Quantum Phenomena
in Simple Optical Systems

Saribek Gevorgyan
AND
Menua Gevorgyan

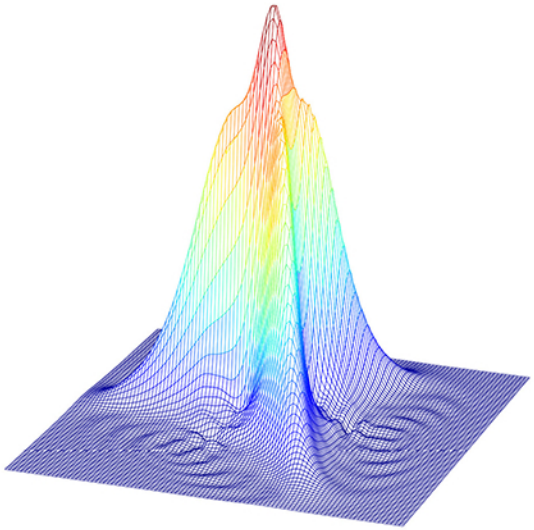

Quantum Phenomena in Simple Optical Systems

Quantum Phenomena in Simple Optical Systems

By

Saribek Gevorgyan and Menua Gevorgyan

Cambridge
Scholars
Publishing

Quantum Phenomena in Simple Optical Systems

By Saribek Gevorgyan and Menua Gevorgyan

This book first published 2020

Cambridge Scholars Publishing

Lady Stephenson Library, Newcastle upon Tyne, NE6 2PA, UK

British Library Cataloguing in Publication Data
A catalogue record for this book is available from the British Library

ISBN (10): 1-5275-4433-8
ISBN (13): 978-1-5275-4433-8

TABLE OF CONTENTS

PREFACE

The book is based on original works of the authors of the book published in peer-reviewed scientific journals. Problems of quantum optics in simple optical systems are studied in the book, namely, generation of the second and third harmonics and generation of the second and third subharmonics, as well as two- and three-photon absorption in the case of two- and three-photon perturbations of the absorbing modes, respectively. Quantum optics problems, such as quantum behaviour of unstable optical systems (second and third harmonic generation), as well as problems related to obtaining squeezed, superposition, and entangled states of optical fields in simple optical systems, are considered. Although the authors tried to write fewer formulas and gave a lot of graphic illustrations of the behaviour of the considered optical systems, some knowledge in the field of quantum optics and Monte Carlo algorithms for studying quantum behaviour of systems is required in order to understand the materials. The authors are grateful to Helen Edwards for the idea of writing this book and the moral support shown during the work on the book.

CHAPTER 1

QUANTUM THEORY OF UNSTABLE BEHAVIOR OF THE INTRACAVITY SECOND HARMONIC GENERATION PROCESS

Introduction

All materials in this chapter are taken from [1–7].

This section investigates the dynamics of quantum fluctuations of the number of photons and phases of the fundamental and second harmonic modes in the unstable region of the system for the process of intracavity generation of the second harmonic. The phase and the number of photon distribution functions of these modes are calculated in the positive P-representation [8]. Joint distribution functions of the number of photons and phases of the field modes are also calculated. It is shown that the dynamics of the semiclassical value of the number of photons of the field modes can differ considerably from the dynamics of the solution to the Langevin equations for the number of photons of the same modes. In particular, in the unstable region, depending on the initial state of the system, the dynamics of the semiclassical value of the number of photons can be without oscillations, whereas the solution to the Langevin equations for the same initial state of the system may have strong oscillations. Algorithms for calculating the distribution functions of photon numbers, as well as for calculating the joint distribution function of photon numbers of the interacting modes of the field, are given in the positive P-

representation. These algorithms can also be applied to calculate both the phase and the joint distribution function of the number of photons and phases of the interacting modes. It is shown that, at the critical point, the distribution functions of the number of photons of the fundamental mode and of the second harmonic mode have single-peak structures, which are asymmetric with respect to the most probable value of the number of photons of the corresponding modes. In the unstable region, the distribution functions of the number of photons of both modes gradually transform into a two-component structure. Each of the components of the distribution functions represents a state of the mode in which it persists most of the time. In the unstable region, the joint distribution function of the photon numbers of the fundamental and second harmonic mode also has a two-peak structure. The above results were obtained in the case of system evolution from an initial state, which has a normal distribution of stochastic amplitudes of the field modes. It is shown that, in the P-representation, in the unstable region of interaction of the system and in the region of large interaction times, the distribution functions of the phases of the field modes also have a two-component structure, which is in contrast to the stable region. Unlike the corresponding photon number distribution functions, the heights of the peaks of the two components of the state of the phase are equal; this means that the system spends the same amount of time in these components of the state. It is shown that the dynamics of the average value of the phase of the field modes depends strongly on the initial state in the unstable region. In the case of evolution of the system from an initial state, which has a normal distribution of stochastic amplitudes of the field modes, the average values of the phases of the field modes do not change in time in the region of large interaction times, whereas in the case of a coherent initial state of both modes and in

the case of a nonzero average value of the phases of the initial state of the system, the average values of the phase oscillate around zero (around the phase of the perturbation field). In the region of instability, in the case of coherent initial states of the field modes, oscillation is observed for both the phase and joint distribution functions of the number of photons and phases, as well as the joint phase distribution functions of the interacting modes of the field. The behaviour of the joint distribution function of the phases of the field modes was studied depending on the system's distance from the critical point. It is shown that, in the unstable region, the joint distribution function of phases of the field modes has a wide dip around the point representing the classical phase matching of the field modes. The latter shows that the classical phase matching has a zero probability of realization in the unstable region. When the system changes into the stable region, a peak is obtained instead of a dip at this point, which corresponds to the classical phase matching of interacting modes.

The dynamics of the quantum entropy, of the Wigner functions, and of the quadrature amplitudes of the field modes are investigated, applying the Monte Carlo wave-function method. It is shown that, depending on the increase in the amplitude of the perturbation field, the quantum entropy of the field modes increases, and the field modes can localize in coherent, squeezed, and unstable states. In the region of a strong perturbation field, the modes of the field first localize in squeezed states, followed by a decay of the squeezed states and a gradual localization of the modes in unstable states.

For the process of intracavity generation of the second harmonic, the dynamics of correlation of quadrature amplitude fluctuations of the fundamental and second harmonic modes is studied, depending on the

nonlinear coupling coefficient between the modes. It is shown that, in this system, depending on the nonlinear coupling coefficient, entangled states of the field in relation to variables of quadrature amplitudes may be obtained. It is also shown that, depending on the value of the nonlinear coupling coefficient, the entanglement of the states of field modes, which is related to one quadrature amplitude, may vanish, whereas the states of the field modes remain entangled in relation to the other quadrature amplitude.

1.1 Nonlinear System, Langevin Equations, and Quantum Noise

We consider a model of second harmonic generation inside a two-mode resonator. A nonlinear medium is placed inside a cavity tuned to the frequencies of the fundamental mode ω_1 and the second harmonic mode $\omega_2 = 2\omega_1$. The system is perturbed externally by a coherent field at a frequency of the fundamental mode. The equations for the density matrix of the optical field of this system may be written in the interaction picture as follows:

$$\frac{\partial \rho}{\partial t} = (i\hbar)^{-1}[H_{\text{int}}, \rho] + L_1(\rho) + L_2(\rho). \tag{1.1.1}$$

Here, the first term represents the external perturbation of the system and the nonlinear interaction of optical fields.

$$H_{\text{int}} = i\hbar E(a_1 - a_1^+) + i\hbar\chi(a_1^2 a_2^+ - a_1^{+2} a_2), \tag{1.1.2}$$

where a_i^+ and a_i $(i = 1,2)$ are the creation and annihilation operators for the corresponding modes, respectively;χ is the coefficient of coupling between the modes, which is proportional to the nonlinear susceptibility

$\chi^{(2)}$; and E is the amplitude of the classical perturbing field at the frequency ω_1.

The $L_1(\rho)$ and $L_2(\rho)$ superoperators describe the damping of the fundamental and second harmonic modes through the resonator mirrors:

$$L_i(\rho) = -\gamma_i(2a_i\rho a_i^+ - a_i^+ a_i\rho - \rho a_i^+ a_i),\ (i = 1,2). \qquad (1.1.3)$$

Here, γ_1 and γ_2 are the damping rates of the respective modes.

From Eqs. (1.1.1)–(1.1.3), in the positive P-representation [8], the following Langevin equations may be derived for the stochastic β_i, α_i amplitudes of the field:

$$\frac{\partial\alpha_1}{\partial t} = E - \gamma_1\alpha_1 - 2\chi\beta_1\alpha_2 + (-2\chi\alpha_2)^{1/2}\xi_1(t),$$

$$\frac{\partial\beta_1}{\partial t} = E - \gamma_1\beta_1 - 2\chi\alpha_1\beta_2 - (-2\chi\beta_2)^{1/2}\xi_2(t),$$

$$\frac{\partial\alpha_2}{\partial t} = -\gamma_2\alpha_2 + \chi\alpha_1^2,$$

$$\frac{\partial\beta_2}{\partial t} = -\gamma_2\beta_2 + \chi\beta_1^2, \qquad (1.1.4)$$

where $\xi_1(t)$ and $\xi_2(t)$ are independent Langevin sources of noise with the following nonzero correlation functions:

$$< \xi_i(t)\xi_j(t') >= \delta_{ij}\delta(t - t'). \qquad (1.1.5)$$

In terms of the stochastic variables of the photon number and phase,

$$n_k = \alpha_k\beta_k,\ \phi_k = \frac{1}{2i} ln\left(\frac{\alpha_k}{\beta_k}\right)\ (k = 1,2). \qquad (1.1.6)$$

From Eq. (1.1.4) and with the help of the Ito formulas, we get

$$\frac{\partial n_1}{\partial t} = 2En_1^{1/2} - 2\gamma_1 n_1 - 4\chi n_1 n_2^{1/2}\, cos(\phi_2 - 2\phi_1) + (-2\chi)^{1/2} n_1^{1/2} n_2^{1/4} \times \{\xi_1(t)\, exp[\, i(\varphi_2 - 2\varphi_1)/2] - \xi_2(t)\, exp[-i(\phi_2 - 2\phi_1)/2]\},$$

$$\frac{\partial n_2}{\partial t} = -2\gamma_2 n_2 + 2\chi n_1 n_2^{1/2}\, cos(\phi_2 - 2\phi_1),$$

$$\frac{\partial \phi_1}{\partial t} = -\frac{E}{n_1^{1/2}} sin(\phi_1) - 2\chi n_2^{1/2}\, sin(\phi_2 - 2\phi_1) + \chi n_1^{-1} n_2^{1/2}\, sin(\phi_2 - 2\phi_1) + \frac{1}{2i}(-2\chi)^{1/2} n_1^{-1/2} n_2^{1/4} \times \{\xi_1(t)\, exp[\, i(\phi_2 - 2\phi_1)/2] - \xi_2(t)\, exp[-i(\phi_2 - \phi_1)/2]\},$$

$$\frac{\partial \phi_2}{\partial t} = \chi n_1 n_2^{-1/2}\, sin(2\phi_1 - \phi_2). \qquad (1.1.7)$$

In a semiclassical approach, i.e., neglecting the noise sources in (1.1.7), for average photon numbers in the steady-state limit ($\gamma_{1,2} t >> 1$), we obtain

$$E(n_1^0)^{1/2} - \gamma_1 n_1^0 - 2\chi n_1^0 (n_2^0)^{1/2} = 0, \qquad -\gamma_2 n_2^0 + \chi n_1^0 (n_2^0)^{1/2} = 0,$$
$$\phi_1^0 = \phi_2^0 = 0. \qquad (1.1.8)$$

After linearization with respect to small fluctuations ($\delta n_i = n_i - n_i^0$, $\delta\phi_i = \phi_i - \phi_i^0$) near the steady-state solutions n_i^0, ϕ_i^0 ($i = 1,2$), equations (1.1.7) are converted to

$$\frac{\partial}{\partial t}\begin{bmatrix}\delta n_1 \\ \delta n_2\end{bmatrix} = A_n \begin{bmatrix}\delta n_1 \\ \delta n_2\end{bmatrix}, \quad \frac{\partial}{\partial t}\begin{bmatrix}\delta \phi_1 \\ \delta \phi_2\end{bmatrix} = A_\phi \begin{bmatrix}\delta \phi_1 \\ \delta \phi_2\end{bmatrix}, \qquad (1.1.9)$$

where A_n and A_ϕ are as follows:

$$A_n = \begin{bmatrix} -\gamma_1 - 2\chi(n_2^0)^{1/2} & -2\gamma_2 \\ 2\chi(n_2^0)^{1/2} & \gamma_2 \end{bmatrix},$$

$$A_\phi = \begin{bmatrix} -\gamma_1 + 2\chi(n_2^0)^{1/2}(1-(n_1^0)^{-1}) & -\chi(n_2^0)^{1/2}(2-(n_1^0)^{-1}) \\ 2\gamma_2 & -\gamma_2 \end{bmatrix}. \quad (1.1.10)$$

We assume that the classically characterized driving field phase is equal to zero. The eigenvalues λ_1 and λ_2 of the $A_n$matrix and $\lambda_3$and λ_4 of the A_φ matrix for $n_1 >> 1$ are

$$\lambda_{1,2} = -\frac{1}{2}(\gamma_1 + \gamma_2 + 2\chi(n_2^0)^{1/2}) \pm$$
$$\tfrac{1}{2}\left[(\gamma_1 - \gamma_2 + 2\chi(n_2^0)^{1/2})^2 - 16\chi\gamma_2(n_2^0)^{1/2}\right]^{1/2},$$

$$\lambda_{3,4} = -\frac{1}{2}(\gamma_1 + \gamma_2 - 2\chi(n_2^0)^{1/2})$$
$$\pm\tfrac{1}{2}\left[(\gamma_1 - \gamma_2 - 2\chi(n_2^0)^{1/2})^2 - 16\chi\gamma_2(n_2^0)^{1/2}\right]^{1/2}. \quad (1.1.11)$$

The real parts of $\lambda_1$and λ_2 are always negative, but the λ_3 and λ_4 coefficients at the critical values

$$n_{2cr} = \left(\frac{\gamma_1+\gamma_2}{2\chi}\right)^2, n_{1cr} = \frac{\gamma_2(\gamma_1+\gamma_2)}{2\chi^2}, \; E_{cr} = (2\gamma_1+\gamma_2)\left[\frac{\gamma_2(\gamma_1+\gamma_2)}{2\chi^2}\right]^{1/2} \quad (1.1.12)$$

become imaginary. It means that, at this point (the Hopf bifurcation point), the small fluctuations of the phase do not damp. This is a physical reason for the unstable behaviour of the entire optical system (to right of the bifurcation point).

The Langevin system of equations (1.1.4) can be written in the following differential form:

$$d\alpha_1 = (\varepsilon - \alpha_1 - 2k\beta_1\alpha_2)d\tau + (-2k\alpha_2)^{1/2}w_1(\tau)(d\tau)^{1/2},$$

$$d\beta_1 = (\varepsilon * -\beta_1 - 2k\alpha_1\beta_2)d\tau + (-2k\beta_2)^{1/2}w_2(\tau)(d\tau)^{1/2},$$

$$d\alpha_2 = (-r\alpha_2 + k\alpha_1^2)d\tau,$$

$$d\beta_2 = (-r\beta_2 + k\beta_1^2)d\tau. \qquad (1.1.13)$$

Here, the quantity $\tau = \gamma_1 t$ is the scaled time, $r = \gamma_2/\gamma_1$ is the ratio of the damping rates of the modes inside the cavity, $k = \chi/\gamma_1$ is the scaled constant of coupling between the modes, and $\varepsilon = E/\gamma_1$ is the scaled perturbation at the frequency of the fundamental mode. The independent noise sources $w_1(\tau)$ and $w_2(\tau)$ have zero mean values: $< w_1(\tau) >=< w_2(\tau) >= 0$. Nonzero values only have the means of squares of these quantities:

$$< [w_1(\tau)]^2 >=< [w_2(\tau)]^2 >= 1. \qquad (1.1.14)$$

Without noise sources and at long times of interaction, the system of equations (1.1.13) has a stable stationary solution only for small values of the perturbing field ($\varepsilon < \varepsilon_{cr}$). The quantity $\varepsilon_{cr}$is the Hopf bifurcation point and is determined by the formula

$$\varepsilon_{cr} = (2 + r)[r(1 + r)/(2k^2)]^{1/2}. \qquad (1.1.15)$$

When $\varepsilon > \varepsilon_{cr}$, small time fluctuations of phases of the fundamental and second harmonic modes cease damping. The system loses its stability around the stationary solutions to Eqs. (1.1.13) without noise terms. In this region, classical solutions for numbers of photons get into a self-

oscillation regime. Our calculations are based on a simulation of noise sources. We model these sources by the following formulas [9]:

$$w_1(\tau) = [-2\,ln(\,z_1)]^{1/2}\,cos(\,2\pi z_2),$$

$$w_2(\tau) = [-2\,ln(\,z_1)]^{1/2}\,sin(\,2\pi z_2), \qquad (1.1.16)$$

where z_1 and z_2 are independent random numbers with a uniform distribution in the interval (0;1). For the random quantities in expression (1.1.16), we have

$$< w_i(\tau) >= 0,\ < w_i(\tau)w_j(\tau) >= \delta_{ij}\ (i,j = 1,2). \qquad (1.1.17)$$

For the solution of the system of equations (1.1.13), the Euler numerical technique for differential equations is used, which is not quick; however, unlike Runge-Kutta methods, it is more correct for solving equations with Langevin noise sources [10]. This approach was initially developed in [11] to calculate the dynamics of the photon numbers in SHG. The lack of numerical solutions to the Langevin equations, in particular, the appearance of nonphysical spikes at large times and at a sufficient distance to the right of the bifurcation point, is discussed in [10]. It was shown in [12] that the deterministic part of the quantum stochastic equations for a wavefunction can be solved with the Runge-Kutta methods, but the stochastic part should be simulated with the more reliable Euler's method.

1.2 Semiclassical and Quantum Solutions of Langevin Equations

Let us consider the semiclassical solutions of Eqs. (1.1.13) for photon numbers that were for the first time discovered in [13]. Figure 1.1 (curve 1) shows the photon number dynamics of the second harmonic with the

initial conditions $\alpha_i(0) = \beta_i(0) = 1,\ (i = 1,2)$, using the semiclassical approach (the noise sources in (1.1.13) are neglected). As one can see, under such conditions, the self-pulsing regime is absent. Curve 2 represents the real part of the photon number

$$Re(\beta_2\alpha_2) = Re\, n_2 \qquad (1.2.1)$$

for a single solution of Langevin equations (with noise sources) under the same conditions. The imaginary part $Im(\beta_2\alpha_2)$ is not taken into account, as it becomes zero when averaged over an ensemble with a large number of realizations.

The absence of a self-pulsing regime in the semiclassical approach can be connected with the fact that the initial values β_i, α_i are absolutely real, so the initial phase is equal to the phase in the steady-state solution ($\delta\Phi = 0$) [13]. Meanwhile, the presence of quantum noise in realizations of Langevin equations leads to small phase fluctuations around the steady-state solution. This is the reason for the change of the system into the self-pulsing region in a separate solution. That is why it is interesting to consider the quantum dynamics of the phase in SHG in order to describe and further investigate the instability in this process.

In the region of instability $E > E_{cr}$, the temporal behaviour of the number of photons of the fundamental mode is analogous to the temporal behaviour of the number of photons of the second harmonic mode.

1.3 Quantum Dynamics of Photon Numbers of the Modes

First, let us study the temporal behaviour of the photon numbers of the fundamental mode and of the second harmonic in the instability region of

the system. The average value of the number of photons of the optical system is calculated as the mathematical expectation of the stochastic quantities: $n_i(\tau) = Re\{\alpha_i(\tau)\beta_i(\tau)\}$, where

$$\langle n_i(\tau)\rangle = \lim_{N\to\infty}\left(\frac{1}{N}\sum_{(j)=1}^{N} n_i^{(j)}(\tau)\right), \quad (i = 1,2). \tag{1.3.1}$$

Here, (j) is the realization number and N is the total number of realizations of the set of equations (1.1.14).

In this section, we calculate the quantum dynamics of the number of photons of the system in the case of a normal distribution of the initial values of stochastic amplitudes of the fundamental mode and of the second harmonic.

$$\alpha_1(0) = [-2\,ln(\,z_1)]^{1/2}\,cos(\,2\pi z_2) + i[-2\,ln(\,z_1)]^{1/2}\,sin(\,2\pi z_2),$$

$$\beta_1(0) = \alpha_1^*(0),$$

$$\alpha_2(0) = [-2\,ln(\,z_3)]^{1/2}\,cos(\,2\pi z_4) + i[-2\,ln(\,z_3)]^{1/2}\,sin(\,2\pi z_4),$$

$$\beta_2(0) = \alpha_2^*(0) \quad , \tag{1.3.2}$$

where z_1, z_2, z_3, z_4 are independent random numbers with a uniform distribution on the interval (0…1). In particular, for these initial values of the amplitudes of the optical field modes, we have

$$< \alpha_i(0) >=< \beta_i(0) >= 0,$$

$$< \beta_i(0)\alpha_j(0) >= 2\delta_{ij}\ (i,j = 1,2). \tag{1.3.3}$$

We also investigate the quantum dynamics of photon numbers of the interacting modes of the optical system in the case of evolution of the

system from initial coherent states of the fundamental and second harmonic modes.

Figure 1.2 demonstrates the dynamics of the average value of the number of photons of the fundamental mode in the region of unstable behaviour of the system (curve 1). According to (1.1.15), the critical perturbation of the system is $\varepsilon_{cr} = 30$. The function was calculated for the value of perturbation $\varepsilon = 50$. To calculate the quantum dynamics of the number of photons of the fundamental mode, we used 1000 realizations for the set of equations (1.1.13) with initial values given in (1.3.2). Curve 2 represents the behaviour of the number of photons of one of the realizations of the set of equations (1.1.13) with the initial values of the stochastic amplitudes of the field modes $\alpha_j(0) = i$ and $\beta_j(0) = -i$ $(j = 1,2)$. Curve 2 was calculated for the same parameter values as for curve 1. At large interaction times, oscillations of curve 2 show that, in this region, the system is in a self-oscillating regime. In the region of instability, the dynamics of the number of photons of the fundamental mode, averaged over an ensemble of realizations of the system (described by the set of equations (1.1.13)), has no oscillations (curve 1), if the interacting modes develop from an initial state that has a normal distribution of stochastic amplitudes (1.3.2) for both modes.

Figure 1.3 shows the time behaviour of the average number of photons of the second harmonic mode (curve 1) in the case of evolution of both modes of the system from an initial state with a normal distribution of the stochastic amplitudes. To calculate this function, we used 1000 independent realizations for the set of equations (1.1.13). The function was calculated for the same parameters and perturbation of the system as the curves in Fig. 1.2. The time behaviour of the second harmonic mode in the

region of instability is similar to the behaviour of the fundamental mode. Curve 2 in Fig. 1.3 represents one realization of the second harmonic mode for the case where the system evolves from the same initial values of the stochastic amplitudes for which curve 2 in Fig. 1.2 was calculated.

Figure 1.4 demonstrates the quantum dynamics of the number of photons of the fundamental mode (curve 1) and of the second harmonic (curve 2) for the case of evolution of the system from the following initial values of the stochastic amplitudes of the field modes: $\alpha_j(0) = 1 + i$ and $\beta_j(0) = 1 - i$ $(j = 1,2)$. To obtain each curve, we used 20 000 independent realizations for the set of equations (1.1.13). Here, unlike in the previous cases, the average numbers of photons of the modes oscillate in the region of large evolution times. The amplitude of oscillations of the fundamental mode is larger than the amplitude of oscillations of the second harmonic. These two cases of evolutions of the system show that, in the region of instability and in the region of long interaction times, the quantum behaviour of the number of photons of the modes depends strongly on the initial state of these modes.

1.4 Distribution Functions for Photon Numbers of the Modes

In this section, we study distribution functions for the number of photons of the fundamental mode and the second harmonic in the vicinity of the bifurcation point of the system. First, let us study the distribution functions of the fundamental mode in the region of large interaction times. Let us describe the algorithm for calculating this function. To calculate the distribution function, first, a segment in the phase space of the number of photons of the fundamental mode should be chosen. This is the region

outside of which the distribution function vanishes. This region can be easily found by studying the dynamics of several realizations of the number of photons of the fundamental mode. We divide the length of this segment into N_p equal parts and calculate the quantity

$$\Delta n_1 = (n_{1\max} - n_{1\min})/N_p. \quad (1.4.1)$$

Then, we choose an array of numbers $A(i)$ with the dimension $N_p + 1$ $(i = 0, N_p)$ and equate all of its elements to zero.

Next, a cycle of calculations begins, and one of its steps is presented below. We calculate the number of photons of the fundamental mode for an instant of time by using the solution to the set of equations (1.1.13). After this, we calculate

$$i = Int[(n_1(\tau) - n_{1\min})/\Delta n_1], \quad (1.4.2)$$

where Int means the calculation of the integer part of the expression in square brackets. The value of the array element should be increased by unity as follows:

$$A(i) \to A(i) + 1. \quad (1.4.3)$$

Then, calculations are repeated until the necessary number of realizations N is obtained. The array elements $A(i)$ represent approximate values of the unnormalized distribution function for the number of photons of the fundamental mode for the instant of time τ at the points $n_{1min} + i\Delta n_1$, $\left(i = 0, N_p\right)$. We construct a curve that passes through these points and normalizes the obtained function to unity. The normalized curve represents an approximate plot of the distribution for the number of photons of the fundamental mode in the positive P representation.

Figure 1.5 shows the distribution function for the number of photons of the fundamental mode ($n_1 = Re(\beta_1\alpha_1)$) at the critical point of the system ($\varepsilon = \varepsilon_{cr} = 30$). To calculate this function, we used 100 000 independent numerical solutions of the set of Langevin equations (1.1.13) with the initial values of stochastic amplitudes of the field modes (1.3.2). The function was calculated in the range of large interaction times ($\tau = 10$) and for the parameter values k = 0.1 and r = 1. This function is asymmetric relative to the most probable value. To the right of the point of the most probable value of the number of photons, the probability of realization is larger than that observed to the left.

Figure 1.6 demonstrates the distribution function for the number of photons of the fundamental mode in the instability region (ε = 50) and for large interaction times (τ = 10). To calculate this function, we used 100 000 independent numerical realizations of the set of Langevin equations (1.1.13). The function was calculated for the same values of the parameters k = 0.1 and r = 1. In this case, the distribution function for the number of photons has two most probable values, each of which corresponds to a state in which the system mostly resides. After the passage of the critical point, as the system penetrates deep into the unstable region, the distribution function of the number of photons gradually changes from the single-component asymmetric structure (Fig.1.5) to the two-component structure (Fig.1.6).

In the region of long interaction times and in the region of instability, the behaviour of the distribution function of the number of photons of the second harmonic is analogous to the behaviour of the distribution function for the number of photons of the fundamental mode. In Fig.1.7, the distribution function for the number of photons of the second mode is

presented in the region of large interaction times ($\tau = 10$) and at the critical point of the system ($\varepsilon = \varepsilon_{cr} = 30$). The function was calculated for the same parameters of the system that were used to calculate the distribution function shown in Fig. 1.5 ($k = 0.1$ and $r = 1$). To obtain this function, we used 100 000 independent realizations of the set of Langevin equations with the initial values (1.3.2). Similarly to the distribution function for the number of photons of the fundamental mode at the critical point (Fig.1.5), this function is also asymmetric relative to the most probable value. However, in this case, the probability of realizing a number of photons that is smaller than the most probable number is greater than the probability of realizing a number of photons that is greater than the most probable number.

Figure 1.8 presents a distribution function for the number of photons of the second harmonic in the region of large interaction times and in the instability region. The function was obtained using 100 000 independent realizations of the set of Langevin equations (1.1.13) with the initial independent values (1.3.2). The function was calculated for the parameters $k = 0.1$ and $r = 1$. The distribution function of the number of photons of the second harmonic has a two-peak structure, as well as the distribution function of the number of photons of the fundamental mode. Each of the most probable values of the distribution function corresponds to a state in which the system resides most of the time.

1.5 Joint Distribution Functions for Photon Numbers of the Modes

In this section, we study the behaviour of the joint distribution function of the number of photons of the fundamental mode and of the second harmonic.

To calculate this function, we use the following algorithm. In the phase space of the number of photons of the fundamental mode and of the second harmonic, we choose a rectangle with the vertices $(n_{1\min}, n_{2\min})$, $(n_{1\min}, n_{2\max})$, $(n_{1\max}, n_{2\max})$, and $(n_{1\max}, n_{2\min})$. This is the region of the phase space outside of which the joint distribution function of the number of photons of the fundamental and second harmonic modes vanishes. We divide the edges of this rectangle into N_p equal parts and calculate the quantities $\Delta n_1 = (n_{1\max} - n_{1\min})/N_p$ and $\Delta n_2 = (n_{2\max} - n_{2\min})/N_p$. Then, we determine the two-dimensional array of numbers $A(i,j)$ with the dimension $(N_p + 1) \times (N_p + 1)$, where $i, j = 0, N_p$, and equate all its elements to zero. Next, a cycle of calculations begins (one of its steps is presented below). Using the solution to the set of equations (1.1.13), we calculate the number of photons of the fundamental mode and of the second harmonic at the instants of time τ, $n_1(\tau)$ and $n_2(\tau)$. Then, we use the following formulas:

$$i = Int[(n_1(\tau) - n_{1\min})/\Delta n_1],$$

$$j = Int[(n_2(\tau) - n_{2\min})/\Delta n_2]. \qquad (1.5.1)$$

Here, as in formula (1.4.2), Int means the calculation of the integer part of the expression in square brackets. We increase the value of the array element $A(i,j)$ with the number (i,j) by 1 as follows:

$$A(i,j) \to A(i,j) + 1. \qquad (1.5.2)$$

After this, calculations are repeated until the required number of realizations N is obtained.

The array elements $A(i,j)$ represent approximate values of the unnormalized joint distribution function of the number of photons of the fundamental mode and of the second harmonic at the points $(n_{1\min} + i\Delta n_1,\ n_{2\min} + j\Delta n_2)$.

Further, we construct a surface that passes through the points $(n_{1\min} + i\Delta n_1,\ n_{2\min} + j\Delta n_2,\ A(i,j))$ of the three-dimensional space. This surface represents the unnormalized joint distribution function of the number of photons of the fundamental mode and of the second harmonic at the instant of time τ. Then, we normalize this function.

Figure 1.9 demonstrates the joint distribution function of the number of photons of the fundamental mode and of the second harmonic at the critical point ($\varepsilon = \varepsilon_{cr} = 30$) and in the region of large interaction times ($\tau = 10$). The function was calculated using 50 000 independent realizations of the set of equations (1.1.13) with the initial values (1.3.2) and for the values of the parameters of the system k = 0.1 and r = 1. The function has a single peak structure but is asymmetric relative to the most probable value of the distribution function. A combination of larger values of the photon number of the fundamental mode with smaller values of photon number of the second harmonic relative to the most probable value of the distribution function has a larger probability of realization than a combination of smaller values of the photon number of the fundamental mode with larger values of the photon number of the second harmonic.

Figure 1.10 demonstrates a joint distribution function of the number of photons of the fundamental mode and of the second harmonic in the region of instability ($\varepsilon = 50$) and in the range of large interaction times ($\tau = 10$). To calculate this function, we used 50 000 independent numerical solutions to the set of Langevin equations (1.1.13) with the initial values (1.3.2). The function was calculated for the parameters of the system k = 0.1 and r = 1. It has a two-peak structure. Each of the most probable values of the distribution function corresponds to a state in which the system spends the majority of its time.

1.6 Dynamics of Phase Fluctuations

In this section, we study the behaviour of the distribution function of phases (1.1.6) $Re\,\phi_i$ $(i = 1,2)$ of the fundamental and second harmonic modes in the case of different initial states of the interacting modes. The algorithm for calculating the phase distribution function of the field modes is similar to the algorithm for calculating the photon number distribution function; hence, we do not provide it here.

Figure 1.11 shows the dynamics of the fundamental mode phase distribution function in the case of the initial coherent states of interacting modes $\alpha_j(0) = \sqrt{2}$ and $\beta_j(0) = \alpha_j(0)^*$, where $j = 1,2$. The function is calculated based on 100 000 independent trajectories of Eqs. (1.1.13) for the following parameter values: $\varepsilon = 50$, $k = 0.1$, and $r = 1$. At these values, we have $\varepsilon_{cr} = 30$. At the moment $\tau = 0$, the phase distribution function of this mode is infinitely narrow. The distribution function broadens gradually with time and, after some time ($\tau = 5$), passes from a single-peak to a two-peak shape. After acquiring a two-peak structure, it does not change its shape later. The two peaks are symmetric with respect

to the zero phase and determine the two components of the phase state of this mode. The phase distribution function of the second harmonic displays a similar time behaviour.

In Fig. 1.12 the dynamics of a certain realization of the fundamental mode phase is shown. The dashed lines correspond to the two most probable values of the phase. The time of transition of the system between these states is about the stay time in them.

Figure 1.13 shows the dynamics of the phase distribution function of the second harmonic mode in the case of Gaussian initial conditions (1.3.2) of the interacting modes and for the following values of parameters: $\varepsilon = 50$, $k = 0.1$, and $r = 1$. The function was calculated using 50 000 independent realizations for the set of equations (1.1.13). At the beginning (t = 0), the function has a sharp single peak form. It is seen in Fig. 3 that the distribution function gradually widens as time progresses and eventually acquires a two-peak form. These two peaks are the two most probable values of the stochastic phase; in fact, with the further evolution of the system, a new macroscopic state is formed.

Figure 1.14 shows the dynamics of the average value of the real part of the second harmonic mode phase in the case of evolution of the system from an initial coherent state with the values of stochastic amplitudes $\alpha_1(0) = 1 + i$, $\beta_1(0) = 1 - i$, $\alpha_2(0) = 1 - i$, and $\beta_2(0) = 1 + i$ (curve 1) and in the case of evolution from an initial state, which has a normal distribution of stochastic amplitudes of the field modes (1.3.2) (curve 2). Both curves represent the temporal behaviour of the average value of the phase of the second-harmonic mode in the unstable region and are calculated for the following values of system parameters: $\varepsilon = 50$, $k = 0.1$, and $r = 1$. Each

curve is calculated using 5000 independent solutions of the system of equations (1.1.13). In the case of evolution from an initial state with a normal distribution of the stochastic amplitudes of the field modes, the average value of the phase of the second harmonic mode does not change with time and is zero (the value of the phase of the perturbation field). In the case of evolution of the system from initial coherent states of the field modes (curve 1), the average value of the phase of the mode does not have a stationary value and oscillates in time around the zero value of the phase. These curves show that, in the unstable region, the dynamics of the average value of the phases of the interacting modes depend strongly on the initial state of these modes. In the case of system evolution from the initial states mentioned above, the average value of the phase of the fundamental mode has a similar temporal behaviour: in the case of normal distributions of the initial values of stochastic amplitudes of the interacting modes, the average value of the phase of the fundamental mode does not change in time and is zero, whereas in the case of coherent initial states of both modes it oscillates around the zero value of the phase.

In the unstable region, not only the dynamics of the average values of the phases but also the dynamics of the phase distribution function of the interacting modes of the field, depend strongly on the initial state of the optical system. In the region of large times, if the system evolves from initial coherent states with zero values of phases of both modes of the system (see Fig. 1.11), as well as if the system evolves from an initial state in which the stochastic amplitudes of the interacting modes of the field have normal distributions (see Fig. 1.13), the distribution functions of the stochastic phases of the modes do not change in time and have a two-component structure.

However, the dynamics of the phase distribution of the field modes changes dramatically in the case of evolution of the optical system from initial coherent states of both modes with a nonzero phase. Figure 6.15 shows the temporal behaviour of the distribution function of the second harmonic mode phase in the case of evolution of the optical system from an initial coherent state with the following values of the stochastic amplitudes of the field modes: $\alpha_1(0) = 1 + i$, $\beta_1(0) = 1 - i$, $\alpha_2(0) = 1 - i$, and $\beta_2(0) = 1 + i$. Here, Figs. 6.15a to 6.15d represent the distribution function of the real part of the phase of the second harmonic mode $Re(\phi_2)$ at the times of evolution of the system $\gamma t = 5.3$, $\gamma t = 6$, $\gamma t = 6.6$, and $\gamma t = 7.3$, respectively. These time points correspond to points a, b, c, and d in Fig. 1.14. The dynamics of the distribution function is calculated for the parameter values $k = 0.1$, $r = 1$, and $\varepsilon = 50$. For calculating the dynamics of this function, 50 000 independent realizations of the Langevin system of equations (1.1.13) were used. At the time point $\gamma t = 5.3$, the average value of the phase of the second harmonic mode is zero (see Fig. 1.14). At this point, the second harmonic mode is localized in a two-component state with the same probability of detection of this mode of the field in each component of the state (Fig. 1.15a). Then, from a two-component state, the system gradually localizes into one component of the state in which the average value of the phase of the second harmonic mode has a positive value (Fig. 1.15b). From here, the system changes back into a two-component state with the same probability of detection of the second harmonic mode in each component of the state (Fig. 1.15c). The average value of the phase of the second harmonic mode in this state is reset to zero. After that, the system localizes in the other component of the state, where the average value of the phase of the second harmonic mode is negative. This behaviour of the phase distribution function of the

second harmonic mode repeats itself with the further evolution of the optical system.

In the unstable region, in the case of evolution of the optical system from initial coherent states with nonzero phases of stochastic amplitudes of both modes, the temporal behaviour of the distribution function of the phase of the fundamental mode $Re\,\phi_1$ is similar to the temporal behaviour of the distribution function of the second harmonic mode phase.

In Fig. 1.16 we demonstrate the dynamics of the phase distribution function for the fundamental mode in the case of the initial coherent states of both modes $\alpha_j(0) = i\sqrt{2}$ and $\beta_j(0) = \alpha_j(0)^*$ $(j = 1{,}2)$, and for the following parameter values: $\varepsilon = 50$, $k = 0.1$, and $r = 1$. The function was calculated using 100 000 independent realizations for the set of equations (1.1.13). In this case, there is no stationary solution for the distribution function, and it passes to an oscillation regime after broadening. The fundamental mode localizes gradually in one component of the state from the two-component state, which has the same probability of detecting the mode in each component of the state. Next, the system returns to the two-component state, and after that localizes in the other component of the state.

In Fig. 1.17 we plot the phase distribution function of the fundamental mode at the moment of time $\tau = 9$ in the case of initial coherent states of both modes $\alpha_j(0) = \sqrt{2}$ and $\beta_j(0) = \alpha_j(0)^*$, where $j = 1{,}2$ ($k = 0.1$ and $r = 1$), versus the amplitude of the driving field ε. The function was calculated using 100 000 independent realizations for the set of equations (1.1.13). At $\varepsilon = 30$ (point of bifurcation), the system is in a one-component state with zero phase values. When the system passes the

bifurcation point, the system branches into a two-component state with opposite values of the phases of the components. The fundamental mode can be detected with the same probability in both of these two components of the state of the mode.

In the region of large interaction times, the dependence of the distribution function of the phase of the second harmonic mode on the amplitude of the perturbation field is similar to the dependence of the distribution function of the phase of the fundamental mode shown in Fig. 1.17.

1.7 Dynamics of Joint Phase Fluctuations of the Modes and Self-Phase Matching

The above-described technique can also be applied for the calculation of the joint distribution function of the phases of the fundamental mode and second harmonic. This function characterizes the phase matching between the interacting modes. Below the critical point, where the system has stable classical solutions for the photon numbers and phases, the phase fluctuations are considerably smaller than unity. In this case, the most probable values of phase pairs coincide with their classical values, and the equality $Re\,\phi_1 = Re\,\phi_2 = 0$ determines the classical phase matching between the modes. Figure 1.18 shows the joint distribution function of phases of the fundamental mode and second harmonic in the case of initial vacuum states of both modes ($\alpha_j(0) = \beta_j(0) = 0$, where $j = 1,2$) and for the following parameter values: $r = 1$, $k = 0.1$, and $\varepsilon = 10$. The function was calculated using 100 000 independent realizations for the set of equations (1.1.13). The function shows the classic matching of the system mode phases.

Above the critical point, the phase fluctuations become of the order of unity. Figure 1.19 shows the joint distribution function of phases of the fundamental mode and the second harmonic in the case of initial vacuum states of both modes ($\alpha_j(0) = \beta_j(0) = 0$, where $j = 1,2$) and for the following values of parameters: $r = 1$, $k = 0.1$, and $\varepsilon = 50$. Events in some region around the point $Re\,\phi_1 = 0, Re\,\phi_2 = 0$ (this point determines the phase matching of the modes in the classical solutions) have zero probability of realization. When the quantum system approaches the bifurcation point from above ($\varepsilon \to \varepsilon_{cr}$), the above-mentioned region is reduced, and, at the critical point, we have a peak at $Re\,\phi_1 = 0, Re\,\phi_2 = 0$ instead of a dip around these values.

In the case of the initial coherent states of both modes $\alpha_j(0) = i\sqrt{2}$ and $\beta_j(0) = \alpha_j(0)^*$, where $j = 1,2$, the distribution function exhibits oscillations and stationary phase matching does not occur in the system. Figure 1.20 shows the joint distribution function of phases of the fundamental mode and second harmonic in the case of initial coherent states of both modes for the following values of parameters: $r = 1$, $k = 0.1$, and $\varepsilon = 50$. For the calculation of these functions, we employed 100 000 independent trajectories of Eqs. (1.1.13).

At the time moment $\tau = 5.96$, the system is localized in one of the state components. In this component, the phases of the modes take simultaneously positive values with respect to the disturbing field phase. At the moment $\tau = 6.63$ (Fig. 20b), the phase of the fundamental mode takes only negative values. These phase values are jointly realized with equal probabilities and with positive and negative values of the second harmonic phase. At the moment $\tau = 7.25$, the system is localized in the

other state component, where the phases of the fundamental mode and second harmonic are negative (Fig. 10c). From here, the system passes to a state in which the phase of the fundamental mode takes only positive values, which are jointly and with equal probabilities realized with either positive or negative values of the second harmonic phase (Fig. 10d).

1.8 Dynamics of Joint Fluctuations in Photon Numbers and Phases

In this section, we study the dynamics of joint fluctuations in photon numbers and phases of the interacting modes. For this purpose, we calculate the joint distribution function of the photon numbers and phases for the fundamental mode and second harmonic.

In the case of the initial coherent states $\alpha_j(0) = \sqrt{2}$ and $\beta_j(0) = \alpha_j(0)^*$ (where $j = 1,2$), the above-mentioned distribution functions pass to a stationary regime for some $\tau >> 1$. In Figs. 1.21a and 1.21b we show the photon number and the phase distribution function at $\tau = 9$ for the fundamental mode and second harmonic, respectively. Both functions are symmetric with respect to the zero phase, and their two branches determine the two components of the phase state of these modes. For either of the modes, the same values of photon numbers are realized in the states with negative and positive phases.

In the case of the initial coherent states $\alpha_j(0) = i\sqrt{2}$ and $\beta_j(0) = \alpha_j(0)^*$ (where $j = 1,2$), the above-mentioned distribution functions have no stationary solutions at $\tau >> 1$. In Fig. 1.22 the dynamics of the joint distribution function of the numbers of photons and phases for the second harmonic mode is shown for this case. At the moment $\tau = 5.96$, the

second harmonic is localized in one component of its state with the most probable positive value of the phase (Fig. 1.22a). At the moment $\tau = 7.25$, the second harmonic is localized in the other component of its state with the most probable negative value of the phase (Fig. 1.22b). The joint distribution function of photon numbers and phases of the fundamental mode also exhibits a similar time behaviour.

1.9 Dynamics of Wigner Function and Quantum Entropy of the Modes

In order to study the quantum properties of the optical system, we calculate the Wigner functions of the field state in polar coordinates $x = r\,cos(\theta)$, using equation [14]:

$$W(r,\theta) = \sum_{m,n} \rho_{mn} w_{mn}(r,\theta), \tag{1.9.1}$$

where ρ_{mn} represents the elements of the density matrix of the field in the Fock basis and

$$w_{mn}(r,\theta) = \begin{cases} \frac{2}{\pi}(-1)^n \left(\frac{n!}{m!}\right)^{1/2} exp(\,i(m-n)\theta) \times \\ \quad exp(-2r^2)(2r)^{m-n} L_n^{m-n}(4r^2), \quad m \geq n \\ \frac{2}{\pi}(-1)^m \left(\frac{m!}{n!}\right)^{1/2} exp(\,i(m-n)\theta) \times \\ \quad exp(-2r^2)(2r)^{n-m} L_m^{n-m}(4r^2), \quad m \leq n \end{cases}. \tag{1.9.2}$$

In the last equation, L_k^{β} represents the Laguerre polynomials.

We also investigate the dynamics of the quantum entropy of the field

$$S = -Tr(\rho\, ln(\,\rho)). \tag{1.9.3}$$

The entropy is calculated using numerical diagonalization of the density matrix of the field in the Fock basis.

The dynamics of the density matrices of the modes of the field is calculated using the Monte Carlo wave function method [15].

The above calculations can also be done using the software package described in [16].

Figure 1.23 shows the dynamics of the Wigner functions of the fundamental and second harmonic modes in the case of evolution of the system from initial vacuum states of both modes (Fig. 1.23a) and for the parameter values of the system $\varepsilon = 6,\ k = 0.3$, and $r = 1$. The functions are calculated using 1000 quantum trajectories of the optical system. Figures 1.24 and 1.25 show the dynamics of the quantum entropy of the fundamental and second harmonic modes, respectively. The dynamics of the quantum entropy of the interacting modes of the system is calculated for the value $k = 0.3$ of the coupling coefficient of the modes and for different values of the perturbation field. In these figures, curves c represent the dynamics of the quantum entropy of the corresponding modes for the value of the perturbation field$\varepsilon = 6$. In the region of interaction times $\tau \leq 0.7$, the quantum entropies of the modes of the field are zero: the modes of the field are in pure states. Figures 1.23b and 1.23c show the Wigner functions of the fundamental mode and of the second harmonic mode, respectively, at the interaction time $\tau = 0.7$. Both functions represent coherent states. After that, the quantum entropy of both modes increases with time, and the modes begin to localize in squeezed states. Figures 1.23d and 1.23e show the Wigner functions of the fundamental mode and of the second harmonic mode, respectively, at the

interaction time $\tau = 1.67$. The figures for the Wigner function show that both modes at this point in time are in a squeezed state. With further evolution of the system, the quantum entropies of both modes continue to grow and change gradually into a stationary region. In the region of large interaction times, the Wigner functions of the interacting modes also change into a stationary limit. In the region of large interaction times, both modes localize in two-component unstable states. The Wigner functions of the fundamental and second harmonic modes at the interaction time $\tau = 8.9$ are shown in Figs. 1.23f and 1.23g, respectively. It can be said that both functions represent a two-component state. With a decrease in the perturbation field, the stationary values of the quantum entropy of the field modes decrease (see Figs. 1.24 and 1.25). In the region of large interaction times and in the case of a small perturbation of the fundamental mode, the interacting modes begin to localize in squeezed or coherent states (more precisely, in states that are a statistical mixture of close coherent states).

Figure 1.26 shows the Wigner functions of the fundamental mode in the region of large interaction times $\tau = 8$, in the case of evolution of both modes from the initial vacuum state, for the value of the coupling coefficient $k = 0.3$, and for the values of the perturbation field $\varepsilon = 1$ in Fig. 1.26a and $\varepsilon = 3$ in Fig. 1.26b. The Wigner function in Fig. 1.26a represents a statistical mixture of close coherent states (the quantum entropy of the state is not equal to zero). Figure 1.26b resembles a Wigner function of a squeezed state that begins to break down.

In the case of system evolution from initial coherent states of both modes, which have a nonzero phase of the state amplitude relative to the phase of the perturbation field, the average values of the quadrature amplitudes of

the field modes $\langle Y_j \rangle = \left(a_j - a_j^+\right)/2i,\ (j = 1{,}2)$ and the Wigner functions of the states of these modes have damped oscillations in time.

Figure 1.27 presents the dynamics of the average values of the quadrature amplitudes of the fundamental $\langle Y_1 \rangle$ (curve 1) and second harmonic $\langle Y_2 \rangle$ (curve 2) modes in the case of evolution from the initial coherent states of the fundamental mode $|-2i\rangle$ and second harmonic mode $|2i\rangle$ for the system parameters $\varepsilon = 6,\ k = 0.3$. The dynamics were calculated using 1000 quantum trajectories of the optical system. The mean values of the quadrature amplitudes of both modes have decayed with time oscillations, which are absent when the system evolves from initial vacuum states of both modes.

Figure 1.28 shows the Wigner function of the fundamental mode in the case of evolution of the fundamental and second harmonic modes from the initial coherent states $|-2i\rangle$ and $|2i\rangle$, respectively, at the interaction times $\tau = 4.9$ (Fig. 1.28a) and $\tau = 8.2$ (Fig. 1.28b) and for the values of the system parameters $\varepsilon = 6,\ k = 0.3$. The functions are computed using 1000 quantum trajectories of the optical system. At the time of interaction $\tau = 4.9$, the fundamental mode is much more localized in the component of the state with negative values of the Y variable than in the component of the state with positive values of this variable (see Fig. 1.28a). At the interaction time $\tau = 8.2$, the fundamental mode is much more localized in the other component of the state, which has positive values of the Y variable (Fig. 1.28b). Such oscillations of the Wigner functions of the states of the field modes are absent when the system evolves from initial vacuum states of both interacting modes.

1.10 Correlation of Quadrature Amplitude Fluctuations and Entangled States of the Field

Now we investigate the dynamics of the normalized correlation function of fluctuations of the quadrature amplitudes of the fundamental and second harmonic modes:

$$g(t) = \frac{\langle((x_1(t)-<x_1(t)>)+(x_2(t)-<x_2(t)>))^2\rangle}{(<x_1(t)^2>-<x_1(t)>^2)+(<x_2(t)^2>-<x_2(t)>^2)}. \quad (1.10.1)$$

Here, $x_i = (a_i + a_i^+)/2$, where i = 1,2 are the quadrature amplitudes of the fundamental and second harmonic modes, respectively. One can rewrite formula (1.10.1) as

$$g(t) = 1 + \frac{2(<x_1(t)x_2(t)>-<x_1(t)><x_2(t)>)}{<x_1(t)^2>-<x_1(t)>^2+<x_2(t)^2>-<x_2(t)>^2}. \quad (1.10.2)$$

In the absence of a correlation between the fluctuations of the quadrature amplitudes of the interacting modes, the value of correlation function (1.10.2) tends to unity.

Let us also investigate the dynamics of the normalized correlation function of fluctuations of the $y_j = (a_j - a_j^+)/2i$ quadrature amplitudes of the interacting modes of the field. The formulas for calculating this value are analogous to formulas (1.10.1) and (1.10.2).

To investigate the quantum properties of the optical system, we also calculate the quantum entropy and the photon numbers of the field modes.

The density matrix of the optical system is solved by means of the numerical Monte Carlo wave function method.

Now investigate the system dynamics in the case of equal values of mode damping factors in the resonator ($\gamma_1 = \gamma_2 = \gamma$) in the dimensionless time $\tau = \gamma t$ and dimensionless system parameters $\varepsilon = E/\gamma$ and $k = \chi/\gamma$. All calculations were performed for system evolution from the initial vacuum state of the fundamental and second harmonic modes. To obtain the dynamics of each correlation function of quadrature amplitude fluctuations of the stationary state of the fundamental and second harmonic modes, 1000 independent quantum trajectories of the optical system were used. The calculations were conducted for the parameter value ε = 1.5.

Let us consider the dynamics of the correlation function of quadrature amplitude fluctuations. Figure 1.29a shows the dynamics of the correlation function of fluctuations of the X quadrature amplitudes, whereas Fig. 1.29b represents the dynamics of the correlation function of fluctuations of the Y quadrature amplitudes of the fundamental and second harmonic modes. These functions are given in the k = 0.03 region of very weak coupling between modes. At the beginning of system evolution, both interacting modes are in a vacuum state at τ = 0, and there is no correlation between quadrature amplitude fluctuations. The correlation function is equal to unity. After some evolution period, the system passes over to a stationary state. In the stationary limit, the correlation function of fluctuations of the X quadrature amplitudes is somewhat less than unity, and the correlation function of fluctuations of the Y quadrature amplitudes slightly exceeds unity. In the stationary limit, both correlation functions are very close to unity, due to which no entangled states of the field modes with respect to the variables of the quadrature amplitudes arise in the system. In the stationary limit, the average values of the photon numbers of the interacting modes are $n_1 \approx 9$ and $n_2 \approx 0.07$, respectively, and the

quantum entropies of these modes are nearly equal and very close to zero: $s_1 \approx 0.0006$ and $s_2 \approx 0.0004$. Both modes are in pure states; therefore, in this case, no entanglement of the states of the field modes would arise in the system for any variable.

Figures 1.30a and 1.30b show the correlation functions g_x and g_y of fluctuations of the quadrature amplitudes of interacting modes X and Y, respectively, for the value k = 0.3 of the nonlinear coupling between the modes. In this case, the correlation function g_x is less than unity in the stationary limit, while the correlation function g_y, on the contrary, is more than unity. In the stationary limit, an entanglement of the states of the field modes arises with respect to both variables. Unlike the previous case, the photon numbers of the fundamental and second harmonic modes of the stationary state of the system are of the same order $n_1 \approx 3.5$ and $n_2 \approx 1$, and the quantum entropies of the field modes are nonzero and approximately equal to each other ($s_1 \approx 0.16$ and $s_2 \approx 0.2$).

With a further increase in the nonlinear coupling coefficient between the modes, the correlation of fluctuations of X quadrature amplitudes of the interacting field modes decreases in the stationary limit and, on the contrary, the correlation of fluctuations of Y quadrature amplitudes increases. The dynamics of the correlation functions g_x and g_y for the value k = 0.8 of the nonlinear coupling coefficient is shown in Figs. 1.31a and 1.31b, respectively. The stationary value of the correlation function g_x is nearly equal to unity, which shows that there is no correlation between fluctuations of X quadrature amplitudes in this interaction region. The latter shows that the entanglement of the states of the field modes vanishes with respect to this variable. In this interaction region, the correlation

functiong_y continues to exceed unity in the stationary limit, because of which the states of the field modes stay entangled with respect to the variables of the Y quadrature amplitudes. Similarly to the previous case, the average values of the photon numbers of the modes are of the same order of magnitude ($n_1 \approx 1.8$ and $n_2 \approx 1$), and the values of quantum entropies are equal ($s_1 \approx 0.6$ and $s_2 \approx 0.6$).

With a subsequent increase in the coefficient of nonlinear coupling of the modes, in the stationary limit, the correlation of fluctuations of X quadrature amplitudes increases, whereas the correlation of fluctuations of Y quadrature amplitudes remains almost the same. The dynamics of the correlation functionsg_x and g_y for the value of the nonlinear coupling coefficient k = 3 is shown in Figs. 1.32a and 1.32b, respectively. In the stationary limit of interaction, both correlation functions exceed unity. Due to this, in this interaction region, the entanglement of the states of the field modes is formed with respect to both X and Y variables. In this case, the average values of the number of photons of the interacting modes of the stationary state of the system are $n_1 \approx 0.9$ and $n_2 \approx 0.4$, respectively, and the quantum entropy values of the field modes $s_1 \approx 0.9$ and $s_2 \approx 0.7$ show that the modes are not in pure states.

With a further increase in the nonlinear coupling between the modes, the correlations of fluctuations of both X and Y quadrature amplitudes decrease gradually and vanish. The dynamics of the correlation functions g_x and g_y are given in Figs. 1.33a and 1.33b, respectively, for a very large value of the nonlinear coupling coefficient (k = 30). In this case, in the stationary limit of interaction, the values of both correlation functions are sufficiently close to unity, indicating that there is almost no correlation

between the fluctuations of the quadrature amplitudes of the interacting modes. Hereupon, no entangled states of the field modes with respect to both X and Y variables arise in the system. In this case, in the stationary limit of interaction, the average value of the number of photons of the fundamental mode exceeds considerably that of the second harmonic: $n_1 \approx 0.5$ and $n_2 \approx 0.05$. The stationary value of the entropy of the fundamental mode also exceeds considerably that of the second harmonic mode: $s_1 \approx 0.6$ and$s_2 \approx 0.03$.

References

1. S. T. Gevorkyan and M. S. Gevorkyan, “Fluctuations in the Number of Photons in the Region of Unstable Behavior in the Process of Intracavity Second Harmonic Generation,” *Optics and Spectroscopy* 110, no. 1 (2011): 83–89.
2. S. T. Gevorgyan and M. S. Gevorgyan, “Distribution of Numbers of Photons in the Region of Unstable Behavior in the Process of Intracavity Second Harmonic Generation,” *Journal of Contemporary Physics (Armenian Academy of Sciences)* 46, no. 2 (2011): 47–53.
3. S. T. Gevorkyan and W. H. Maloyan, “Critical Phenomena in Temporal Behavior of Phase in Second Harmonic Generation,” *J. Modern Optics* 44, no. 8 (1997): 1443 –1452.
4. S. T. Gevorgyan and V. A. Maloyan, “Phase Matching in Second Harmonic Generation,” *Proceedings of the National Academy of Sciences of Armenia, Physics* 33, no. 1 (1998): 3–8. [In Russian]
5. S. T. Gevorkyan, “Bifurcation and Coherence Superposition States in Second Harmonic Generation,” *Phys. Rev. A* 62, 013813 (2000).

6. S. T. Gevorgyan, G. Yu. Kruchkyan, and N. T. Muradyan, "Quantum Fluctuations in Unstable Dissipative Systems," *Phys. Rev. A* 61, 043805 (2000).
7. M. S. Gevorgyan, “Correlation of Quadrature Amplitude Fluctuations during the Intracavity Generation of Second Harmonic,” *Journal of Contemporary Physics (Armenian Academy of Sciences)* 52, no. 3 (2017): 189–194.
8. C. W. Gardiner. *Handbook of Stochastic Methods* (Berlin: Springer, 1986).
9. S. M. Yermakov and G. A. Mikhaylov. *Statistical Modeling* (Moscow: Nauka, 1982). [In Russian]
10. A. M. Smith and C. W. Gardiner, *Phys. Rev. A* 38 (1988): 4073.
11. M. Dorfele and A. Schenzle, *Z. Phys. B* 65 (1986): 113.
12. R. Schack, T. A. Brun, and I. C. Percival, *J. Phys.,* A 28 (1995): 1995.
13. P. D. Drummond, K. J. McNeil, and D. F. Walls, *Optica Acta* 27 (1980): 321.
14. L. Gilles, B. M. Garraway, and P. L. Knight, “Generation of Nonclassical Light by Dissipative Two-Photon Processes,” *Phys. Rev.* A 49 (1994): 2785–2799.
15. K. Molmer, Y. Castin, and J. Dalibard, “Monte Carlo Wave-Function Method in Quantum Optics,” *JOSA* B 10 (1993), 524–538.
16. J. R. Johansson, P. D. Nation, and F. Nori, "QuTiP 2: A Python Framework for the Dynamics of Open Quantum Systems," *Comp. Phys. Comm.* 184 (2013): 1234.

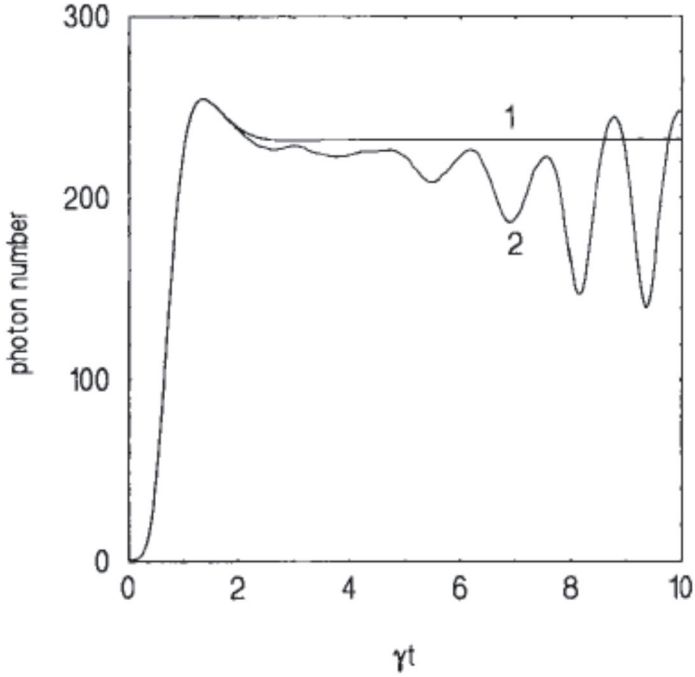

Fig.1.1. Photon number dynamics of the second harmonic mode. Numerical solution of Eqs. (1.1.13) for $\gamma_1 = \gamma_2 = \gamma$, $E/\gamma = 50$, and $\chi/\gamma = 0.1$ and initial conditions $\alpha_i(0) = \beta_i(0) = 1$ $(i = 1,2)$ with a semiclassical approach (curve 1) and for a single trajectory with noise sources in Langevin equations (curve 2).

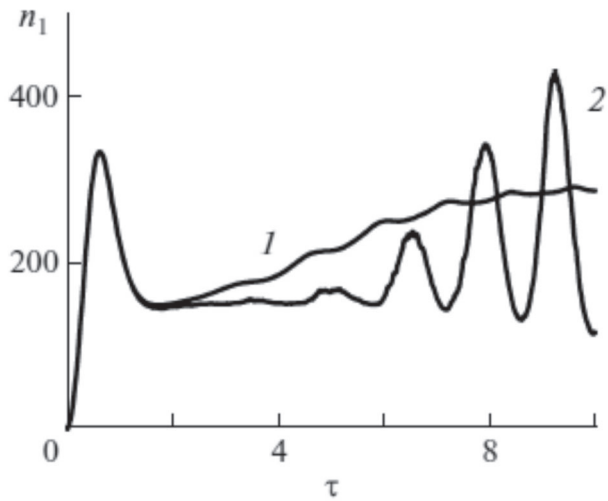

Fig. 1.2. Dynamics of the average value of the number of photons of the fundamental mode in the region of instability of the system (curve 1) in the case when the optical system evolves from an initial state with a normal distribution of stochastic amplitudes of the field modes (1.3.2). To calculate this function, 1000 realizations for the set of equations (1.1.13) were used. Curve 2 corresponds to one realization of the dynamics of the number of photons of the fundamental mode in the case when the evolution of the system begins from an initial state with the values of the stochastic amplitudes of the field modes $\alpha_j(0) = i$ and $\beta_j(0) = -i$ $(j = 1,2)$. Both curves were calculated for the parameter values k = 0.1, r = 1, and ε = 50.

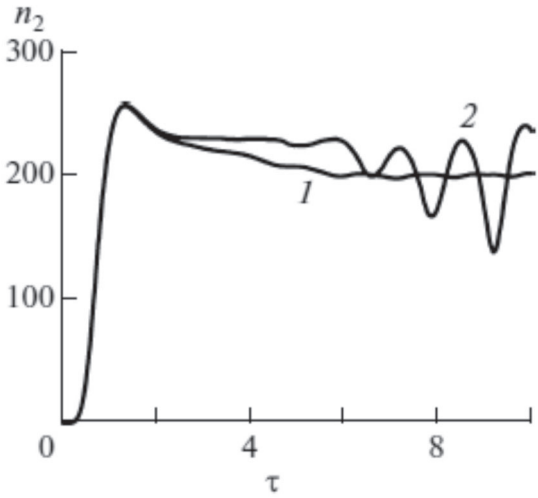

Fig. 1.3. Dynamics of the average value of the number of photons of the second harmonic mode in the instability region of the system (curve 1) in the case of evolution of the system from an initial state with a normal distribution of stochastic amplitudes of the field modes (1.3.2). To calculate this function, 1000 independent realizations of the set of equations (1.1.13) were used. Curve 2 corresponds to one realization of the dynamics of the number of photons of the second harmonic, when system evolution begins from an initial state with the stochastic amplitude values of field modes $\alpha_j(0) = i$ and $\beta_j(0) = -i$ $(j = 1,2)$. Both curves were calculated for the parameter values k = 0.1, r = 1, and ε = 50.

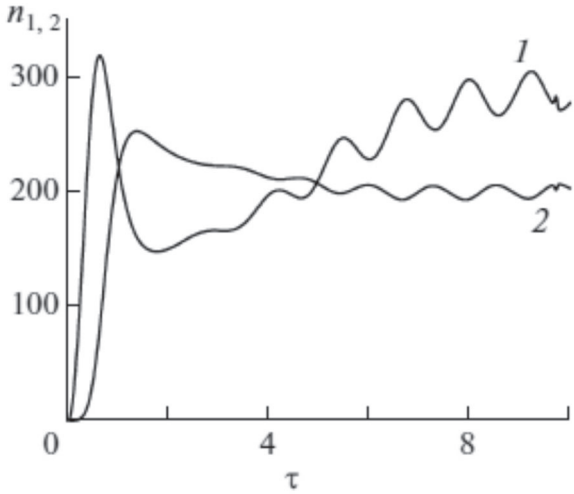

Fig. 1.4. Quantum dynamics of the number of photons of the fundamental mode (1) and second harmonic (2) in the case of system evolution from an initial state with the stochastic amplitude values of field modes $\alpha_j(0) = 1 + i$ and $\beta_j(0) = 1 - i$ $(j = 1,2)$. $k = 0.1$, r = 1, and ε = 50. Both curves were calculated using 20 000 independent realizations for the set of Langevin equations (1.1.13).

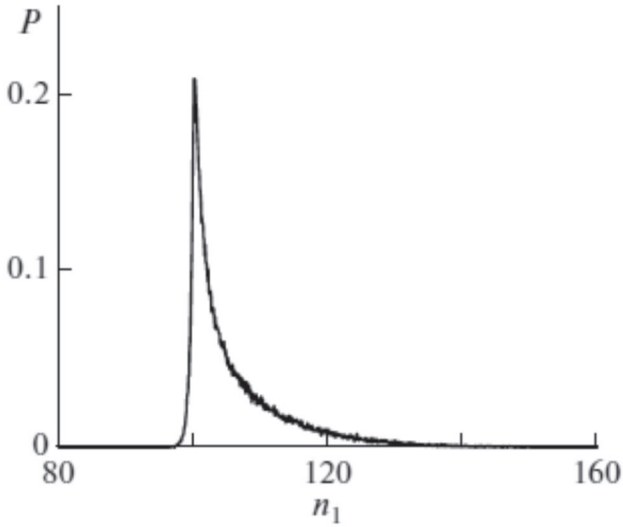

Fig. 1.5. Distribution function of the number of photons of the fundamental mode at a critical point of the system ($\varepsilon = \varepsilon_{cr} = 30$) and in the range of large interaction times (τ = 10), when the system evolution begins from an initial state with a normal distribution of stochastic amplitudes of field modes (1.3.2). k = 0.1 and r = 1. The curve was obtained using 100 000 independent solutions for the set of equations (1.1.13).

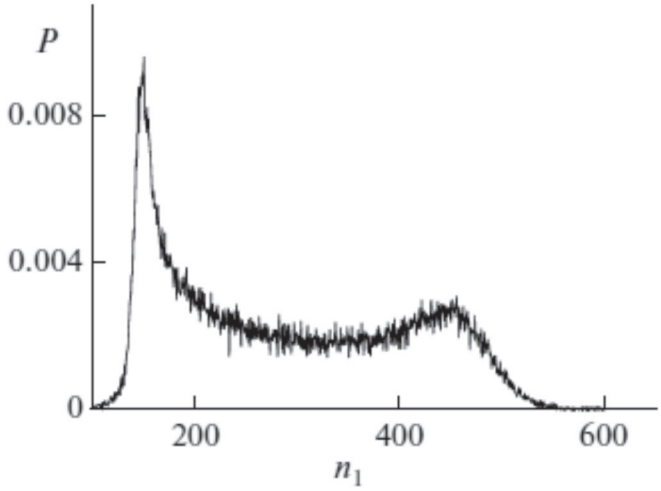

Fig. 1.6. Distribution function for the number of photons of the fundamental mode in the region of instability (ε=50) and the range of large interaction times (τ = 10), when system evolution begins from an initial state with a normal distribution of stochastic amplitudes of field modes. k = 0.1 and r = 1. To calculate the function, 100 000 independent solutions for the set of equations (1.1.13) were used.

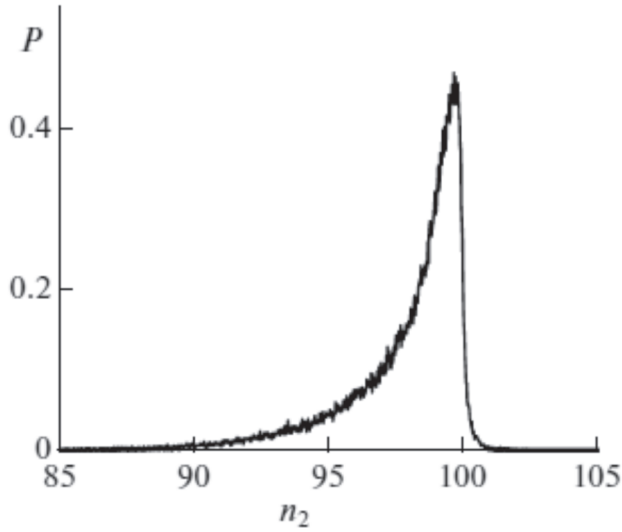

Fig. 1.7. Distribution function of the number of photons of the second harmonic mode at the critical point of the system ($\varepsilon = \varepsilon_{cr} = 30$) and in a range of large interaction times ($\tau = 10$) in the case of system evolution from an initial state with a normal distribution of stochastic amplitudes of field modes (1.3.2). k = 0.1 and r = 1. The curve was calculated using 100 000 independent solutions for the set of Langevin equations (1.1.13).

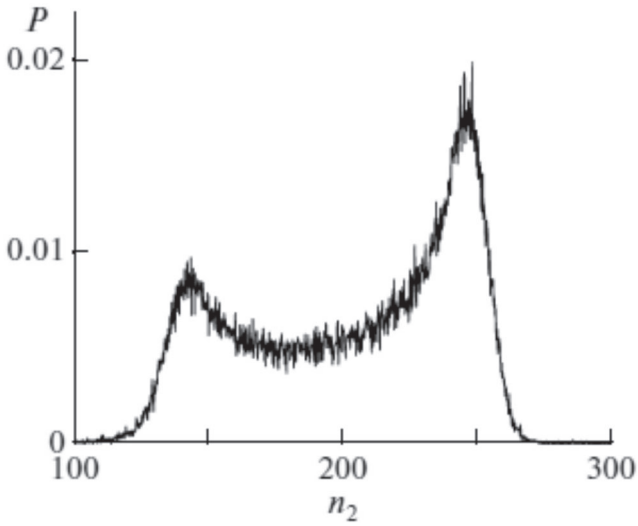

Fig. 1.8. Distribution function of the number of photons of the second harmonic above the bifurcation point of the optical system ($\varepsilon = 50$) and in the range of large interaction times ($\tau = 10$) in the case of system evolution from an initial state with a normal distribution of stochastic amplitudes of interacting modes (1.3.2). $k = 0.1$ and $r = 1$. The curve was calculated using 100 000 independent realizations for the set of Langevin equations (1.1.13).

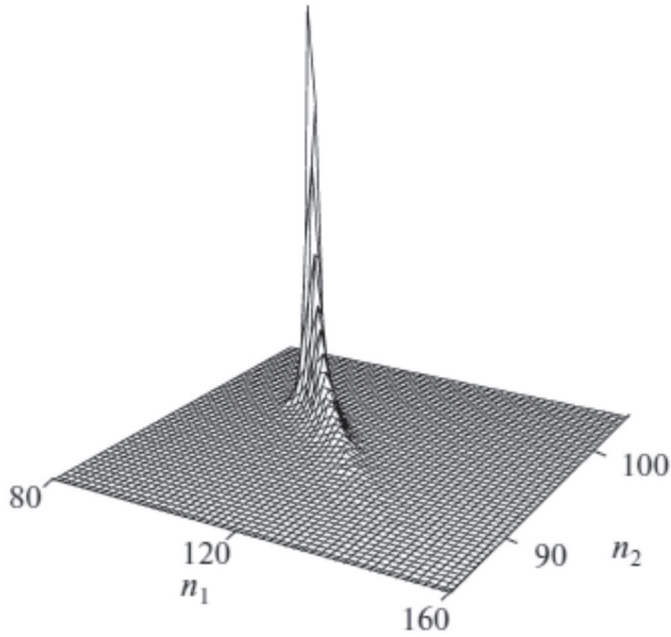

Fig. 1.9. Function of joint distribution of the number of photons of the fundamental mode and of the second harmonic at the critical point of the system ($\varepsilon = \varepsilon_{cr} = 30$) and in the range of large interaction times (τ = 10), when the evolution of the system begins from an initial state with a normal distribution of stochastic amplitudes of field modes (1.3.2). k = 0.1 and r = 1. To calculate the function, 50 000 independent realizations of the set of Langevin equations (1.1.13) were used.

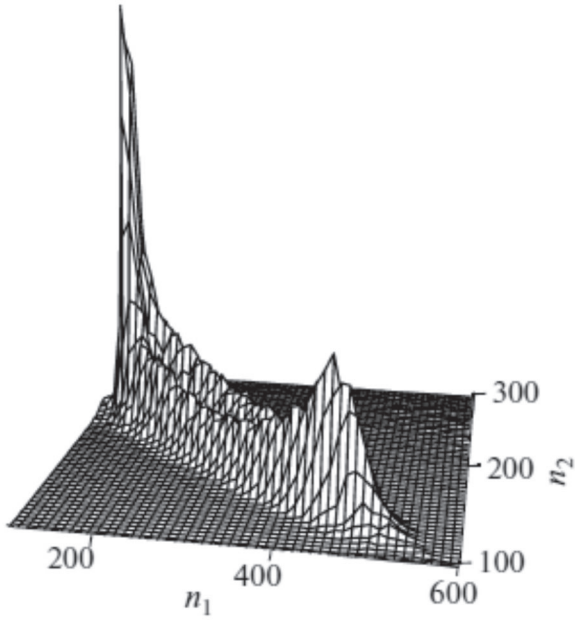

Fig. 1.10. Joint distribution function of the number of photons of the fundamental and second harmonic modes in the region of instability of the system ($\varepsilon = 50$) and in the range of large interaction times ($\tau = 10$) in the case of evolution of the system from an initial state with a normal distribution of stochastic amplitudes of field modes (1.3.2). $k = 0.1$ and $r = 1$. The function was calculated using 50 000 independent realizations for the set of equations (1.1.13).

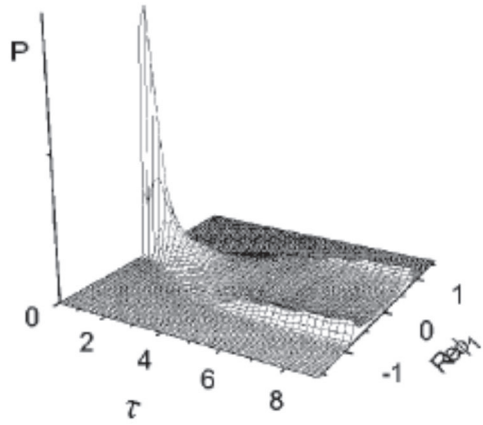

Fig. 1.11. Dynamics of the phase distribution function for the fundamental mode in the case of the initial coherent states of both $\alpha_j(0) = \sqrt{2}$ and $\beta_j(0) = \alpha_j(0)^*$ modes ($j = 1,2$) and for the following parameter values: $\varepsilon = 50$, $k = 0.1$, and $r = 1$. The function is computed by means of 100 000 independent trajectories of Eqs. (1.1.13).

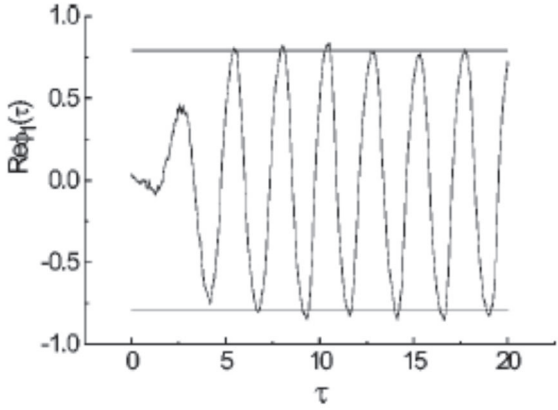

Fig. 1.12. Realization of the phase for the fundamental mode in the case of the initial coherent states of both $\alpha_j(0) = \sqrt{2}$ and $\beta_j(0) = \alpha_j(0)^*$ modes ($j = 1,2$) and for the following parameter values: $\varepsilon = 50$, $k = 0.1$, and $r = 1$. The dashed lines lead to the two most probable values of the phase.

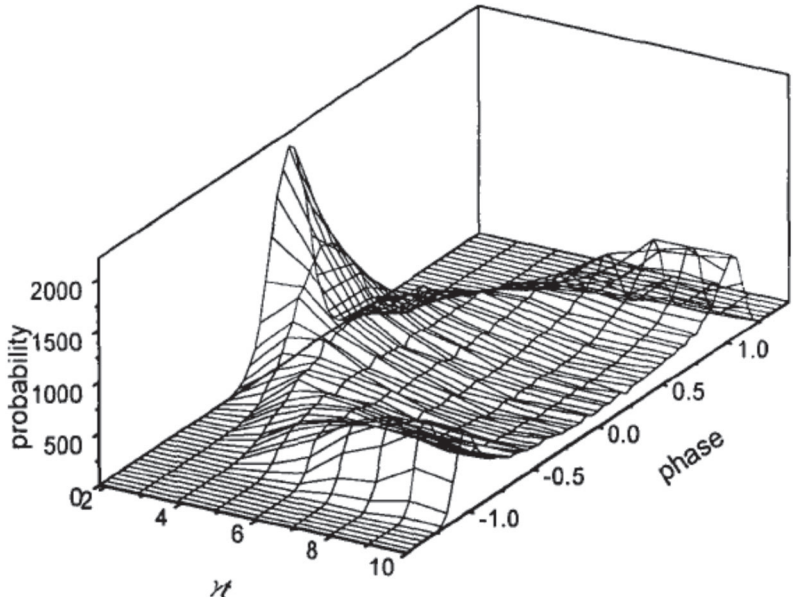

Fig. 1.13. Distribution function dynamics of a stochastic phase for the second harmonic mode obtained after 50 000 trials under Gaussian conditions (1.3.2). $\varepsilon = 50$, $k = 0.1$, and $r = 1$.

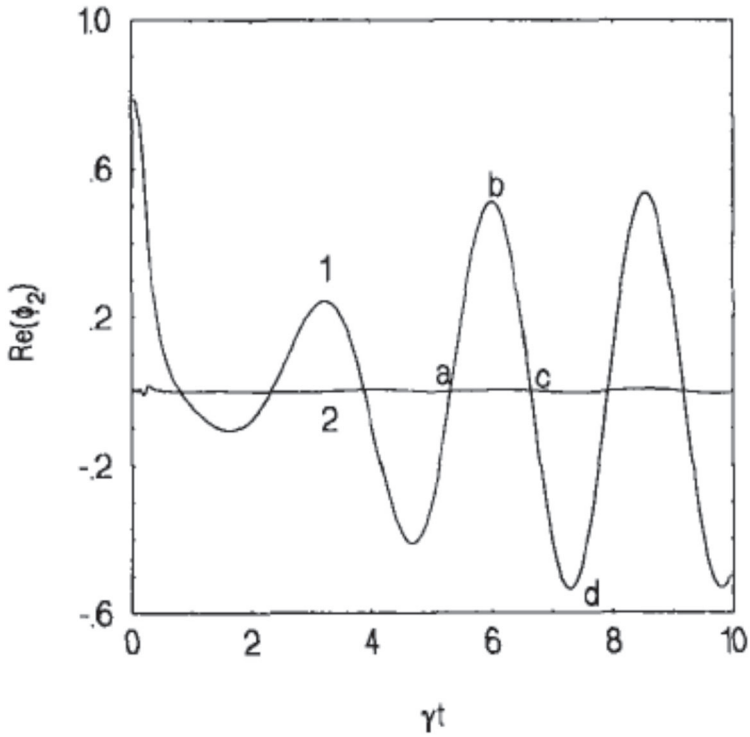

Fig. 1.14. Quantum dynamics of the real part of the phase of the second harmonic mode with initial coherent (curve 1) and Gaussian (curve 2) distributions of the amplitudes $\alpha_j(0)$ and $\beta_j(0)$ $(j = 1,2)$, averaged over 5000 trials. $\varepsilon = 50$, $k = 0.1$, and $r = 1$.

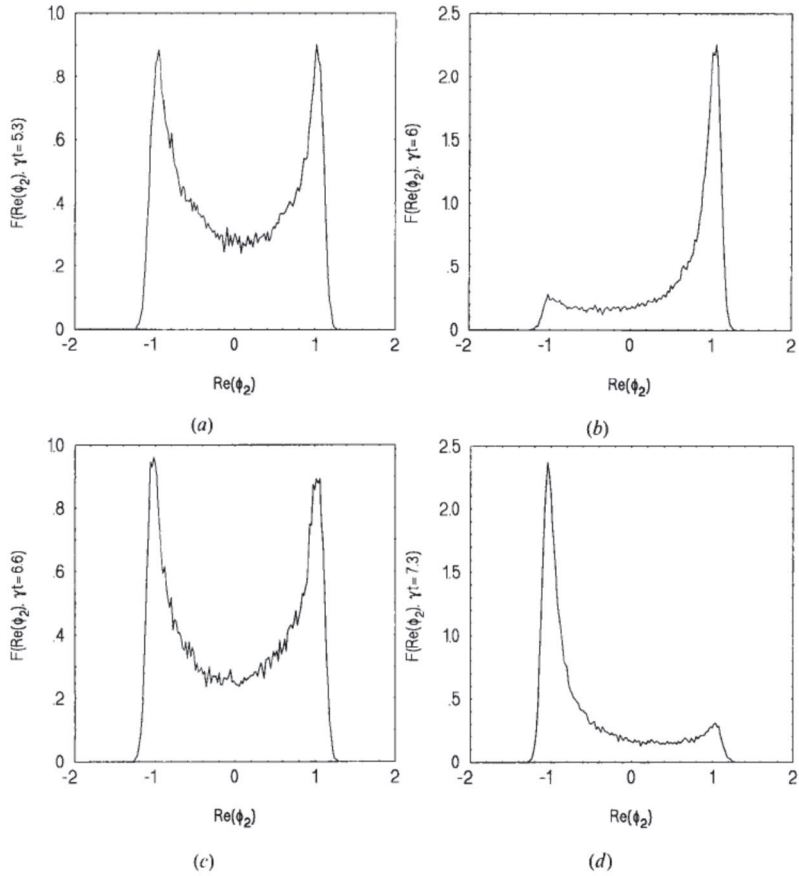

Fig. 1.15. Four pictures that represent the second harmonic phase distribution function with the coherent initial conditions $\alpha_1(0) = 1 + i$,$\beta_1(0) = 1 - i$ and $\alpha_2(0) = 1 - i$, $\beta_2(0) = 1 + i$ for different fixed moments in time that correspond to points a-d marked in Fig. 1.1.14 (50 000 trials). $\varepsilon = 50$, $k = 0.1$, and $r = 1$.

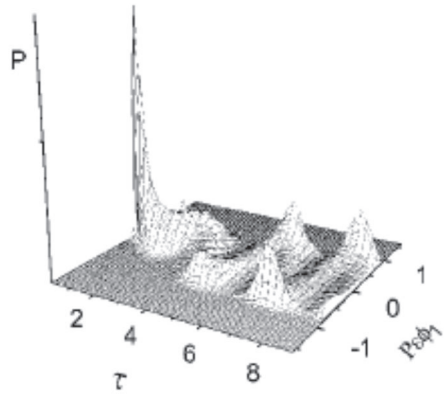

Fig. 1.16. Dynamics of the phase distribution function of the fundamental mode in the case of initial coherent states of both modes $\alpha_j(0) = i\sqrt{2}$ and $\beta_j(0) = \alpha_j(0)^*$ $(j = 1,2)$ and for the following parameter values: $\varepsilon = 50$, $k = 0.1$, and $r = 1$. The function was calculated based on 100 000 independent trajectories of Eqs. 1.1.13.

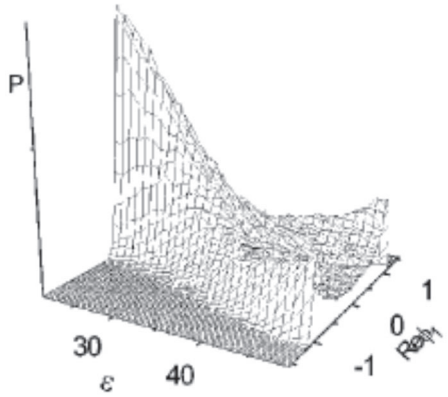

Fig. 1.17. Dependence of the phase distribution function of the fundamental mode with the initial coherent distribution of amplitudes $\alpha_j(0) = \sqrt{2}$ and $\beta_j(0) = \alpha_j(0)^*$ $(j = 1,2)$ on ε $(k = 0.1,\ r = 1)$ at the moment $\tau = 9$ (stationary limit). Calculated based on 100 000 trajectories of Eqs. (1.1.13).

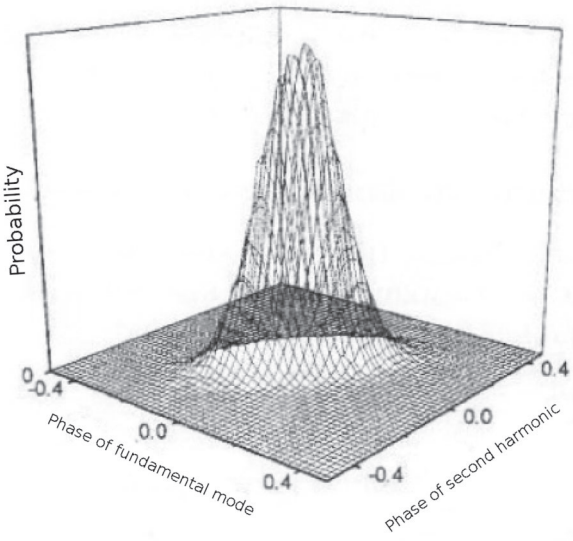

Fig 1.18. Joint phase distribution function of the fundamental mode and second harmonic with initial vacuum states of both modes; $\alpha_j(0) = \beta_j(0) = 0$ $(j = 1,2)$ at the moment $\tau = 10$, $\varepsilon = 10$, $k = 0.1$, and $r = 1$. Calculated based on 100 000 trajectories of Eqs. (1.1.13).

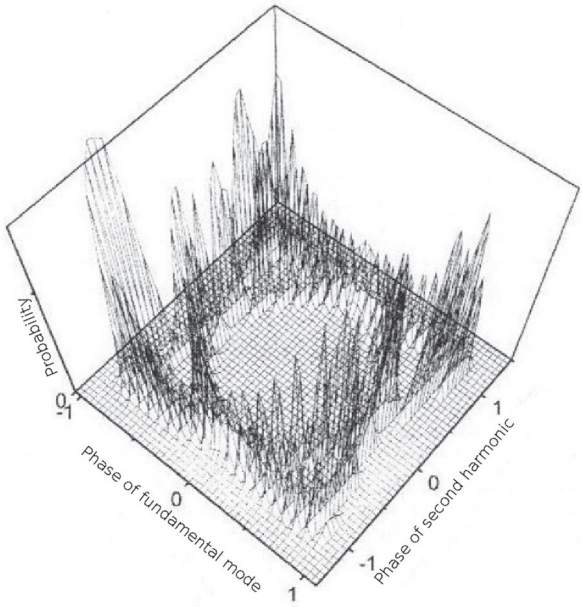

Fig. 1.19. Joint phase distribution function of the fundamental mode and second harmonic with initial vacuum states of both modes at the moment $\tau = 10$; $\varepsilon = 50$, $k = 0.1$, and $r = 1$. Calculated based on 100 000 trajectories of Eqs. (1.1.13).

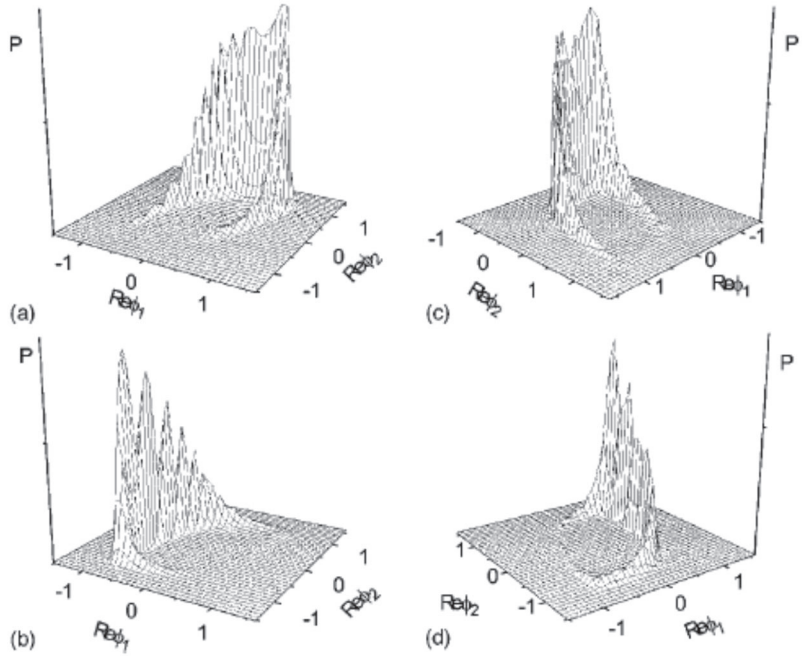

Fig. 1.20. Joint distribution function of the fundamental and second harmonic phases in the case of the initial coherent states of both modes $\alpha_j(0) = i\sqrt{2}$ and $\beta_j(0) = \alpha_j(0)^*$, $(j = 1,2)$ at the moments $\tau = 5.96$ (a), $\tau = 6.63$ (b), $\tau = 7.25$ (c), and $\tau = 7.88$ (d). Computed by means of 100 000 trajectories of Eqs. (1.1.3). $\varepsilon = 50$, $k = 0.1$, and $r = 1$.

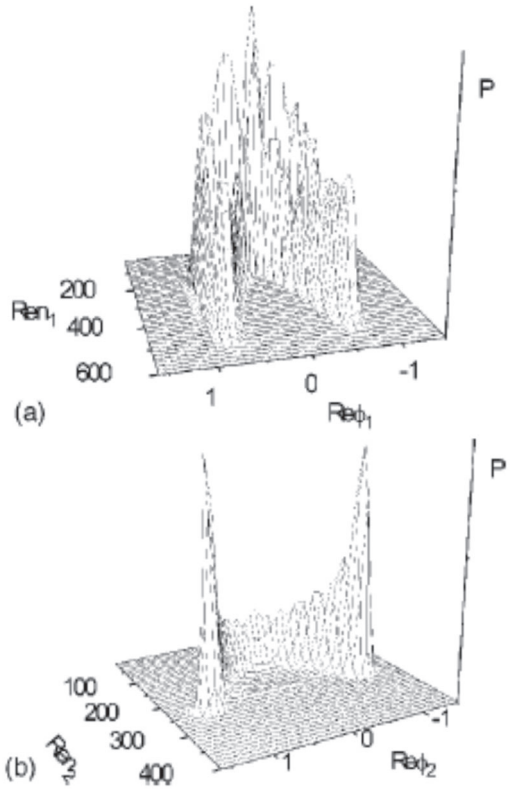

Fig. 1.21. Joint distribution function of photon numbers and phases of the fundamental (a) and second harmonic (b) modes at the moment $\tau = 9$. Calculated based on 100 000 trajectories of Eqs. (1.1.13). $\varepsilon = 50$, $k = 0.1$, and $r = 1$. $\alpha_j(0) = \sqrt{2}$ and $\beta_j(0) = \alpha_j(0)^*$ $(j = 1,2)$.

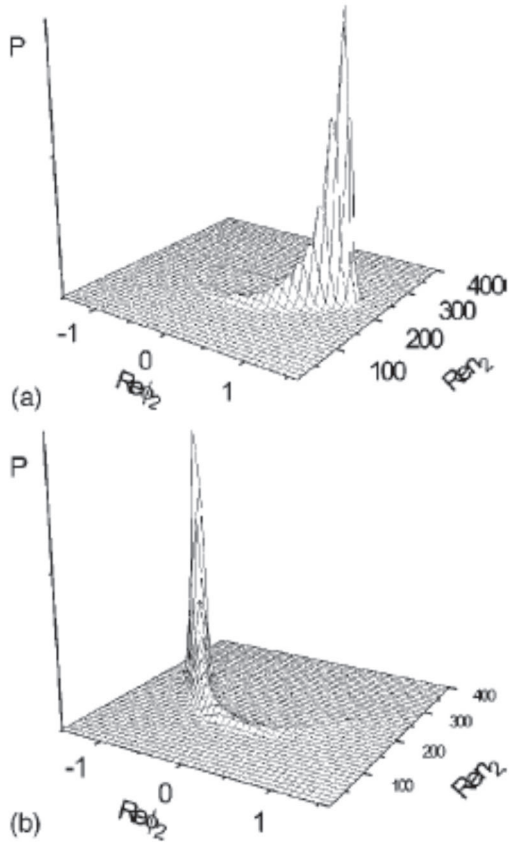

Fig. 1.22. Joint distribution function of the numbers of photons and phases for the second harmonic at the moments $\tau = 5.96$ (a) and $\tau = 7.25$ (b). Calculated based on 50 000 trajectories of Eqs. (1.1.13). The parameter values are as in Fig. 1.21. $\alpha_j(0) = i\sqrt{2}$ and $\beta_j(0) = \alpha_j(0)^*$ $(j = 1,2)$.

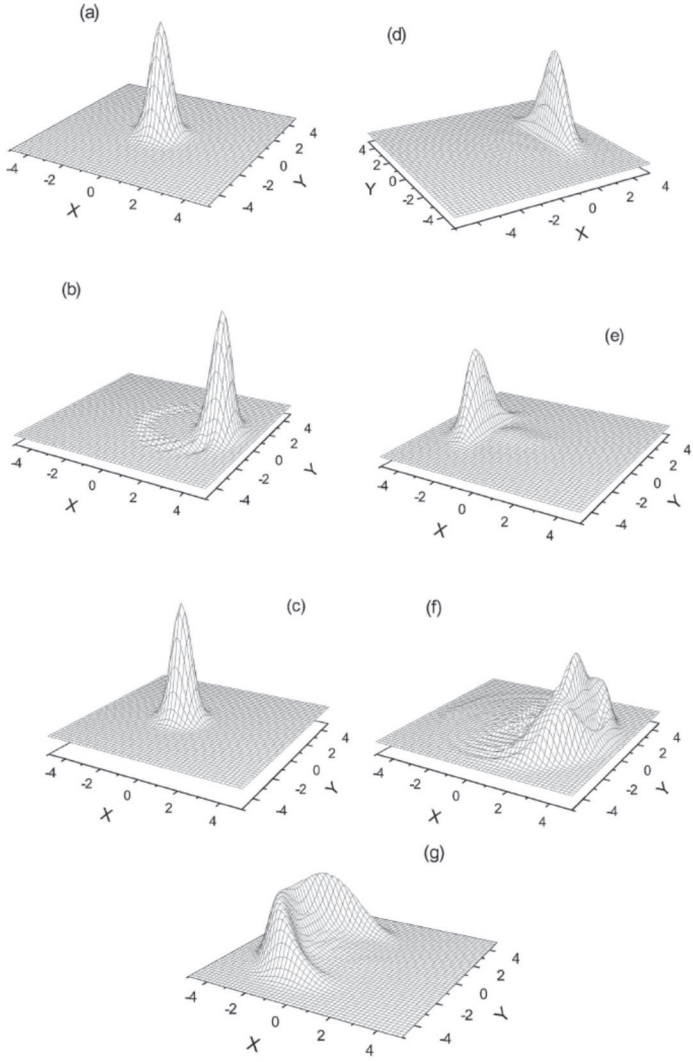

Fig. 1.23. Wigner functions at $\tau = 0$ are the same for both modes (a); $\tau = 0.7$of the fundamental mode (b) and second harmonic mode (c); $\tau = 1.67$ of the fundamental mode (d) and the second harmonic mode (e); and $\tau = 8.9$ of the fundamental mode (f), the second harmonic mode (g), and for $\varepsilon = 6$ and $k = 0.3$, averaged over 1000 realizations.

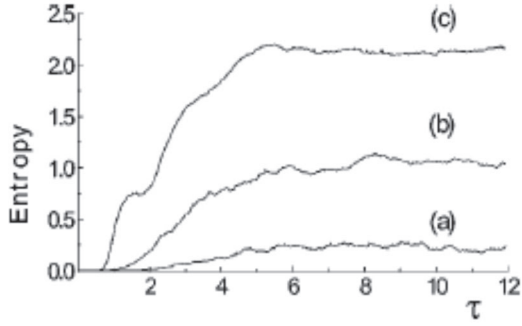

Fig. 1.24. Time evolution of the entropy of the fundamental mode, initially prepared in a vacuum state for $\varepsilon = 1$ (a) over 150 realizations; for $\varepsilon = 3$ (b), over 150 realizations; and for $\varepsilon = 6$ (c), over 1000 realizations. $k = 0.3$ ($\tau = \gamma_1 t$).

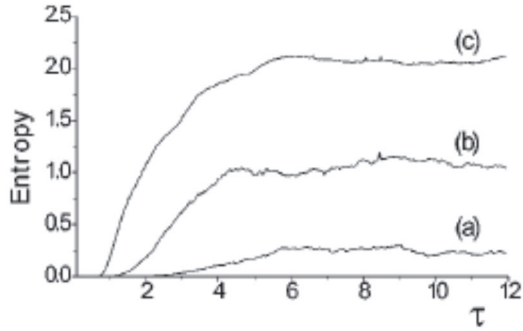

Fig. 1.25. Time evolution of the entropy of the second harmonic mode, which was initially prepared in a vacuum state for $\varepsilon = 1$ (a) over 150 realizations; for $\varepsilon = 3$ (b), over 150 realizations; and for $\varepsilon = 6$ (c), over 1000 realizations.

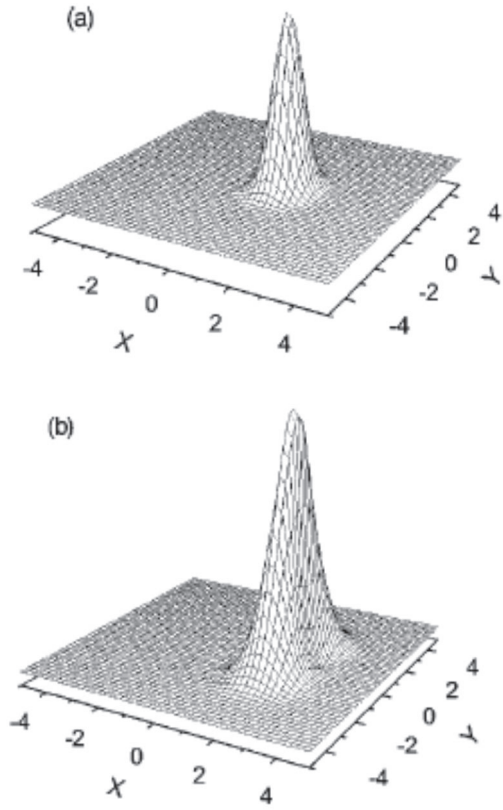

Fig. 1.26. Wigner functions of the fundamental mode, initially prepared in a vacuum state for $\varepsilon = 1$ (a) and $\varepsilon = 3$ (b) ($\tau = 8$), averaged over 150 realizations ($k = 0.3$).

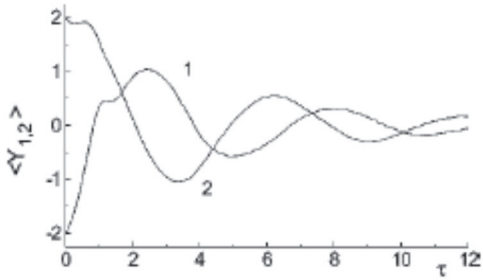

Fig. 1.27. Time evolution of the quadrature components $\langle Y_1 \rangle$ (curve 1) and $\langle Y_2 \rangle$ (curve 2) for the initial coherent states of the modes and the parameters $\varepsilon = 6,\ k = 0.3$, ensemble-averaged over 1000 realizations.

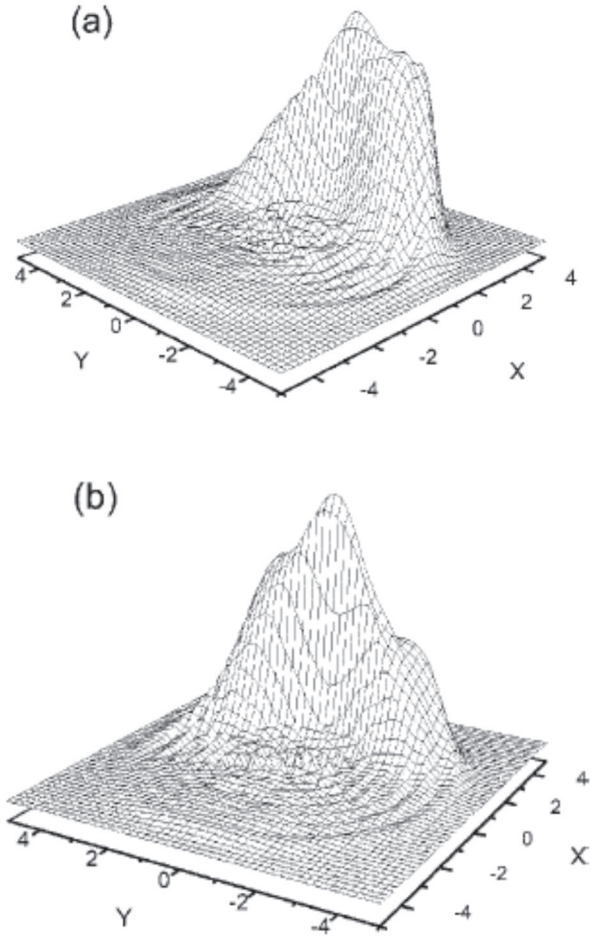

Fig. 1.28. Wigner functions of the fundamental mode, which was initially prepared in a coherent state at $\tau = 4.9$ (a) and $\tau = 8.2$ (b) and $\varepsilon = 6,\ k = 0.3$, ensemble-averaged over 1000 realizations.

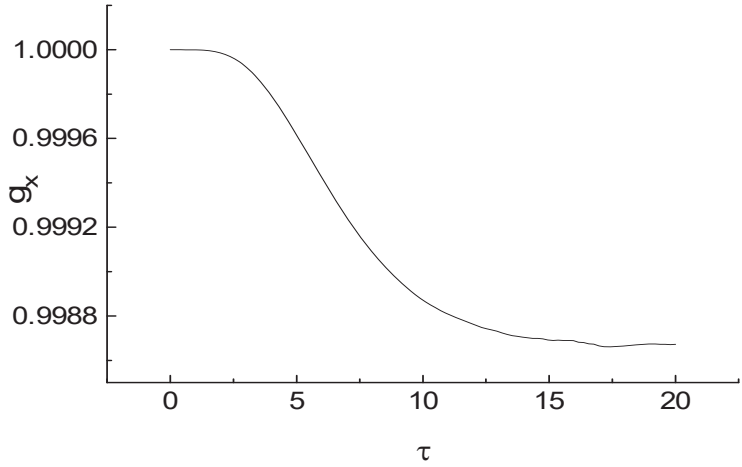

Fig. 1.29a

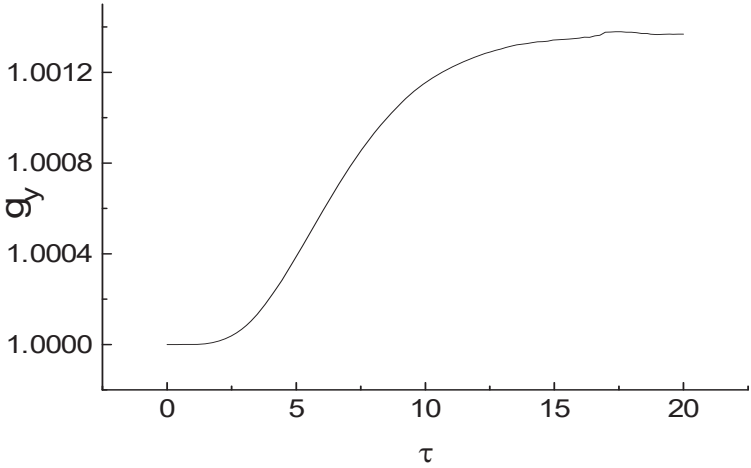

Fig. 1.29b

Fig. 1.29. Dynamics of the correlation function of fluctuations of the (a) x and (b) y quadrature amplitudes of interacting modes in the case of very weak coupling between the modes k = 0.03.

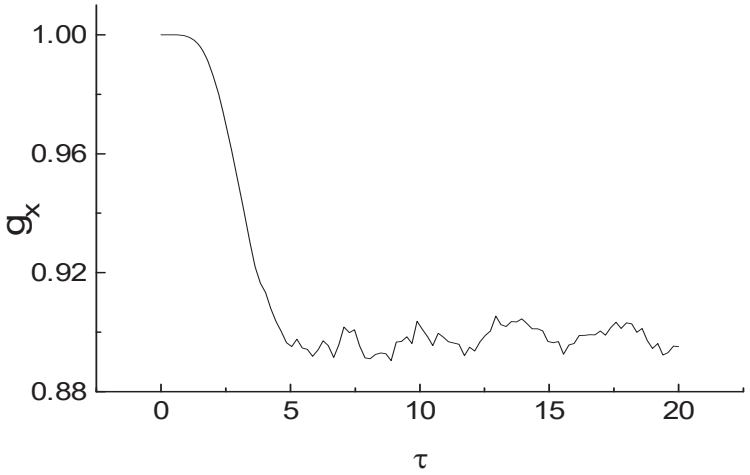

Fig. 1.30 a

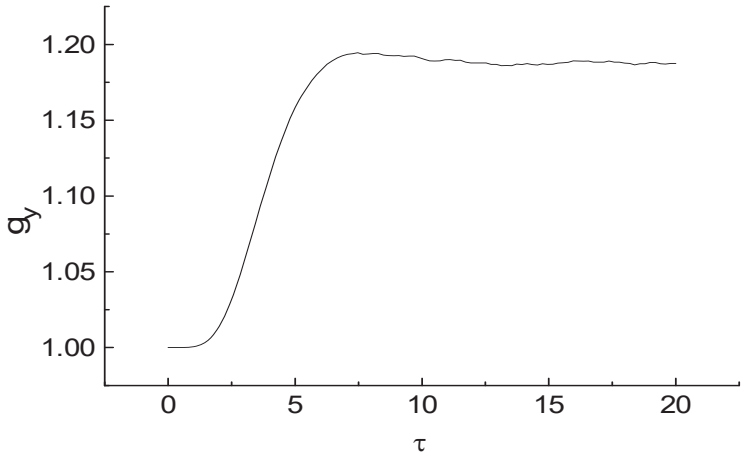

Fig. 1.30 b

Fig. 1.30. Dynamics of the correlation function of fluctuations of the (a) x and (b) y quadrature amplitudes of interacting modes for the k = 0.3 value of the system parameter.

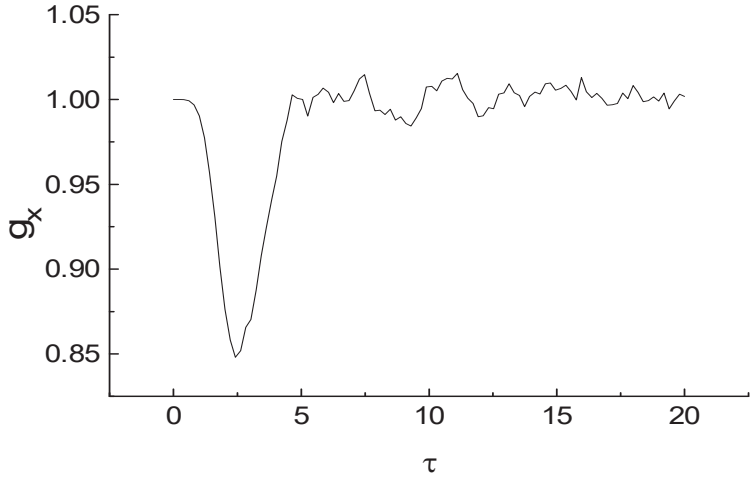

Fig. 1.31a

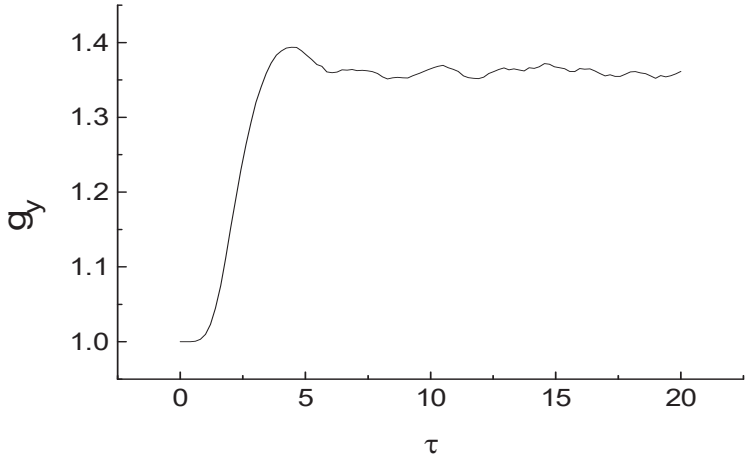

Fig. 1.31b

Fig. 1.31. Dynamics of the correlation function of fluctuations of the (a) x and (b) y quadrature amplitudes of interacting modes for the k = 0.8 value of the system parameter.

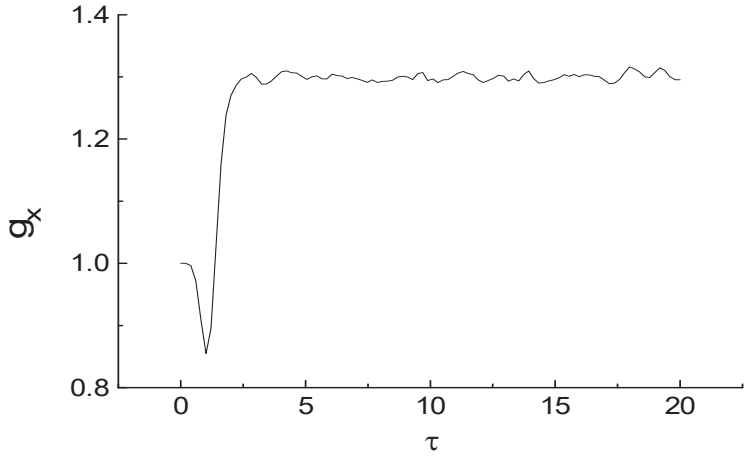

Fig. 1.32a

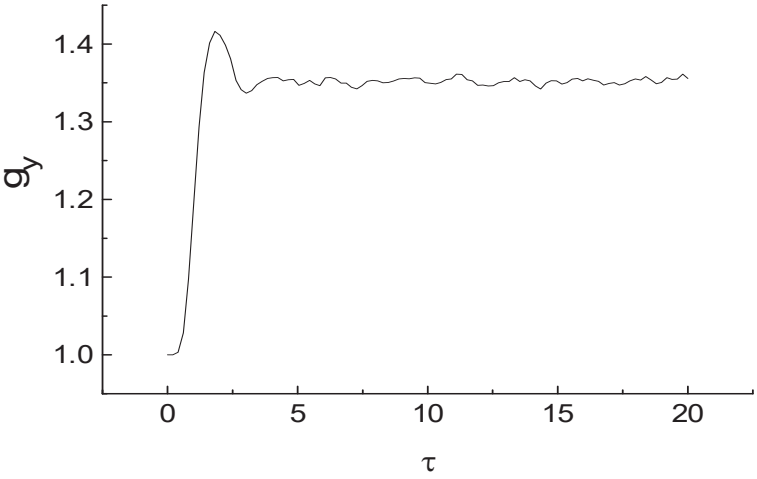

Fig. 1.32b

Fig. 1.32. Dynamics of the correlation function of fluctuations of the (a) x and (b) y quadrature amplitudes of interacting modes in the case of strong coupling between the modes (k = 3).

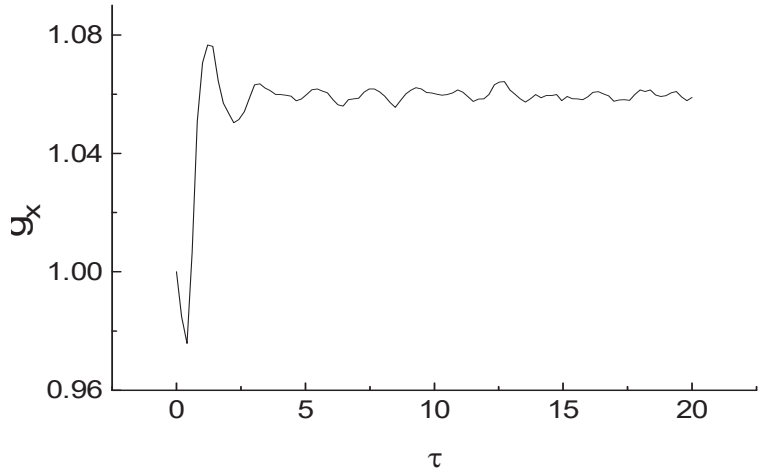

Fig. 1.33a

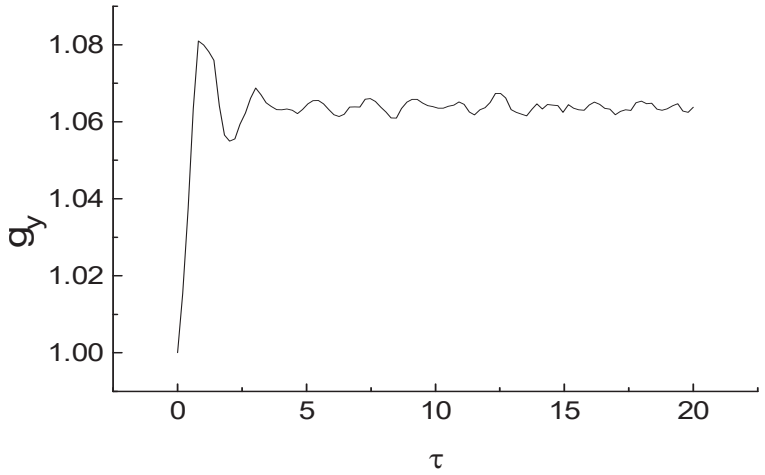

Fig. 1.33b

Fig. 1.33 Dynamics of the correlation function of fluctuations of the (a) x and (b) y quadrature amplitudes of interacting modes in the case of very strong coupling between the modes (k = 30).

CHAPTER 2

QUANTUM THEORY OF UNSTABLE BEHAVIOUR OF INTRACAVITY THIRD HARMONIC GENERATION PROCESS

Introduction

All materials in this chapter are taken from works [1–10].

This chapter presents a quantum theory of intracavity third harmonic generation. Third-order noise is considered, and corresponding Langevin equations are obtained for the motion of stochastic amplitudes of the interacting modes [1]. Variable transformation formulas, which include contributions of third-order noise, are obtained (generalized Ito formulas). Semiclassical solutions for the stationary state are found. A linear analysis of stability is performed. Above the bifurcation point of the optical system, in the unstable region, an auto-oscillation temporal behaviour of the fundamental and third harmonic modes is found. The influence of third-order noise on higher order moments of operators of the field is also discussed.

Section 2.4 presents a system of Langevin equations in the P-representation in a differential form [3,5]. We suppose that third-order noise has very little effect on the dynamics of the system in the region of large interaction times; therefore, third-order noise is reduced from the

Langevin system of equations, and the latter is solved by applying the Euler method.

Further, in Section 2.5, in the unstable region of the optical system, the dynamics of one realization of the number of photons of the fundamental and third harmonic modes is investigated. It is shown that both quantities are in an auto-oscillation mode in the unstable region [2]. In this section, the dynamics of the average number of photons of the interacting modes is also investigated in the unstable region and in the case of evolution of the system from an initial state, which has a Gaussian distribution of the stochastic amplitudes of the field modes. In the latter case, it is shown that the average values of the number of photons do not have self-oscillations. In this section, the dynamics of the average values of the number of photons of the field modes is also investigated in the unstable region and in the case of evolution from initial coherent states of the modes. It is shown that, in the latter case, the average values of the photon numbers are in a self-oscillation mode.

In Section 2.6, the distribution functions of the number of photons of the fundamental and third harmonic modes are investigated near the bifurcation point of the system and in the unstable region in the case of evolution of both modes from initial states, which have a Gaussian distribution of stochastic amplitudes. It is shown that these distribution functions have a single-peak asymmetric structure near the critical point, whereas they have a two-peak structure in the unstable region. Each of these peaks of the distribution functions represents a state of the mode in which it spends most of the time. A joint distribution function of the photon numbers of the interacting modes is also investigated. This

function also has a single-peak asymmetric structure near the critical point and a two-peak structure in the unstable region.

In Section 2.7, quantum fluctuations of the phases of the fundamental and third-harmonic modes [3], as well as the joint fluctuations of the phases of these modes [3, 4], are investigated. The dynamics of the distribution functions of the phases of the fundamental and third harmonic modes is investigated in the instability region of the system and in the case of evolution of the system from initial states with a Gaussian distribution of the stochastic amplitudes of both modes. It is shown that, in the region of large evolution times, both functions have a stationary two-component structure. The dynamics of the distribution functions of phases of the field modes is investigated in the case of system evolution from initial coherent states with a nonzero phase of the stochastic amplitudes of the interacting modes [3]. It is shown that, in this case, the phase distribution functions of both modes change into an auto-oscillation mode in the instability region and in the region of large times. In this section, the dynamics of the joint distribution function of phases of the fundamental and third harmonic modes is also investigated. It is shown that, in the case of evolution of the system from an initial state with a Gaussian distribution of stochastic phases of both modes, the joint distribution function of phases changes into a stationary mode in the region of large interaction times. Some domain of events, which surround the point corresponding to the classical phase matching of the system, has a zero probability of realization [3, 4]. The latter shows that the classical phase matching has a zero probability of realization in the unstable region. When the optical system transitions from the unstable to the stable region, a peak is gradually formed near the point corresponding to the classical phase matching, which is in

accordance with the classical phase matching of the interacting modes. In the case of evolution of the system from initial coherent states with a nonzero phase of the stochastic amplitudes of both modes, the joint distribution function of the phases of the field modes changes into an auto-oscillation mode in the unstable region and in the region of large interaction times [3].

In Section 2.8, the dynamics of the joint distribution function of the phase and the photon number is investigated for both the fundamental and third harmonic modes. It is shown that in the case of evolution of the system from an initial state with a Gaussian distribution of the stochastic amplitudes of the field modes, the distribution functions are symmetric around the zero phase (the phase of the fundamental mode perturbation field) and have a two-component structure [3, 4, 5] in the unstable region and in the region of large interaction times. Each component of these functions represents a component of the state of field mode in which it spends most of the time. In the case of evolution of the system from initial coherent states of both modes, which have nonzero phases of stochastic amplitudes relative to the phase of the perturbation field, the functions of the joint distribution of the number of photons and phases of the interacting modes switch to an auto-oscillation mode [3]. Further, the dynamics of the number of photons, quantum entropy, and the Wigner function of the field modes is numerically investigated applying the Monte Carlo wave function method [6, 7, 8].

In Section 2.9, the quantum dynamics of the system is investigated in the case of evolution of the field modes from initial vacuum states. With the help of an investigation into the dynamics of the Wigner functions, it is shown that, in the case of a strong coupling between the modes and a

strong external perturbation of the fundamental mode, the fundamental mode from an initial vacuum state localizes in a pure coherent state with zero quantum entropy in the region of short evolution times. From the coherent state, the mode localizes gradually into a squeezed state, the quantum entropy of which is greater than zero. With the increase in the quantum entropy, the squeezed state begins to decay gradually, and the system changes gradually from a stable to an unstable state. Further, the quantum entropy of the fundamental mode changes to a stationary value. The Wigner function of the stationary state of the fundamental mode has a two-component structure [6, 7, 8]. The dynamics of the state of the third harmonic mode is similar to the dynamics of the state of the fundamental mode: the mode of the third harmonic first localizes in a coherent state; then, in a squeezed state, from which it changes into an unstable stationary state. The Wigner function of the unstable state has a cylindrical shape and represents the state of the third harmonic mode; hence, it represents a state, which has a completely undefined phase. The system is in an unstable state with an undefined phase. The quantum dynamics of the system is also investigated in the case of a weak perturbation of the fundamental mode and strong nonlinear coupling between them. In this case, in the region of large evolution times, the fundamental mode localizes in a squeezed stationary state, and the third harmonic mode localizes in a state, which has a Wigner function similar to the Wigner function of a coherent state; however, the state has nonzero quantum entropy. Wigner functions of the states of the system in the region of large interaction times show that, in this case, the system is in a stable state. In this section, the dynamics of the system is also investigated in the case of a strong external perturbation of the fundamental mode and weak coupling between the interacting modes. In the latter case, in the region of large interaction

times, both modes localize in stationary unstable states, the Wigner function of which have a two-component structure with a connection between the components of the states.

In Section 2.10, the quantum dynamics of the system is investigated in the case of the system evolution from initial coherent states of the field modes [9]. It is shown that, in the unstable region, in the case of evolution of the system from initial coherent states of interacting modes and in the case when the amplitude of the state of at least one mode has an imaginary part, the quadrature amplitudes and Wigner functions of the field modes oscillate. In the region of large interaction times, the oscillation amplitude gradually tends to zero. Oscillations of the above values disappear when the system changes into the stable region [9]. The correlation between fluctuations of the quadrature amplitudes of the interacting modes is studied for the process of intracavity third harmonic generation in the instability region [10]. It is shown that this correlation strongly depends on the value of the nonlinear mode coupling coefficient. For small values of the coupling coefficient, the correlation between fluctuations of the quadrature amplitudes is small. With an increase in the coupling coefficient, the correlation increases (states of the subsystems become entangled). Then, starting from a certain value of the coupling coefficient, it begins a gradual decrease and tends to zero (the entanglement of the states of the subsystems decreases). The correlation between fluctuations of the quadrature amplitudes also decreases when the amplitude of the fundamental mode perturbing field is decreased.

2.1 Basic Equations and Third-Order Noise

Consider a model of third harmonic generation inside a two-mode cavity. A nonlinear medium is placed inside a cavity tuned to the frequencies of the fundamental mode ω_1 and of the third harmonic ω_2, where $\omega_2 = 3\omega_1$. The fundamental mode is resonantly perturbed by an external classical field. The density matrix equation, which describes this optical system, can be written in the following form:

$$\frac{\partial \rho}{\partial t} = (i\hbar)^{-1}\left[H_{sys}, \rho\right] + L(\rho), \tag{2.1.1}$$

where

$$H_{sys} = \frac{i\hbar\chi}{2}(a_1^{+3}a_2 - a_1^3 a_2^+) + i\hbar(E a_1^+ - E * a_1), \tag{2.1.2}$$

$$L(\rho) = \sum_{i=1}^{2} \frac{\gamma_i}{2}(2a_i \rho a_i^+ - \rho a_i^+ a_i - a_i^+ a_i \rho). \tag{2.1.3}$$

Here, a_i and a_i^+ $(i = 1,2)$ are the annihilation and creation operators of photons of the fundamental and the third harmonic modes, respectively; χ is the coupling coefficient of the modes, which is proportional to the nonlinear susceptibility $\chi^{(3)}$ of the medium; E is the classical amplitude of the perturbing field at the frequency ω_1; and γ_i $(i = 1,2)$ are the damping coefficients of the interacting modes.

This equation is then transformed into a Fokker Planck equation for the quasi-probability distribution function $P(x)$ in the generalized P-representation [11], which we write in the general form by introducing a four-component variable: $x \equiv (x_1, x_2, x_3, x_4) \equiv (\alpha_1, \beta_1, \alpha_2, \beta_2)$

$$\frac{\partial P(x)}{\partial t} = \left(-\sum_i \frac{\partial}{\partial x_i} A_i(x) + \frac{1}{2}\sum_{i,j} \frac{\partial^2}{\partial x_i \partial x_j} D_{ij}(x) - \right.$$
$$\left. \frac{1}{6}\sum_{ijk} \frac{\partial^3}{\partial x_i \partial x_j \partial x_k} C_{ijk}(x)\right) P(x). \qquad (2.1.4)$$

The α_1, β_1, α_2, and β_2 quantities are independent complex variables corresponding to the a_1, a_1^+, a_2, and a_2^+ operators, respectively. The elements of the drift vector are equal to

$$A_1 = E - \gamma_1 \alpha_1 - 3\chi \beta_1^2 \alpha_2,$$

$$A_2 = E^* - \gamma_1 \beta_1 - 3\chi \alpha_1^2 \beta_2.$$

$$A_3 = -\gamma_2 \alpha_2 + \chi \alpha_1^3,$$

$$A_4 = -\gamma_2 \beta_2 + \chi \beta_1^3. \qquad (2.1.5)$$

The nonvanishing noise terms are

$$D_{11} = -6\chi \beta_1 \alpha_2,$$

$$D_{22} = -6\chi \alpha_1 \beta_2, \qquad (2.1.6)$$

$$C_{111} = -6\chi \alpha_2,$$

$$C_{222} = -6\chi \beta_2. \qquad (2.1.7)$$

Equation (2.1.4) has a complicated form due to the third order derivatives. We can obtain stochastic equations of motion, which are equivalent to Eq. (2.1.4), by following the Ito method (see, for example, [11]). When applied to Eq. (2.1.4), this method is not so simple and well-known as in the case of diffusion equations without the tensor C_{ijk}, and it leads naturally to the concept of third order noise sources. For the one-dimensional problem, a stochastic equation approach, containing third-

order noise, has been developed by Gardier [11]. For a general multi-dimensional case of Eq. (2.1.4), it can be shown that the system of equivalent stochastic equations for x_i variables has the following form:

$$\frac{\partial x_i}{\partial t} = A_i(x) + \sum_j B_{ij}(x)\xi_j(t) + \sum_{n,m} R_{inm}(x)\eta_{nm}(t), \qquad (2.1.8)$$

where the noise terms $\xi_j(t)$ and $\eta_{nm}(t)$ correspond to the contributions, arising from the second- and third-order derivatives, respectively, in the Fokker-Planck equation (2.1.4). Their nonvanishing correlation functions are

$$< \xi_i(t)\xi_j(t`) >= \delta_{ij}\delta(t - t`), \qquad (2.1.9)$$

$$< \eta_{im}(t)\eta_{jk}(t`)\eta_{kl}(t``) >= \delta_{ij}\delta_{jk}\delta_{mn}\delta_{nl}\delta(t - t`)\delta(t` - t``). \qquad (2.1.10)$$

The B_{ij} and R_{imn} coefficients in the system of equations (2.1.8) are obtained from the relations

$$\sum_k B_{ik}B_{jk} = D_{ij}, \qquad (2.1.11)$$

$$\sum_{n,m} R_{inm}R_{jnm}R_{knm} = C_{ijk}. \qquad (2.1.12)$$

Equations (2.1.4) and (2.1.8), as well as Eqs. (2.1.9)-(2.1.12), are written in a general form. For the case of third harmonic generation, Eqs. (2.1.5)-(2.1.7) (with account of Eqs. (2.1.11) and (2.1.12)) give

$$B_{11} = \sqrt{D_{11}}, B_{22} = \sqrt{D_{22}}, \qquad (2.1.13)$$

$$R_{111} = \sqrt[3]{C_{111}}, R_{222} = \sqrt[3]{C_{222}}. \qquad (2.1.14)$$

This leads to the following Langevin equations:

$$\frac{\partial \alpha_1}{\partial t} = A_1 + \sqrt{-6\chi\beta_1\alpha_2}\xi_1(t) + \sqrt[3]{-6\chi\alpha_2}\eta_{11}(t),$$

$$\frac{\partial \beta_1}{\partial t} = A_2 + \sqrt{-6\chi\alpha_1\beta_2}\xi_2(t) + \sqrt[3]{-6\chi\beta_2}\eta_{22}(t),$$

$$\frac{\partial \alpha_2}{\partial t} = A_3,$$

$$\frac{\partial \beta_2}{\partial t} = A_4. \qquad (2.1.15)$$

2.2 Semiclassical Steady States and Instability

To analyze the system of equations (2.1.15), it is convenient to transform them to the photon number and phase variables of the modes:

$$n_j = \alpha_j\beta_j, \qquad (2.2.1)$$

$$\phi_j = \frac{1}{2i} ln\left(\frac{\alpha_j}{\beta_j}\right), \ (j = 1,2). \qquad (2.2.2)$$

It can be shown that the variable change formula (Ito form) in the case of stochastic equations with third-order noise terms is

$$\frac{df(x)}{dt} = \sum_i \frac{\partial f}{\partial x_i} A_i(x) + \frac{1}{2}\sum_{i,j} \frac{\partial^2 f}{\partial x_i \partial x_j} D_{ij}(x) + \frac{1}{6}\sum \frac{\partial^3 f}{\partial x_i \partial x_j \partial x_k} C_{ijk}(x) + \sum_i \frac{\partial f}{\partial x_i}\left(\sum_k B_{ik}(x)\xi_k(t) + \sum_{n,m} R_{inm}(x)\eta_{nm}(t)\right). \qquad (2.2.3)$$

In the variables (2.2.1) and (2.2.2), the equations of motion become

$$\frac{\partial n_1}{\partial t} = 2|E|n_1^{1/2}\cos(\phi - \phi_1) - 2\gamma_1 n_1 - 6\chi n_1^{3/2} n_2^{1/2}\cos(3\phi_1 - \phi_2) + \Gamma(t),$$

$$\frac{\partial n_2}{\partial t} = -2\gamma_2 n_2 + 2\chi n_1^{3/2} n_2^{1/2}\cos(3\phi_1 - \phi_2),$$

$$\frac{\partial \phi_1}{\partial t} = \frac{|E|}{\sqrt{n_1}}\sin(\phi - \phi_1) + \left(3\chi n_1^{1/2} n_2^{1/2} - 3\chi n_1^{-1/2} n_2^{1/2} + 2\chi n_1^{-3/2} n_2^{1/2}\right)\sin(3\phi_1 - \phi_2) + \varphi(t),$$

$$\frac{\partial \phi_2}{\partial t} = \chi n_1^{3/2} n_2^{-1/2}\sin(3\phi_1 - \phi_2), \qquad (2.2.4)$$

where ϕ is the phase of the driving field $E = |E|\exp(i\phi)$, and the noise terms are

$$\Gamma(t) = \beta_1 B_{11}\xi_1(t) + \alpha_1 B_{22}\xi_2(t) + \beta_1 R_{111}\eta_{11}(t) + \alpha_1 R_{222}\eta_{22}(t),$$

$$\varphi(t) = \frac{1}{2i}\left(\frac{B_{11}}{\alpha_1}\xi_1(t) - \frac{B_{22}}{\beta_1}\xi_2(t) + \frac{R_{111}}{\alpha_1}\eta_{11}(t) - \frac{R_{222}}{\beta_1}\eta_{22}(t)\right). \quad (2.2.5)$$

An analysis of the steady-state solutions n_j^0 and ϕ_j^0 $(j = 1,2)$ of these equations in a semiclassical approximation and of the conditions of their stability with respect to small fluctuations (linear stability analysis) leads to the following results:

$$\phi_1^0 = \phi_2^0/3 = \phi,$$

$$3k(n_1^0)^{5/2} + (n_1^0)^{1/2} = \varepsilon,$$

$$n_2^0 = \frac{k}{r}(n_1^0)^3. \qquad (2.2.6)$$

Here, we have used the following notations:

$$r = \gamma_2/\gamma_1,\ k = \frac{\chi^2}{\gamma_1\gamma_2},\ \text{and}\ \varepsilon = \frac{|E|}{\gamma_1}. \tag{2.2.7}$$

This solution is stable if $\varepsilon < \varepsilon_{cr}$, where

$$\varepsilon_{cr} = \frac{1}{\sqrt[4]{6k}}\left\{(1+r)^{1/4} + \frac{1}{2}(1+r)^{5/4}\right\} \tag{2.2.8}$$

is the critical point. The critical photon number in the fundamental mode is

$$n_1^{cr} = \left(\frac{1+r}{6k}\right)^{1/2}, \tag{2.2.9}$$

and the dependence of n_1^0 and n_2^0 on $|\varepsilon|^2$ is shown in Fig. 2.1. Above the critical point($\varepsilon > \varepsilon_{cr}$), i.e., for a sufficiently strong driving field, the real parts of the eigenvalues of the matrices of the linearized equations of motion become negative, which leads to instability. In the instability region, the intensities of the third harmonic and fundamental modes exhibit a self-pulsing temporal behaviour. The mode dynamics depends on the initial conditions and is illustrated in Fig. 2.2 for a particular realization.

2.3.Higher-Order Moments and Third-Order Noise

This section discusses the role of third-order noise in physical quantities. As it may be expected, third-order noise effects will be manifested in higher order operator moments, which describe, in particular, the photon correlation phenomena.

At first, let us consider this question in the small time approximation $t << \gamma_{1,2}^{-1}$. For this purpose, we turn to the solution of stochastic equations of

motion (2.1.15) for small time intervals in the case of the vacuum initial conditions $\alpha_j(t=0)=\beta_j(t=0)=0$ $(j=1,2)$. Initially, we write down the amplitudes of the fundamental mode in the form

$$\alpha_1(t)=\alpha_1^d(t)+F_1(t), \tag{2.3.1}$$

$$\beta_1(t)=\beta_1^d(t)+F_2(t), \tag{2.3.2}$$

where we separate the $F_{1,2}$ noise contributions from the α_1^d and β_1^d deterministic parts; then, we use the Euler iteration method. This yields the following results in the third order of iteration:

$$\alpha_1^d(\tau)=\beta_1^d(\tau)=\varepsilon\tau-\varepsilon\frac{\tau^2}{3}+\varepsilon\left(\frac{\tau}{3}\right)^3-4kr\varepsilon^5\frac{\tau^7}{3^6}+\ldots, \tag{2.3.3}$$

$$F_j(\tau)=\sqrt[3]{-6kr}\varepsilon W_j(\tau)\left(\frac{\tau}{3}\right)^{5/3}+\sqrt{-12kr}\varepsilon^2V_j(\tau)\left(\frac{\tau}{3}\right)^3+\cdots,$$

$$\tau=\gamma_1 t \tag{2.3.4}$$

where we have chosen $\varepsilon=\varepsilon*$ for simplicity purposes. $V_j(\tau)$ and $W_j(\tau)$ are second- and third-order noise sources, respectively, which are connected with $\xi_j(\tau)$ and $\eta_{jj}(\tau)$ by

$$\xi_j(\tau)d\tau=V_j(\tau)\sqrt{d\tau}, \tag{2.3.5}$$

$$\eta_{jj}(\tau)\sqrt{d\tau}=W_j(\tau)\sqrt[3]{d\tau}. \tag{2.3.6}$$

Their nonzero correlators are

$$<V_j(\tau)^2>=<W_j(\tau)^3>=1. \tag{2.3.7}$$

Using the results in (2.3.3)-(2.3.7), we calculate the second- and the third-order correlators for the fundamental mode. In the lowest approximation in τ, the normalized second-order correlator

$$g_1^{(2)} = \frac{<(a_1^+)^2 a_1^2>}{<a_1^+ a_1>^2} \tag{2.3.8}$$

contains a contribution from the second-order noise source and is determined as

$$g_1^{(2)} - 1 \approx \frac{2<F_1^2>}{(\alpha_1^d)^2} \approx -\frac{8}{3} kr\varepsilon^2 \left(\frac{\tau}{3}\right)^4. \tag{2.3.9}$$

We see that the quantity $g_1^{(2)} - 1$ is proportional to the squared amplitude of the driving field and that the pair correlation of photons is of an antibunched character.

In respect to the normalized third-order correlator

$$g_1^{(3)} = \frac{<(a_1^+)^3 a_1^3>}{<a_1^+ a_1>^3}, \tag{2.3.10}$$

the leading contribution (in the lowest order in τ) arises from the third-order noise source. Indeed, using solutions (2.3.3) and (2.3.4), we obtain

$$g_1^{(3)} - 1 \approx \frac{1}{(\alpha_1^d)^3}(< F_1^3 > + 3\alpha_1^d < F_1^2 >) \approx$$
$$-\frac{4}{9} kr \left(\frac{\tau}{3}\right)^2 - 8kr\varepsilon^2 \left(\frac{\tau}{3}\right)^4 + \ldots, \tag{2.3.11}$$

where the first term is originated from the third-order noise source W_1, while the second one is determined by the second-order noise source V_1. Note that the correlation between photons, described by $g_1^{(3)}$, is also of an antibunched character.

For the case of the third-harmonic mode, one may arrive at similar conclusions regarding the role of the third-order noise, but the corresponding results for $g_2^{(2)}$ and $g_2^{(3)}$ are more complicated to be reproduced here.

2.4. Langevin Equations in a Differential Form

The Langevin equations in (2.1.15), which describe the dynamics of the stochastic amplitudes of the fundamental and third harmonic modes, can be written in the following differential form:

$$d\alpha_1 = (\varepsilon - \alpha_1 - 3k\beta_1^2\alpha_2)d\tau + \sqrt{-6k\beta_1\alpha_2}w_1(\tau)\sqrt{d\tau} + \sqrt[3]{-6k\alpha_2}v_1(\tau)\sqrt[3]{d\tau},$$

$$d\beta_1 = (\varepsilon - \beta_1 - 3k\alpha_1^2\beta_2)d\tau + \sqrt{-6k\alpha_1\beta_2}w_2(\tau)\sqrt{d\tau} + \sqrt[3]{-6k\beta_2}v_2(\tau)\sqrt[3]{d\tau},$$

$$d\beta_2 = (-r\beta_2 + k\beta_1^3)d\tau,$$

$$d\beta_2 = (-r\beta_2 + k\beta_1^3)d\tau. \quad (2.4.1)$$

Here, $\tau = \gamma_1 t$ is the normalized time, $\varepsilon = E/\gamma_1$, $k = \chi/\gamma_1$, and $r = \gamma_2/\gamma_1$; $w_1(\tau)$, $w_2(\tau)$, $v_1(\tau)$, and $v_2(\tau)$ are independent Langevin noise sources with the following nonzero correlation functions:

$$\langle w_1^2\rangle = \langle w_2^2\rangle = 1,$$

$$\langle v_1^3\rangle = \langle v_2^3\rangle = 1. \quad (2.4.2)$$

In the range of large interaction times, the set of equations (2.4.1) without noise terms only has the steady-state stable solution for the photon number and phases

$$n_j = \alpha_j\beta_j,\ \varphi_j = \frac{1}{2i}ln\left(\frac{\alpha_j}{\beta_j}\right)\ (j = 1,2) \qquad (2.4.3)$$

in the case of small perturbations of the field $\varepsilon < \varepsilon_{cr}$. Here, ε_{cr} is the critical value of the perturbation field (the Hopf bifurcation point), which is defined by Eq. (2.2.8) [1]:

$$\varepsilon_{cr} = \frac{1}{\sqrt[4]{6\frac{k^2}{r}}}\left[(1+r)^{1/4} + \frac{1}{2}(1+r)^{5/4}\right]. \qquad (2.4.4)$$

In the case of strong perturbations, small fluctuations of phases of the fundamental mode and the third harmonic do not decay with time (the system loses its stability in the vicinity of the steady-state solutions to Eqs. (2.4.1) without noise terms). The semiclassical solutions for the number of photons of the modes change to a regime of self-sustained oscillations.

Our calculations are based on modelling noise sources in Eqs. (2.4.1). We assume that the third-order noises in the range of large interaction times have a weak affect on the time behaviour of the system and can therefore be neglected.

$$d\alpha_1 = (\varepsilon - \alpha_1 - 3k\beta_1^2\alpha_2)d\tau + \sqrt{-6k\beta_1\alpha_2}w_1(\tau)\sqrt{d\tau},$$

$$d\beta_1 = (\varepsilon - \beta_1 - 3k\alpha_1^2\beta_2)d\tau + \sqrt{-6k\alpha_1\beta_2}w_2(\tau)\sqrt{d\tau},$$

$$d\alpha_2 = (-r\alpha_2 + k\alpha_1^3)d\tau,$$

$$d\beta_2 = (-r\beta_2 + k\beta_1^3)d\tau. \qquad (2.4.5)$$

The second-order noises are simulated by the formulas [12]

$$w_1(\tau) = [-2\,ln(\,z_1)]^{1/2}\,cos(\,2\pi z_2),$$

$$w_2(\tau) = [-2\,ln(\,z_1)]^{1/2}\,sin(\,2\pi z_2), \qquad (2.4.6)$$

where z_1 and z_2 are independent random numbers with a uniform distribution on the interval (0, 1). In particular, for these noises, we have

$$\langle w_i(\tau)\rangle = 0,$$

$$\langle w_i(\tau)w_j(\tau)\rangle = \delta_{ij}\ (i,j = 1,2). \qquad (2.4.7)$$

To solve the set of equations (2.4.5), we use the numerical Euler method.

The average values of the number of photons of the modes are calculated with the formula

$$\langle n_k(\tau)\rangle = Re\langle\alpha_k(\tau)\beta_k(\tau)\rangle = Re\left(\lim_{N\to\infty}\left(\frac{1}{N}\sum_{j=1}^{N}\alpha_k^{(j)}(\tau)\,\beta_k^{(j)}(\tau)\right)\right), \quad (k = 1,2), \qquad (2.4.8)$$

where $\alpha_k^{(j)}(\tau)$ and $\beta_k^{(j)}(\tau)$ are the numerical realizations of the corresponding quantities of Eqs. (2.4.5).

2.5 Quantum Dynamics of Photon Numbers

First, let us study the time behaviour of the number of photons of the fundamental mode and of the third harmonic.

Figure 2.3 demonstrates one particular realization of the dynamics of the number of photons of the fundamental mode (1) and of the third harmonic (2) in the region of unstable behaviour of the system. The curves were obtained from numerical solutions of Eqs. (2.4.5) with the initial values of the stochastic amplitudes of the field modes

$$\alpha_1(0) = i,\ \alpha_2(0) = i,\ \beta_1(0) = \alpha_1^*(0), \text{ and } \beta_2(0) = \alpha_2^*(0) \qquad (2.5.1)$$

and for the following values of the system parameters: $\varepsilon = 380$, $k^2 = 10^{-9}$, and $r = 1$. For these parameter values, the critical perturbation of the field is $\varepsilon_{cr} \approx 270$. In the range of large evolution times, both modes are in a regime of self-oscillation of the photon number.

Figure 2.4 shows the dynamics of the average number of photons of the fundamental mode (1) and of the third harmonic (2) in the case of evolution of the system from an initial state with a Gaussian distribution of stochastic amplitudes of both modes. The initial values of the stochastic amplitudes of the system were simulated by the formulas

$$\alpha_1(0) = [-2\,ln(z_1)]^{1/2}\,cos(2\pi z_2) + i[-2\,ln(z_1)]^{1/2}\,sin(2\pi z_2),$$

$$\beta_1(0) = \alpha_1^*(0),$$

$$\alpha_2(0) = [-2\,ln(z_3)]^{1/2}\,cos(2\pi z_4) + i[-2\,ln(z_3)]^{1/2}\,sin(2\pi z_4),$$

$$\beta_2(0) = \alpha_2^*(0), \qquad (2.5.2)$$

where z_1, z_2, z_3, and z_4 are independent random numbers with a uniform distribution on the interval (0…1). Both curves were obtained with the help of 1000 realizations of the set of equations (2.4.5) and for the values of the parameters corresponding to Fig. 2.3. We can state that there are no oscillations in the average values of the number of photons of the fundamental mode and of the third harmonic.

The temporal behaviour of the average values of the photon numbers in the unstable region of the system depends on the initial state.

Figure 2.5 demonstrates the dynamics of the average values of the number of photons of the fundamental mode (1) and of the third harmonic (2) in the case of evolution of the system from an initial state with the values of stochastic amplitudes presented in formula (2.5.1). The curves were calculated with the help of 1000 realizations of the set of equations (2.4.5) for the values of the parameters in Fig. 2.3. It can be said that both curves have small amplitude oscillations. The oscillation amplitude of the number of photons of the fundamental mode is larger than that of the third harmonic.

2.6 Distribution functions for the number of photons

In this section, we study distribution functions for the number of photons of the fundamental mode and of the third harmonic in the region of unstable behaviour of the system. First, we will calculate the distribution function for the number of photons of the fundamental mode in the region of large interaction times. An algorithm for calculating this function is given in the fourth section of the previous chapter.

Figure 2.6 demonstrates a distribution function for the number of photons of the fundamental mode in the region of unstable behaviour of the system and for large interaction times ($\tau = 15$). The function was calculated for system evolution from an initial state with a Gaussian distribution of stochastic amplitudes of the field modes. To obtain this function, 30 000 independent realizations of numerical solutions of the set of stochastic equations (2.4.5) were used. The distribution function for the number of photons of the fundamental mode has a two-peak structure. Each of the two most probable values of the photon numbers corresponds to a state, in which the system can be found most of the time. The time during which

the system is in a state with a small number of photons is longer than the time during which the system is in a state with a large number of photons.

Figure 2.7 demonstrates a distribution function for the number of photons of the fundamental mode close to the bifurcation point of the optical system (ε = 300). To calculate this function, we used 30 000 independent solutions to the set of Langevin equations (2.4.5). The function was calculated in the range of large interaction times (τ = 15) and for the parameter values $k^2 = 10^{-9}$ and $r = 1$. Unlike the previous case, the distribution function for the number of photons of the fundamental mode has a single-peak structure close to the point of bifurcation of the optical system. Passing to the unstable region, the distribution function gradually transforms from a single- to a two-peak structure.

Figure 2.8 demonstrates the distribution function for the number of photons of the third harmonic in the region of unstable behaviour of the system and for large interaction times (τ = 15). The function was calculated with the help of 30 000 independent realizations of the set of stochastic equations (2.4.5). The curve was calculated for the case of evolution of the system from an initial state with a Gaussian distribution of stochastic amplitudes of the field modes and for the parameter values in Fig. 2.3. This function is similar to the distribution function for the number of photons of the fundamental mode and has a two-peak structure. Each peak corresponds to a component of the state of the system. In this case, the system spends more time in the state component with a large value of the number of photons than in the state component with a small value.

Figure 2.9 corresponds to the distribution function for the number of photons of the third harmonic close to the bifurcation point of the optical

system ($\varepsilon = 300$) and to the same values of the parameters as the distribution function shown in Fig. 2.7. To calculate this function, 30 000 independent solutions to the set of Langevin equations (2.4.5) were used. In this case, the distribution function has a single-peak structure.

In this section, we also study joint fluctuations in the number of photons of the fundamental mode and of the third harmonic. For this purpose, a joint distribution function for the number of photons of the interacting modes was calculated. The algorithm for calculating this function is given in the fifth section of the previous chapter.

Figure 2.10 demonstrates a joint distribution function of the photon numbers of the fundamental mode and third harmonic. The function was calculated for the case of system evolution from an initial state with a Gaussian distribution of stochastic amplitudes of the interacting modes, in the range of large evolution times, and for the parameter values in Fig. 2.3. To calculate this function, we used 50 000 independent realizations of numerical solutions to Eqs. (2.4.5); the function has a two-peak structure. Each peak corresponds to a state in which the system resides during the main part of the interaction time. The residence time of the system in the state component with a large number of photons of the fundamental mode and a small number of photons of the third harmonic is shorter than in the state component with a small number of photons of the fundamental mode and a large number of photons of the third harmonic.

Figure 2.11 demonstrates a joint distribution function of the number of photons of the fundamental and third harmonic modes in the range of large interaction times ($\tau = 15$) and close to the bifurcation point of the optical system ($\varepsilon = 300$). The function was calculated for the same parameter

values as the function presented in Fig. 2.9. To calculate this function, we used 50 000 independent solutions to the set of Langevin equations (2.4.5). In this case, the function has a single-peak structure close to the bifurcation point, being distinct from the previous case where the system was in the instability region.

2.7. Quantum Fluctuations of Phases of the Modes

In this section, we study quantum fluctuations of the phases of the fundamental and third harmonic modes, as well as joint fluctuations of the phases of these modes. For this purpose, we calculate the phase distribution functions of the interacting modes, as well as the joint distribution functions of phases of the field modes. The method for calculating the dynamics of these functions is given in the fourth and fifth sections of the previous chapter.

Figure 2.12 shows the dynamics of the distribution function of the fundamental mode phase for the Gaussian initial condition of both modes (2.5.2). Here and below, the following parameter values are used for calculations: $\varepsilon = 380$, $k^2 = 10^{-9}$, and $r = 1$. At these values, the critical perturbation is $\varepsilon_{cr} \approx 270$.

At $\tau = 0$, we have a uniform distribution of phases in the interval $(-\pi/2, \pi/2)$. After some very small period, due to the classical perturbation field, the fundamental mode moves towards the coherent state with a very narrow phase distribution. Then, the system moves gradually towards the state with the two most probable phase values. States with two components are formed in the system. Hereafter, the distribution function does not vary.

In Fig. 2.13 the dynamics of a certain realization of the fundamental mode phase is shown. The dashed lines correspond to the two most probable values of the phase. The transition time of the system between these states is about the stay time in them.

In the unstable region and in the case of system evolution from an initial state with a Gaussian distribution of the stochastic amplitudes of both interacting modes, the dynamics of the phase distribution function of the third harmonic mode is similar to the dynamics of the phase distribution function of the fundamental mode under the same conditions. Figure 2.14 shows the dynamics of the phase distribution function of the third harmonic mode for this case. The dynamics of the distribution function is calculated for the following values of system parameters: $\varepsilon = 380$, $k^2 = 10^{-9}$, and $r = 1$. To calculate the temporal behaviour of this function, 100 000 independent solutions of the Langevin system of equations (2.4.5) were used. In the region of small interaction times ($\tau < 1$), from the initial uniform distribution in the interval $(-\pi/2, \pi/2)$, the phase distribution function of the third harmonic mode starts to narrow. After that, it expands. Next, it transforms into a two-component structure in the region of large interaction times($\tau \cong 10$). After that, the distribution function does not change in time. The two most likely phase values represent the two components of the state, where the system spends most part of the time.

In the region of unstable behaviour, the temporal behaviour of the phase distribution functions of the fundamental and third harmonic modes depends strongly on the initial state of the modes. In the case of evolution of the system from initial coherent states of both modes, in the region of

large interaction times, the phase distribution functions of the fundamental and third harmonic modes do not exhibit any stationary behaviour.

Figure 2.15 shows the dynamics of the phase distribution functions of the fundamental (Fig. 2.15a) and third harmonic (Fig 2.15b) modes in the case of evolution of the system from initial coherent states of both modes with the stochastic amplitude values of the field modes

$$\alpha_1(0) = 1 + i,\ \alpha_2(0) = 1 + i,\ \beta_1(0) = \alpha_1^*(0), \text{ and } \beta_2(0) = \alpha_2^*(0) \quad (2.7.1)$$

and for the system parameter values $\varepsilon = 380$, $k^2 = 10^{-9}$, and $r = 1$. To calculate the dynamics of these functions, 100 000 independent solutions of the Langevin system of equations (2.4.5) were used. In the region of instability, the temporal behaviours of the phase distribution functions of the interacting modes are similar to each other. In the region of large evolution times and in the case of evolution of the system from initial coherent states of both modes, the phase distribution functions of the field modes switch to an auto-oscillation mode. The modes localize gradually in one component of the state from the two-component one, then return to the two-component state, and then localize gradually into the other component of the state.

Figure 2.16 shows one trajectory of the optical system in the phase space $(Re\,\phi_1, Re\,\phi_2)$. The trajectory of the system is represented in the time interval $(0{,}55)$. The density of the points represents the amount of time spent by the system in that area of the phase space. The time interval between two adjacent points is $\Delta\tau = 0.01$. The trajectory is calculated for the following values of system parameters: $\varepsilon = 380$, $k^2 = 10^{-9}$, and $r = 1$. In the region of small times $\tau << 1$, after the beginning of interaction, in the cavity volume $(Re\,\phi_1 = 0, Re\,\phi_2 = 0)$, classical phase matching of

the interacting modes occurs. From the initial point in the phase space, marked in the figure, the system passes very quickly to the point of the phase space, which corresponds to the classical phase matching of the interacting modes. After that, it leaves this point and never returns there. The system spends most of the time in two regions of the phase space. In these regions, both phases of the interacting modes have either positive or negative values. These two clusters of points in the phase space represent the two states of the system.

In this section, we also study the dynamics of the joint distribution function of the phases of the fundamental and third harmonic modes. For the parameter values of the system in Fig. 2.12 at the time point $\tau = 9.5$, this function is shown in Fig. 2.17 for the case of evolution of the system from an initial state with a Gaussian distribution of stochastic amplitudes of both modes (2.5.2). The distribution function has a two-peak structure. Each peak represents a state of the system, in which it spends most of the time. Some area of events that surround the point corresponding to the classical phase matching of the system ($Re\,\phi_1 = 0, Re\,\phi_2 = 0$) has a zero probability of realization. The latter shows that the classical phase matching has a zero probability of realization in the unstable region. When the optical system transitions from the unstable to the stable region, the well surrounding the point decreases gradually and a peak forms gradually at the point corresponding to the classical phase matching of the interacting modes.

In the case of evolution of the system from initial coherent states with nonzero phases of both modes, the joint distribution function of phases of the interacting modes switches to an auto-oscillation mode. Figure 2.18 presents the joint distribution function of the phases of the interacting

modes at the time $\tau = 9.43$ and for evolution from the initial coherent states of both modes $\alpha_1(0) = 1 + i$, $\alpha_2(0) = 1 + i$, $\beta_1(0) = \alpha_1^*(0)$, and $\beta_2(0) = \alpha_2^*(0)$, as well as for the following parameter values of the system: $\varepsilon = 380$, $k^2 = 10^{-9}$, and $r = 1$. To calculate the dynamics of this function, 100 000 independent solutions of the Langevin system of equations (2.4.5) were used. At this point in time, the system localizes in the component of the state, in which the phases of both modes have negative values. The probability of detection of the system in a state, in which the phases of both modes have positive values, is equal to zero. Over time, the system oscillates between the two components of the state.

2.8 Joint Fluctuations in Photon Numbers and Phases of the Modes

In this section, we study the dynamics of the joint distribution function of the number of photons and phases of the fundamental and third harmonic modes. The algorithm for calculating these functions is similar to the algorithm for calculating the corresponding functions for the process of second harmonic generation, which is given in the previous chapter.

Figure 2.19 shows the joint distribution function of the number of photons and phases of the fundamental (Fig. 2.19a) and third harmonic (Fig. 2.19b) modes at the time point $\tau = 9.5$ and in the case of evolution of both modes from initial states, which have a Gaussian distribution of stochastic amplitudes (2.5.2). The functions are computed for the following parameters of the system: $\varepsilon = 380$, $k^2 = 10^{-9}$, and $r = 1$. In order to compute these functions, 100 000 independent solutions to the Langevin system of equations (2.4.5) were used. Both distribution functions are symmetric with respect to the zero phase (the phase of the perturbation

field of the fundamental mode) and have a two-component structure. Each component of these functions represents a component of the state of the field mode, in which it spends most of the time. For each mode, the same value of the number of photons is realized in the components of states with a positive phase and in the components of states with a negative phase.

In the case of system evolution from initial coherent states of both modes with the values of stochastic amplitudes (2.7.1), the joint distribution functions of photon numbers and phases of the interacting modes go into an auto-oscillation mode. Figure 2.20 shows the joint distribution function of the number of photons and phases of the third harmonic mode at the time $\tau = 9.43$ and in the case of evolution from initial coherent states of both modes with the values of stochastic amplitudes of the field modes $\alpha_1(0) = 1 + i,\ \alpha_2(0) = 1 + i,\ \beta_1(0) = \alpha_1^*(0),$ and $\beta_2(0) = \alpha_2^*(0),$ as well as for the system parameter values $\varepsilon = 380$, $k^2 = 10^{-9}$, and $r = 1$. To calculate the dynamics of this function, 100 000 independent solutions of the Langevin system of equations (2.4.5) were used. At this moment in time, the third harmonic mode is localized in the component of the state, which has a negative phase.

2.9 Quantum Dynamics of the Field in the Case of Evolution from Initial Vacuum States

In this section and in the following sections of this chapter, we investigate the quantum dynamics of intracavity third harmonic generation using the Monte Carlo wave function method [13, 14].

We investigate the dynamics of the system using the dimensionless time $\tau = \gamma_t t$ and the dimensionless parameters

$\varepsilon = E/\gamma_1, r = \gamma_2/\gamma_1$, and $k = \chi/\gamma_1$, (2.9.1)

for the ratio of damping coefficients of the modes r =1 and in the case of system evolution from initial vacuum states of both modes. The mean number of photons, the quantum entropy, and the Wigner functions of the modes are calculated using 1000 independent quantum trajectories of the optical systems.

First, we study the quantum dynamics of the interacting modes of the optical system in the region of strong coupling of the modes (k = 0.3) and in the case of a strong external perturbation of the fundamental mode (ε = 3).

Figure 2.21 shows the quantum dynamics of the number of photons of the fundamental mode (curve a) and the dynamics of the number of photons of the same mode for an arbitrarily chosen quantum trajectory of the optical system (curve b). In the region of long interaction times, the dynamics of the number of photons of a single trajectory differs considerably from the dynamics of the mean number of photons of the mode. The latter observation shows that there are strong fluctuations in the number of photons of the fundamental mode in the region of long interaction times ($\tau > 1$). In the region of short interaction times ($\tau < 1$), the dynamics of the mean number of photons of the mode is the same as the dynamics of the number of photons of the arbitrarily chosen quantum trajectory. For long interaction times, small fluctuations in the number of photons do not decay, which leads to a significant difference between the dynamics of the mean number of photons and the dynamics of the photon number of the arbitrarily chosen quantum trajectory.

Figure 2.22 shows the quantum dynamics of the number of photons of the third harmonic mode (curve a) and the dynamics of the number of photons of an arbitrarily chosen quantum trajectory of the same mode (curve b). As in the case of the fundamental mode, in the region of short interaction times ($\tau < 1$), the dynamics of the number of photons of a single quantum trajectory is the same as the dynamics of the mean number of photons. However, in the region of large interaction times ($\tau > 1$), the number of photons of a single quantum trajectory fluctuates strongly around the mean number of photons of the mode. The latter observation shows that the system turns to the region of unstable behaviour, where small fluctuations in the number of photons of the interacting modes do not damp.

Figure 2.23 shows the dynamics of the quantum entropy of the fundamental mode. In the region of short interaction times ($\tau < 1$), the quantum entropy of the mode is equal to zero, which indicates that, in this region of interaction, the mode is in a pure state and the ensemble of the quantum trajectories consists of a single term. The latter observation explains the coincidence of the dynamics of the number of photons of a single quantum trajectory and of the dynamics of the mean number of photons (see Fig. 2.21). After that, the quantum entropy of the mode starts to grow. Then, in the region of long interaction times ($\tau > 4$), it obtains a stationary value. In this region of interaction times, the state of the system almost does not change any further, representing a statistical mixture of pure states.

Figure 2.24 shows the dynamics of the quantum entropy of the third harmonic mode. As in the case of the fundamental mode, the quantum entropy of the third harmonic mode is equal to zero in the region of small interaction times. The mode is in a pure state and the ensemble of the

quantum trajectories consists of a single term, which explains the coincidence of the dynamics of the number of photons of a single quantum trajectory and the dynamics of the mean number of photons in the region of small interaction times (see Fig. 2.22). Then, the quantum entropy of the mode starts growing, and, in the region of long interaction times ($\tau > 4$), it turns into a stationary value. After that, the state of the system remains almost unchanged. The stationary value of the quantum entropy of the third harmonic is less than that of the quantum entropy of the fundamental mode (see Figs. 2.23 and 2.24).

Figure 2.25 shows the dynamics of the Wigner function of the state of the fundamental mode. Here, Fig. 2.25a shows the Wigner function of the initial vacuum state. Figures 2.25b to 2.25f show the Wigner function of the state of the fundamental mode at the times of interaction $\tau = 1$, $\tau = 1.5$, $\tau = 2$, $\tau = 3$, and $\tau = 10$, respectively. At the time $\tau = 1$, the system is in a pure coherent state with zero quantum entropy, into which it changed from the initial vacuum state. At that moment, the number of photons has already reached almost a maximum value and does not change any further (see Fig. 2.21). After that, there is a sharp increase in quantum entropy. The latter observation shows that, although the energy of the mode does not change, the state starts to change sharply. Near the time $\tau = 1.5$, the mode has already changed from a coherent state to a squeezed one (see Fig. 2.25c). In this state, the quantum entropy of the fundamental mode is approximately 0.3, which shows that the system is not in a pure state. After that, with an increase in the quantum entropy, the squeezed state of the fundamental mode begins to decay gradually, and the system changes gradually from a stable state to an unstable one at the time $\tau \approx 2$ (see Fig. 2.25d). At the time $\tau \approx 3$, the quantum entropy of the mode

already almost reaches a maximal value of 1.7 (the stationary value of the quantum entropy of the mode is approximately 1.9), and the system changes to an unstable state, the Wigner function of which is shown in Fig. 2.25e. After that, the quantum entropy of the fundamental mode changes to a stationary value. The Wigner function of the stationary state of the fundamental mode at the time $\tau = 10$ is shown in Fig. 2.25f. It only differs slightly from the Wigner function shown in Fig. 2.25e and represents the unstable stationary state of the fundamental mode, which has two state components.

Figure 2.26 shows the dynamics of the Wigner function of the state of the third harmonic mode. Figures 2.26a to 2.26e show the Wigner function of the state of the third harmonic mode at the interaction times of the optical system modes $\tau = 1$, $\tau = 1.5$, $\tau = 2$, $\tau = 3$, and $\tau = 10$, respectively. The mode changed from an initial vacuum state to a pure coherent state (Fig. 2.26a) with zero quantum entropy at the time $\tau \approx 1$ (see Fig. 2.24). Meanwhile, the number of photons of the mode (see Fig. 2.22) grew insignificantly, and the coherent state of the system was close to the vacuum one, which also reflects the Wigner function in Fig. 2.26a. After that, the quantum entropy of the system starts to grow, and, at the time $\tau \approx 1.5$, it reaches a value of 0.3. The Wigner function of the state of the mode at the time $\tau = 1.5$ is shown in Fig. 2.26b. It represents a squeezed state with a slightly squeezed quadrature component. After that, as the quantum entropy of the system grows, the squeezed state of the system begins to decay. The Wigner function of the state of the mode at the time $\tau = 2$ is shown in Fig. 2.26c. The quantum entropy of this state is approximately equal to 0.9. A stationary unstable state begins to form in the system, the Wigner function of which at the time $\tau = 3$ is shown in Fig. 2.26d. The

quantum entropy of this state is approximately equal to 1.5, and it almost reaches the stationary value. After that, the state of the system almost does not change. The Wigner function of the state of the third harmonic mode in the region of long interaction times ($\tau = 10$) is shown in Fig. 2.26e. It has a cylindrical form. The quantum entropy of the stationary state is approximately equal to 1.6.

Figures 2.27 and 2.28 represent the Wigner functions of two arbitrarily chosen quantum trajectories of the optical system in the region of long interaction time $\tau = 10$. Figure 2.27a represents the Wigner function of the state of the fundamental mode, and Fig. 2.27b represents the Wigner function of the state of the third harmonic mode of an arbitrarily chosen quantum trajectory. Figures 2.28a and 2.28b represent the Wigner functions of the states of the fundamental and third harmonic modes of another arbitrarily chosen quantum trajectory, respectively. The Wigner functions of the corresponding modes of two different quantum trajectories differ considerably from each other. The latter explains the high values of the quantum entropy of the modes in this region of interaction times.

Now we consider the quantum dynamics of the system, when the perturbation of the fundamental mode is weak ($\varepsilon = 1$) and the coupling coefficient remains the same ($k = 0.3$).

Figure 2.29 illustrates the quantum dynamics of the number of photons of the fundamental mode (curve a) and the dynamics of the number of photons of an arbitrarily chosen quantum trajectory (curve b). In the region of short interaction times ($\tau < 2$), the dynamics of the mean number of photons coincides with the dynamics of the number of photons of the

arbitrarily chosen quantum trajectory of the fundamental mode. In the region of long interaction times, we explain the slight fluctuations in the number of photons of the arbitrarily chosen quantum trajectory of the system is due to a weak perturbation of the fundamental mode. The system is in a stable state.

Figure 2.30 illustrates the quantum dynamics of the mean number of photons (curve a) and of the number of photons of an arbitrarily chosen trajectory (curve b) of the third harmonic. In the region of short interaction times ($\tau < 2$), the dynamics of the mean number of photons of the third harmonic coincides with the dynamics of the number of photons of an arbitrarily chosen quantum trajectory. In the region of long interaction times, we explain the large fluctuations in the number of photons of an arbitrarily chosen trajectory around the mean number of photons to be due to a small value of the number of photons.

Figures 2.31 and 2.32 show the dynamics of the quantum entropy of the fundamental and the third harmonic modes, respectively. In the region of short interaction times ($\tau < 2$), the quantum entropies of the modes are equal to zero, which shows that the modes are in pure states in this region of interaction times. Later, the quantum entropy of the modes begins growing. In the region of long interaction times ($\tau = 10$), it is approximately equal to 0.4. In contrast to the case of a strong external perturbation of the fundamental mode, the stationary values of the quantum entropies of the modes are equal in this case, and they are smaller than the corresponding values in the case of a strong perturbation. The fact that the quantum entropy values are small shows that the ensemble of quantum trajectories consists of fewer terms in the present case than in the former one.

Figures 2.33 and 2.34 show the quantum dynamics of the Wigner functions of the states of the fundamental and third harmonic modes, respectively. Figures 2.33a and 2.34a represent the Wigner functions of the states of the fundamental and third harmonic modes, respectively, at the interaction time $\tau = 2$. Both functions represent a pure coherent state (the quantum entropy is equal to zero) (see Figs. 2.31 and 2.32). At this interaction time, the number of photons of the third harmonic (see Fig. 2.30) is still small, and the Wigner function of the state of the mode represents a coherent state, which is close to a vacuum state. Figures 2.33b and 2.34b represent the Wigner functions of the states of the fundamental and third harmonic modes, respectively, in the region of long interaction times ($\tau = 10$). In the region of long interaction times, the fundamental mode changes from a pure coherent state to a squeezed stationary state, the value of the quantum entropy of which is equal to 0.4. The third harmonic mode changes to a state, which has a Wigner function similar to the Wigner function of a coherent state, but the value of quantum entropy is equal to 0.4. The Wigner functions show that the system is in a stable state in the region of long interaction times.

Now we consider the quantum dynamics of the system in the case of a weak coupling of the modes (k = 0.1) and a strong external resonant perturbation (ε = 3) of the fundamental mode.

Figure 2.35 shows the quantum dynamics of the number of photons of the fundamental mode (curve a) and of an arbitrarily chosen quantum trajectory of the fundamental mode (curve b). The dynamics of the number of photons and of the arbitrarily chosen quantum trajectory coincide in the region of short interaction times ($\tau < 2$). Later, the number of photons of the arbitrarily chosen quantum trajectory fluctuates around the mean

number of photons of the fundamental mode. We explain the fact that the magnitude of fluctuations is small in comparison to the fluctuation magnitude of the arbitrarily chosen quantum trajectory shown in Fig. 2.21 by the weak coupling of the interacting modes.

Figure 2.36 shows the quantum dynamics of the number of photons of the third harmonic mode (curve a) and of an arbitrarily chosen quantum trajectory of the third harmonic mode (curve b). In the region of short interaction times ($\tau < 2$), the dynamics of the mean number of photons coincides with the dynamics of the arbitrary quantum trajectory. Later, the number of photons of the arbitrary quantum trajectory fluctuates around the mean number of photons of the mode.

Figures 2.37 and 2.38 show the dynamics of the quantum entropy of the fundamental and third harmonic modes, respectively. In the region of short interaction times ($\tau < 2$), the quantum entropy values of the modes are equal to zero. The latter observation shows that the ensemble of quantum trajectories of the system consists of a single element in this region of interaction times, which explains the coincidence of the dynamics of the mean number of photons with the dynamics of the number of photons of the arbitrarily chosen quantum trajectory of the corresponding modes. In the region of long interaction times, the dynamics of the quantum entropies of the modes changes to a stationary behaviour. In the region of long interaction times, in contrast to the case of strong coupling of the modes shown in Figs. 2.23 and 2.24, the stationary values of the quantum entropies of the modes are equal.

Figures 2.39 and 2.40 present the dynamics of the Wigner functions of the fundamental and third harmonic modes, respectively. At time of interaction $\tau \approx 2$, the fundamental mode changes from a vacuum state to a pure squeezed one. The quantum entropy of this state is equal to zero. After that, the squeezed state decays, and, in the region of long interaction times ($\tau = 10$), the fundamental mode localizes in an unstable state, the Wigner function of which is shown in Fig. 2.39b. The Wigner function represents a two-component state with a coupling of the components of the state. The quantum entropy of this state is approximately equal to 1.4. Near the interaction time $\tau = 2$, the mode of the third harmonic localizes in a pure coherent state (see Fig. 2.40a) (the quantum entropy is equal to zero) from an initial vacuum state. After that, the coherent state of the mode decays, and, in the region of long interaction times ($\tau = 10$), the mode localizes in a stationary unstable state, the Wigner function of which is shown in Fig. 2.40b.

In this case, the Wigner function has a two-component structure with a coupling between the state components. This observation contrasts with the case of a strong coupling of the modes and a strong perturbation of the fundamental mode, where the Wigner function has a cylindrical form (see Fig. 2.26e) in the region of long interaction times and where the behaviour of the system is unstable.

2.10 Quantum Dynamics of the Field in the Case of Evolution from Initial Coherent States

We study the quantum dynamics of the system when the interacting modes evolve from the initial coherent states [15]

$$a_j|\alpha_j\rangle = \alpha_j|\alpha_j\rangle,$$

$$|\alpha_j\rangle = exp(-|\alpha_j|^2/2) \sum_{n=0}^{\infty} \frac{\alpha_j^n}{(n!)^{1/2}} |n\rangle \ (j = 1,2). \qquad (2.10.1)$$

Here, α_j is the amplitude of the coherent state, and $|n\rangle$ is the Fock state. We study the dynamics of the system in the dimensionless time $\tau = \gamma_1 t$ and for the dimensionless parameters

$$\varepsilon = E/\gamma_1, \ r = \gamma_2/\gamma_1, \text{ and } k = \chi/\gamma_1 , \qquad (2.10.2)$$

when r = 1 and k = 0.3. We calculate the Wigner functions of the states of the system modes, the quantum entropy of the modes, and the mean values of the number of photons and of the quadrature amplitudes of the field using 1000 independent quantum trajectories of the optical system.

Let us first consider the dynamics of the mean value of the quadrature amplitudes $y_j = (a_j - a_j^+)/2i \ \ (j = 1,2)$ of the interacting modes of the optical system in the case of evolution from initial coherent states of the fundamental mode with the state amplitude $\alpha_1 = i$ and of the third harmonic mode with the state amplitude $\alpha_1 = -i$. Note that the phase of the classical perturbation field of the fundamental mode is considered to be zero. First, we study the dynamics of the system in the case of strong perturbation fields ($\varepsilon = 3$). Figure 2.41 presents the dynamics of the mean value of the quadrature amplitude of the fundamental mode in the above-mentioned case. The quadrature amplitude begins its evolution from its initial value and oscillates around the zero value. In the region of large interaction times, the oscillation amplitude tends gradually to zero. Figure 2.42 presents the dynamics of the quadrature amplitude of the third harmonic mode. It begins its evolution from the initial value and, similarly to the behaviour of the quadrature amplitude of the fundamental mode, oscillates around the zero value and tends to zero in the region of large

interaction times. The oscillation of the quadrature amplitude of the third harmonic mode is less than that of the fundamental mode.

For the above-considered case of system dynamics, the Wigner functions of the state of the fundamental and third harmonic modes also have decaying oscillations. Figure 2.43 presents the dynamics of the Wigner function of the state of the fundamental mode for the above-mentioned case of optical system evolution. The Wigner functions of the state of the fundamental mode are presented for interaction times, at which the quadrature amplitude of this mode takes peak values. Figure 2.43a presents the Wigner function of the initial coherent state of the fundamental mode with the amplitude $\alpha_1 = i$ of the state. Figure 2.43b presents the Wigner function of the state of the fundamental mode at τ = 2.35. At this moment in time, the quadrature amplitude of the mode has a maximal negative value, which is approximately equal to –1. The Wigner function is also mainly localized in the region of negative values of the y variable. Figure 2.43c presents the Wigner function of the state of the fundamental mode at τ = 4.3. For this moment, the mean value of the quadrature amplitude is the maximal positive value $y_1 \approx 0.35$, and the Wigner function is somewhat more strongly localized in the region of positive values of the y variable. At $\tau \approx 7.5$, the mean value of the quadrature amplitude of the fundamental mode takes again the maximal negative value $y_1 \approx 0.12$. It is rather close to zero, and the Wigner function of the fundamental mode at τ = 7.5 is already almost symmetric with respect to the zero value of the y variable (Fig. 2.43d).

The Wigner function of the state of the third harmonic mode also oscillates for the aforesaid case of system evolution in the (x, y) plane, similarly to the Wigner function of the state of the fundamental mode. This temporal

behaviour of the Wigner function of the third harmonic mode is presented in Fig. 2.44. Here, Fig. 2.44a represents the Wigner function of the initial coherent state with the amplitude $\alpha_2 = -i$ of the state. Figures 2.44b to 2.44d present the Wigner functions of the states of the third harmonic mode at $\tau = 2.45$, 4.3, and 7.5, respectively. At these times, the mean value of the y_2 quadrature amplitude takes peak values. At $\tau = 2.45$, the quadrature amplitude of the mode has a positive maximal value ($y_1 \approx 0.6$) and the Wigner function of the state of the third harmonic mode is much more localized in the region of positive values of the y variable (Fig. 2.44b). At $\tau = 4.3$, the quadrature amplitude has a maximal negative value that is approximately equal to –0.2 and the Wigner function of the state of this mode that is presented in Fig. 2.44c is somewhat more localized in the region of negative values of the y variable. At this moment, the Wigner function of the third harmonic has the shape of a cylinder that is somewhat broken in the region of positive values of the y variable. This means that this function is somewhat more localized in the region of negative values of the y variable. At $\tau = 7.5$, the y_2 external resonant quadrature amplitude takes the maximally positive value; it is so close to zero ($y_2 \approx 0.05$) that it has almost no effect on the localization of the Wigner function in the (x, y) plane. At this moment, the Wigner function of the third harmonic mode has a cylindrical shape and is almost symmetrically localized with respect to the zero value of the y variable (Fig. 2.44b).

Similarly to the case discussed above, it was shown in [16] (see also Section 9 in Chapter 1) that, for the process of intracavity generation of the second harmonic in the region of unstable behavior of the system and in the case of evolution of the interacting modes from initial coherent states,

the quadrature amplitudes and Wigner functions of the state of the modes can have oscillations, which decay in time.

In contrast to the behavior of the mean value of the quadrature amplitude y_j $(j = 1,2)$ of the interacting modes and of the Wigner function of the state of the fundamental and third harmonic modes, the dynamics of the mean value of the number of photons, as well as of of the quantum entropy of these modes in the above-mentioned region of system evolution, also have no oscillations in the case of the aforesaid initial states of the system modes. Figure 2.45 presents the dynamics of the mean value of the number of photons of the fundamental (curve a) and third harmonic (curve b) modes for the above-mentioned region of evolution of the system and for the evolution of the interacting modes from the above-presented initial coherent states. Both curves have no oscillations. The drop in the mean value of the number of photons of the third harmonic mode in the region of small interaction times is not connected with the unstable behaviour of the system. This behaviour is explained by the fact that the dissipation of the energy of the initial state of the third harmonic mode at this interaction time occurs faster than the ingress of energy into the mode due to the interaction with the fundamental mode, because the energy of the fundamental mode is rather small for these interaction times (curve a).

Figure 2.46 presents the dynamics of the quantum entropy of the fundamental (curve a) and third harmonic (curve b) modes for the above case. Neither curve has oscillations. The stationary quantum entropy values of the fundamental and third harmonic modes are not equal.

The mean values of both quadrature amplitudes y_j $(j = 1,2)$ of the modes in the region of unstable interaction of the system oscillate when at least

one amplitude of the initial coherent states of the interacting modes has an imaginary part or is imaginary. Figures 2.47 and 2.48 present the temporal behaviour of the mean values of quadrature amplitudes of the fundamental and third harmonic modes, respectively, in the above-mentioned interaction region and in the case of evolution of the system modes from initial coherent states with the state amplitudes $\alpha_1 = i$ and $\alpha_2 = -1$. The mean values of both quadrature amplitudes have oscillations, which decay in time. The Wigner functions of the state of these modes also oscillate. Oscillations of the mean values of the quadrature amplitudes disappear when the amplitudes of the initial coherent states of both modes become real.

When the system begins its evolution from initial coherent states with real state amplitudes, the mean values of the quadrature amplitudes y_j $(j = 1, 2)$ have no oscillations and are represented by the straight lines $y_j(\tau) = 0$. In this case, the Wigner functions also do not oscillate and are symmetric with respect to the zero value of the y variable.

Figure 2.49 presents the quantum entropy dynamics of the fundamental (curve a) and third harmonic (curve b) modes in the above-mentioned region of system evolution and in the case of evolution of the interacting modes from initial coherent states with the amplitude of the states $\alpha_1 = 1$ and $\alpha_2 = -1$. Comparing Figs. 2.49 and 2.46, one can see that the stationary values of the quantum entropies of the corresponding modes are equal. However, the quantum entropies of the interacting modes in the case of evolution from initial coherent states with real amplitudes of the states reach their stationary values faster than in the case of evolution from initial states with imaginary amplitudes of the state. The mean value of the

number of photons of the initial states of the interacting modes equals unity in both cases.

Decaying oscillations of the quadrature amplitudes y_j $(j = 1,2)$ disappear when the system transitions from an unstable state to a stable one. The system can be brought to a stable state by reducing the perturbation of the fundamental mode from the outside or by decreasing the coefficient of mode coupling. Figures 2.50 and 2.51 present the dynamics of the quadrature amplitudes of the fundamental y_1 and third harmonic mode y_2 modes, respectively, for $\alpha_1 = i$ and $\alpha_2 = -i$ and at a weak perturbation of the fundamental mode (ε = 1). Neither curve had oscillations. This is connected with the fact that the system is in the stable region of interaction. The Wigner functions of the fundamental and third harmonic modes for this case in the region of large interaction times τ = 10 are presented in Figs. 2.52 and 2.53, respectively. They show that the modes are in stable states. The fundamental mode is in a squeezed state, and the third harmonic is in a state close to the vacuum one.

2.11. Correlation Dynamics of Quadrature Amplitude Fluctuations and Entangled States

In the present section, we use the Monte Carlo wave function method to investigate the correlation between fluctuations in quadrature amplitudes of the fundamental and third harmonic modes in the case of evolution of both modes from initial vacuum states. We show the possibility of entanglement of the states of the interacting modes of the system in the region of its unstable behaviour.

We investigate the system dynamics in terms of dimensionless time ($\tau = \gamma_1 t$) and dimensionless system parameters ($k = \chi/\gamma_1$ and $\varepsilon = E/\gamma_1$) for

the case of equal mode damping coefficients in the cavity ($\gamma_1 = \gamma_2$). All calculations were made for system evolution from initial vacuum states of the fundamental and third harmonic modes. To find the dynamics of each correlation function of fluctuations in the quadrature amplitudes and Wigner functions of the stationary state of the system, we used 1000 independent quantum trajectories of the optical system.

Let us investigate the dynamics of the normalized correlation function of fluctuations in the quadrature amplitudes of the fundamental and third harmonic modes:

$$g(t) = \frac{\langle((x_1(t)-<x_1(t)>)+(x_2(t)-<x_2(t)>))^2\rangle}{(<x_1(t)^2>-<x_1(t)>^2)+(<x_2(t)^2>-<x_2(t)>^2)}. \qquad (2.11.1)$$

Here, $x_i = (a_i + a_i^+)/2$ (i = 1, 2) are the quadrature amplitudes of the fundamental and third harmonic modes, respectively. Formula (2.11.1) can be presented in the form

$$g(t) = 1 + \frac{2(<x_1(t)x_2(t)>-<x_1(t)><x_2(t)>)}{<x_1(t)^2>-<x_1(t)>^2+<x_2(t)^2>-<x_2(t)>^2}. \qquad (2.11.2)$$

In the absence of correlation between fluctuations of quadrature amplitudes of the interacting modes, correlation function (2.11.2) tends to unity.

Let us analyze the dynamics of the correlation function of fluctuations of the quadrature amplitudes. The dynamics of the correlation function of the quadrature amplitudes of the fundamental and third harmonic modes is depicted in Fig. 2.54. This function is plotted for the case of weak mode coupling (k = 0.1) and a strong perturbation of the fundamental mode (ε = 3). At the beginning of system evolution (τ = 0), both interacting modes occupy vacuum states and there is no correlation between fluctuations of

the quadrature amplitudes. The correlation function is equal to unity. After some time of evolution, the state of the system changes to an unstable stationary one [6] and fluctuations of the quadrature amplitudes of the interacting modes start to grow. This can be seen from the Wigner functions of the stationary states of these modes, which are presented in Fig. 2.55 for the same parameter values. The fluctuations of the quadrature amplitudes of the interacting modes are correlated, leading to the correlation function becoming slightly smaller than unity. This shows that there appeared some entanglement of the states of the fundamental and third harmonic modes.

The dynamics of the correlation function of fluctuations of the quadrature amplitudes of the interacting modes for the same value of perturbation of the fundamental mode as in the previous case ($\varepsilon = 3$), but a relatively large value of the mode coupling coefficient ($k = 0.5$), is shown in Fig. 2.56. In this case, the steady-state value of the correlation function is much smaller than unity (in contrast to the previous case). This is a manifestation of increased entanglement of the states of the fundamental and third harmonic modes. Figure 2.57 illustrates the Wigner functions of the states of the fundamental (Fig. 2.57a) and third harmonic (Fig. 2.57b) modes for this case. The plots show that fluctuations of the quadrature amplitudes of the interacting modes became larger. This leads to a decrease in the correlation function and to an increase in the entanglement of the states of the interacting modes.

Any further increase in the mode coupling coefficient does not lead to a decrease in the correlation function of the quadrature amplitudes but, on the contrary, results in its increase: the value of the correlation function tends to unity, which indicates a decrease in the correlation of fluctuations

and a decrease in the entanglement of the states of the interacting modes. The dynamics of the correlation function of the quadrature amplitudes for the coupling coefficient $k = 2$ and perturbation amplitude $\varepsilon = 3$ (just as in the previous case) is illustrated in Fig. 2.58. It can be seen that the steady-state value of the correlation function is close to unity. The Wigner functions of the stationary states of the fundamental and third-harmonic modes are presented in Fig. 2.59. They show that fluctuations of quadrature components became smaller relative to the previous case.

The correlation of fluctuations of the quadrature amplitudes not only decreases upon a further increase in the mode coupling coefficient but also upon a decrease in the perturbation amplitude of the fundamental mode. The dynamics of the correlation function of fluctuations of the quadrature amplitudes of the interacting modes for the mode coupling coefficient $k = 0.5$ and perturbation amplitude of the fundamental mode $\varepsilon = 1$ is shown in Fig. 2.60. The only difference between this case and the case with the correlation function presented in Fig. 2.56, which corresponds to the maximum correlation between fluctuations of the quadrature amplitudes, is the small perturbation amplitude of the fundamental mode. This leads to a decrease in the correlation between fluctuations of the quadrature amplitudes of the interacting modes in the steady-state regime (the correlation function in this interval is relatively close to unity) and a corresponding decrease in the entanglement of the states of these modes. The corresponding Wigner functions of the states of the fundamental and third-harmonic modes of the stationary state of the field are illustrated in Fig. 2.61. They demonstrate that the fluctuations of the quadrature amplitudes of these modes became smaller.

References

1. S. T.Gevorkyan, G. Yu. Kryuchkyan, and K. V. Kheruntsyan, "Noise, Instability, and Squeezing in Third-Harmonic Generation," *Optics Comm.* 134 (1997): 440–446.
2. S. T. Gevorkyan and M. S. Gevorkyan, “Fluctuations in the Number of Photons above the Bifurcation Point in the Process of Third Harmonic Generation,” *Optics and Spectroscopy* 107, no. 1 (2009): 122–128.
3. S. T. Gevorkyan, "Quantum Superposition States in Third Harmonic Generation," *Phys. Rev A* 58, no. 6 (1998): 4862–4867.
4. S. T. Gevorgyan, “Critical Phenomenon and Quantum Fluctuations in Third Harmonic Generation,” Proceedings of NAS of Armenia, Physics 33, no. 3 (1998): 103–108. [In Russian]
5. S. T. Gevorkyan, “Schroedinger Cat-Like States in Third Harmonic Generation,” in Proceedings Conference on Laser Physics-97, Ashtarak, Armenia, 1997 (Oct. 20-24), 78–83.
6. S. T. Gevorkian and M. S. Gevorkian, “Quantum Dynamics of Formation of an Unstable Field State in the Process of Intracavity Third Harmonic Generation,” *Optics and Spectroscopy* 112, no. 3 (2012): 457–464.
7. S. T. Gevorgyan and M. S. Gevorgyan, “Quantum Description of the Unstable Behavior of the Intracavity Third Harmonic Generation Process,” *Armenian Journal of Physics* 5, no. 3 (2012): 122 –140.
8. M. Gevorgyan and S. Gevorgyan, “Quantum Dynamics of Interacting Modes in Intracavity Third Harmonic Generation

Process" *ISRN optics* 2012, Article ID 476817 (2012), doi: 10.5402/476817(2012).

9. S. T. Gevorgyan and M. S. Gevorgyan, "Evolution Dynamics of Initial Coherent States of a Field in an Unstable Region of Behavior in the Process of Intracavity Third Harmonic Generation," *Optics and Spectroscopy* 113, no. 5 (2012): 522–529.
10. M. S. Gevorgyan, "Correlation of Fluctuations of the Quadrature Amplitudes of Interacting Modes in the Instability Region of Intracavity Third Harmonic Generation," *Optics and Spectroscopy* 116, no. 4 (2014): 661–665.
11. C. W. Gardiner, "Handbook of Stochastic Methods" (Springer, Berlin, 1986).
12. S.M. Yermakov, G.A. Mikhaylov. *Statistical Modeling* (Moscow: Nauka, 1982). [in Russian]
13. K. Molmer, Yv. Castin, and J. Dalibard, "Monte Carlo Wave-Function Method in Quantum Optics," *JOSA B* 10 (1993): 524–538.
14. J. R. Johansson, P. D. Nation, and F. Nori, "QuTiP 2: A Python Framework for the Dynamics of Open Quantum Systems," *Comp. Phys. Comm.* 184 (2013): 1234.
15. R. J. Glauber, "Coherent and Incoherent States of the Radiation Field," *Phys Rev* 131 (1963): 2766.
16. S. T. Gevorgyan, G. Yu. Kruchkyan, N. T. Muradyan, "Quantum Fluctuations in Unstable Dissipative Systems," *Phys. Rev. A* 61, 043805 (2000).

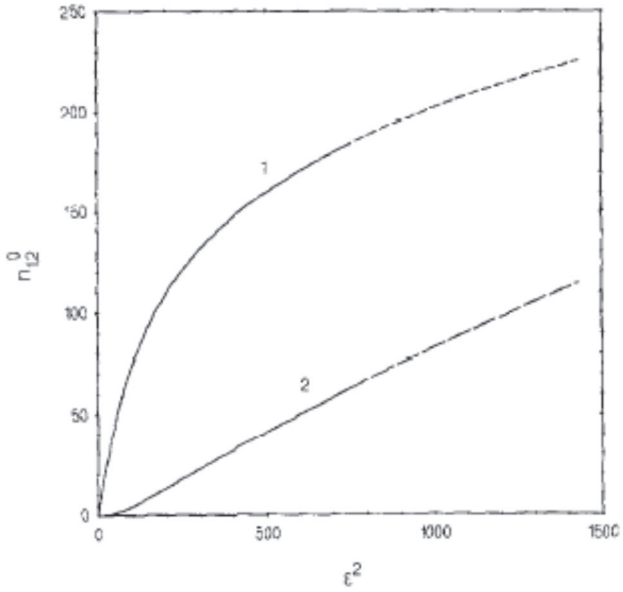

Fig. 2.1. Semiclassical steady-state photon numbers for the fundamental and third harmonic modes n_1^0 (curve *1*) and n_2^0 (curve *2*) versus the pump intensity parameter $\boldsymbol{\varepsilon^2}$ for $k = 10^{-5}$ and $r = 1$. The solid parts of the curves correspond to the stable solutions, while the broken parts describe the unstable region.

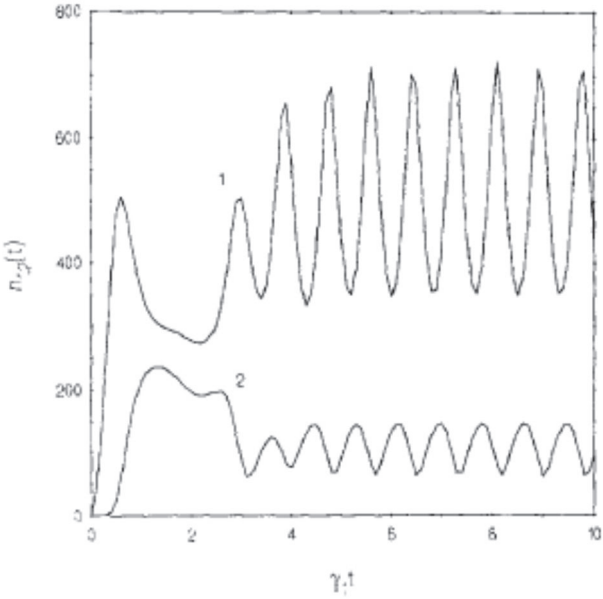

Fig. 2.2. Demonstration of the self-pulsing behaviour of the fundamental and third harmonic mode photon numbers $n_1(t)$ (curve *1*) and $n_2(t)$ (curve *2*) versus $\gamma_1 t$; the numerical solution to Eqs. (2.1.15) in the semiclassical approximation for $k = 10^{-5}$, $r = 1$, and $\varepsilon = 60$ and the initial conditions $\alpha_1(0) = 1 + i$ and $\alpha_2(0) = 0$.

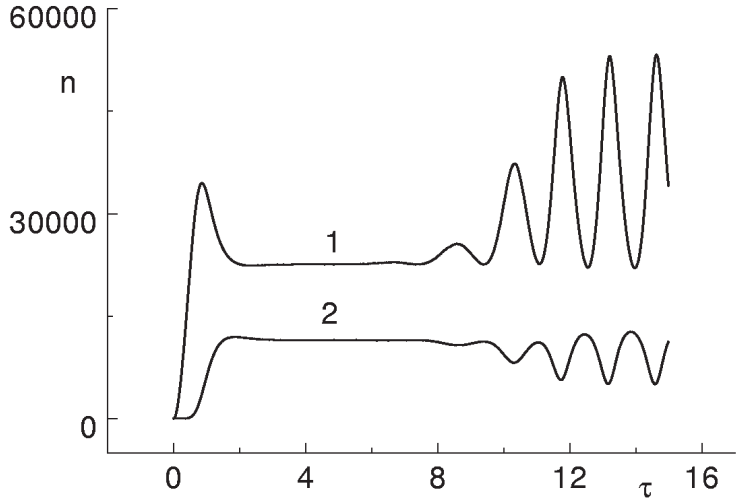

Fig. 2.3. One realization of the dynamics of the number of photons (*1*) of the fundamental mode and (*2*) of the third harmonic in the case of evolution of the system from the initial values $\alpha_1(0) = i$, $\alpha_2(0) = i$, $\beta_1(0) = \alpha_1^*(0)$, and $\beta_2(0) = \alpha_2^*(0)$ of the field amplitudes. $\varepsilon = 380$, $k^2 = 10^{-9}$, and $r = 1$.

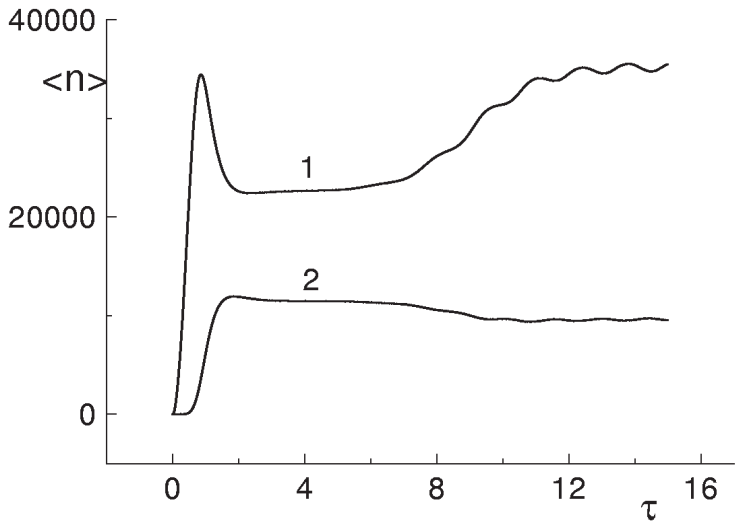

Fig. 2.4. Dynamics of the average number of photons (*1*) of the fundamental mode and (*2*) of the third harmonic in the case of evolution of the system from an initial state with a Gaussian distribution of stochastic amplitudes of the field modes $\varepsilon = 380$, $k^2 = 10^{-9}$, and $r = 1$. To obtain each of these curves, 1000 independent solutions of the set of equations (2.4.5) were used.

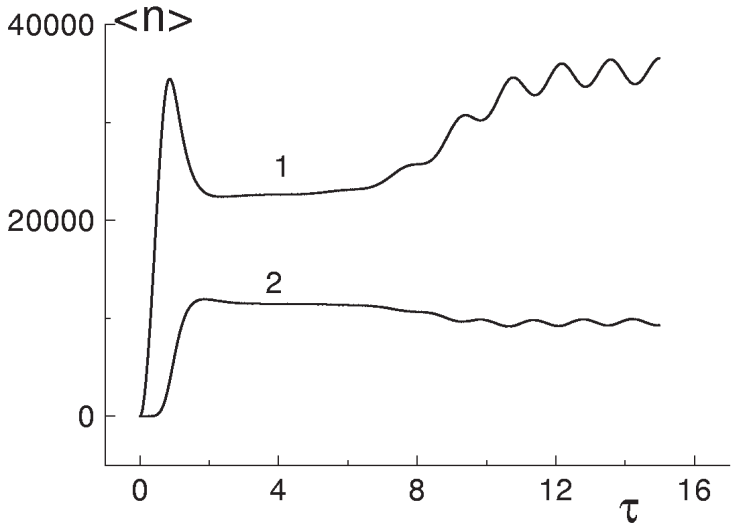

Fig. 2.5. Dynamics of the average number of photons (*1*) of the fundamental mode and (2) of the third harmonic in the case of evolution of the system from the initial values $\alpha_1(0) = i$, $\alpha_2(0) = i$, $\beta_1(0) = \alpha_1^*(0)$, and $\beta_2(0) = \alpha_2^*(0)$ of stochastic amplitudes of the field modes. $\varepsilon = 380$, $k^2 = 10^{-9}$, and $r = 1$. To obtain each of these curves, 1000 independent solutions to the set of equations (2.4.5) were used.

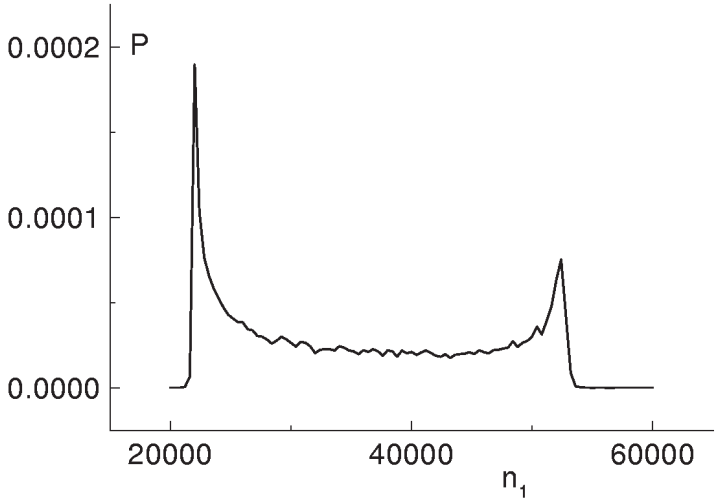

Fig. 2.6. Distribution function for the number of photons of the fundamental mode in the range of large interaction times (τ = 15) and in the case of evolution of the system from an initial state with a Gaussian distribution of stochastic amplitudes of the field modes. $\varepsilon = 380$, $k^2 = 10^{-9}$, and $r = 1$. The curve was obtained using 30 000 independent solutions to the set of equations (2.4.5).

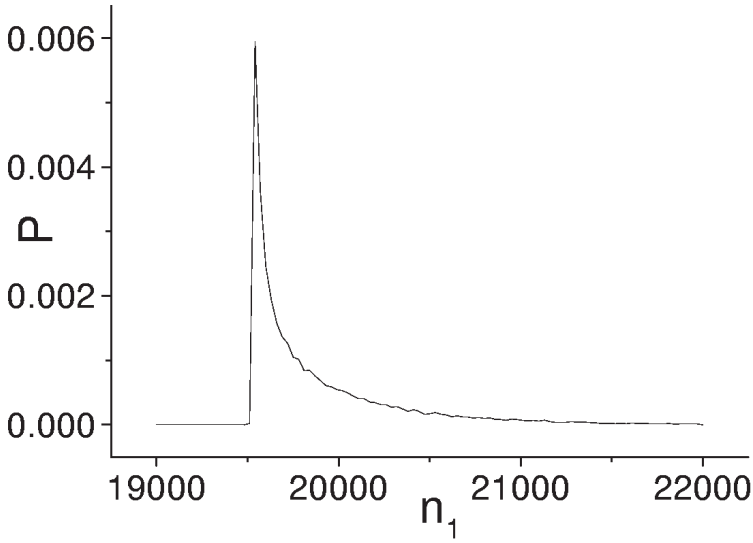

Fig. 2.7. Distribution function for the number of photons of the fundamental mode close to the bifurcation point of the optical system and in the range of large interaction times (τ = 15). The function was calculated for the evolution of the system from an initial state with a normal distribution of stochastic amplitudes of the fundamental mode and of the third harmonic. $k^2 = 10^{-9}$ and $r = 1$. To calculate the function, 30 000 independent realizations of the set of Langevin equations were used.

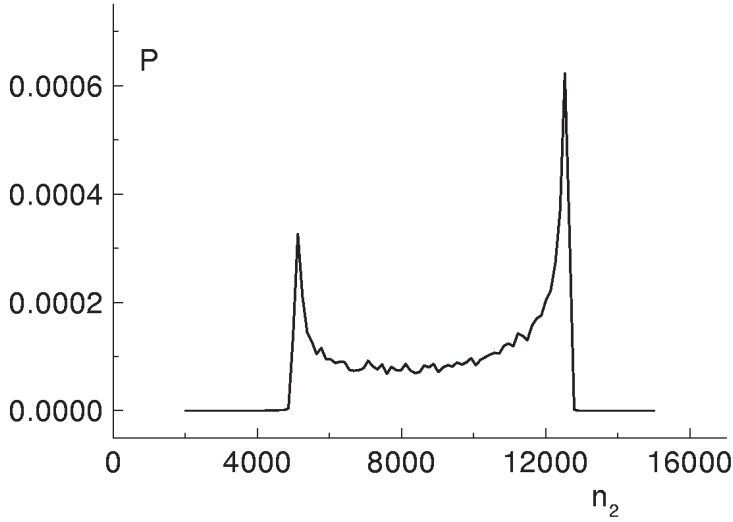

Fig. 2.8. Distribution function for the number of photons of the third harmonic in the range of large interaction times (τ = 15) and in the case of evolution of the system from an initial state with a Gaussian distribution of stochastic amplitudes of the field modes. $\varepsilon = 380$, $k^2 = 10^{-9}$, and $r = 1$. The curve was obtained using 30 000 independent solutions of the set of equations (2.4.5).

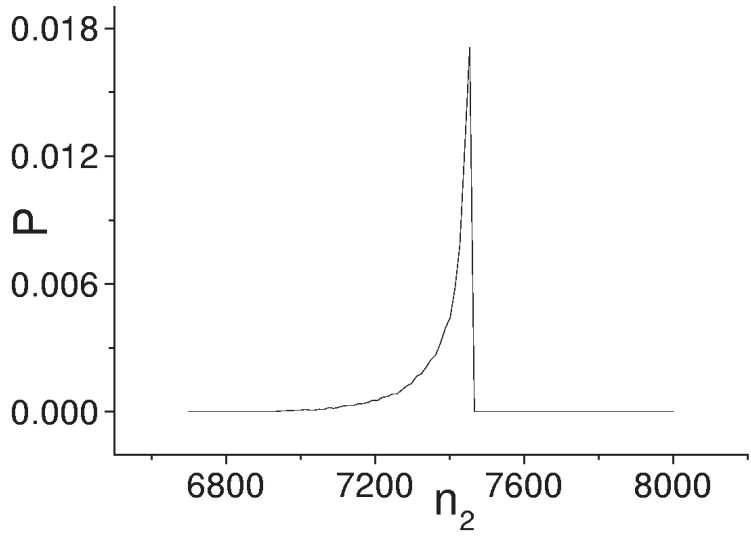

Fig. 2.9. Distribution function for the number of photons of the third harmonic close to the bifurcation point of the optical system ($\varepsilon = 300$) and in the range of large interaction times ($\tau = 15$). The function was calculated for the evolution of the system from an initial state with a normal distribution of stochastic amplitudes of the fundamental mode and of the third harmonic. To calculate the function, 30 000 independent realizations of the set of Langevin equations were used.

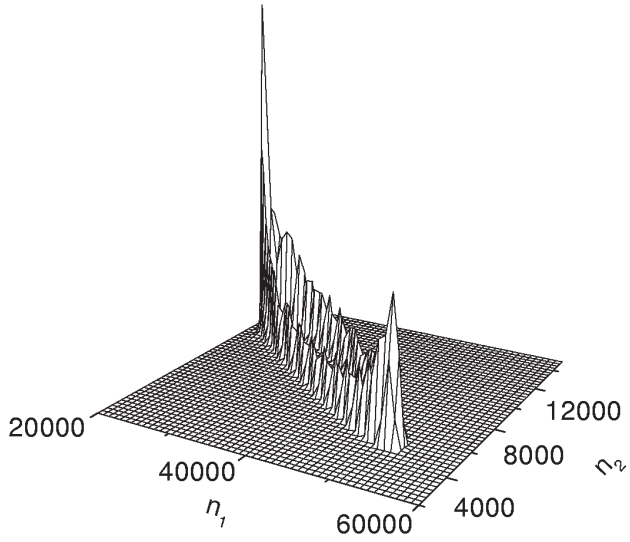

Fig. 2.10. Joint distribution function of the number of photons of the fundamental mode and of the third harmonic in the range of large interaction times (τ = 15) and in the case of evolution of the system from an initial state with a Gaussian distribution of stochastic amplitudes of the field modes. $\varepsilon = 380$, $k^2 = 10^{-9}$, and $r = 1$. The function was calculated using 50 000 independent realizations of the set of equations (2.4.5).

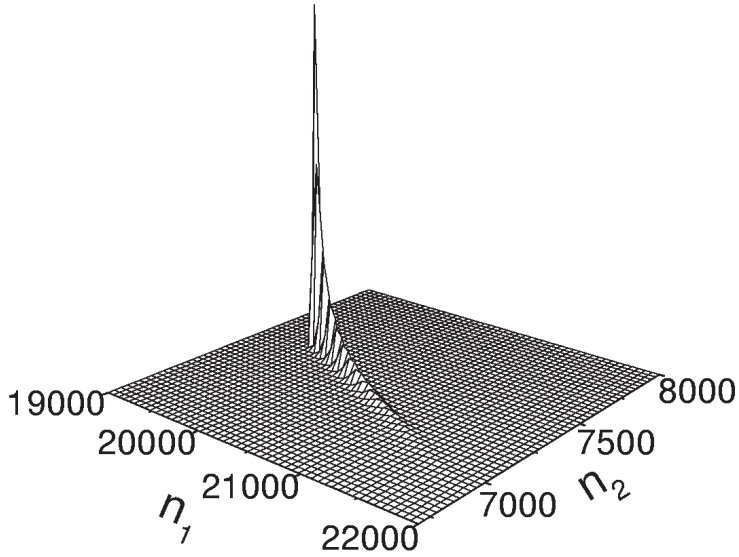

Fig. 2.11. Joint distribution function of the number of photons of the fundamental mode and of the third harmonic close to the bifurcation point of the optical system (ε =300) and in the range of large interaction times (τ = 15). The function was calculated in the case of evolution of the system from an initial state with a normal distribution of stochastic amplitudes of the fundamental mode and of the third harmonic. To calculate this function, 30 000 independent realizations of the set of Langevin equations were used.

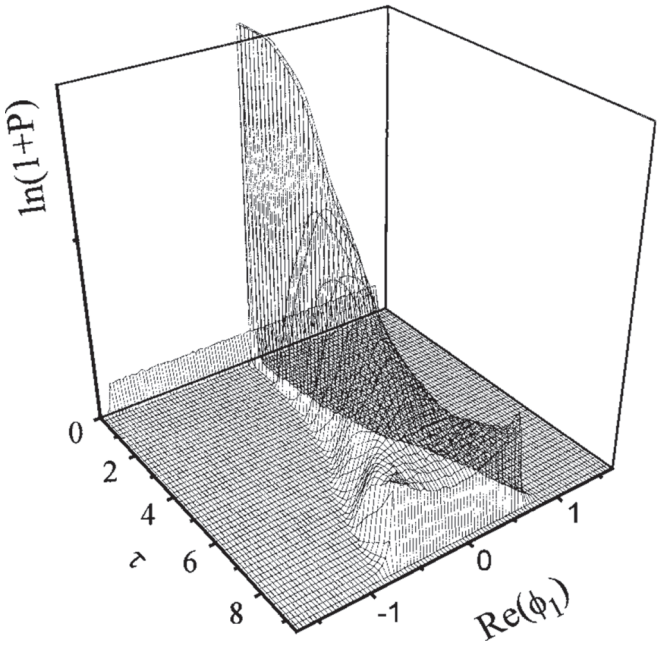

Fig. 2.12. Dynamics of the distribution function of the phase for the fundamental mode in the case of an initial Gaussian state of both modes and for the following parameter values: $\varepsilon = 380$, $k^2 = 10^{-9}$, and $r = 1$. The function is calculated with the help of 100 000 independent trajectories of Eqs. (2.4.5).

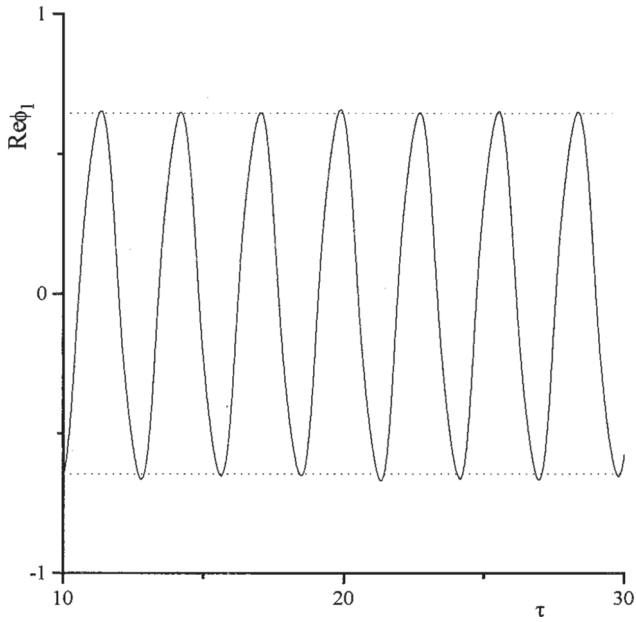

Fig. 2.13. Realization of the phase for the fundamental mode. Dashed lines lead to the two most probable values of the phase. The function is calculated for the case of the parameters in Fig. 2.12.

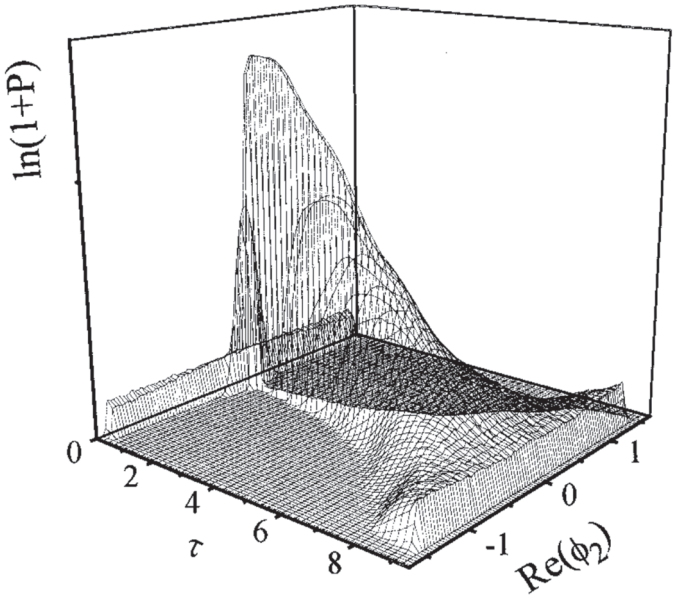

Fig. 2.14. Phase distribution dynamics for the third harmonic in the case of an initial Gaussian state of both modes and for the parameter values in Fig. 2.12 (100 000 trajectories).

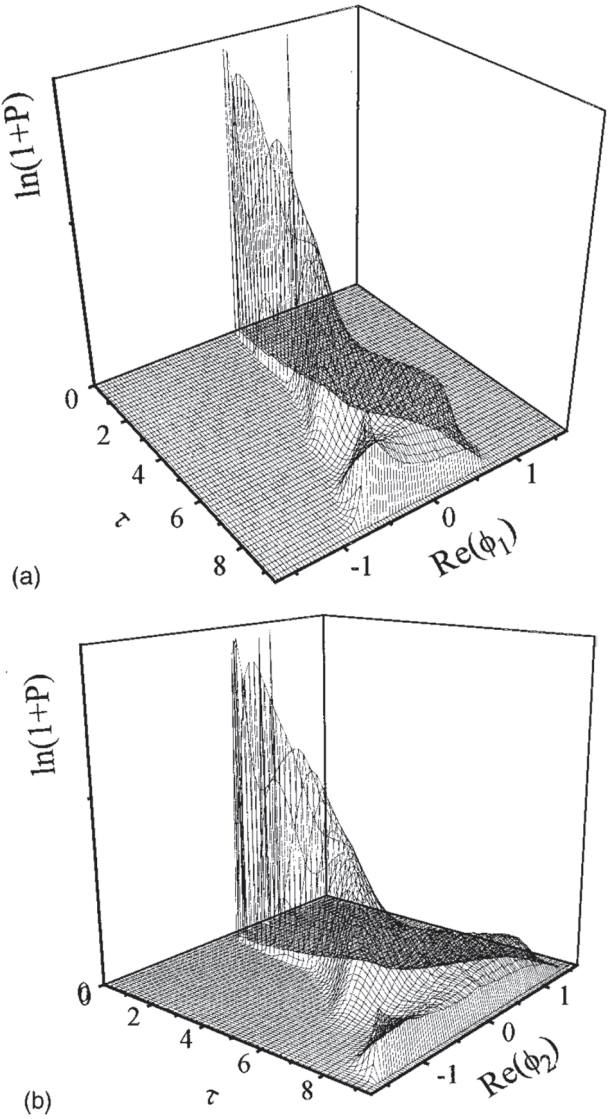

Fig. 2.15. Dynamics of the distribution function of the phase for the fundamental mode (a) and third harmonic (b) in the case of a coherent initial state of both modes (100 000 trajectories).

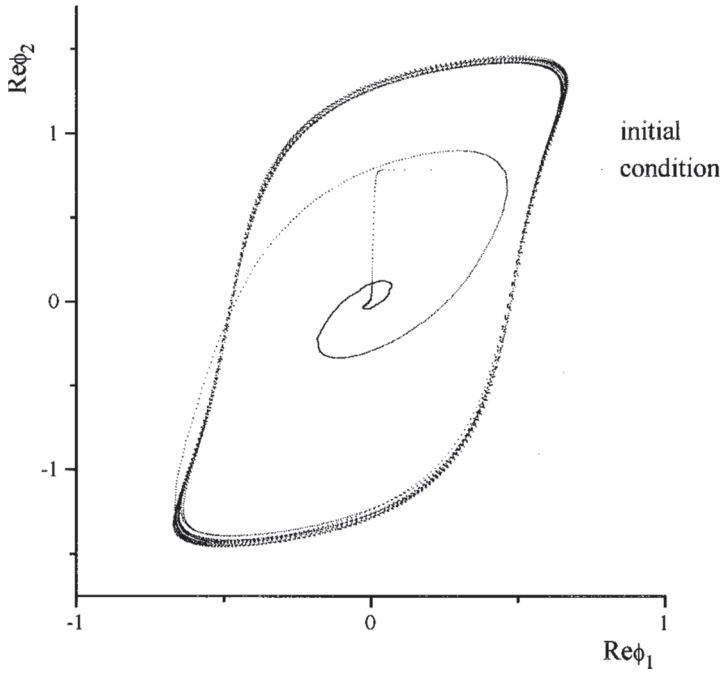

Fig. 2.16. Trajectory of the optical system in the phase space $(Re\,\phi_1, Re\,\phi_2)$. The trajectory is shown in the interval $(0{,}55)$ of time τ. The density of points is proportional to the stay time of the optical system in this area of phase space. The temporal interval between neighboring points is $\Delta\tau = 0.01$.

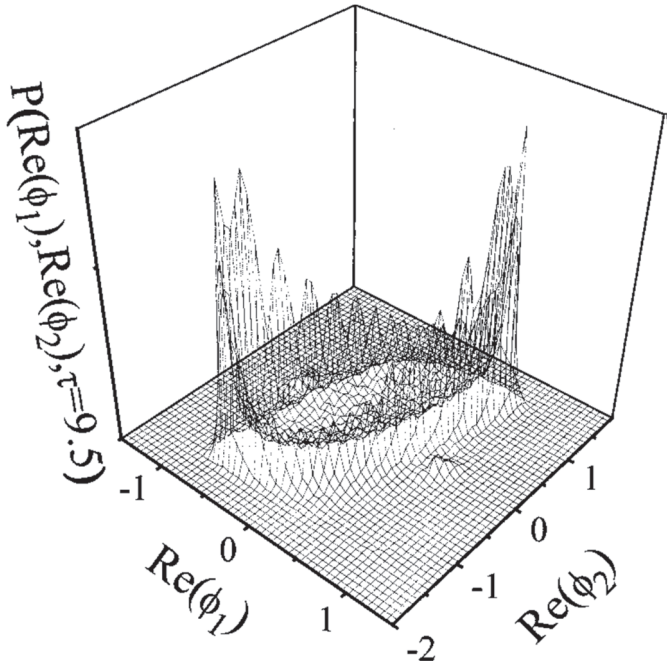

Fig. 2.17. Joint distribution function of phases for the fundamental and third harmonic modes at the moment $\tau = 9.5$ and in the case of an initial Gaussian state of both modes. The function is calculated for the parameter values in Fig. 2.12 based on 100 000 trajectories.

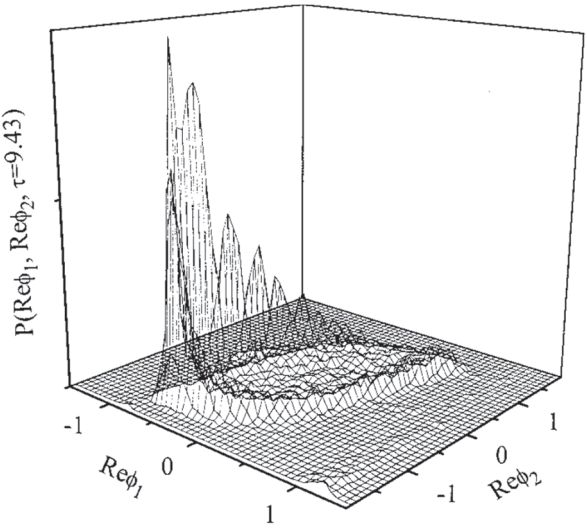

Fig. 2.18. Joint distribution function of phases for the fundamental mode and third harmonic at the moment $\tau = 9.43$ and in the case of a coherent initial state of both modes (100 000 trajectories).

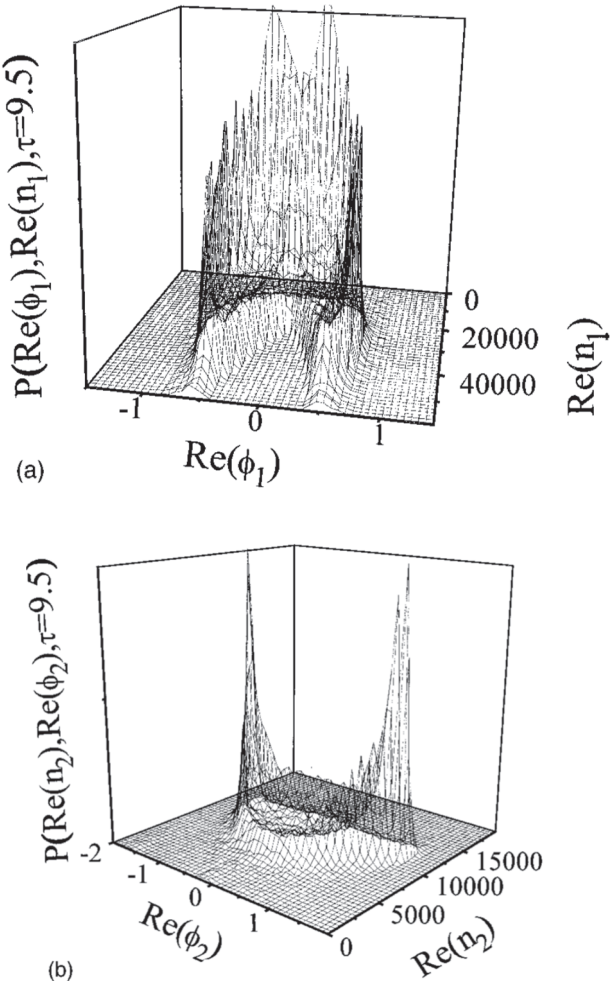

Fig. 2.19. Joint distribution function of the photon number and phase for the fundamental mode (a) and third harmonic (b) at the moment $\tau = 9.5$ and for the parameter values in Fig. 2.12 (100 000 trajectories).

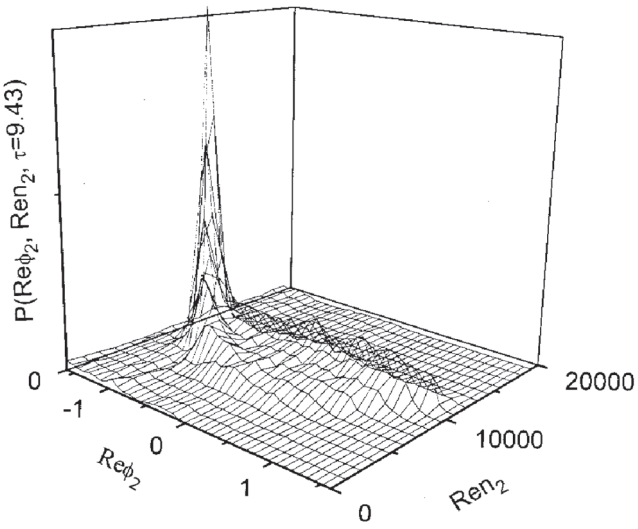

Fig. 2.20. Joint distribution function of the photon number and phase for the third harmonic at the moment $\tau = 9.43$ and in the case of a coherent initial state of both modes (100 000 trajectories).

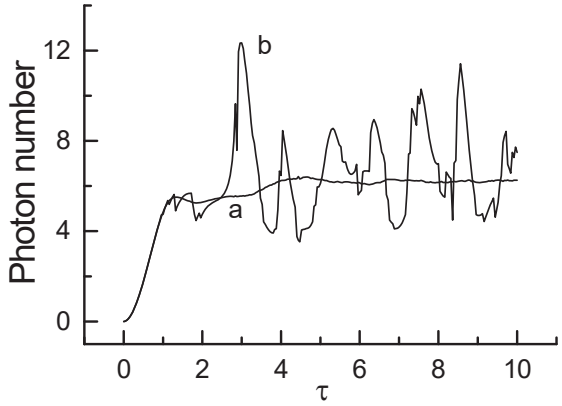

Fig. 2.21. Dynamics of the mean number of photons (curve a) and of the number of photons of an arbitrarily chosen quantum trajectory (curve b) of the fundamental mode for the system parameter values ε = 3 and k = 0.3.

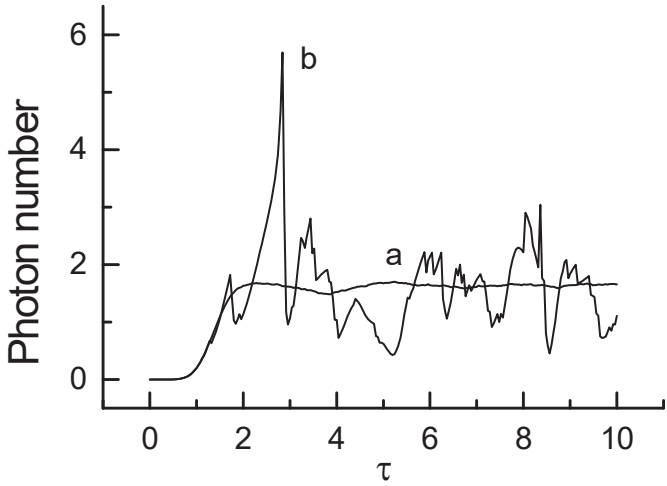

Fig. 2.22. Dynamics of the mean number of photons (curve a) and the number of photons of an arbitrarily chosen quantum trajectory (curve b) of the third harmonic mode; ε = 3 and k = 0.3.

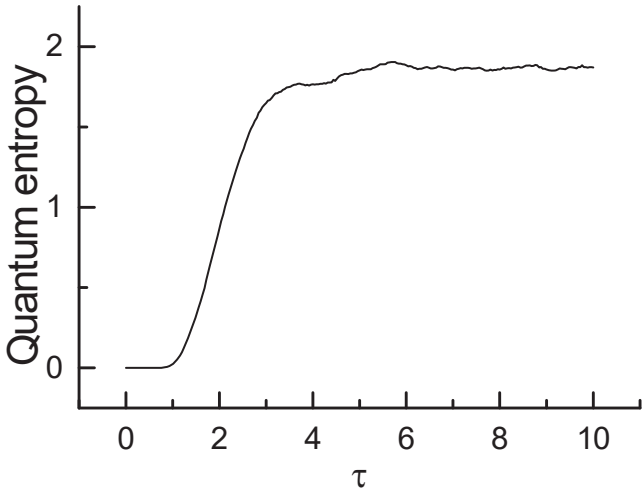

Fig. 2.23. Dynamics of the quantum entropy of the fundamental mode for the system parameter values ε = 3 and k = 0.3.

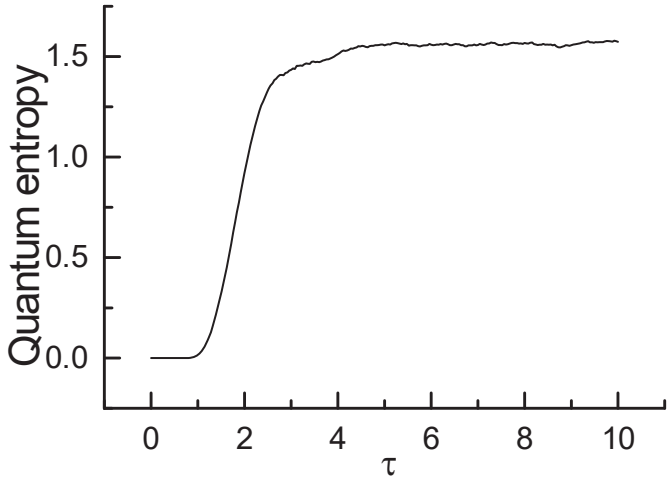

Fig. 2.24. Dynamics of the quantum entropy of the third harmonic mode for the system parameter values $\varepsilon = 3$ and $k = 0.3$.

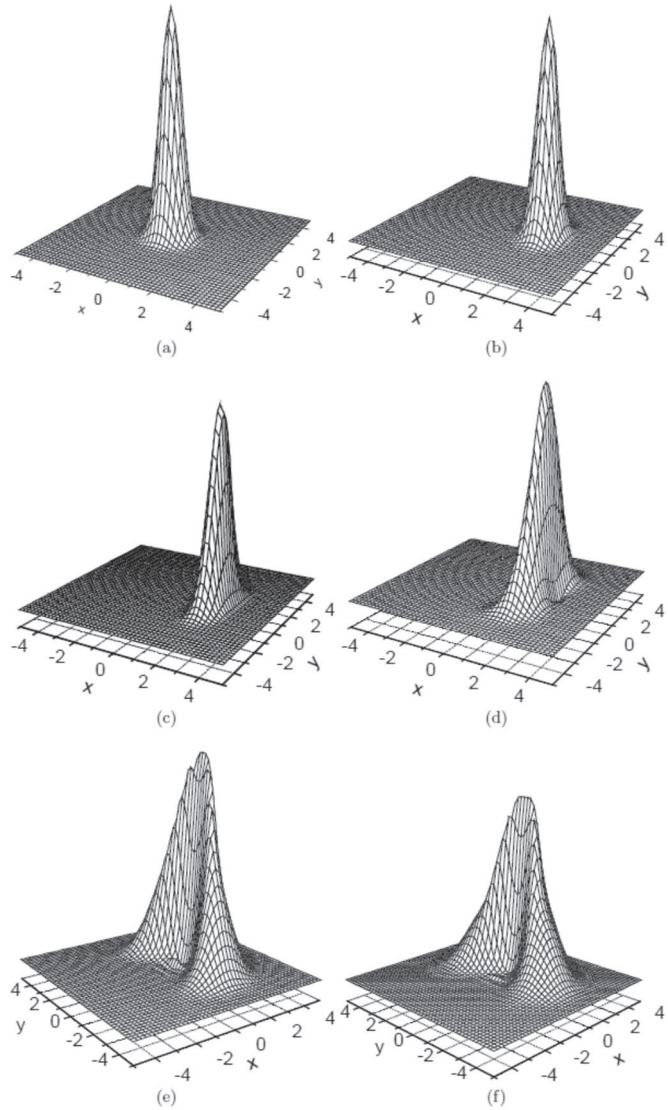

Fig. 2.25. Dynamics of the Wigner function of the state of the fundamental mode for the system parameter values ε = 3 and k = 0.3; (b) to (f) illustrate the Wigner functions of the fundamental mode at the mode interaction times $\tau = 1$, $\tau = 1.5$, $\tau = 2$, $\tau = 3$, and $\tau = 10$, respectively.

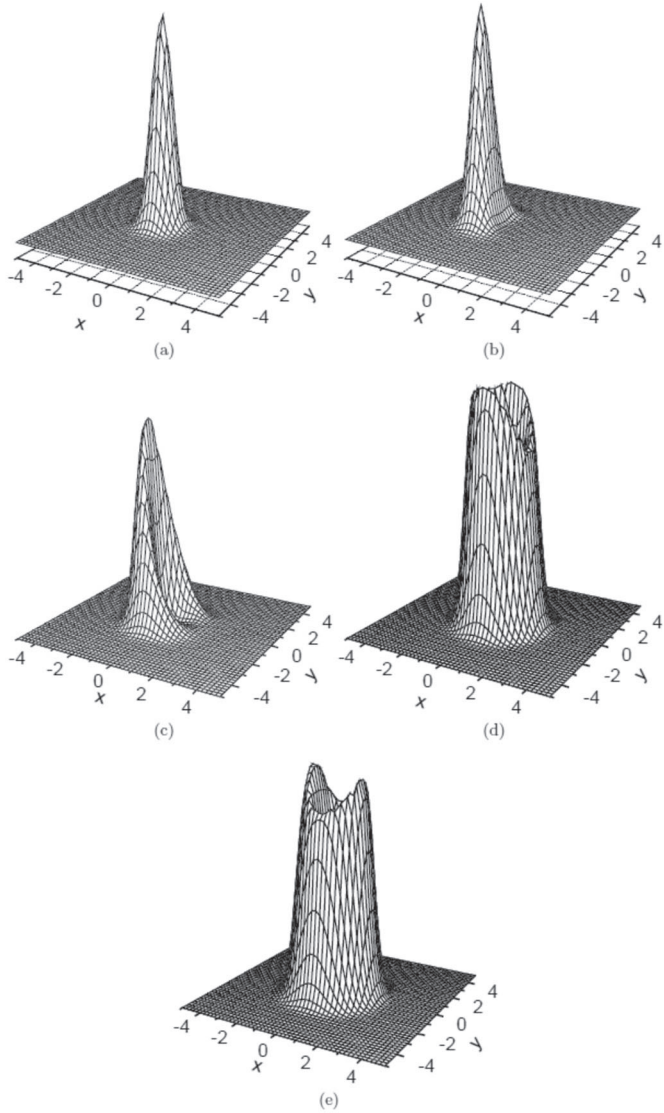

Fig. 2.26. Dynamics of the Wigner function of the state of the third harmonic for the system parameter values ε = 3 and k = 0.3; (a) to (e) illustrate the Wigner functions of the third harmonic mode at the interaction times $\tau = 1$, $\tau = 1.5$, $\tau = 2$, $\tau = 3$, and $\tau = 10$, respectively.

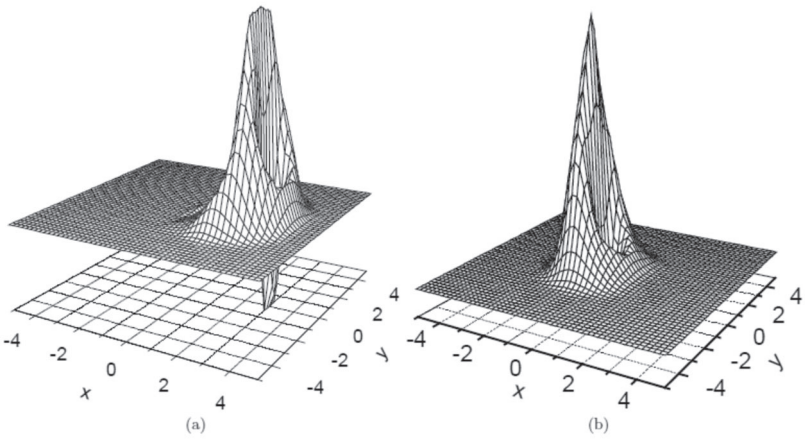

Fig. 2.27. Wigner functions of the states of the fundamental mode (a) and the third harmonic mode (b) of an arbitrary quantum trajectory of the optical system in the region of long interaction times ($\tau = 10$) and for the system parameter values ε = 3 and k = 0.3.

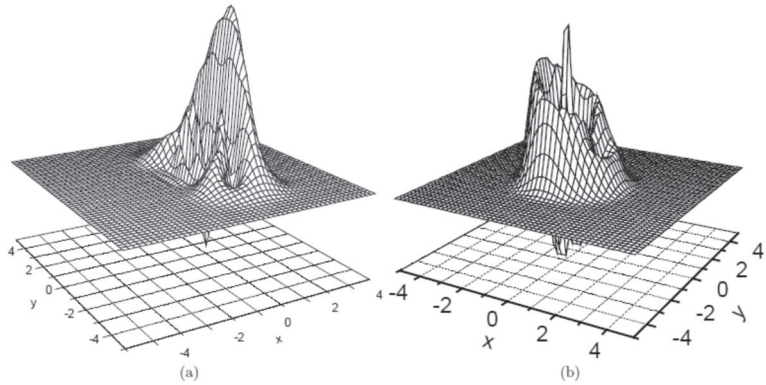

Fig. 2.28. Wigner functions of the states of the fundamental (a) and third harmonic (b) modes of an arbitrary quantum trajectory of the optical system in the region of long interaction times ($\tau = 10$) and for the system parameter values ε = 3 and k = 0.3.

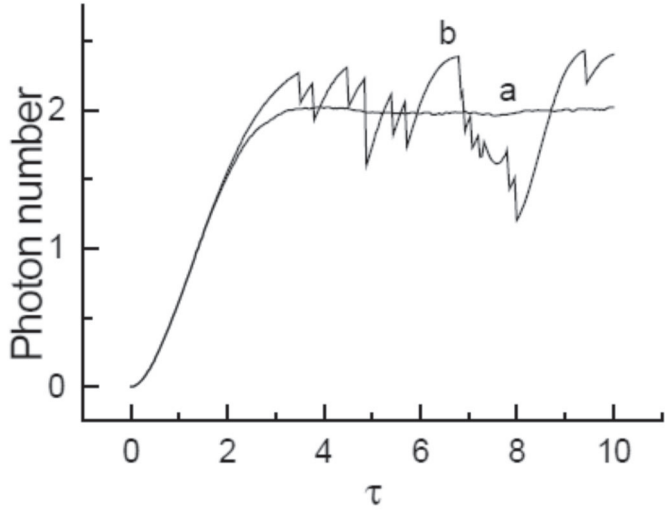

Fig. 2.29. Dynamics of the mean number of photons (curve a) and of the number of photons of an arbitrary quantum trajectory of the fundamental mode for the system parameter values ε = 1 and k = 0.3.

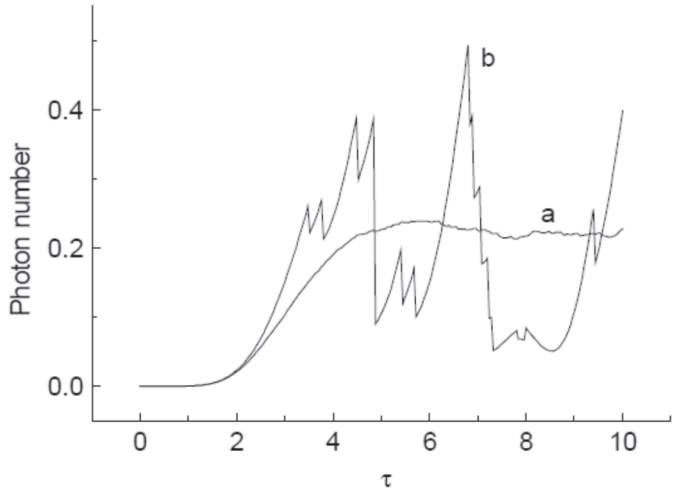

Fig. 2.30. Dynamics of the mean number of photons (curve a) and of the number of photons of an arbitrary quantum trajectory of the third harmonic mode for the system parameter values ε = 1 and k = 0.3.

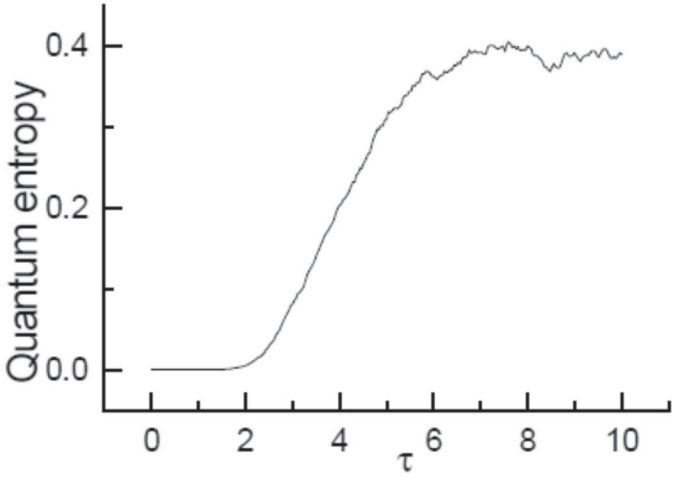

Fig. 2.31. Dynamics of the quantum entropy of the fundamental mode for the system parameter values ε = 1 and k = 0.3.

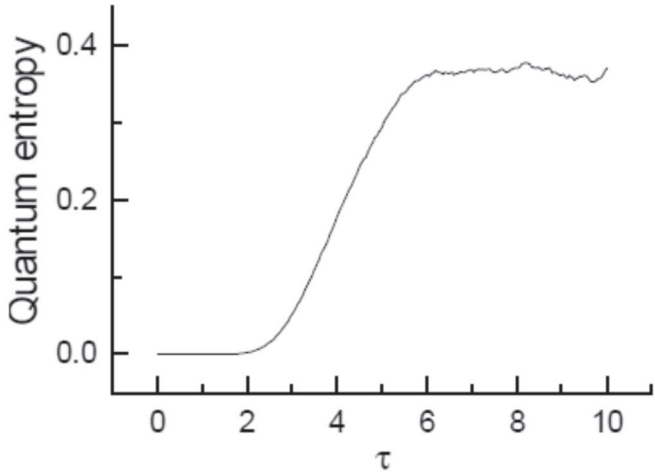

Fig. 2.32. Dynamics of the quantum entropy of the third harmonic mode for the system parameter values ε = 1 and k = 0.3.

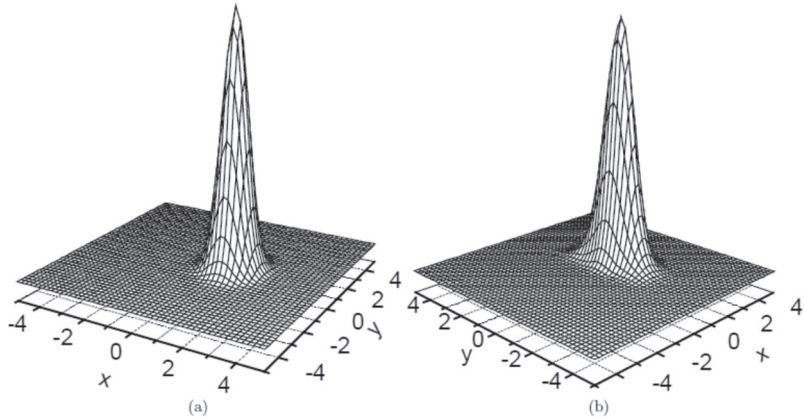

Fig. 2.33. Dynamics of the Wigner function of the state of the fundamental mode for the system parameter values ε = 1 and k = 0.3; (a) and (b) illustrate the Wigner function at the mode interaction moments $\tau = 2$ and $\tau = 10$, respectively.

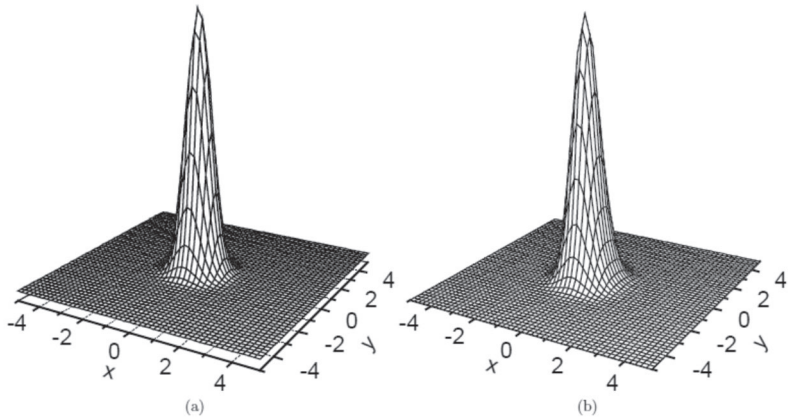

Fig. 2.34. Dynamics of the Wigner function of the state of the third harmonic mode for the system parameter values $\varepsilon = 1$ and $k = 0.3$; (a) and (b) illustrate the Wigner function at mode interaction times $\tau = 2$ and $\tau = 10$, respectively.

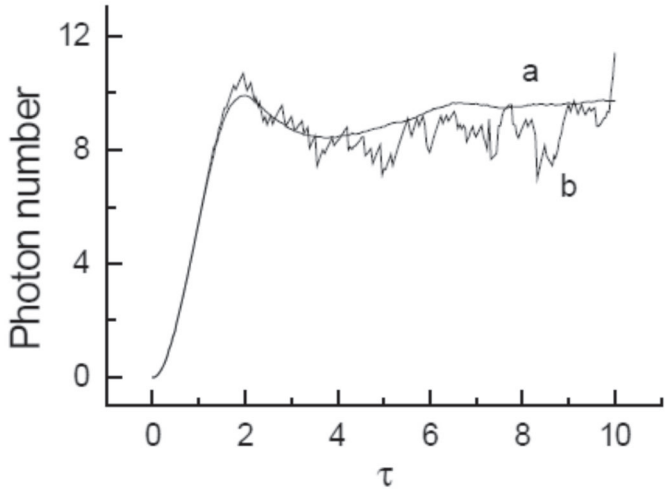

Fig. 2.35. Dynamics of the mean number of photons (curve a) and of the number of photons of an arbitrary quantum trajectory (curve b) of the fundamental mode for the system parameter values $\varepsilon = 3$ and $k = 0.1$.

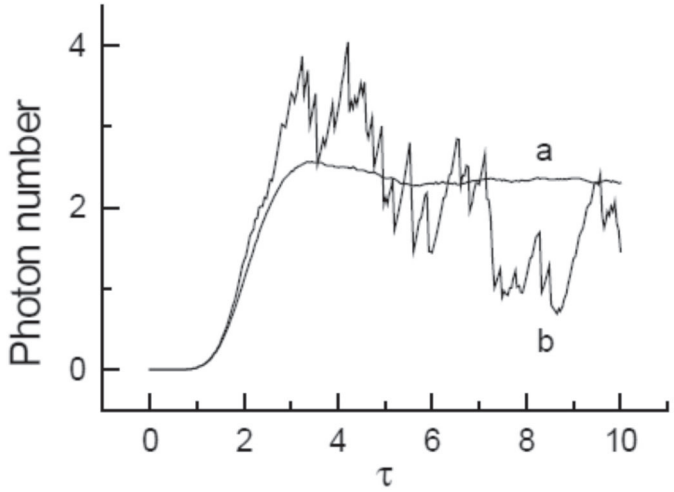

Fig. 2.36. Dynamics of the mean number of photons (curve a) and of the number of photons of an arbitrary quantum trajectory (curve b) of the third harmonic mode for the system parameter values $\varepsilon = 3$ and $k = 0.1$.

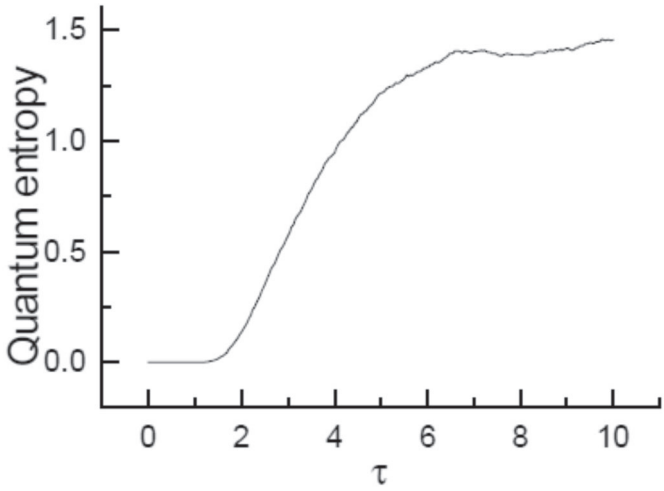

Fig. 2.37. Dynamics of the quantum entropy of the fundamental mode for the system parameter values $\varepsilon = 3$ and $k = 0.1$.

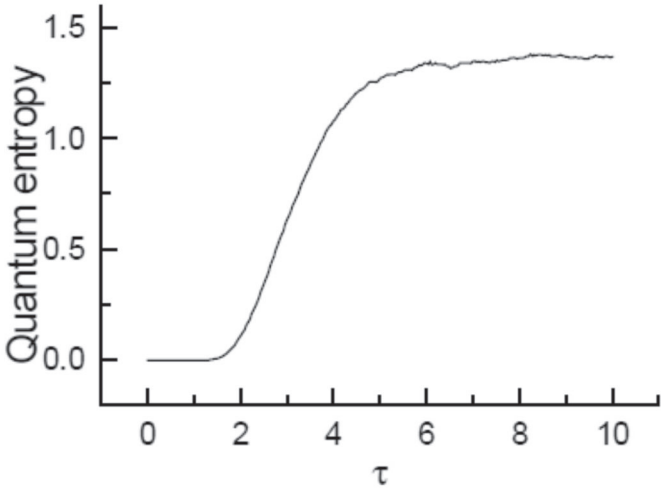

Fig. 2.38. Dynamics of the quantum entropy of the third harmonic mode for the system parameter values $\varepsilon = 3$ and $k = 0.1$.

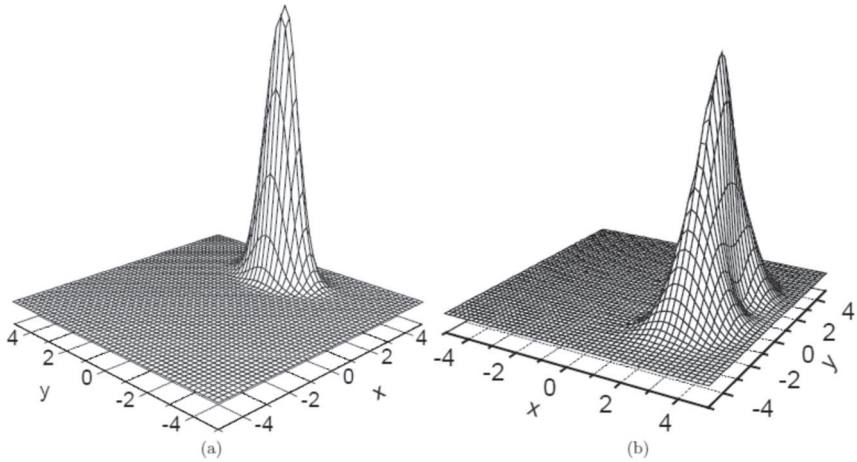

Fig. 2.39. Dynamics of the Wigner function of the state of the fundamental mode for the the system parameter values $\varepsilon = 3$ and $k = 0.1$; (a) and (b) illustrate the Wigner function at the mode interaction moments $\tau = 2$ and $\tau = 10$, respectively.

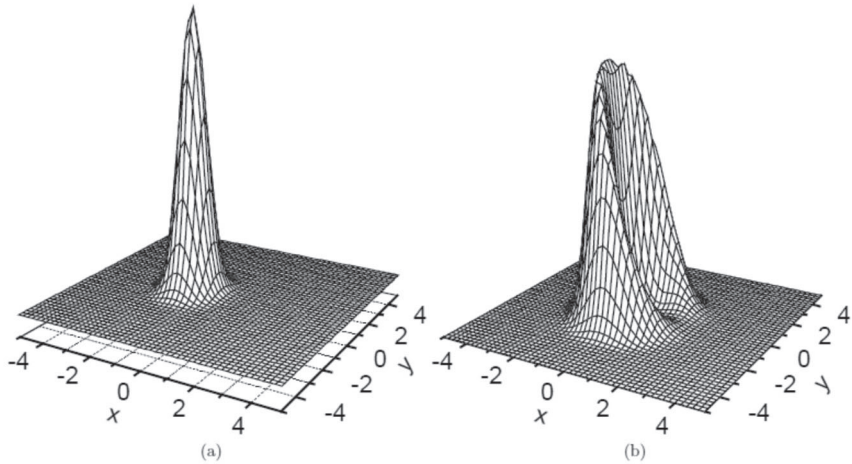

Fig. 2.40. Dynamics of the Wigner function of the state of the third harmonic mode for the system parameter values $\varepsilon = 3$ and $k = 0.1$. (a) and (b) illustrate the Wigner function at the mode interaction times $\tau = 2$ and $\tau = 10$, respectively.

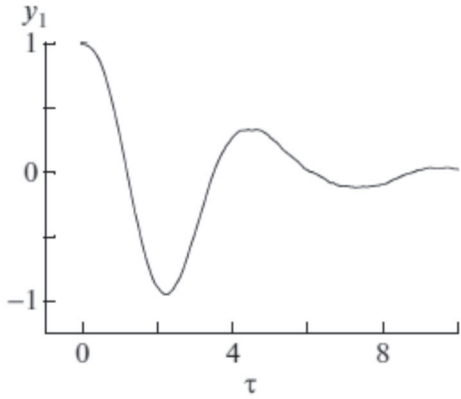

Fig. 2.41. Dynamics of the mean value of the quadrature amplitude of the fundamental mode in the case $\alpha_1 = i$ and $\alpha_2 = -i$ for the perturbation value ε = 3.

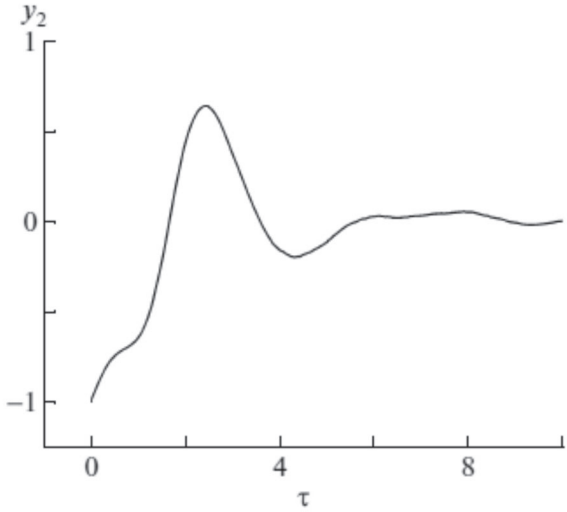

Fig. 2.42. Dynamics of the mean value of the quadrature amplitude of the third harmonic mode in the case $\alpha_1 = i$ and $\alpha_2 = -i$ and for the perturbation value ε = 3.

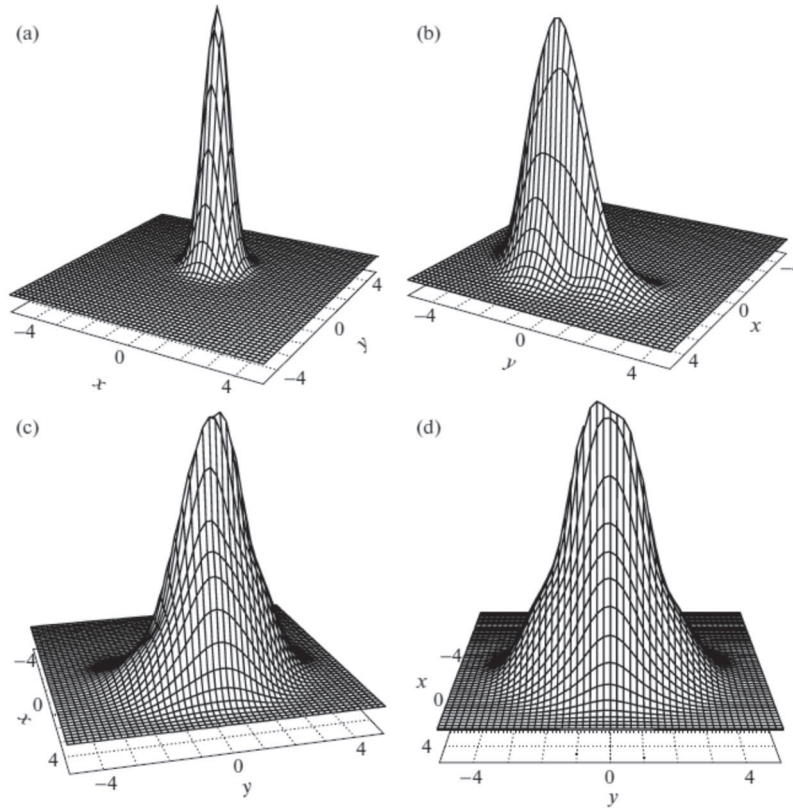

Fig. 2.43. Dynamics of the Wigner function of the state of the fundamental mode when $\alpha_1 = i$ and $\alpha_2 = -i$ and for the perturbation value ε = 3: (a) initial coherent state with the amplitude of the state; (b-d) Wigner functions of the state of the fundamental mode at τ = 2.35, 4.5, and 7.5, respectively.

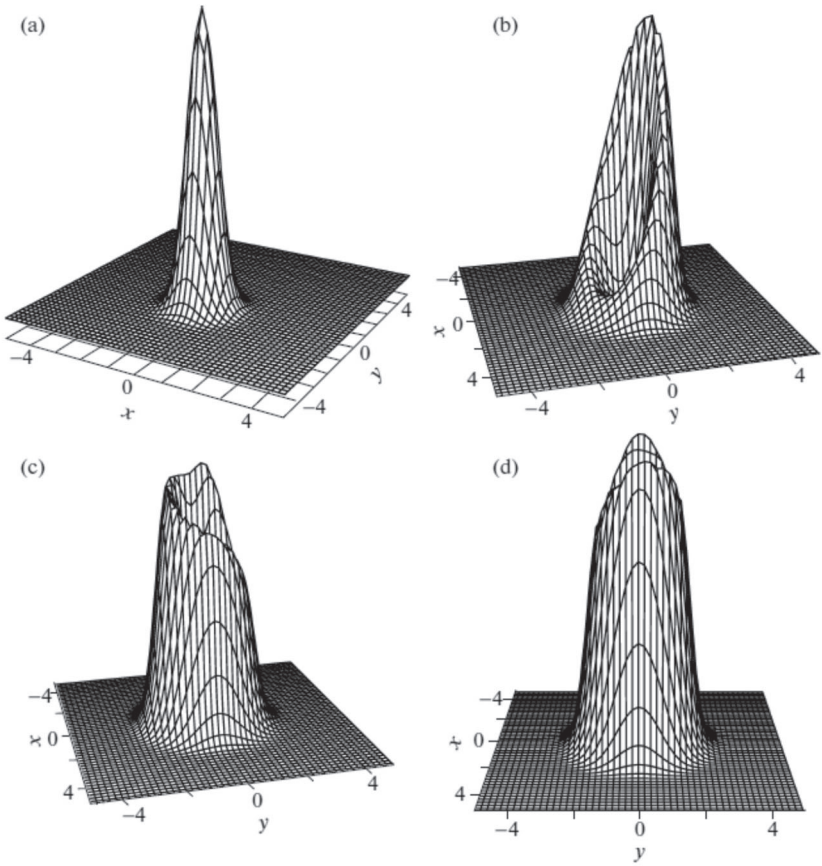

Fig. 2.44. Dynamics of the Wigner function of the state of the third harmonic mode in the case case $\alpha_1 = i$ and $\alpha_2 = -i$ and for the perturbation value ε = 3: (a) initial coherent state with the amplitude of the state; (b-d) Wigner functions of the state of the third harmonic mode at τ = 2.45, 4.3, and 7.5, respectively.

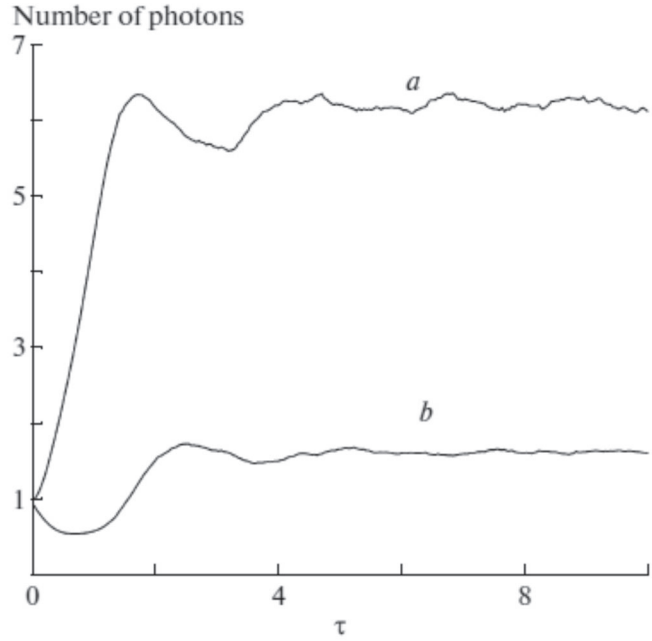

Fig. 2.45. Dynamics of the mean value of the number of photons (a) of the fundamental mode and (b) of the third harmonic mode for $\alpha_1 = i$ and $\alpha_2 = -i$ and for the perturbation value ε = 3.

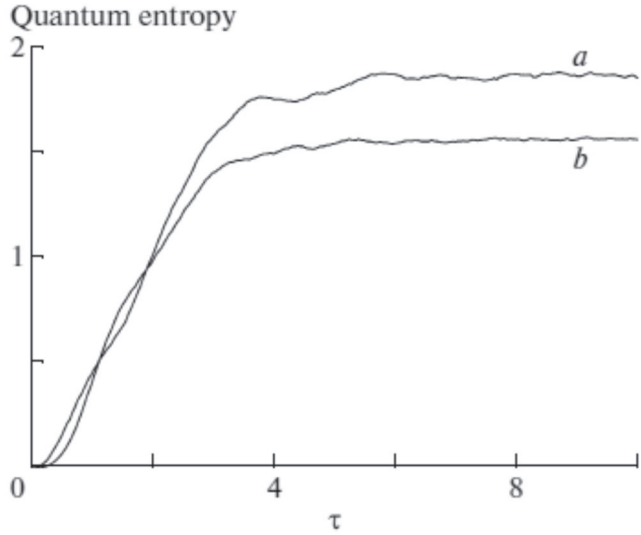

Fig. 2.46. Dynamics of the quantum entropy (a) of the fundamental and (b) third harmonic modes in for $\alpha_1 = i$ and $\alpha_2 = -i$ and for the perturbation value ε = 3.

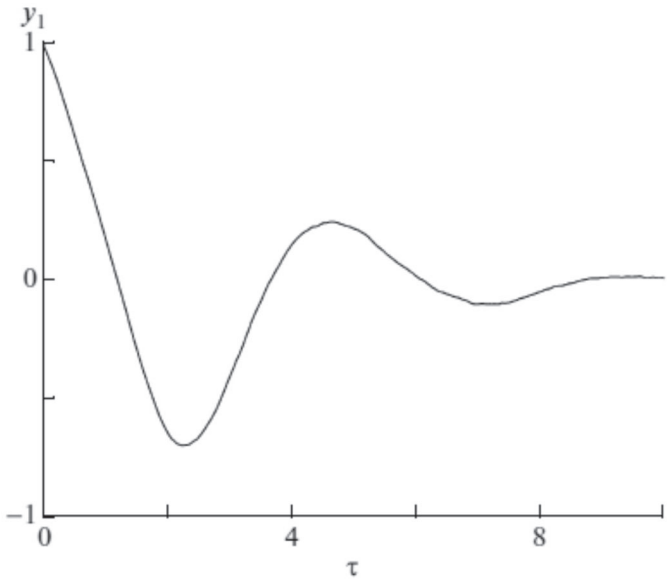

Fig. 2.47. Dynamics of the mean value of the quadrature amplitude of the fundamental mode for $\alpha_1 = i$ and $\alpha_2 = -i$ and for the perturbation value ε = 3.

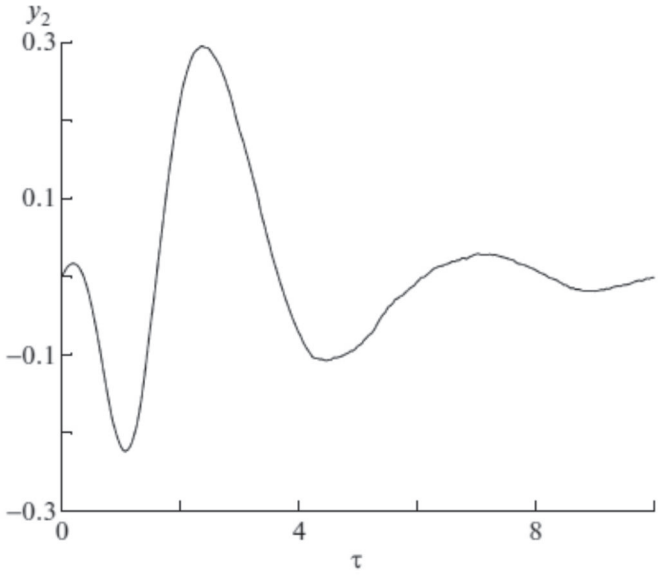

Fig. 2.48. Dynamics of the mean value of the quadrature amplitude of the third harmonic mode for $\alpha_1 = i$ and $\alpha_2 = -i$ and for the perturbation value ε = 3.

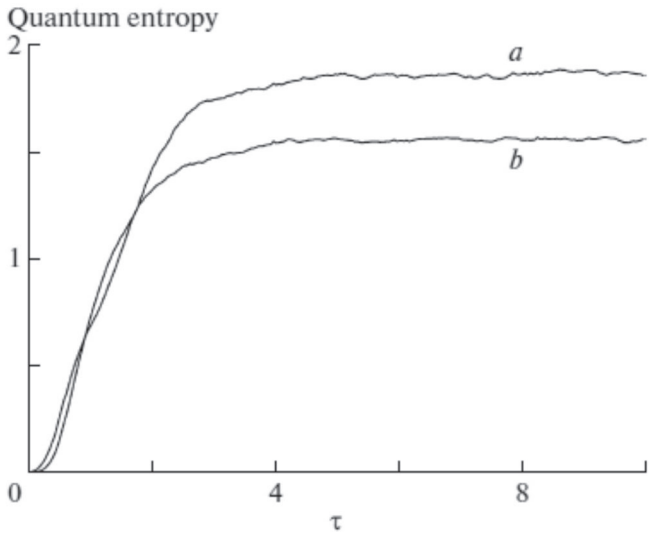

Fig. 2.49. Dynamics of the quantum entropy (a) of the fundamental and (b) third harmonic modes for $\alpha_1 = 1$ and $\alpha_2 = -1$ and for the perturbation value $\varepsilon = 3$.

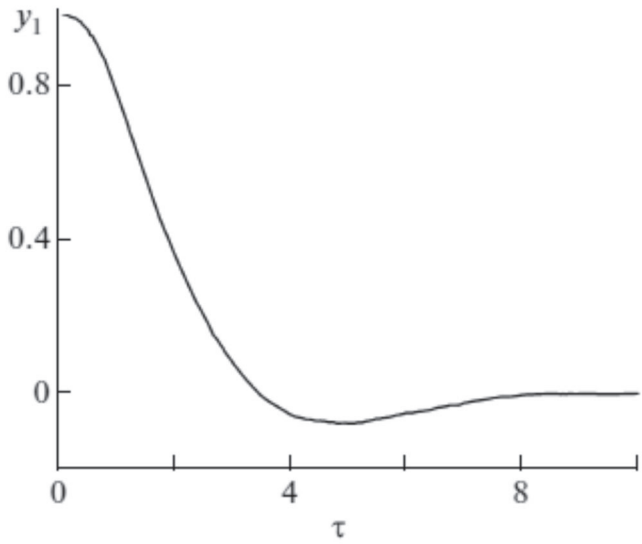

Fig. 2.50. Dynamics of the mean value of the quadrature amplitude of the fundamental mode for $\alpha_1 = i$ and $\alpha_2 = -i$ and for the perturbation value ε = 1.

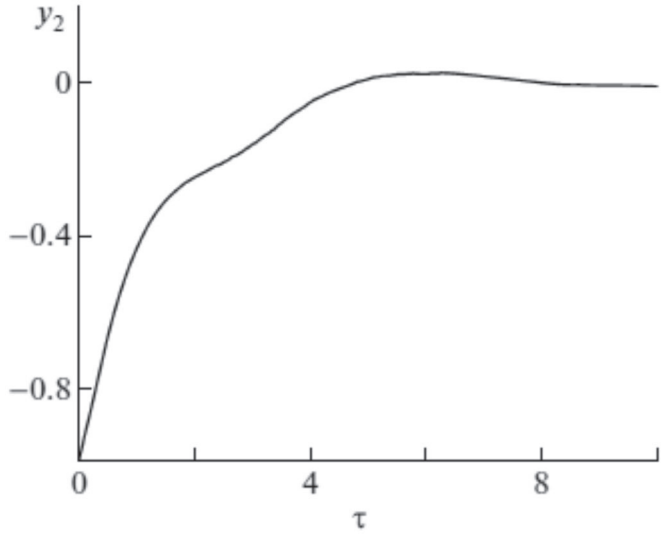

Fig. 2.51. Dynamics of the mean value of the quadrature amplitude of the third harmonic mode for $\alpha_1 = i$ and $\alpha_2 = -i$ and for the perturbation value ε = 1.

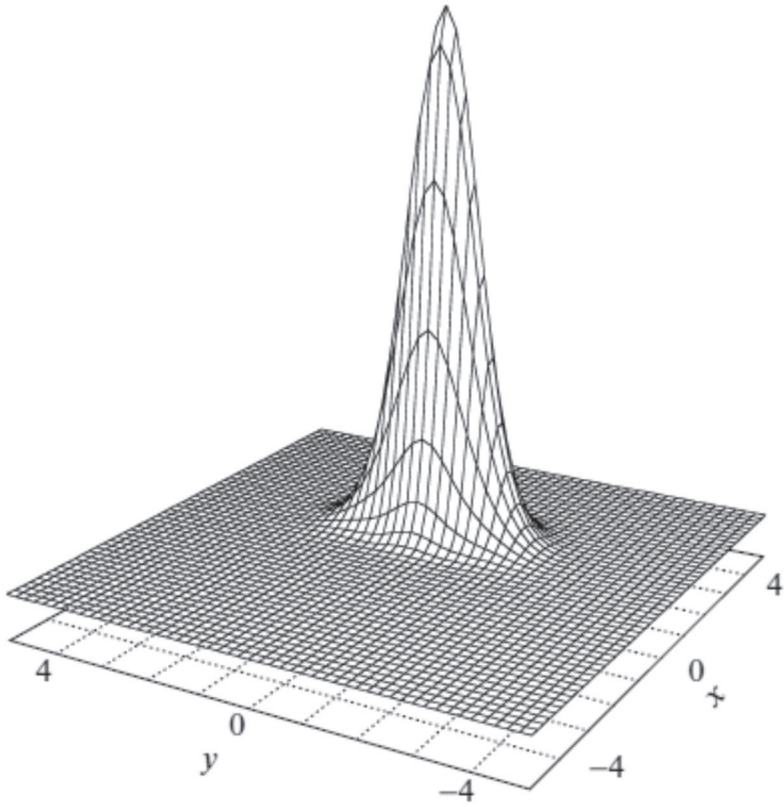

Fig. 2.52. Wigner function of the state of the fundamental mode at the time $\tau = 10$ for $\alpha_1 = i$ and $\alpha_2 = -i$ and for the perturbation value $\varepsilon = 1$.

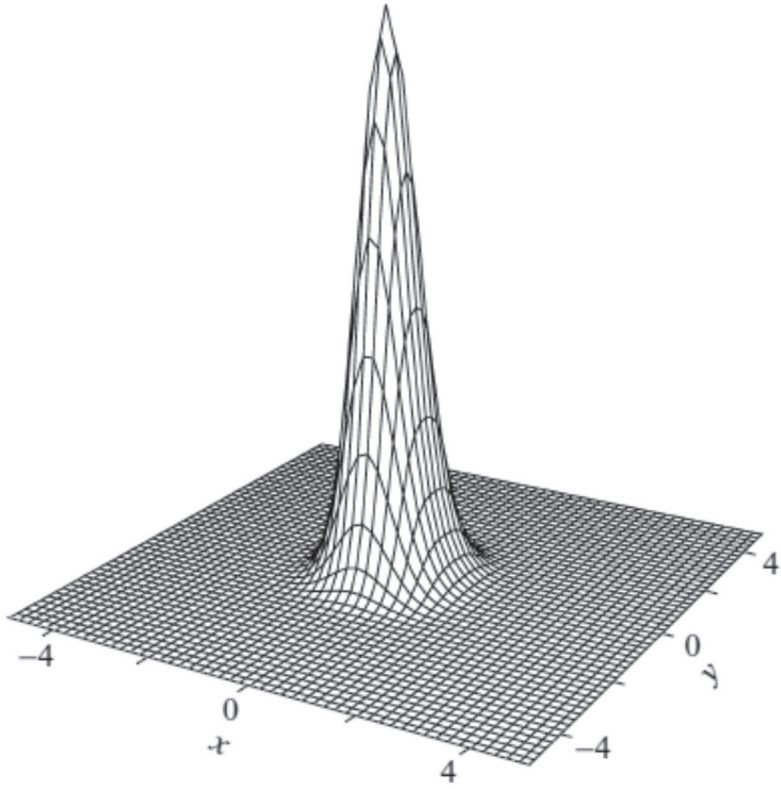

Fig. 2.53. Wigner function of the state of the third harmonic mode at the time τ = 10 for $\alpha_1 = i$ and $\alpha_2 = -i$ and for the perturbation value ε = 1.

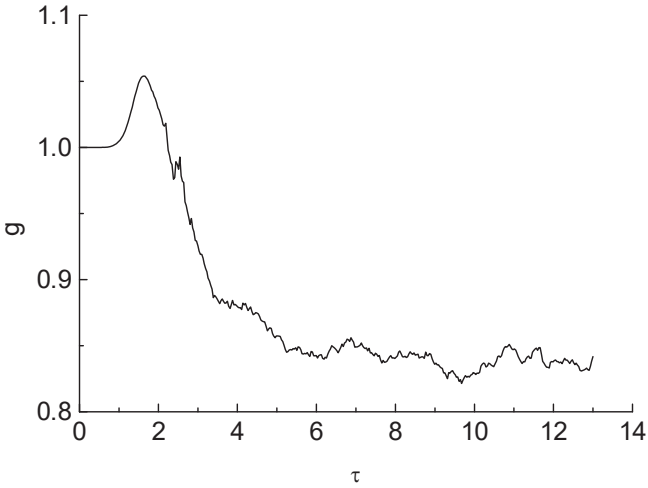

Fig. 2.54. Dynamics of the correlation function of fluctuations of quadrature amplitudes of interacting modes in the case of weak coupling between the modes ($k = 0.1$) and a strong perturbation of the fundamental mode ($\varepsilon = 3$). The function was calculated by using 1000 quantum trajectories of the optical system.

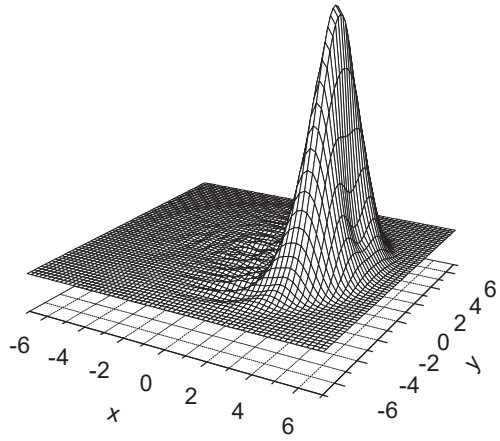

(a)

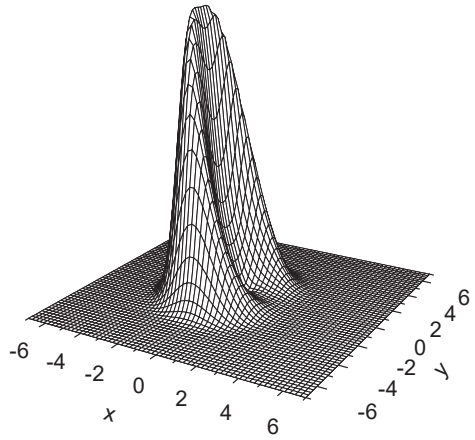

(b)

Fig. 2.55. Wigner functions of states of the (a) fundamental and (b) third harmonic modes in the region of long interaction times ($\tau = 10$) and for the system parameter values $k = 0.1$ and $\varepsilon = 3$.

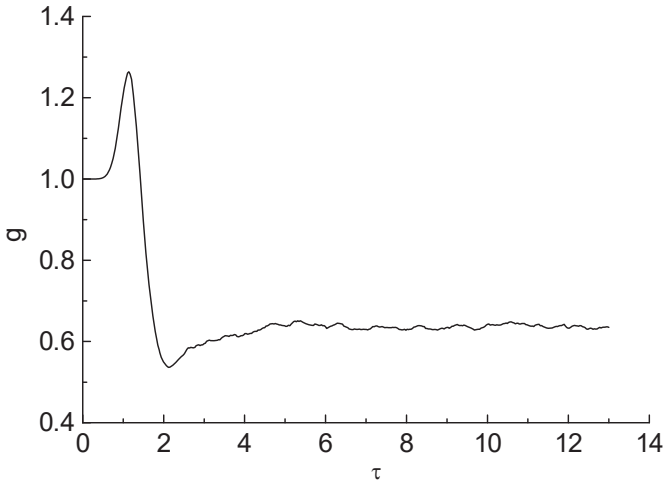

Fig. 2.56. Dynamics of the correlation function of fluctuations of the quadrature amplitudes for the system parameter values k = 0.5 and ε = 3.

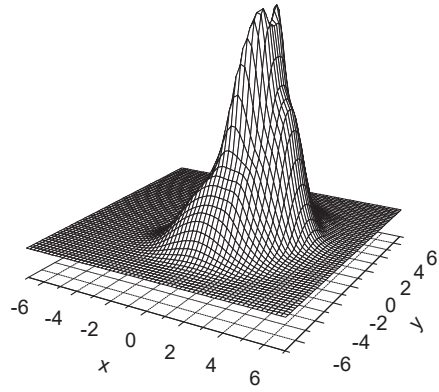

(a)

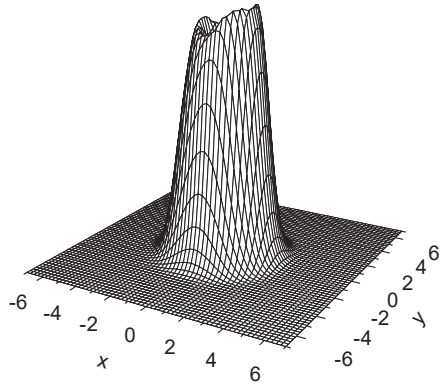

(b)

Fig. 2.57. Wigner functions of the stationary states of the (a) fundamental and (b) third harmonic modes for the system parameter values k = 0.5 and ε = 3.

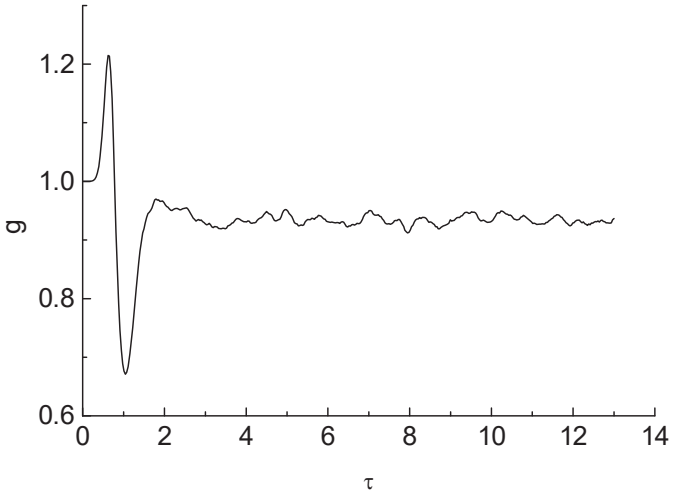

Fig. 2.58. Dynamics of the correlation function of fluctuations of the quadrature amplitudes of interacting modes in the case of strong mode coupling (k = 2) and the perturbation amplitude ε = 3.

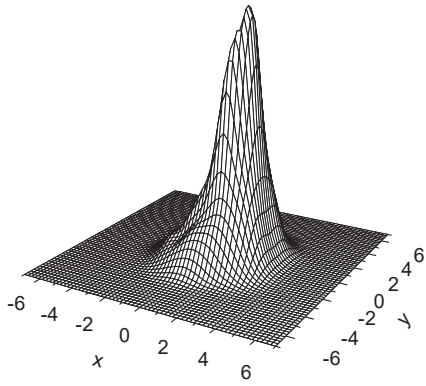

(a)

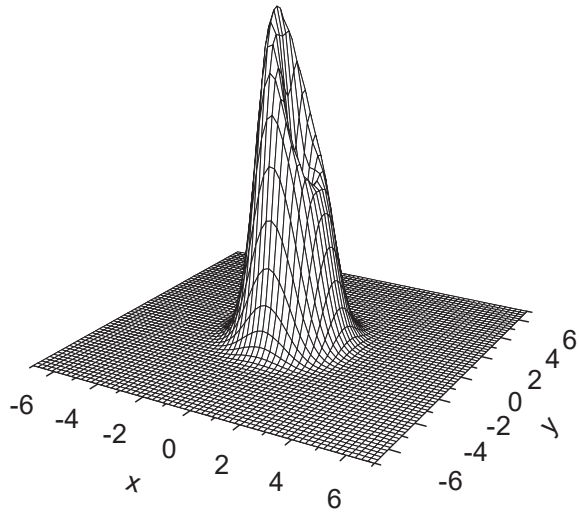

(b)

Fig. 2.59. Wigner functions of the stationary states of the (a) fundamental and (b) third harmonic modes for the system parameter values k = 2 and ε = 3.

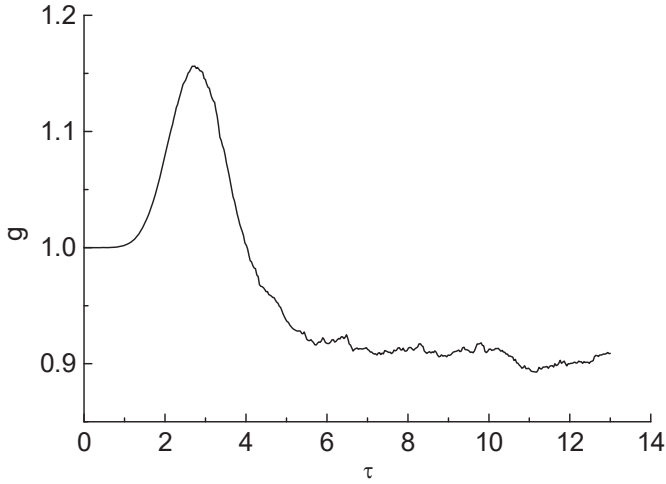

Fig. 2.60. Dynamics of the correlation function of fluctuations of quadrature amplitudes of interacting modes in the case of a weak perturbation of the fundamental mode ($\varepsilon = 1$) and the mode coupling coefficient $k = 0.5$.

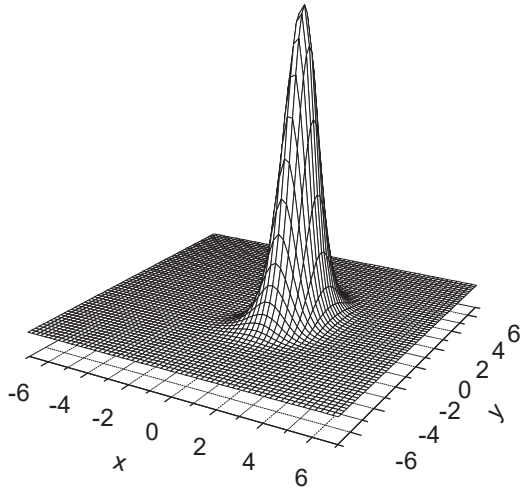

(a)

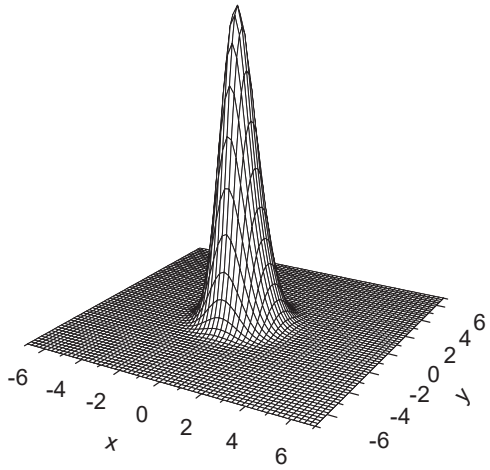

(b)

Fig. 2.61 Wigner functions of the stationary states of the (a) fundamental and (b) third harmonic modes for the system parameter values $\varepsilon = 1$ and $k = 0.5$.

CHAPTER 3

DYNAMICS OF FORMATION OF SUPERPOSITION STATES OF LIGHT IN AN ABSORBING MEDIUM

Introduction

All materials in this chapter are taken from [1,2].

This chapter considers the process of simultaneous absorption of two photons in a medium in the presence of weak one-photon absorption. The medium is perturbed from outside in a two-photon parametric manner. The formation of a stationary even-parity superposition state of light in such a medium is shown to be possible in the region of small amplitudes of the state (weak perturbations of the system). This is associated with the fact that, in this region of interaction, the field spends considerably more time in the even superposition state than in the odd state. It is shown that a nonstationary superposition state of light with a large amplitude of the state (large photon numbers) can be obtained for interaction times that are longer than the time required for the formation of a superposition state of the field in the optical system in the absence of single-photon dissipation and shorter than the most probable time of the first one-photon jump of the field state. The formation dynamics of the quantum entropy of the field is studied by a numerical simulation of quantum trajectories of the system. The Wigner functions of the state of the field are calculated. Analytical results are obtained for the density matrix of the stationary state of the system in the presence of weak one-photon absorption.

3.1. Model of the Nonlinear System and Basic Equations

We consider the statistical properties of the mode of an electromagnetic field interacting with a two-photon absorbing medium. We assume that this mode is perturbed from outside in a two-photon parametric manner [3]. The Hamiltonian of this interaction can be described with the help of the squares of the field operators. We also assume the presence of weak one-photon absorption of the field in the medium. The equation for the density matrix for this model can be written as

$$\frac{\partial \rho}{\partial t} = L_p(\rho) + \sum_{i=1,2} L_i(\rho). \tag{3.1.1}$$

In this equation, the $L_i(\rho)$ superoperators $(i = 1,2)$ describe the one- and two-photon absorption of the field in the medium, respectively:

$$L_i(\rho) = -\frac{\gamma_i}{2}(a^{+i}a^i\rho + \rho a^{+i}a^i - 2a^i\rho a^{+i}), \tag{3.1.2}$$

where γ_i $(i = 1,2)$ are the corresponding absorption rates of the field in the medium. The first term in Eq. (3.1.1) describes the two-photon parametric perturbation of the field mode from outside;

$$L_p(\rho) = (i\hbar)^{-1}\left[H_p, \rho\right]. \tag{3.1.3}$$

The Hamiltonian H_p has the form

$$H_p = i\hbar\frac{\varepsilon}{2}(a^2 - a^{+2}) \tag{3.1.4}$$

(the phase of the perturbing field is omitted for simplicity). To study the quantum properties of the optical system, we calculate the Wigner functions of the field state [3].

We also study the dynamics of the quantum entropy of the field S = – Tr(ρln(ρ)). We calculate the entropy by the numerical diagonalization of the field density matrix in the Fock basis [3].

By using the Monte Carlo method for calculating the wave functions [4], we study quantum trajectories of the optical system. Here we present an algorithm of this method for calculating a quantum trajectory of the field of our optical system.

For calculating the field state at the moment t + δt, we find the probability of a quantum jump of the field state at the t moment:

$$\delta p = \delta p_1 + \delta p_2 = \gamma_1 \delta t \langle \Psi(t)|a^+ a|\Psi(t)\rangle + \gamma_2 \delta t \langle \Psi(t)|a^{+2} a^2|\Psi(t)\rangle, \quad (3.1.5)$$

where $|\psi(t)\rangle$ is the field state at the t moment. The first and second terms of Eq. (3.1.5) describe, respectively, the probabilities of one- and two-photon quantum jumps of the field state. After this, a random number ξ is generated, which has a uniform distribution within the interval (0, 1). If ξ < δp, a quantum jump in the field state occurs in the system. In this case, we calculated the normalized probabilities of one- and two-photon jumps of the field state

$$p_1 = \frac{\delta p_1}{\delta p_1 + \delta p_2},$$

$$p_2 = \frac{\delta p_2}{\delta p_1 + \delta p_2}. \quad (3.1.6)$$

Then, a second random number η is generated, which has a uniform distribution within the interval (0, 1). If $\eta < p_1$, the field state of the system undergoes a one-photon jump and the field changes to the state

$$|\Psi(t+\delta t)\rangle \sim a|\Psi(t)\rangle. \quad (3.1.7)$$

If $\eta > p_1$, the field state undergoes a two-photon jump and the field changes to the new state

$$|\Psi(t+\delta t)\rangle \sim a^2|\Psi(t)\rangle. \quad (3.1.8)$$

In both cases, the new state of the system is normalized. If ξ > δp, the system evolves in a continuous manner:

$$|\Psi(t+\delta t)\rangle \sim |\Psi(t)\rangle + (i\hbar)^{-1}H_{ef}\delta t|\Psi(t)\rangle, \quad (3.1.9)$$

where

$$H_{ef} = H_p - i\hbar\frac{\gamma_1}{2}a^+a - i\hbar\frac{\gamma_2}{2}a^{+2}a^2 \quad (3.1.10)$$

is the non-Hermitian Hamiltonian of continuous system evolution. After each step of continuous evolution, the new state is normalized.

The field density matrix is calculated as the mathematical expectation of the matrices of the trajectory of the system:

$$\rho(t) = \lim_{N\to\infty}\left(\frac{1}{N}\sum_{(m)=1}^{N}\left|\Psi(t)^{(m)}\right\rangle\left\langle\Psi(t)^{(m)}\right|\right). \quad (3.1.11)$$

3.2. Quantum Dynamics of the Field in the Absence of One-Photon Absorption

In this section, we study the quantum dynamics of the field in the absence of one-photon absorption. In this case, to calculate one step of the quantum trajectory of the system, it is necessary to introduce $\gamma_1 = 0$ into the algorithm for calculating quantum trajectories of the system, which was described in the preceding section.

Figures 3.1 and 3.2 demonstrate the Wigner functions of the field state of two random trajectories of the optical system in the cases when the field evolves from initial vacuum and one-photon Fock states, respectively. The trajectories were calculated for the following values of the parameters of the system: $\varepsilon/\gamma_2 = 5$ and $\gamma_1 = 0$. Figures 3.1a and 3.2a correspond to the initial vacuum and one-photon Fock states of the field, respectively. Figures 3.1b, 3.1c, 3.2b, and 3.2c correspond to the field state before (b) and after (c) the first two-photon quantum jump of the field state at the moments $\gamma_2 t \approx 0.575$ and $\gamma_2 t \approx 0.435$, respectively, for the corresponding trajectories of the system. Figures 3.1d and 3.2d represent the Wigner function of the optical system in the corresponding trajectories at the moment $\gamma_2 t = 10$. In the region of large interaction times, the quantum entropy of the optical system approaches a stationary zero value (see Fig. 3.3, curves 1 and 2), as a result of which the Wigner functions presented in Figs 3.1d and 3.2d represent stationary states of the optical system in the case of evolution from initial vacuum and single-photon Fock states, respectively.

The Wigner functions presented in Figs. 3.1d and 3.2d only differ from each other by oscillations between the two coherent components of the state. They demonstrate the formation of different types of interference between the coherent components of the state [3]. The Wigner function in Fig. 3.1d represents the even-parity superposition state

$$|\alpha\rangle_e = \sqrt{N_e}(|\alpha\rangle + |-\alpha\rangle), \qquad (3.2.1)$$

and the Wigner function in Fig. 3.2d represents the odd-parity superposition state [3]

$$|\alpha\rangle_o = \sqrt{N_o}(|\alpha\rangle - |-\alpha\rangle). \quad (3.2.2)$$

In Eqs. (3.2.1) and (3.2.2), the N_e and N_o coefficients are the normalization factors of the corresponding states

$$N_{e,o}^{-1} = 2(1 \pm exp(-2|\alpha|^2)), \quad (3.2.3)$$

and |α⟩ and |–α⟩ denote the coherent states of the field [5]

$$|\alpha\rangle = exp(-|\alpha|^2/2)\sum_{n=0}^{\infty}\frac{\alpha^n}{\sqrt{n!}}|n\rangle. \quad (3.2.4)$$

Here, $\alpha = \sqrt{-\varepsilon/\gamma_2}$ [3].

In the region of large interaction times, the field localizes in an even parity superposition state in the case of evolution of the system from an initial vacuum state; in contrast, it localizes in an odd parity superposition state in the case of evolution from an initial single-photon Fock state.

Figure 3.3 (curve 1) demonstrates the dynamics of the quantum entropy of the field in the case of evolution of the system from an initial vacuum state of the field for the system parameter values $\varepsilon/\gamma_2 = 5$ and $\gamma_1 = 0$. The dynamics of the entropy was calculated using 5000 independent quantum trajectories of the optical system.

Figure 3.3 (curve 2) demonstrates the dynamics of the quantum entropy of the field in the case of evolution from an initial one-photon Fock state of the field and for the same values of the system parameters as for curve 1. The dynamics of the entropy was calculated based on 5000 independent quantum trajectories of the system. In this case, relative to the previous one (Fig.3.3, curve 1), the time, at which entropy reaches its stationary

zero value, decreases; this is also the case for the maximum value of entropy.

In the curves, the amount of time necessary for the transition of the quantum entropy of the system to the stationary zero value is the amount of time necessary for the formation of even parity (curve 1) and odd parity (curve 2) superposition states of the field. In the region of larger evolution times, the optical field localizes in superposition states of the corresponding parities and the ensemble of quantum trajectories of the system consists of a single element, which is in contrast to the evolution of the system in the region of small interaction times.

Figure 3.4 demonstrates the dynamics of the quantum entropy of the field in the case of evolution from an initial vacuum state of the field for the system parameter values $\varepsilon/\gamma_2 = 2$ and $\gamma_1 = 0$. The entropy dynamics was calculated based on 5000 independent quantum trajectories of the optical system. For these values of the parameters, as compared to the case presented in Fig. 3.3 (curve 1), the time necessary for the entropy to reach its stationary zero value increases and the maximum value of the entropy decreases.

3.3. Quantum Dynamics of the Field in the Presence of Weak One-Photon Absorption. Quantum Coherence and Dissipation

In this section, we will consider the dynamics of the optical system in the presence of weak one-photon absorption $\gamma_1 << \gamma_2$. Although the one-photon absorption is small compared to the two-photon absorption, it affects substantially the behaviour of the system in quantum trajectories

and the formation of a stationary ensemble of field states at long times of evolution of the optical system.

Figure 3.5 demonstrates the Wigner functions of the field state of one random trajectory of the optical system in the case of evolution from an initial vacuum state of the field and for the following system parameter values: $\varepsilon/\gamma_2 = 5$ and $\gamma_1/\gamma_2 = 0.01$.

At the time point$\gamma_2 t \approx 12.420$, before the first one-photon jump, the field state was localized in the even-parity superposition state $|\alpha\rangle_e$, where $\alpha \approx \sqrt{-\varepsilon/\gamma_2}$ (3.2.1). During further evolution, the field state only changes after each one-photon jump that changes the type of interference between the coherent components of the superposition state

$$a|\alpha\rangle_{e,o} = \sqrt{\frac{N_{e,o}}{N_{o,e}}}\alpha|\alpha\rangle_{o,e}. \qquad (3.3.1)$$

After the first one-photon jump, the field changed its states from $|\alpha\rangle_e$ to $|\alpha\rangle_o$ (Figs. 3.5a and 3.5b); after the second quantum jump, it was again localized in the $|\alpha\rangle_e$ state (Figs. 3.5c and 3.5d). In the region of long evolution times $\gamma_1 t > 1$, other trajectories of the optical system that originate from an initial vacuum state have a similar behaviour in time. In the region of long interaction times, the system is in a superposition state of type (3.2.1) or (3.2.2) until a one-photon quantum jump changes the type of interference between the coherent components of the superposition state. The probability of finding the system in each of these states is proportional to the field lifetime $T_{e,o}$ in these states. As a result, the field density matrix in the region of long interaction times can be represented in the form

$$\rho = \frac{T_e}{T_e+T_o}|\alpha\rangle_{ee}\langle\alpha| + \frac{T_o}{T_e+T_o}|\alpha\rangle_{oo}\langle\alpha|. \quad (3.3.2)$$

The field lifetime in each of these superposition states $|\alpha\rangle_{e,o}$ is inversely proportional to the probability of the system to leave the state. The field leaves its state only after a one-photon jump. The continuous evolution of the system and two-photon jumps do not change the field state. Under the condition that, at the t moment, the field was in the state $|\alpha\rangle_{e,o}$, the probability of a one-photon jump of the field state $\delta p_{e,o}$ within the δt time interval is proportional to the number of photons in this state [4] (see also formula (3.1.5)):

$$\delta p_{e,o} = \gamma_{1o,e}\langle\alpha|a^+a|\alpha\rangle_{e,o}\delta t = \gamma_1|\alpha|^2\frac{1\mp exp(-2|\alpha|^2)}{1\pm exp(-2|\alpha|^2)}\delta t \equiv \frac{\delta t}{T_{e,o}}. \quad (3.3.3)$$

Formula (3.3.3) defines the dependence of the field lifetime in the superposition states $|\alpha\rangle_{e,o}$ on the amplitude of the state α.

Figure 3.6 presents the dependences of the probabilities of finding the field in the superposition states $|\alpha\rangle_{e,o}$ for long evolution times in the presence of small one-photon absorption

$$P_{e,o} = \frac{T_{e,o}}{T_e+T_o} \quad (3.3.4)$$

on the absolute value of the amplitude of the state $\beta = |\alpha|$. The probabilities were calculated using Eqs. (3.3.4) and (3.3.3).

In the region of large values of the state amplitude $|\alpha| >> 1$, the field can be found with the same probability of 1/2 in each of the superposition states $|\alpha\rangle_{e,o}$. For this case, the field density matrix can be presented in the form

$$\rho = \frac{1}{2}|\alpha\rangle_{ee}\langle\alpha| + \frac{1}{2}|\alpha\rangle_{oo}\langle\alpha|. \quad (3.3.5)$$

In the region of large values of the amplitude of the state, the normalization factors of the states (3.2.1) and (3.2.2) are equal to each other, $N_e \approx N_o \approx 1/2$, and the density matrix of the system can be represented as a statistical mixture of two coherent states with the same probability of finding the field in each coherent component of the state

$$\rho = \frac{1}{2}|\alpha\rangle\langle\alpha| + \frac{1}{2}|-\alpha\rangle\langle-\alpha|. \quad (3.3.6)$$

The quantum entropy of this state is equal to the maximum entropy of the two-component system ln(2).

Figure 3.7 demonstrates the Wigner function of the stationary state of the system in the case of a large value of the amplitude of the state $\alpha = i\sqrt{5}$. It was calculated based on Eqs. (3.3.6), (3.2.1), and (3.2.2). The function represents a statistical mixture of two coherent components with the same probability of finding the field in each coherent component of the state.

In the region of small values of the amplitude of the state $|\alpha| < 1$ (small perturbations of the system), the field begins to spend more time in the superposition state $|\alpha\rangle_e$ than in $|\alpha\rangle_o$ (3.6). This leads to a decrease in the quantum entropy of the field; i.e., the optical system begins to acquire quantum-mechanical coherence.

Figure 3.8 shows the dependence of the quantum entropy of the stationary field state on the absolute value of the amplitude of the state $\beta = |\alpha|$. In the region of large values of the state amplitude $|\alpha| >> 1$, the system can be found with the same probability in each of the superposition states (3.2.1) and (3.2.2), which results in the maximum value of the entropy of

the two-component state. As the amplitude of the state decreases, the field begins to remain predominantly in the even superposition state, which manifests itself as a decrease in the quantum entropy of the stationary state of the system.

Figure 3.9 presents the Wigner function of the stationary state of the field in the presence of small one-photon absorption and in the region of a small value of the state amplitude ($\alpha = i0.8$). The Wigner function was calculated using Eqs. (3.3.2) and (3.3.3). The function shows the presence of quantum-mechanical interference between the two coherent components of the field state.

The possibility of formation of superposition states of light in the process of second subharmonic generation was demonstrated in [6]. In this work, it is shown that in the above-mentioned system, in the region of small values of the number of photons, the subharmonic localizes in a stationary superposition state of even type. This result can be explained with the help of our research described above. Since the system investigated in this work is dissipative, if the subharmonic mode has localized in an even type superposition state, then, after some time, a single-photon quantum jump of the field state will change it into an odd-type superposition state. In the region of small values of the number of photons, the subharmonic mode will spend more time in an even-type superposition state, which will lead to the appearance of quantum coherence in this optical system. A similar result was obtained for this system in [7], using the Monte Carlo wave function method (see also Chapter 5).

3.4. Possibility of Formation of a Schrödinger Cat Type Nonstationary Field State

In this section, we investigate the possibility of formation of a Schrödinger cat type nonstationary superposition state in the optical system described above and in the presence of weak single-photon absorption.

Figure 3.10 demonstrates the dynamics of the quantum entropy of the field in the presence of weak one-photon absorption ($\gamma_1/\gamma_2 = 0.01$) in the case of evolution from an initial vacuum state of the field. The quantum entropy was calculated for $\varepsilon/\gamma_2 = 5$. The function was calculated with 5000 independent quantum trajectories of the system. In the region of long evolution times $\gamma_2 t >> 1$, the entropy tends to the stationary value $ln(2)$. This shows that, at these times, a stationary ensemble of quantum trajectories is formed in the system and it consists of elements of two types in the same numbers. The time necessary for the formation of this stationary ensemble is connected to the times at which one-photon quantum jumps in the field state take place. These jumps begin to create a stationary ensemble consisting of elements of two types (the even- and odd-parity superposition states) from an ensemble of elements of the same type (an even-parity superposition state).

As was shown in Section 3.2, in the absence of single-photon absorption of the optical system, some evolution time is required in order to form a superposition state of the field. The latter is the time at which the quantum entropy of the field decreases after an increase and at which it starts to change into a stationary zero value (see Fig. 3.3).

In Fig. 3.10, in this region of evolution, one can see a certain decrease in the quantum entropy, but the entropy does not reach a zero value. This can

be explained by the fact that, at these evolution times, the first one-photon jumps of the field state begin to destroy the formation of a pure ensemble of the field state, consisting only of the even superposition state $|\alpha\rangle_e$, adding the new type of the state $|\alpha\rangle_o$ to the ensemble of trajectories of the system; this leads to an increase in the quantum entropy in this region of interaction times. By increasing the most probable time of formation of the first one-photon jump of the field state, one can attain a considerable decrease in the field entropy in the time region mentioned above.

Figure 3.11 illustrates the dynamics of the quantum entropy of the field in the case where the coefficient of one-photon absorption is smaller than in the previous case. This decreases the probability of a one-photon jump of the field state and leads to an increase in the most probable time of the first one-photon jump. As a result, in the regions, where the evolution time is longer than the time required for the formation of a superposition state of the field in the optical system in absence of single-photon dissipation, the quantum entropy begins to decrease and almost vanishes ($S \approx 0.05$ for $\gamma_2 t \approx 1.44$). In this region of evolution times, the field can be found in a pure even-parity superposition state.

In the presence of small absorption in the system at long evolution times, the ensemble of trajectories of the field originating from the initial one-photon Fock state does not differ from the ensemble in the case of evolution from an initial vacuum state. Similarly to the case of evolution from an initial vacuum state at long evolution times, the field is in one of the superposition states $|\alpha\rangle_{e,o}$ until a one-photon jump changes this type of superposition state to the other type. In this case, it is possible to obtain an odd nonstationary superposition stat in the optical system.

As distinct from the case, where one-photon absorption is absent, in the presence of small one-photon absorption at long evolution times, the stationary ensemble of trajectories of the field is independent of the initial state of the field. This ensemble is the same for evolution cases from both initial vacuum and one-photon Fock states.

References

1. S. T. Gevorgyan, "Dynamics of Formation of Superposition States of Light in an Absorbing Medium," *Optics and Spectroscopy* 99, no. 1 (2005): 116–125.
2. S. T. Gevorgyan and V. O. Chaltykyan, "Quantum Coherence of Optical Systems and Dissipation," *J. of Modern Optics* 51, no 13 (2004): 1911–1917.
3. L. Gilles, B. M. Garraway, and P. L. Knight, "Generation of Nonclassical Light by Dissipative Two-Photon Processes," *Phys. Rev.* A 49 (1994): 2785–2799.
4. K. Molmer, Y. Castin, and J. Dalibard, "Monte Carlo Wave-Function Method in Quantum Optics," *JOSA B* 10 (1993): 524–538.
5. R. J. Glauber, "Coherent and Incoherent States of the Radiation Field" *Phys Rev* 131 (1963): 2766.
6. M. Wolinsky and H. J. Carmichael, "Quantum Noise in the Parametric Oscillator: From Squeezed States to Coherent-State Superpositions," *Phys. Rev. Lett.* 60 (1988): 1836–1839.
7. S. T. Gevorgyan and M. S. Gevorgyana, "Quantum Dynamics of Interacting Modes in the Process of Intracavity Subharmonic Generation," *Optics and Spectroscopy* 116, no. 4 (2014): 619–625.

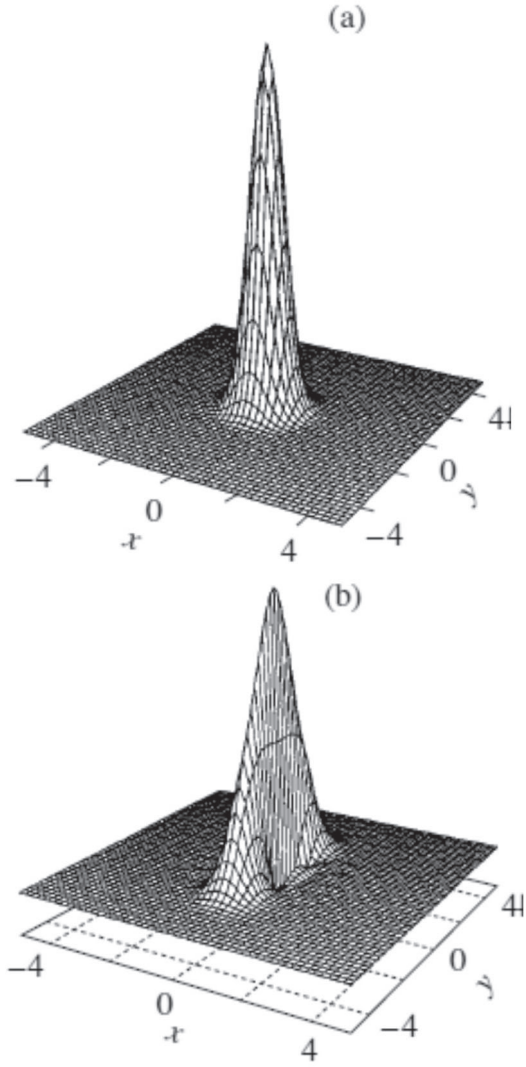

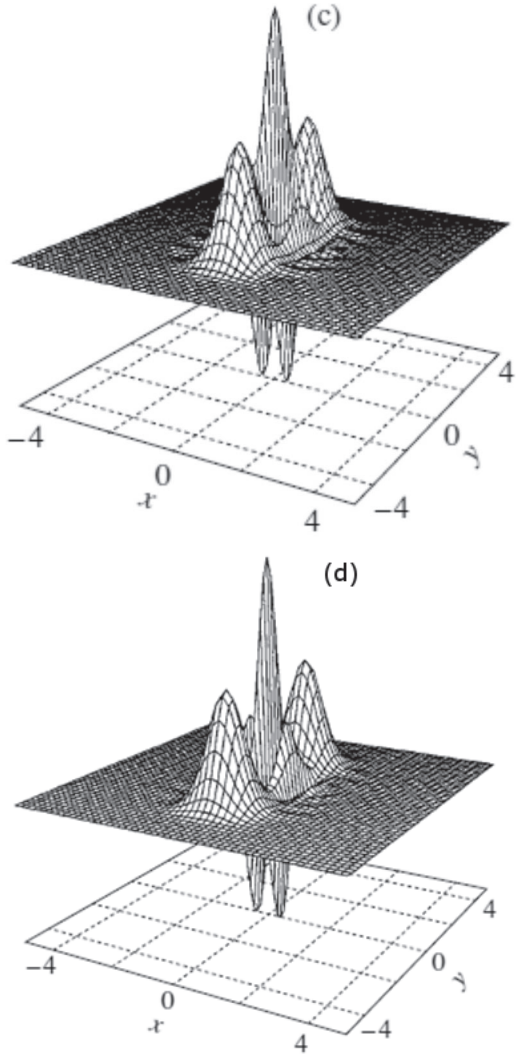

Fig. 3.1. Wigner functions of the field state of one quantum trajectory of the system in the case of evolution (a) from an initial vacuum state of the field and (b) before and (c) after the first two-photon jump of the field state at the moment $\gamma_2 t \approx 0.575$; (d) represents the Wigner function of the field state in the region of large interaction times $\gamma_2 t = 10$. $\varepsilon/\gamma_2 = 5$ and $\gamma_1 = 0$.

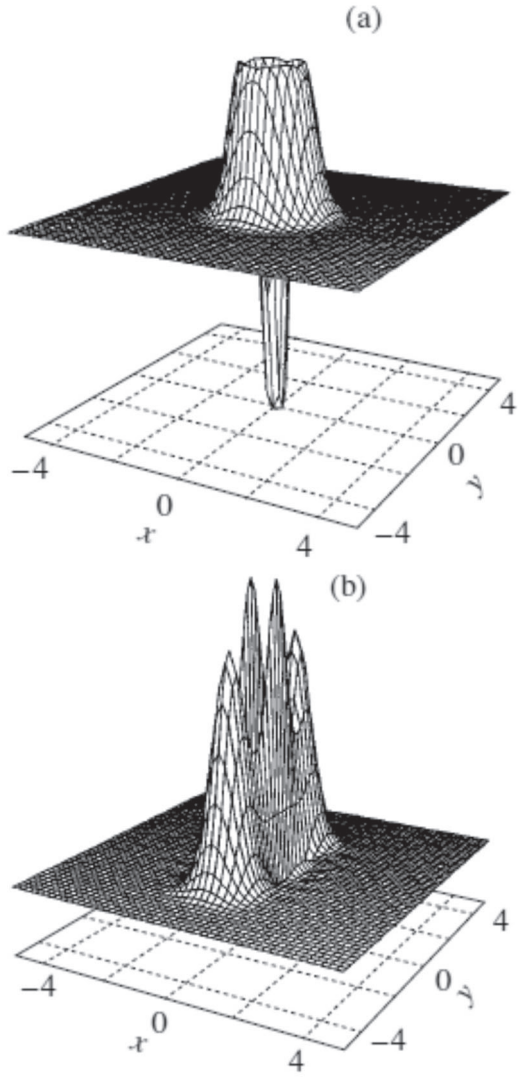

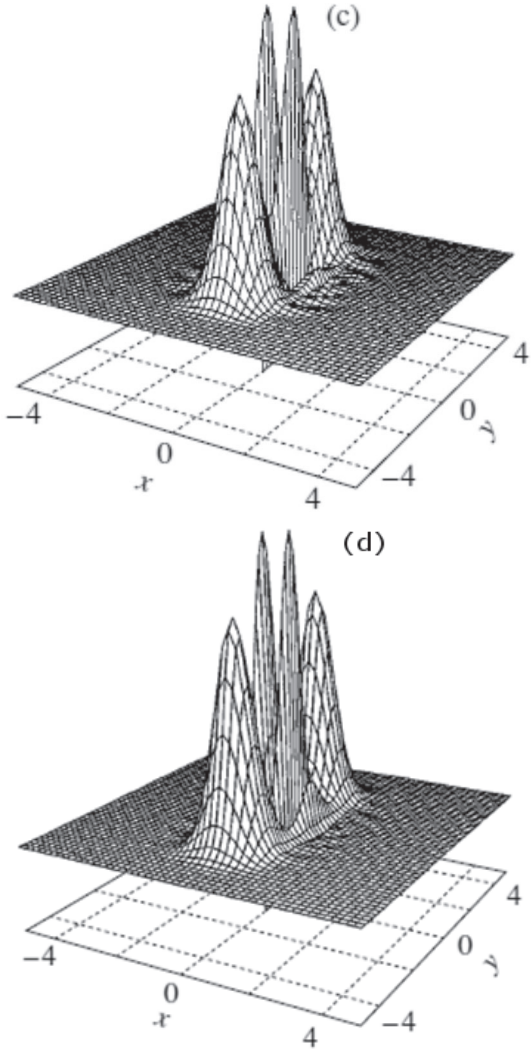

Fig. 3.2. Wigner functions of the field state of one quantum trajectory of the system in the case of evolution (a) from an initial one-photon Fock state of the field and (b) before and (c) after the first two-photon jump of the field state at the moment $\gamma_2 t \approx 0.435$; (d) represents the Wigner function of the field state in the region of large interaction times $\gamma_2 t = 10$. $\varepsilon/\gamma_2 = 5$ and $\gamma_1 = 0$.

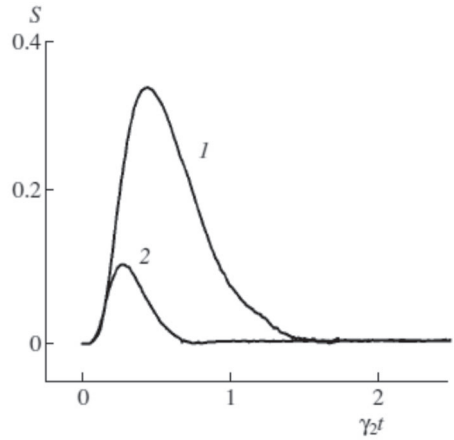

Fig. 3.3. Dynamics of the quantum entropy of the field in the cases of evolution from an initial (1) vacuum and (2) one-photon Fock states of the field. Each curve was calculated, using 5000 independent quantum trajectories of the optical system. $\varepsilon/\gamma_2 = 5$ and $\gamma_1 = 0$.

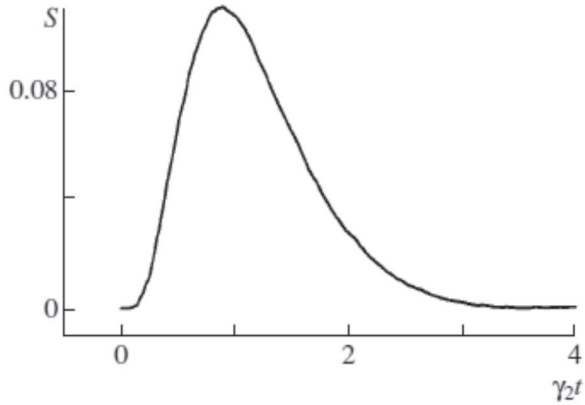

Fig. 3.4. Dynamics of the quantum entropy of the field in the case of evolution from an initial vacuum state of the field. The dynamics of the entropy was calculated, using 5000 independent quantum trajectories of the optical system. $\varepsilon/\gamma_2 = 2$ and $\gamma_1 = 0$.

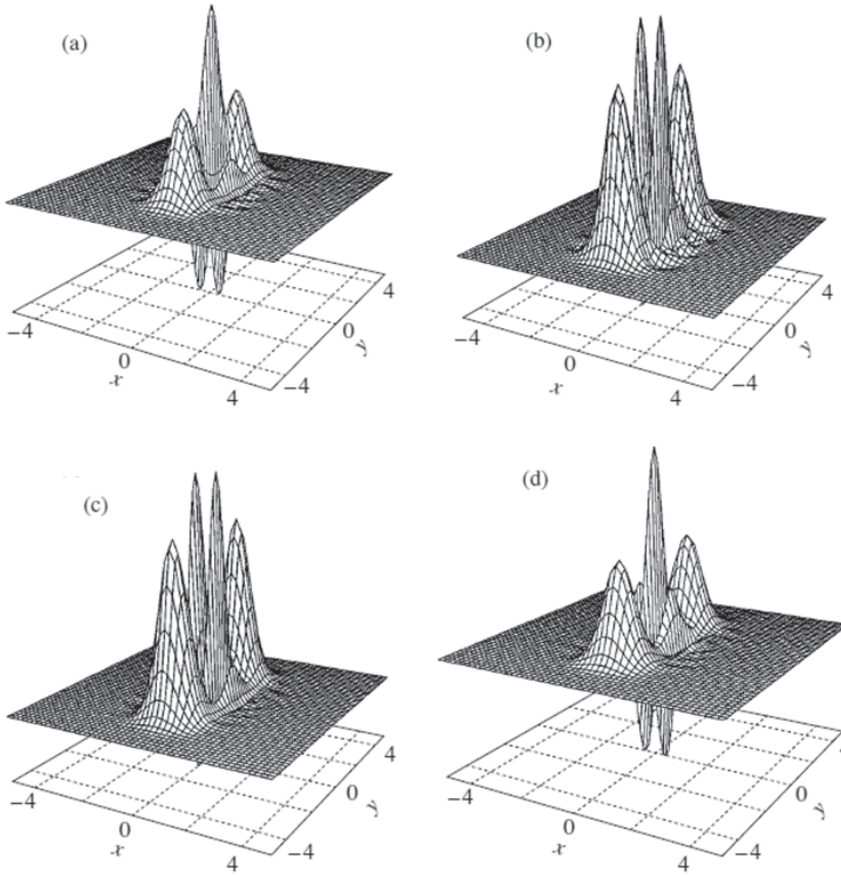

Fig. 3.5. Wigner functions of the field state of one quantum trajectory of the optical system in the case of evolution from an initial vacuum state and in the presence of weak one-photon absorption; $\gamma_1/\gamma_2 = 0.01$. Panels (a)--(b) and (c)--(d) represent the field state Wigner functions before and after the first and before and after the second one-photon quantum jumps of the field state at the moments $\gamma_2 t \approx 12.420$ and$\gamma_2 t \approx 22.51$, respectively ($\varepsilon/\gamma_2 = 5$).

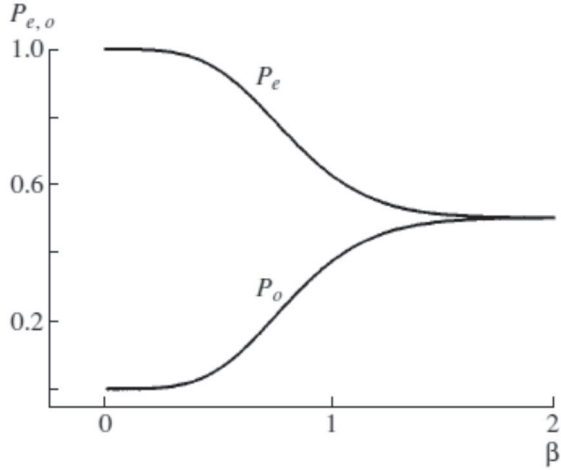

Fig. 3.6. Dependence of the probabilities of finding the field in the even-parity (P_e) and odd-parity (P_o) superposition states at long evolution times $\gamma_1 t >> 1$ and in the presence of weak one-photon absorption $\gamma_1/\gamma_2 << 1$ on the absolute value of the amplitude of the state β = |α|.

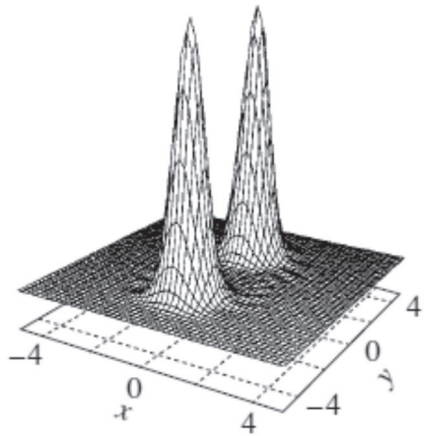

Fig. 3.7. Wigner function of the stationary state of the field in the presence of weak one-photon absorption ($\gamma_1/\gamma_2 << 1$) in the region of a large value of the state amplitude ($\alpha = i\sqrt{5}$).

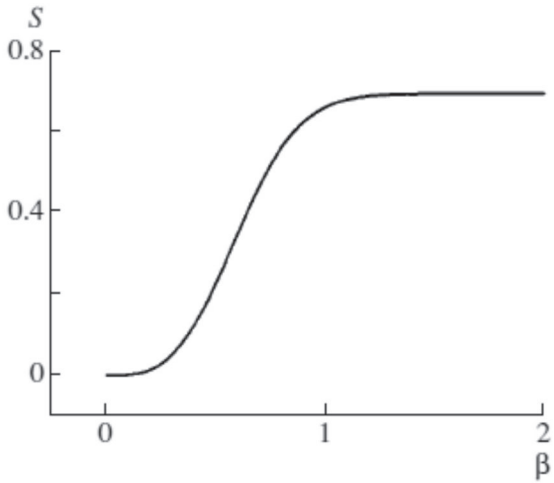

Fig. 3.8. Dependence of the quantum entropy of the stationary state of the field in the presence of weak one-photon absorption $\gamma_1/\gamma_2 << 1$ on the absolute value of the state amplitude β = |α|.

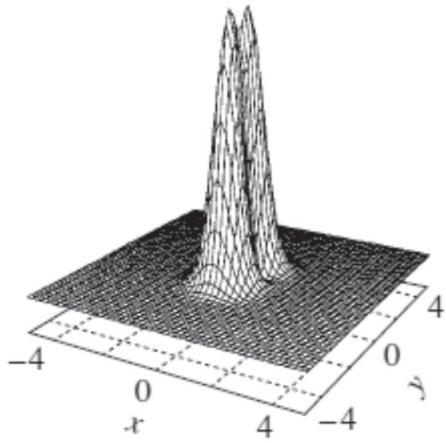

Fig. 3.9. Wigner function of the stationary state of the field in the presence of weak one-photon absorption ($\gamma_1/\gamma_2 << 1$) in the region of a small value of the amplitude of the state (α = i0.8).

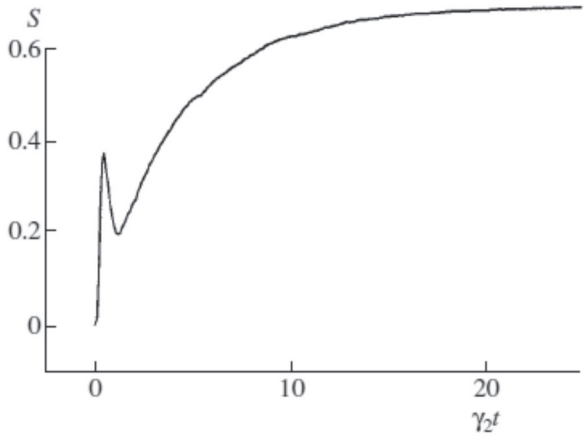

Fig. 3.10. Dynamics of the quantum entropy of the field in the case of evolution from an initial vacuum state of the field in the presence of weak one-photon absorption ($\gamma_1/\gamma_2 = 0.01$). The dynamics of the entropy was calculated, using 5000 independent trajectories of the optical system ($\varepsilon/\gamma_2 = 5$).

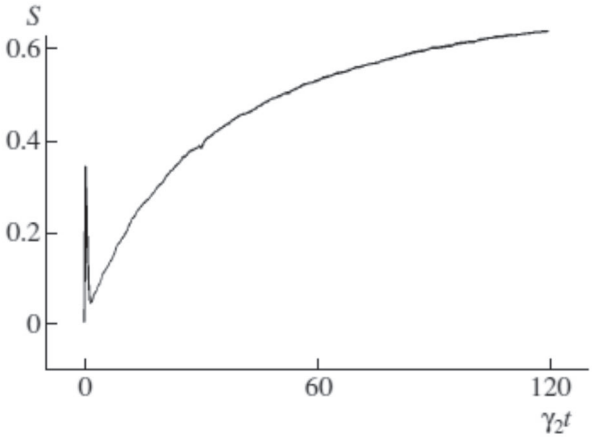

Fig. 3.11. Dynamics of the quantum entropy of the field in the case of evolution from an initial vacuum state of the field in the presence of weak one-photon absorption ($\gamma_1/\gamma_2 = 0.001$). The dynamics of the entropy was calculated, using 5000 independent trajectories of the optical system ($\varepsilon/\gamma_2 = 5$).

CHAPTER 4

THREE-COMPONENT COHERENT SUPERPOSITION STATES OF LIGHT

Introduction

All materials in this chapter are taken from [1–6].

For the process of three-photon absorption in the case of a cubic parametric perturbation, a possibility to obtain quantum superposition states of three coherent components is shown [1,2,3]. The one- and two-photon absorption processes are shown to destroy the interference between the state components: the quantum superposition state decays into a classical mixture of its components. It is shown that, depending on the initial state of the field, the interference between different three-component coherent superposition states formed in the system can result in almost full localization of the optical system in a two-component state or in the destruction of the interference between different coherent components. An analytical solution is obtained for the density matrix of the field in the region of large interaction times. It is shown that the stationary solution of the field density matrix is an eigenstate of the cube of the field annihilation operator.

The Wigner functions and quantum entropy of the system are calculated for a variety of initial states. The quantum properties of three-component superposition field states are studied [4]. It is shown that the action of the

annihilation operator on the superposition state of three coherent components changes the type of interference between coherent components and the superposition state of one type changes into another.

The dependence of the number of photons, as well as of fluctuations in the number of photons of three types of superposition states, on the amplitude of the state is studied. It is shown that, in the region of large values of the amplitude of the state, the numbers of photons of different types of superposition states coincide and Poisson statistics of the number of photons takes place in the system. In the region of small values of the state amplitude, in two types of superposition states, antigrouping of photons is realized, whereas grouping is observed in one. In this region, the photon numbers of different states also differ.

The process of simultaneous absorption of three photons in a medium possessing weak one-photon absorption is analyzed. The mode experiencing absorption is perturbed externally via a three-photon parametric process. It is shown that a steady-state three-component superposition state of light can exist in this system in the range, where the amplitude of the state is small (small perturbations of the system). The latter condition is due to the fact that, in this range of interaction, the field spends significantly more time in one of the three types of superposition states of light that form an ensemble of quantum trajectories of the system than in the other two [5,6]. It is also shown that it is possible to obtain unstable three-component superposition states of light with a large value of the state amplitude (large values of the number of photons) in a range of interaction times, which is larger than the necessary time for the formation of a superposition state in the absence of single-photon dissipation and smaller than the most probable time of the first single-photon jump of the

field state. Using numerical simulation of the quantum trajectories of the system, the formation dynamics of quantum entropy of the field is studied. The Wigner functions of the field state are calculated. Analytical results are obtained for the density matrix of the stationary state of the system in the presence of weak single-photon absorption [5, 6].

4.1. Model of the Nonlinear System and Basic Equations

Let us consider statistical properties of an electromagnetic field mode interacting with a three-photon absorbing medium. This mode is assumed to be excited externally in a three-photon parametric way, which can be described by a cubic, with respect to the field operators (Hamiltonian). We also assume one- and two-photon absorption to occur in the medium. According to such a model, we can write the density matrix equation for the problem in the form

$$\frac{\partial \rho}{\partial t} = L_p(\rho) + L_1(\rho) + L_2(\rho) + L_3(\rho). \qquad (4.1.1)$$

In this equation the superoperators $L_1(\rho)$, $L_2(\rho)$, and $L_3(\rho)$ describe the one-, two-, and three-photon absorption, respectively:

$$L_1(\rho) = -k_1(a^+a\rho + \rho a^+a - 2a\rho a^+),$$

$$L_2(\rho) = -k_2(a^{+2}a^2\rho + \rho a^{+2}a^2 - 2a^2\rho a^{+2}),$$

$$L_3(\rho) = -k_3(a^{+3}a^3\rho + \rho a^{+3}a^3 - 2a^3\rho a^{+3}), \qquad (4.1.2)$$

where k_i $(i = 1,2,3)$ are the corresponding absorption rates in the medium. The first term in Eq. (4.1.1) describes the three-photon parametric pumping,

$$L_p(\rho) = (i\hbar)^{-1}\left[H_p, \rho\right], \tag{4.1.3}$$

with H_p being the corresponding Hamiltonian:

$$H_p = i\hbar\frac{\varepsilon}{2}(a^3 - a^{+3}) \tag{4.1.4}$$

(the pumping phase is omitted here).

Equation (4.1.1) leads to the following equations for the matrix elements of the density matrix in the basis of the Fock states $\rho_{m,n} \equiv \langle m|\rho|n\rangle$:

$$\begin{aligned}\frac{\partial\rho_{m,n}}{\partial\tau} = \frac{\varepsilon}{4k_3}[&[(m+1)(m+2)(m+3)]^{1/2}\rho_{m+3,n} - \\ &[m(m-1)(m-2)]^{1/2}\rho_{m-3,n} - [n(n-1)(n-2)]^{1/2}\rho_{m,n-3} + \\ &[(n+1)(n+2)(n+3)]^{1/2}\rho_{m,n+3}] - \\ &\frac{k_1}{2k_3}[(m+n)\rho_{m,n} - 2[(m+1)(n+1)]^{1/2}\rho_{m+1,n+1} - \\ &\frac{k_2}{2k_3}\{[m(m-1)+n(n-1)]\rho_{m,n} - \\ &2[(m+1)(m+2)(n+1)(n+2)]^{1/2}\rho_{m+2,n+2}\} - \\ &\frac{1}{2}\{[m(m-1)(m-2)+n(n-1)(n-2)]\rho_{m,n} - \\ 2[(m+1)(m+2)(m+3)&(n+1)(n+2)(n+3)]^{1/2}\rho_{m+3,n+3}\},\end{aligned} \tag{4.1.5}$$

where $\tau = 2k_3t$ is the dimensionless time. These are the basic equations of the problem under consideration. We solve them numerically by the Runge–Kutta method (for small photon numbers, it proves to be more efficient to directly solve Eqs. (4.1.5) than to apply the stochastic methods).

In order to investigate quantum properties of the optical system, we calculate the Wigner function (1.9.1) and (1.9.2), which is rather convenient for these purposes. Particularly, the oscillations of this function between the components of a state indicate the occurrence of quantum–mechanical interference between these components.

We also examine the dynamics of the quantum entropy of the field defined as $S(\tau) = -Tr\{\rho(\tau)\, ln\, \rho\,(\tau)\}$. We calculate this quantity by means of numerical diagonalization of the density matrix in the Fock basis. The quantum entropy equals zero in pure states, and it increases, when the system loses its coherence properties.

The Monte Carlo wave function method [7] was applied to investigate quantum trajectories of the optical system when two- and weak one-photon absorption is absent. An algorithm of this technique is given below for calculating a single quantum trajectory of the field of the system under consideration.

In order to obtain the field state at the time $t + \delta t$, we calculate the probability of a quantum jump of this state at the t time:

$$\delta p = \delta p_1 + \delta p_3 = \gamma_1 \delta t \langle \psi(t)|a^+ a|\psi(t)\rangle + \gamma_3 \delta t \langle \psi(t)|a^{+3} a^3|\psi(t)\rangle, \quad (4.1.6)$$

where $|\psi(t)\rangle$ is the field state at the t time. The first and second terms in Eq. (4.1.6) describe the probabilities of one- and three-photon quantum jumps of the field state, respectively. After such an event, a random ξ number is generated, which has a uniform distribution in the interval $(0; 1)$. When $\xi < \delta p$, a quantum jump of the field state occurs in the system, and we calculate the normalized probabilities of these jumps as

$$p_1 = \frac{\delta p_1}{\delta p_1 + \delta p_3}, p_3 = \frac{\delta p_3}{\delta p_1 + \delta p_3}. \quad (4.1.7)$$

Then the second random number is generated, which also has a uniform distribution in the interval $(0; 1)$. When $\eta < p_1$, a one-photon quantum jump of the field state occurs in the system and the field passes to the state

$$|\psi(t + \delta t)\rangle \sim a|\psi(t)\rangle. \quad (4.1.8)$$

In the opposite case, when $\eta > p_1$, a three-photon field state jump occurs in the system and the field changes into a new state:

$$|\psi(t + \delta t)\rangle \sim a^3|\psi(t)\rangle. \quad (4.1.9)$$

The new states are normalized in both cases. In the case of $\xi > \delta p$, the system evolves continuously as follows:

$$|\psi(t + \delta t)\rangle \sim |\psi(t)\rangle + (i\hbar)^{-1} H_{ef} \delta t|\psi(t)\rangle, \quad (4.1.10)$$

where

$$H_{ef} = H_p - i\hbar \frac{\gamma_1}{2} a^+ a - i\hbar \frac{\gamma_3}{2} a^{+3} a^3 \quad (4.1.11)$$

is the non-Hermitian Hamiltonian of continuous evolution. After every step of continuous evolution, the state of the system is normalized.

The density matrix of the field is calculated as the mathematical expectation of the trajectory matrices of the system:

$$\rho(t) = \lim_{N \to \infty} \left(\frac{1}{N} \sum_{(m)=1}^{N} \left| \psi(t)_{(m)} \right\rangle \left\langle \psi(t)_{(m)} \right| \right). \quad (4.1.12)$$

4.2. Formation and Decay of Coherent Superposition States

Firstly, we consider the dynamics of the optical system, when there are no one- and two-photon absorption processes (i.e., $k_1 = k_2 = 0$).

For the case when the system is initially in the vacuum state ($\rho(0) = |0\rangle\langle 0|$) and is then driven strongly ($\varepsilon >> k_3$), the dynamics of the Wigner function is demonstrated in Figs. 4.1a to 4.1c, while the evolution of the quantum entropy for this case is given in Fig. 4.2 (curve 1). At the time $\tau = 0$, the system is in a vacuum (pure) state and has zero entropy and is described by the Wigner function in Fig. 4.1a. Then, the entropy increases and reaches its maximum value at the moment $\tau \approx 0.49$. At this time, the Wigner function appears as in Fig. 4.1b. The system is in a three-component state with equal probabilities to be found in each of the components. Oscillations between the components show that quantum-mechanical interference occurs. Since the entropy is greater than zero, the system is not in a pure state and only partial coherence is realized between the components of this state.

At times $\tau > 0.49$, the entropy tends to its steady-state zero value. The system goes to a pure state, which is a quantum superposition of the three components. The steady-state Wigner function is shown in Fig. 4.1c. The mean number of photons in this state ($n = Tr\{\rho a^+ a\} = \langle a^+ a\rangle$) is equal to ~4.65.

In the case of a weak driving field ($\varepsilon \approx k_3$), the components of the Wigner function overlap and are not seen well. This is demonstrated in Fig. 4.3. The entropy dynamics for this case is shown by curve 2 in Fig. 4.2.

If one- or two-photon absorption (even if weak) occurs in the system, it destroys the interference between the components of the steady state, and the pure state decays into a statistical mixture of the three components. The steady-state ($\tau = 4$) Wigner function in the case of one-photon absorption ($k_2 = 0$ and $k_1/k_3 = 0.2$) and strong driving ($\varepsilon/k_3 = 20$) is shown in Fig. 4.4. Here, oscillations are absent; i.e., there is no interference between the components. The system is in a state, which is a statistical mixture of the three components with equal probabilities of finding the system in each of them. The quantum entropy of such a state should be equal to ln3. In this case, the steady-state limit of curve 3 in Fig. 2, which shows the entropy evolution, is close to $1.09 \approx ln\,3$.

Figure 4.2 shows the dynamics of the system entropy in the cases, where two-photon absorption ($k_1 = 0$ and $k_2/k_3 = 0.2$) occurs in the system (curve 4) and where either one- or two-photon absorption is present ($k_1/k_3 = 0.2$ and $k_2/k_3 = 0.2$), in addition to three-photon absorption (see curve 5). It is seen that, at equal rates of one- and two-photon absorption, the latter destroys the quantum coherence in the system much faster.

Figure 4.5 shows the photon number distribution $p(n) = \langle n|\rho|n\rangle$ in the steady state of the system when one- and two-photon absorption is absent and a coherent superposition state is formed (Fig. 4.5a) and for the presence of one-photon absorption when the steady state is a statistical mixture of the three components (Fig. 4.5b). In both cases, the system evolves from an initial vacuum state.

The oscillations in Fig. 4.5a express the three-photon nature of the coherent superposition state: the distribution function only has

nonvanishing values for the numbers of photons equal to $n = 3k$ ($k = 0,1,2,\ldots$). These oscillations are absent in Fig. 4.5b.

Similarly, coherent superposition states are formed in the system by evolving from initial one- and two-photon Fock states ($\rho(0) = |1\rangle\langle 1|$ and $\rho(0) = |2\rangle\langle 2|$). In these cases, the photon number distribution function $p(n)$ has nonvanishing values for $n = 3k + 1$ and $n = 3k + 2$, respectively ($k = 0,1,2,\ldots$).

4.3. Evolution from Multicomponent Mixed Initial States

Consider now cases, when the system is not initially found in a pure state and one- and two-photon dissipation does not take place. Figure 4.6 represents the dynamics of the quantum entropy of the system when $\varepsilon/k_3 = 20$ and for the following initial states, which are statistical mixtures of Fock states: $\rho(0) = (1/2)(|0\rangle\langle 0| + |1\rangle\langle 1|)$ (curve 1), $\rho(0) = (1/2)(|1\rangle\langle 1| + |2\rangle\langle 2|)$ (curve 2), $\rho(0) = (1/2)(|0\rangle\langle 0| + |2\rangle\langle 2|)$ (curve 3); $\rho(0) = 1/3)(|0\rangle\langle 0| + |1\rangle\langle 1| + |2\rangle\langle 2|)$ (curve 4), and $\rho(0) = (1/2)(|0\rangle\langle 0| + |3\rangle\langle 3|)$ (curve 5). Of all these cases, only in the last one does the system evolve to a pure steady state (see Fig. 4.6, curve 5). Starting from the value $\sim 0.7 \approx ln\,2$, corresponding to a statistical mixture of two components, the entropy decreases, tending to the steady-state zero value. This pure state is a quantum superposition of the three components, as can be seen from the shape of the Wigner function presented in Fig. 4.7b (Fig. 4.7a shows the initial shape of the Wigner function for this case).

In the case of initial mixed two-component states $\rho(0) = (1/2)(|m\rangle\langle m| + |n\rangle\langle n|)$ with the photon number difference in the

components $m-n\neq 3k$ $(k=0,1,2..)$, the entropy increases from the $ln\,2$ value, reaches a maximum value, and then decreases tending to the steady-state $ln\,2$ value (see Fig. 4.6, curves l–3)). In these cases, a state, which is a statistical mixture of two three-component quantum superposition states, is formed in the system. So, Fig. 4.8 shows the Wigner function of the initial $\rho(0)=(1/2)(|0\rangle\langle 0|+|1\rangle\langle 1|)$ (Fig. 4.8a) and steady (Fig. 4.8b) states at $\varepsilon/k_3=20$ and without one- and two-photon dissipation. Although, in this case, the stationary state of the system is a statistical mixture of two quantum three-component states, there are oscillations of the Wigner function between the coherent components, which shows that quantum-mechanical interference exists between the coherent components of the state. The latter is explained by the fact that the quantum entropy of the field ($ln\,2$) is less than the maximum quantum entropy of the three-component state, which is equal to $ln\,3$. This leads to the formation of quantum-mechanical coherence in the stationary state of the field.

If the initial state is a three-component mixture $\rho(0)=(1/3)(|n\rangle\langle n|+|m\rangle\langle m|+|l\rangle\langle l|)$ ($m-n\neq 3k$, $m-l\neq 3k'$, and $n-l\neq 3k''$, where k, k', and $k''$are integers), the quantum entropy of the system starts from the value $\sim 1.09\approx ln\,3$; increases; then reaches its maximum value; and, after this, tends to decrease to the $ln\,3$ value; i.e., a statistical mixture of three quantum superposition states is formed at $\tau\to\infty$ with equal probabilities of finding the system in each of them. An example of such evolution shows the Wigner function of the initial state $\rho(0)=(|0\rangle\langle 0|+|1\rangle\langle 1|+|2\rangle\langle 2|)/3$ and the steady state given in Figs. 4.9a and 4.9b, respectively.

4.4. Steady states of the System and the Eigenstates of the Field Amplitude Cube

If one- and two-photon losses are not important, it is easy to find steady-state solutions to the density matrix equation (4.1.1). For this purpose, we represent the density matrix as an expansion in the coherent state basis:

$$\rho(\infty) = \sum_{\alpha,\alpha'} b_{\alpha,\alpha'} |\alpha\rangle\langle\alpha'|, \tag{4.4.1}$$

where $b_{\alpha,\alpha'}$ are constants determined by the standard conditions that $\rho(\infty)$must be satisfied. Substituting this expansion into the density matrix equation

$$L_p(\rho) + L_3(\rho) = 0, \tag{4.4.2}$$

we obtain

$$\sum_{\alpha,\alpha'} b_{\alpha,\alpha'} \left\{ \left[-\frac{\varepsilon}{2} - k_3(\alpha'^*)^3 \right] |\alpha\rangle\langle\alpha'|\alpha^3 + \left[-\frac{\varepsilon}{2} - k_3\alpha^3 \right] \alpha^{+3} |\alpha\rangle\langle\alpha'| \right.$$
$$\left. + \left[\frac{\varepsilon}{2} + k_3(\alpha'^*)^3 \right] |\alpha\rangle\langle\alpha'|\alpha^3 + \left[\frac{\varepsilon}{2} + k_3\alpha^3 \right] |\alpha\rangle\langle\alpha'|(\alpha'^*)^3 \right\} = 0. \tag{4.4.3}$$

To satisfy this equation for each $b_{\alpha,\alpha'}$, the α and α' quantities should be equal to

$$\alpha^3 = (\alpha'*)^3 = -\frac{\varepsilon}{2k_3}, \tag{4.4.4}$$

which gives

$$\alpha_m = \beta\, exp(\,2\pi i m/3),$$

$$\alpha'_m = \beta\, exp(\,2\pi i m/3),\ m = -1,0,1, \tag{4.4.5}$$

with

$$\beta = \left(-\frac{\varepsilon}{2k_3}\right)^{1/3}. \tag{4.4.6}$$

Using Eqs. (4.4.5) and (4.4.6), we can represent the steady-state solution for the density matrix as

$$\begin{aligned}\rho(\infty) = {} & P_0|\beta\rangle\langle\beta| + a_{0,2\pi/3}|\beta\rangle\langle exp(2\pi i/3)\beta| + \\ & a_{0,-2\pi/3}|\beta\rangle\langle exp(-2\pi i/3)\beta| + a_{2\pi/3,0}|exp(2\pi i/3)\beta\rangle\langle\beta| + \\ & P_{2\pi/3}|exp(2\pi i/3)\beta\rangle\langle exp(2\pi i/3)\beta| + \\ & a_{2\pi/3,-2\pi/3}|exp(2\pi i/3)\beta\rangle\langle exp(-2\pi i/3)\beta| + \\ & a_{-2\pi/3,0}|exp(-2\pi i/3)\beta\rangle\langle\beta| + \\ & a_{-2\pi/3,2\pi/3}|exp(-2\pi i/3)\beta\rangle\langle exp(2\pi i/3)\beta| + \\ P_{-2\pi/3}|exp(-2\pi i/3)\beta\rangle & \langle exp(-2\pi i/3)\beta|. \end{aligned} \tag{4.4.7}$$

Here, P_0, $P_{2\pi/3}$, $P_{-2\pi/3}$ are the probabilities of finding the system in the coherent states $|\beta\rangle$, $|exp(2\pi i/3)\beta\rangle$, and $|exp(-2\pi i/3)\beta\rangle$, respectively. The coefficients $a_{p,q} = a_{q,p}*$ $(p, q = 0, -2\pi/3, 2\pi/3)$ describe the interference between the components $|exp(ip)\beta\rangle$ and $|exp(iq)\beta\rangle$. It is seen from Eq. (4.4.7) that the steady-state density matrix is an eigenstate of the cube of the annihilation operator with the eigenvalueβ^3:

$$a^3\rho(\infty) = \beta^3\rho(\infty). \tag{4.4.8}$$

We now construct a linear combination of the three possible coherent states $|exp(2\pi mi/3)\beta\rangle$ $(m = -1,0,1)$ with arbitrary relative phases ϕ_2 and ϕ_3:

$$\begin{aligned}|\xi\rangle = {} & N^{1/2}\{|\beta\rangle + exp(i\phi_2)|exp(2\pi i/3)\beta\rangle + \\ & exp(i\phi_3)|exp(-2\pi i/3)\beta\rangle\}, \end{aligned} \tag{4.4.9}$$

where N represents the normalizations. We now calculate the diagonal elements of the density matrix $|\xi\rangle\langle\xi|$:

$$\langle n|\xi\rangle\langle\xi|n\rangle = N\frac{|\beta|^{2n}}{n!}exp(-|\beta|^2)\left\{3 + 2\,cos\left(\frac{2\pi n}{3} + \phi_2\right) + 2\,cos\left(\frac{2\pi n}{3} - \phi_3\right) + 2\,cos\left(\frac{4\pi n}{3} + \phi_2 - \phi_3\right)\right\}.$$

. (4.4.10)

Conditions, when the diagonal elements are equal to zero if $n = 3k + 1$ and $n = 3k + 2$ $(k = 0,1,2,\ldots)$, result in the zero phases $\phi_2 = 0$ and $\phi_3 = 0$. The same conditions for the case $n = 3k$ and $n = 3k + 2$ produce $\phi_2 = 2\pi/3$ and $\phi_3 = -2\pi/3$; while for the case $n = 3k$ and $n = 3k + 1$, we have $\phi_2 = -2\pi/3$ and $\phi_3 = 2\pi/3$. Thus, we have three quantum superposition states:

$$|\beta\rangle_m = N_m^{1/2}\{|\beta\rangle + exp(2\pi im/3)|exp(2\pi im/3)\beta\rangle + exp(-2\pi im/3)|exp(-2\pi i/3)\beta\rangle\},\ m = -1,0,1. \quad (4.4.11)$$

Here, the normalizations are determined by the following expressions:

$$N_m^{-1} = 3\left\{1 + 2\,exp(-3|\beta|^2/2)\,cos\left(\frac{2\pi m}{3} + \frac{3^{1/2}}{2}|\beta|^2\right)\right\},\ m = -1,0,1. \quad (4.4.12)$$

It is easy to verify that Eq. (4.4.11) has the property

$$|\beta\rangle_{m+3} \equiv |\beta\rangle_m, \quad (4.4.13)$$

and, instead of the index value $m = -1$, the value $m = 2$ can be used, which we will use in the future.

Coherent superposition states (4.4.11) with the three components are the eigenstates of the cube of the field amplitude operator:

$$a^3|\beta\rangle_m = \beta^3|\beta\rangle_m, \qquad m = 0,1,2. \tag{4.4.14}$$

They have the following scalar products with Fock states:

$$\langle n|\beta\rangle_m = N_m^{1/2}\, exp(-|\beta|^2/2)\frac{\beta^n}{(n!)^{1/2}}\left[1 + 2\,cos\left(\frac{2\pi}{3}(n+m)\right)\right]. \tag{4.4.15}$$

We can now calculate the steady-state solutions to the density matrix (4.4.7) in terms of the states (4.4.11). To do this, we note the following: if the system evolves from an initial vacuum state, in the steady-state limit, it comes to a pure state, which is the quantum-mechanical superposition of the three components (see Section 4.2). In this state, the density matrix diagonal elements $\rho_{n,n} = \langle n|\rho(\infty)|n\rangle$ are only nonzero at $n = 3k$ ($k = 0,1,2,\ldots$). From the expression for the density matrix and the above consideration, it follows that the density operator may in this case be represented as $\rho(\infty) = |\beta\rangle_{00}\langle\beta|$, where $|\beta\rangle_0$ is defined by Eq. (4.4.11) at m = 0. Similarly, if the system evolves from the states $\rho(0) = |1\rangle\langle 1|$ or $\rho(0) = |2\rangle\langle 2|$, we will have $\rho(\infty) = |\beta\rangle_{11}\langle\beta|$ or $\rho(\infty) = |\beta\rangle_{22}\langle\beta|$, respectively. Here, the $|\beta\rangle_{1,2}$ states are defined by Eq. (4.4.11) when $m = 1,2$. Since, in the case of a steady state and without one- and two-photon losses, Eq. (4.1.5) couples Fock states with $n = 3k$ ($k = 0,1,2,\ldots$) to Fock states with $n = 3l$ ($l = 0,1,2,\ldots$); states with $n = 3k + 1$ to states with $n = 3l + 1$; and states with $n = 3k + 2$ to states with $n = 3l + 2$, the steady-state density matrix may in general be represented in the following form:

$$\rho(\infty) = p_0|\beta\rangle_{00}\langle\beta| + p_1|\beta\rangle_{11}\langle\beta| + p_2|\beta\rangle_{22}\langle\beta| + a_{0,1}|\beta\rangle_{01}\langle\beta| + a_{0,2}|\beta\rangle_{02}\langle\beta| + a_{1,0}|\beta\rangle_{10}\langle\beta| + a_{1,2}|\beta\rangle_{12}\langle\beta| + a_{2,0}|\beta\rangle_{20}\langle\beta| + a_{2,1}|\beta\rangle_{21}\langle\beta| \ . \quad (4.4.16)$$

Here p_0, p_1, and p_2 are the probabilities to find the system in the coherent superposition states $|\beta\rangle_0$, $|\beta\rangle_1$, and $|\beta\rangle_2$, respectively ($p_0 + p_1 + p_2 = 1$), while $a_{m,k}$ ($m = 0,1,2$ and $k = 0,1,2$) are the coherences ($a_{m,k} = a *_{k,m}$), determining the interference between these superposition states. Since $Tr\rho$ is the integral of motion, the p_0, p_1, and p_2 probabilities can be calculated as

$$p_0 = \sum_{n=3k} \rho_{n,n}(0),$$

$$p_1 = \sum_{n=3k+1} \rho_{n,n}(0),$$

$$p_2 = \sum_{n=3k+2} \rho_{n,n}(0). \quad (4.4.17)$$

4.5. Quantum-Mechanical Interference Between Superposition States

In this section, we consider the formation of a steady state, if the system evolves from initially pure states, which are quantum-mechanical superpositions of Fock states.

Figure 4.10 shows the dynamics of the quantum entropy of the field in the case of a strong perturbation of the absorbing field ($\varepsilon/k_3 = 20$), in the absence of single- and two-photon absorption, and in the case of evolution of the system from an initial pure state, which is a quantum-mechanical superposition of Fock states. Curves 1–4 represent the dynamics of the quantum entropy of the field in the case of evolution of the system from initial states ($\rho(0) = |\psi(0)\rangle\langle\psi(0)|$) $|\psi(0)\rangle = (|0\rangle + |1\rangle)/2^{1/2}$, $|\psi(0)\rangle = (|1\rangle + |2\rangle)/2^{1/2}$, $|\psi(0)\rangle = (|0\rangle + |2\rangle)/2^{1/2}$, and $|\psi(0)\rangle = (|0\rangle + |1\rangle +$

$|2\rangle)/3^{1/2}$, respectively. In the first three cases, the system starts evolution from an initial state, which is a superposition of two Fock states. The stationary value of quantum entropy for these cases is less than $ln\,2$, which shows that, for these three cases, there is quantum-mechanical interference between two three-component superposition states that form in the system.

Figure 4.11 shows the dynamics of the Wigner function in the absence of single- and two-photon absorption and in the case of a large perturbation ($\varepsilon/k_3 = 20$). Figure 4.11a represents the Wigner function of the initial state of the field $|\psi(0)\rangle = (|1\rangle + |2\rangle)/2^{1/2}$. The Wigner function of the stationary state of the field is shown in Fig. 4.11b. Mainly, the field is localized in a two-component state. There is a very low probability of detection of the field in the third state. This is the result of interference between the two three-component superposition states $|\beta\rangle_1$ and $|\beta\rangle_2$. In this case, the stationary solution (4.4.16) can be represented as follows ($p_0 = 0$ and $p_1 = p_2 = 1/2$):

$$\rho(\infty) = \frac{1}{2}|\beta\rangle_{11}\langle\beta| + \frac{1}{2}|\beta\rangle_{22}\langle\beta| + a|\beta\rangle_{12}\langle\beta| + a*|\beta\rangle_{21}\langle\beta|. \quad (4.5.1)$$

In this expression, a is the coherence coefficient, which characterizes the interference between the two three-component superposition states represented in Eq. (4.4.11) with the indices $m = 1$ and $m = 2$. By expanding solution (4.5.1) in coherent states $|\beta\rangle$, $|\beta\, exp(\,2\pi i/3\rangle$, and $|\beta\, exp(\,-2\pi i/3\rangle$, probabilities of detection of the system $P_{0,\pm 2\pi i/3}$ in the coherent states $|\beta\rangle$, $|\beta\, exp(\,2\pi i/3\rangle$, and $|\beta\, exp(\,-2\pi i/3\rangle$ are obtained:

$$P_0 = \frac{1}{2}(N_1 + N_2 + 4\,Re\; a\,(N_1N_2)^{1/2}),$$
$$P_{2\pi/3} = \frac{1}{2}(N_1 + N_2 + 4\,Re(\,a\,exp(\,4\pi i/3))(N_1N_2)^{1/2}),$$

$$P_{-2\pi/3} = \frac{1}{2}(N_1 + N_2 + 4\,Re(\,a\,exp(-4\pi i/3))(N_1 N_2)^{1/2}), \quad (4.5.2)$$

where $N_{1,2}$ is defined by formula (4.4.12). In the region of a strong perturbation field ($\varepsilon >> k_3$ and $|\beta|^2 = (\varepsilon/2k_3)^{2/3} > 1$), the normalization coefficients (4.4.12) are approximately equal ($N_1 \approx N_2 \approx 1/3$) and Eq. (4.5.2) takes the following simple form:

$$P_0 \approx \frac{1}{3}(1 + 2\,Re\,a),$$

$$P_{2\pi/3} \approx \frac{1}{3}(1 + 2\,Re(\,a\,exp(\,4\pi i/3))),$$

$$P_{-2\pi/3} \approx \frac{1}{3}(1 + 2\,Re(\,a\,exp(-4\pi i/3))) \quad . \qquad (4.5.3)$$

These values depend only on the interference coefficient a between two three-component superposition states. The system can localize in a two-component coherent state with equal probabilities of detection of the field in each component of the state, when the interference coefficient between two three-component superposition states is a real negative number. When the a coefficient takes a maximum negative value of $-1/2$, the field is completely localized in a two-component state. The P_0 probability of detecting the system in a coherent state $|\beta\rangle$ is zero.

Figure 4.12 shows the dynamics of the Wigner function in the absence of one- and two-photon absorption in the region of strong perturbations of the absorbed mode ($\varepsilon/k_3 = 20$). Figure 12a represents the Wigner function of the initial state of the field $|\psi(0)\rangle = (|0\rangle + |2\rangle)/2^{1/2}$, and Fig. 12b represents the Wigner function of the stationary state of the field. In this case, the field is considerably more localized in the $|\beta\rangle$ state, and the

interference between the coherent components $|\beta\, exp(\,2\pi i/3)\rangle$ and $|\beta\, exp(\,-2\pi i/3)\rangle$ is destroyed.

4.6 Quantum Properties of Three-Component Coherent Superposition States of Light

Let us consider the quantum properties of three-component coherent superposition states of an optical field

$$|\beta\rangle_m = N_m^{1/2}\{|\beta\rangle + exp(\,2\pi im/3)|exp(\,2\pi i/3)\beta\rangle + exp(\,-2\pi im/3)|exp(\,-2\pi i/3)\beta\rangle\}, \quad (4.6.1)$$

$$N_m^{-1} = 3\{1 + 2\, exp(\,-3|\beta|^2/2)\, cos(\,2\pi m/3 + \sqrt{3}|\beta|^2/2)\}. \quad (4.6.2)$$

Here $|\beta\rangle_m$, where $m = (0,1,2)$, are three-component superposition states of the optical field; $|\beta\rangle$, $|exp(\,2\pi i/3)\beta\rangle$, and $|exp(\,-2\pi i/3)\beta\rangle$ are coherent states; and $m = (0,1,2)$ are the normalization coefficients of the superposition states. Firstly, we study the number of photons of superposition states $|\beta\rangle_m$, where $m = (0,1,2)$. The action of the annihilation operator on a superposition state $|\beta\rangle_m$ gives

$$a|\beta\rangle_m = \left(\frac{N_m}{N_{m+1}}\right)^{1/2} \beta|\beta\rangle_{m+1}. \quad (4.6.3)$$

In this expression, the normalization coefficients N_m are determined by Eq. (4.6.2). From Eq. (4.6.3), we can obtain an expression for the number of photons of three-component superposition states $|\beta\rangle_m$, using formula (4.6.2) for the normalization coefficients

$$n_m =_m \langle\beta|a^+a|\beta\rangle_m = \frac{N_m}{N_{m+1}}|\beta|^2. \quad (4.6.4)$$

In the case of large $|\beta|^2$ values ($|\beta|^2 >> 1$), the ratio of normalization coefficients is close to one and superposition states of different types have the same average value of the number of photons, which is equal to $|\beta|^2$. Figure 4.13 shows the dependence of the number of photons of coherent three-component superposition states $|\beta\rangle_m$ on the squared amplitude of the state $|\beta|^2$. In the region of large values of the squared amplitude of the state ($|\beta|^2 >> 1$), the numbers of photons of the three types of coherent superposition states are all equal to $|\beta|^2$. In the case of a decrease in the amplitude of the state, in the region of values $|\beta|^2 << 1$, the number of photons in different coherent superposition states depends strongly on the state type. For the states $|\beta\rangle_0$, $|\beta\rangle_1$, and $|\beta\rangle_2$, in the region of small amplitude values of the state, the photon numbers are equal to 0, 1, and 2, respectively.

Let us consider the statistics of the number of photons of coherent superposition states $|\beta\rangle_m$. Using formula (4.6.3), we can obtain the following formula for the relative dispersion of the number of photons of these states:

$$Q_m = \frac{m\langle\beta|(\Delta n)^2|\beta\rangle_m}{m\langle\beta|n|\beta\rangle_m} = 1 + \left(\frac{N_{m+1}}{N_{m+2}} - \frac{N_m}{N_{m+1}}\right)|\beta|^2, \qquad (4.6.5)$$

where $n = a^+a$ is the operator for the number of photons, and $\Delta n = a^+a - {}_m\langle\beta|a^+a|\beta\rangle_m$. When $|\beta|^2 >> 1$, from Eq. (4.6.2), we have $N_m \approx N_{m+1}$, $N_{m+1} \approx N_{m+2}$; for the relative dispersion of the number of photons of three-component superposition states, we obtain $Q \approx 1$. For all three types of superposition states, Poisson statistics of the number of photons takes place in this region of the state amplitude.

In the case of small values of the state amplitude $|\beta|^2 << 1$, the statistics of the number of photons depends strongly on the type of a superposition state. Figure 4.14 shows the dependence of the relative dispersion of the number of photons of superposition states on the squared amplitude of the state. In this figure, curve a represents the variance of the number of photons of the three-component superposition state $|\beta\rangle_m$, where $m = 0$; curve b represents the variance of the number of photons of the state $|\beta\rangle_1$; and curve c represents the variance of the number of photons of the state $|\beta\rangle_2$. In the region of small values of the β state amplitude, in the $|\beta\rangle_0$ superposition state, grouping of photons is realized ($Q > 1$); in the $|\beta\rangle_1$ and $|\beta\rangle_2$ superposition states, antigrouping of photons is realized ($Q < 1$).

Consider the destruction of three-component quantum superposition states $|\beta\rangle_m$ in the presence of single-photon dissipation of the optical field. The destruction of the quantum coherence of two-component superposition field states (Schrödinger cat) in the presence of dissipation of the field was studied in [8,9]. In these works, the destruction mechanisms of the quantum coherence of these states were studied by modelling quantum trajectories of the field, using the quantum jump [7] and quantum state diffusion [10] methods. It is shown that, in the case of modelling the behaviour of superposition state of the Schrödinger cat type, using the quantum jump method, the field state jumps from an even-type superposition state to an odd-type one and returns back, which leads to the formation of an ensemble of field states, consisting of two elements (from even- and odd-type superposition states). This leads to the destruction of the interference between the coherent components of the superposition state, and the field changes into a state that is a statistical mixture of two types of superposition states. In the case of a large value of the state

amplitude, the state can be represented as a statistical mixture of two coherent states. The destruction of the quantum coherence of the field state occurs much faster than energy dissipation. The destruction speed of the quantum coherence of the field state depends linearly on the number of photons in the state.

When the dynamics of the field state is modelled using the Quantum state diffusion method, in trajectories, the field localizes in one randomly selected coherent component of a two-component superposition state in the region of large values of the state amplitude. In this case, the ensemble of trajectories of the system consists of two types of coherent states that have opposite signs of the amplitude. This shows that the quantum coherence of the state collapsed and the field passed into a state that is a statistical mixture of two coherent states.

When a quantum system interacts with a large reservoir, the destruction of coherence can be studied using the following equation for the density matrix of the field [11]:

$$\frac{\partial \rho}{\partial t} = \frac{\gamma}{2}(2a\rho a^{+} - a^{+}a\rho - \rho a^{+}a), \qquad (4.6.6)$$

where ρ is the density matrix of the optical field and γ is the energy damping factor.

Both above-mentioned methods for modelling the behaviour of the field state are based on obtaining an ensemble of pure states $\{|\varphi(t)\rangle\}$ of a quantum system. In both cases, the density matrix of the system is calculated as the mathematical expectation of the density matrices of the pure states

$\rho(t) = M\{|\varphi(t)\rangle\langle\varphi(t)|\}$.

First, we study the temporal behavior of one quantum trajectory of the field state, described by the equation for density matrix (4.6.6) in the case of system evolution from the initial three-component superposition state $|\beta\rangle_0$ and in the case of simulation of quantum trajectories by applying the Monte Carlo wave function method (the method of quantum jumps of the field state).

In this case, to obtain the state of the field at the time $t + \Delta t$, the probability of a quantum jump of the field state at the t time is calculated:

$\Delta p = \gamma \Delta t \langle\varphi(t)|a^+ a|\varphi(t)\rangle$,

where $|\varphi(t)\rangle$ is the field state at the t time. Next, a random number ε is generated that has a uniform distribution in the interval $(0\ldots1)$. When $\varepsilon < \Delta p$, a jump of the field state occurs, and the field changes into a new state, defined by the following formula:

$$|\varphi(t + \Delta t)\rangle = \frac{a|\varphi(t)\rangle}{\sqrt{\langle\varphi(t)|a^+ a|\varphi(t)\rangle}}. \quad (4.6.7)$$

Otherwise ($\varepsilon > \Delta p$), the state of the system changes continuously:

$$|\varphi(t + \Delta t\rangle = \frac{\left\{1 - \frac{\gamma}{2}\Delta t a^+ a\right\}|\varphi(t)\rangle}{\sqrt{1 - \Delta p}}. \quad (4.6.8)$$

As can be seen from Eq. (4.6.7), if the field is in a three-component superposition state $|\beta\rangle_m$ at the t time, then, after a quantum jump of the state of the optical system, it changes into the corresponding superposition state$|\beta\rangle_{m+1}$. The state changes the interference type between coherent components (“the cat jumps”).

To study the continuous evolution of the system state, we expand the state of the field at the t time in the Fock basis:

$$|\varphi(t)\rangle = \sum c_n(t)|n\rangle. \quad (4.6.9)$$

For the $c_n(t)$ coefficients, we can obtain the following expression from Eq. (4.6.8):

$$\frac{dc_n}{dt} = \frac{\gamma}{2}\{n - \sum_k |c_k|^2\, k\}c_n. \quad (4.6.10)$$

The latter equation for the expansion coefficients c_n of the field state in the Fock basis shows that different quantum field states can have significantly different behaviours during continuous evolution of the system. In particular, it can be verified easily that a Fock state does not change and that even and odd quantum superposition states of the field do not change their type during continuous evolution of the system (only the state amplitude attenuates) [8, 9]. For three-component quantum superposition field states, it is only the attenuation of the state amplitude that occurs during continuous evolution of the system. In this case, the amplitude of the superposition state of the field at the t moment is determined by the following formula:

$$\beta(t) = exp(-\gamma t/2)\beta(0)\,. \quad (4.6.11)$$

When the dynamics of states $|\varphi(t)\rangle$ is modelled, using the Quantum state diffusion method, the evolution of an element of the ensemble of quantum trajectories is determined by a nonlinear stochastic differential equation. The stochastic equation for one element of the ensemble of trajectories ($|\varphi(t)\rangle$), corresponding to the solution of the density matrix equation (4.6.6), has the following form [8,9,10]:

$$|\varphi(t+\delta t)\rangle = \frac{\gamma}{2}\{2\langle a^+\rangle a - a^+a - \langle a^+\rangle\langle a\rangle\}|\varphi(t)\rangle\delta t +$$

$$\sqrt{\frac{\gamma}{2}}\{a - \langle a\rangle\}d\xi(t). \qquad (4.6.12)$$

Here, $d\xi(t)$ is a random complex Wiener variable with the following properties: $< d\xi(t) >= 0$, $< (d\xi(t))^2 >= 0$, and $< |d\xi(t)|^2 >= 2dt$. Figure 4.15 shows the dynamics of the Wigner function of the initial state $|\beta\rangle_0$, where $\beta = -5^{1/2}$, for one trajectory of quantum state diffusion. Four of the figures represent the Wigner function of the field state for different moments of evolution of the system: Fig. 4.15a, for $\gamma t = 0$; Fig. 4.15b, for $\gamma t = 0.005$; Fig. 4.15c, for $\gamma t = 0.1$; and Fig. 4.15d, for $\gamma t = 0.5$. The evolution of the Wigner function shows that the system localizes in one random component of the superposition state. In different quantum trajectories, the field localizes with the same probability in different components of the three-component superposition state. Note that the quantum coherence of the system is destroyed much faster than the dissipation of energy of the state.

4.7. System Behaviour in the Absence of One-Photon Absorption

In this section, we study the quantum dynamics of the field, when one-photon absorption is not considered. For calculating one step for a single quantum trajectory of the system, we should take $\gamma_1 = 0$ in the algorithm described in Section 4.1.

Figures 4.16 to 4.18 represent the Wigner function of the field state for three random trajectories of the system for field evolution from an initial vacuum, single-, and two-photon Fock states, respectively. The trajectories

are calculated for the parameter values $\varepsilon/\gamma_3 = 10$ and $\gamma_1 = 0$. These figures depict Wigner functions of the field state at long interaction times ($\gamma_3 t = 10$). These Wigner functions only differ from each other in respect of oscillations between the three coherent components of the state, which show the formation of different types of interference between them. The field states, corresponding to the Wigner functions presented in Figs. 4.16 to 4.18, may be presented in the following general form [1]:

$$|\alpha\rangle_m = N_m^{1/2}\{|\alpha\rangle + exp(2\pi im/3)|exp(2\pi i/3)\alpha\rangle + exp(-2\pi im/3)|exp(-2\pi i/3)\alpha\rangle\}, \quad (4.7.1)$$

where $m = 0,\ 1,\ 2$.

The normalization factors N_m are determined by

$$N_m^{-1} = 3\{1 + 2\,exp(-3|\alpha|^2/2)\,cos(2\pi m/3 + \sqrt{3}|\alpha|^2/2)\}, \quad (4.7.2)$$

and $|\alpha\rangle$, $|exp(2\pi i/3)\alpha\rangle$, and $|exp(-2\pi i/3)\alpha\rangle$ are coherent states of the field [13]

$$|\alpha\rangle = exp(-|\alpha|^2/2)\sum_{n=0}^{\infty}\frac{\alpha^n}{(n!)^{1/2}}|n\rangle. \quad (4.7.3)$$

Here, $\alpha = (-\varepsilon/\gamma_3)^{1/3}$ [1].

The Wigner functions in Figs. 4.16–4.18 correspond to the three-component superposition states $|\alpha\rangle_m$ with $m = 0$, $m = 1$, and $m = 2$, respectively.

Figure 4.19 gives the dynamics of the quantum entropy of the field for system evolution from an initial vacuum (curve 1), initial single-photon Fock (curve 2), and an initial two-photon Fock (curve 3) states of the field,

respectively. Each of the curves is calculated, using 5000 independent quantum trajectories of the system for $\varepsilon/\gamma_3 = 10$ and $\gamma_1 = 0$. For long evolution times, all curves in Fig. 4.19 decay down to the stationary zero value. This shows that, after a long interaction time, the ensemble of quantum trajectories consists of one element. The system localizes in one of the superposition states $|\alpha\rangle_m$ $(m = 0,\ 1,\ 2)$.

The three-component superposition states $|\alpha\rangle_m$ $(m = 0,\ 1,\ 2)$ are the eigenstates of the cube of the annihilation operator, and

$$a^3|\alpha\rangle_m = \alpha^3|\alpha\rangle_m \ (m = 0,\ 1,\ 2). \qquad (4.7.4)$$

Therefore, at large interaction times, three-photon quantum jumps do not change the field state. This is associated with the fact that the cube of the annihilation operator is the operator of the three-photon quantum jump of the field state (see Eq. (4.1.9)).

4.8. System Behaviour in the Presence of Weak One-Photon Absorption, Quantum Coherence, and Dissipation

Here, we consider the dynamics of the system in the case of weak one-photon absorption $(\gamma_1 << \gamma_3)$. Although one-photon absorption is weak compared to three-photon absorption, it affects significantly system behaviour on quantum trajectories and the formation of a stationary ensemble of field states at long system evolution times.

Figure 4.20 shows Wigner functions of the field state for a single random quantum trajectory in the case of system evolution from an initial vacuum state and for the system parameter values $\varepsilon/\gamma_3 = 10$ and $\gamma_1/\gamma_3 = 0.1$. At $\gamma_3 t \approx 1.64$, after the first one-photon quantum jump of the system state, the field makes a transition from the three-component superposition state

$|\alpha\rangle_0$ to the state $|\alpha\rangle_1$ (Figs. 4.20a and 4.20b). Then, the system state does not change up to the second one-photon jump at $\gamma_3 t \approx 2.18$ (Fig. 4.20c). After the second jump, the field passes from the $|\alpha\rangle_1$ to the $|\alpha\rangle_2$ state (Fig. 4.20d). Then, the system state does not change again up to the third one-photon jump at $\gamma_3 t \approx 2.33$ (Fig. 4.20e). After the third jump, the field localizes in the $|\alpha\rangle_0$ state again. Such behaviour of the system is due to the fact that the annihilation operator is the operator of a single-photon jump of the field state (see formula (4.1.8)) and only changes the type of superposition (4.7.1):

$$a|\alpha\rangle_m = \sqrt{\frac{N_m}{N_{m+1}}}\alpha|\alpha\rangle_{m+1} \text{ and } |\alpha\rangle_{m+3} = |\alpha\rangle_m \ (m = 0,\ 1,\ 2). \quad (4.8.1)$$

At large evolution times ($\gamma_1 t >> 1$), other trajectories of the system, which start to evolve from the initial vacuum state, also have a similar time behaviour. At large interaction times, the system spends its time in one of the three types of the superposition states $|\alpha\rangle_m$ $(m = 0,\ 1,\ 2)$ until a one-photon quantum jump changes the type of interference between the coherent components of this state. The probability to find the system in each of these states is proportional to the lifetime T_m $(m = 0,\ 1,\ 2)$ of the field in these states. Therefore, at large interaction times, the density matrix of the field may be represented as

$$\rho = \frac{T_0}{T_0 + T_1 + T_2}\left|\alpha\right\rangle_{0\,0}\left\langle\alpha\right| + \frac{T_1}{T_0 + T_1 + T_2}\left|\alpha\right\rangle_{1\,1}\left\langle\alpha\right| + \frac{T_2}{T_0 + T_1 + T_2}\left|\alpha\right\rangle_{2\,2}\left\langle\alpha\right| \quad . \quad (4.8.2)$$

The lifetime of the field in each of these superposition states $|\alpha\rangle_m$ is inversely proportional to the probability of leaving this state. The field leaves its state only after a one-photon jump in the system. The continuous evolution of the system and three-photon jumps do not change the state of the field. The probability δp_m of a one-photon jump of the field state within the time interval δt (under the condition that, at the t time, the field was in the state $|\alpha\rangle_m$) is proportional to the number of photons in this state [7] (see also formula (4.1.6)):

$$\delta p_m = \gamma_{1_m} \langle \alpha | a^+ a | \alpha \rangle_m \delta t = \frac{\delta t}{T_m}, \ (m = 0,\ 1,\ 2). \tag{4.8.3}$$

Equation (4.8.3) determines the dependence of the lifetime of the field in the superposition states $|\alpha\rangle_m$ with the α state amplitude.

Figure 4.21 shows the probabilities

$$p_m = \frac{T_m}{T_0 + T_1 + T_2} \ (m = 0,\ 1,\ 2) \tag{4.8.4}$$

to find the field in the superposition states $|\alpha\rangle_m$ for weak one-photon absorption at long evolution times from the absolute value $\beta = |\alpha|$ of the state amplitude. The probabilities were calculated with the use of Eqs. (4.8.4), (4.8.3), and (4.7.1).

For large values of the state amplitude $|\alpha| >> 1$, with an equal probability of 1/3, the field can be found in each of the superposition states $|\alpha| >> 1$. In this case, the field density matrix may be represented in the following form:

$$\rho = \frac{1}{3} |\alpha\rangle_{0\,0} \langle \alpha| + \frac{1}{3} |\alpha\rangle_{1\,1} \langle \alpha| + \frac{1}{3} |\alpha\rangle_{2\,2} \langle \alpha| \,. \tag{4.8.5}$$

This means that, for large values of the states, the normalizations are equal (Eq. (4.7.2)); i.e., $N_0 \approx N_1 \approx N_2 \approx 1/3$, and the density matrix is a statistical mixture of the three coherent states with an equal probability to find the field in each coherent component of the state:

$$\rho = \frac{1}{3}|\alpha\rangle\langle\alpha| + \frac{1}{3}|exp(2\pi i/3)\alpha\rangle\langle exp(2\pi i/3)\alpha| + \frac{1}{3}|exp(-2\pi i/3)\alpha\rangle\langle exp(-2\pi i/3)\alpha|. \quad (4.8.6)$$

The quantum entropy of this state is $ln(3)$; i.e., the maximal entropy of the three-component state.

Figure 4.22 shows the Wigner function of the steady state of the system for a large state amplitude value ($\alpha = 2$). It is calculated from Eqs. (4.8.6) and (4.7.1) and represents the above-mentioned statistical mixture of the three coherent components with an equal probability to find the field in each of them.

For small values of the field amplitude ($|\alpha| < 1$, i.e., the perturbation of the system is weak), the field spends more time in the superposition state $|\alpha\rangle_0$ than in the states $|\alpha\rangle_1$ and $|\alpha\rangle_2$ (Fig. 4.21). This may be explained by the fact that, when the field state amplitude goes to zero ($\alpha \to 0$), the photon numbers in the superposition states $|\alpha\rangle_0$, $|\alpha\rangle_1$, and $|\alpha\rangle_2$ tend to 0, 1, and 2, respectively, and the time that the system spends in a superposition state is inversely proportional to the numbers of photons in the state (see formulas (4.8.3) and (4.8.4)). This leads to a decrease in the quantum entropy of the field (i.e., the system acquires quantum-mechanical coherence).

Figure 4.23 shows the dependence of the quantum entropy of the steady state of the field on the absolute value of the state amplitude $\beta = |\alpha|$. It is seen that, in the range $|\alpha| > 1$, the system may be found with the same probability in each of the superposition states (4.7.1) leading to a maximum value of the entropy of the three-component state. However, when the state amplitude decreases, the system spends most of the time in the superposition state $|\alpha\rangle_0$, and the quantum entropy of the steady state of the system decreases.

Figure 4.24 shows a Wigner function of the steady state of the field in the presence of weak one-photon absorption and for a small value of the field amplitude ($\alpha = 0.9$). This Wigner function is calculated, using Eqs. (4.8.2), (4.8.3), (4.7.1), (1.9.1), and (1.9.2).

In Section 4.7, we have shown that, in the absence of one-photon absorption, the system under consideration needs some time to form pure stationary three-component superposition states. In such a case, the quantum entropy of the system takes its stationary zero value. If the one-photon absorption is very weak, single-photon quantum jumps will not hinder the formation of a pure state in the system, and a nonstationary superposition state of the field is formed.

Figure 4.25 demonstrates the dynamics of the quantum entropy of the field when the system evolves from an initial vacuum state. The entropy is calculated for cases of weak one-photon absorption with $\gamma_1/\gamma_3 = 0.1$ (curve 1), $\gamma_1/\gamma_3 = 0.01$ (curve 2), and $\gamma_1/\gamma_3 = 0.001$ (curve 3), respectively. Each of these curves is calculated based on 5000 quantum trajectories of the system. Curves 1 and 2 show that the formation of a pure state in the system is hindered. The third curve shows that the single-

photon absorption, being as weak as $\gamma_1/\gamma_3 = 0.001$, does not have a considerable impact on the system and a pure state is formed in the system; at $\gamma_3 t \sim 0.63$, the quantum entropy of the system goes to zero. At this time, a three-component superposition state ($|\alpha\rangle_0$) is formed. After this, only one-photon quantum jumps raise the quantum entropy of the field by adding the new $|\alpha\rangle_1$ state to the ensemble of trajectories of the system.

In the case of weak one-photon absorption, at long evolution times, the ensemble of trajectories, evolving from initial one- or two-photon Fock states, does not differ from those in the case of evolution from an initial vacuum state. Therefore, similar to the case of evolution from a vacuum state, at long times, the field is in one of the superposition states $|\alpha\rangle_m$ ($m = 0,\ 1,\ 2$) until a single-photon quantum jump changes the type of the superposition state from one to another.

For the cases of system evolution from initial one- and two-photon Fock states, consideration similar to that for the case of evolution from an initial vacuum state shows that, in these cases, the system may form nonstationary three-component superposition states of the $|\alpha\rangle_1$ and $|\alpha\rangle_2$ types, respectively.

References

1. S. T. Gevorgyan and V. O. Chhaltykyan, "Coherent Superposition States of Light and their Interference in Three-Photon Absorption Process," *J. of Modern Opt.* 46 (1991): 1447 –1463.

2. S. T. Gevorkyan and V. O. Chaltykyan, " Formation of Nonclassical States of Light in Media with a Three-Photon Resonance," *Optics and Spectroscopy* 89, no. 4 (2000): 563–568.
3. S. T. Gevorkyan and V. O. Chaltykyan, ”Quantum Superposition States of Light in Three-Photon Absorbing Media,” in Proceedings of the Conference on Laser Physics-98, (Ashtarak, Armenia, October 19–23, 1998), 5–10.
4. S. T. Gevorkyan and V. O. Chaltykyan, “Three-Photon Superposition States of Light,” in the Proceedings of Conference on Laser Physics-99 (October 18–22, 1999), 48–54.
5. S. T. Gevorgyan, Min Xiao, and V. O. Chaltykyan, “Superposition States of Light in a Three-Photon Absorbing Dissipative Medium,” *J. Modern Optics* 55, no. 12 (2008): 1923–1935.
6. S. T. Gevorkyan and M. S. Gevorkyan, “Three-Component Superposition States of Light in a Dissipative Medium,” *Optics and Spectroscopy* 109, no. 1 (2010): 126–132.
7. K. Molmer, Y. Castin, and J. Dalibard, “Monte Carlo Wave-Function Method in Quantum Optics,” *JOSA B* 10 (1993): 524–538.
8. B. M. Garraway, P. L. Knight, and J. Steinbach, “Dissipation of Quantum Superpositions- Localization and Jumps,” *J. Appl. Phys.* B 60 (1995): 63–68.
9. B. M. Garraway, P. L. Knight, and M. B. Plenio, “Generation and Preservation of Coherence in Dissipative Quantum Optical Environments,” *Physica Scripta* T 76 (1998): 152.
10. N. Gisin and I. C. Percival, “Quantum-State Diffusion Model Applied to Open Systems,” *J. Phys. A* 25 (1992): 5677.

11. W. H. Zurek, “Decoherence and Transition from Quantum to Classical,” *Phys. Today* 44 (1991): 36.
12. W. H. Zurek, S. Habib, and J. P. Paz, “Coherent States via Decoherence,” *Phys. Rev. Lett.* 70 (1993): 1187–1190.
13. R. J. Glauber, “Coherent and Incoherent States of the Radiation Field” *Phys Rev* 131 (1963): 2766.

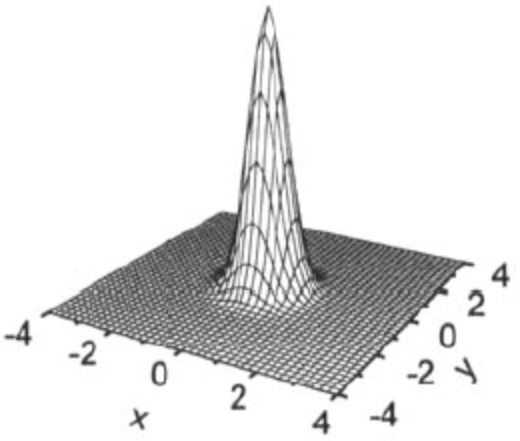

(*a*)

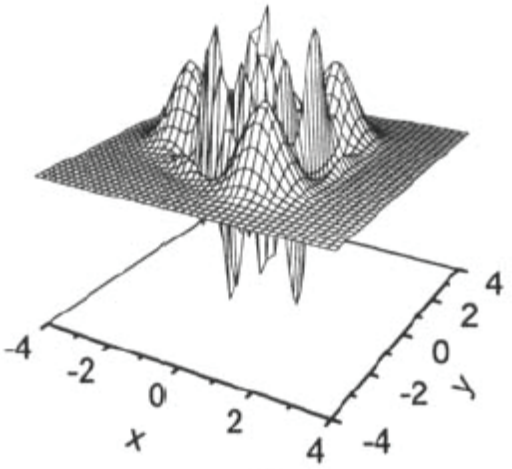

(*b*)

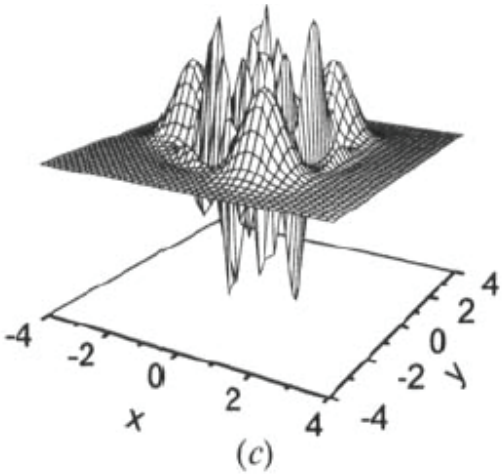

Fig. 4.1. Evolution of the Wigner function when there are no one- and two-photon losses ($k_1 = 0, k_2 = 0$) and $\varepsilon/k_3 = 20$: (a) the initial vacuum state $\tau = 0$; (b) the state of the system at $\tau \approx 0.49$, when the quantum entropy has its maximum value; and (c) the stationary quantum superposition state at $\tau = 4$.

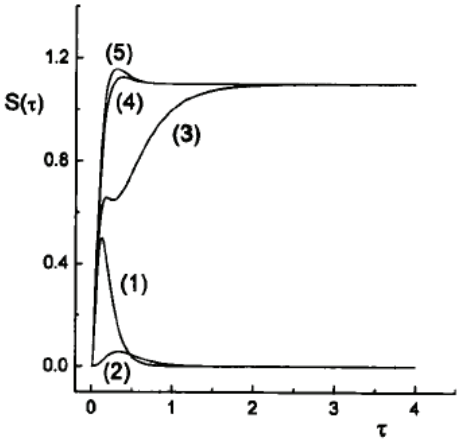

Fig. 4.2. Dynamics of the field quantum entropy in the case when $\varepsilon/k_3 = 20$ and $k_1 = 0, k_2 = 0$ (curve 1); $\varepsilon/k_3 = 4$ and $k_1 = 0, k_2 = 0$ (curve 2); $k_1/k_3 = 0.2$ and $k_2 = 0$ (curve 3); $\varepsilon/k_3 = 20$, $k_1 = 0$, and $k_2/k_3 = 0.2$ (curve 4); and $\varepsilon/k_3 = 20$, $k_1/k_3 = 0.2$, and $k_2/k_3 = 0.2$ (curve 5). The initial state is a vacuum one.

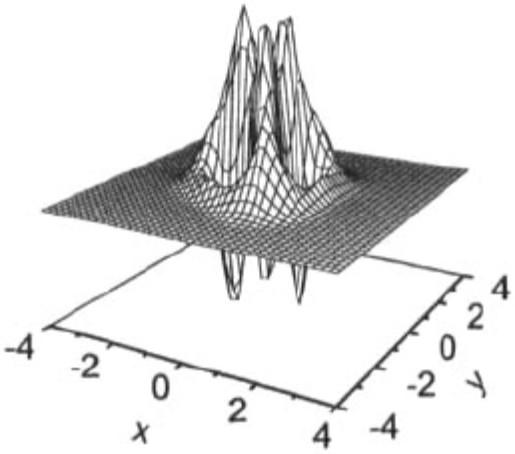

Fig. 4.3. Steady-state Wigner function without one- and two-photon losses for $k_1 = 0, k_2 = 0$ and $\varepsilon/k_3 = 4$. The initial state is vacuum; $n \approx 1.29$.

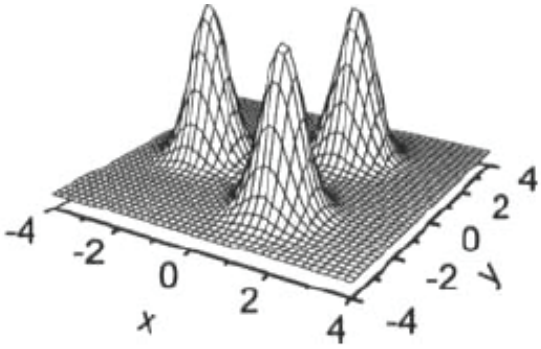

Fig. 4.4. Steady-state Wigner function in the case of weak one-photon dissipation ($k_1/k_3 = 0.2$) and for $\varepsilon/k_3 = 20$. The initial state is vacuum.

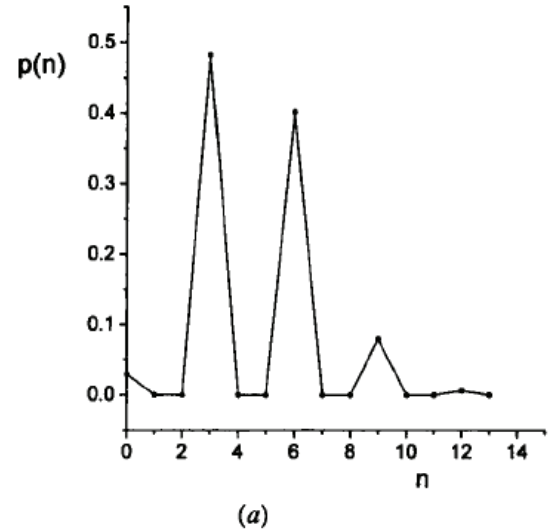

(*a*)

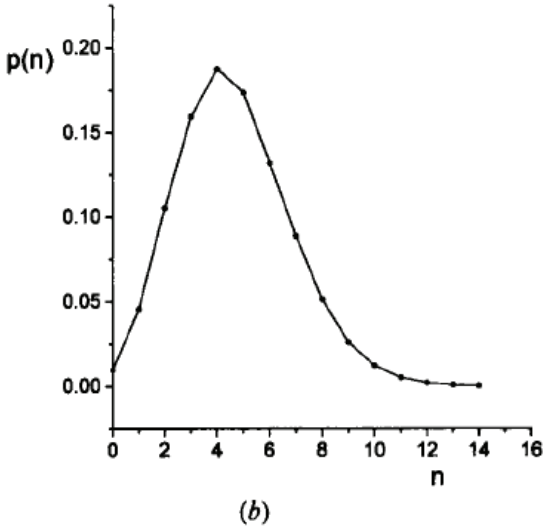

(*b*)

Fig. 4.5. Steady-state photon statistics at $\varepsilon/k_3 = 20$ (a) in the absence of one- and two-photon losses ($k_1 = 0, k_2 = 0$) and (b) in the presence of weak one-photon absorption ($k_1/k_3 = 0.2$). The initial state is vacuum.

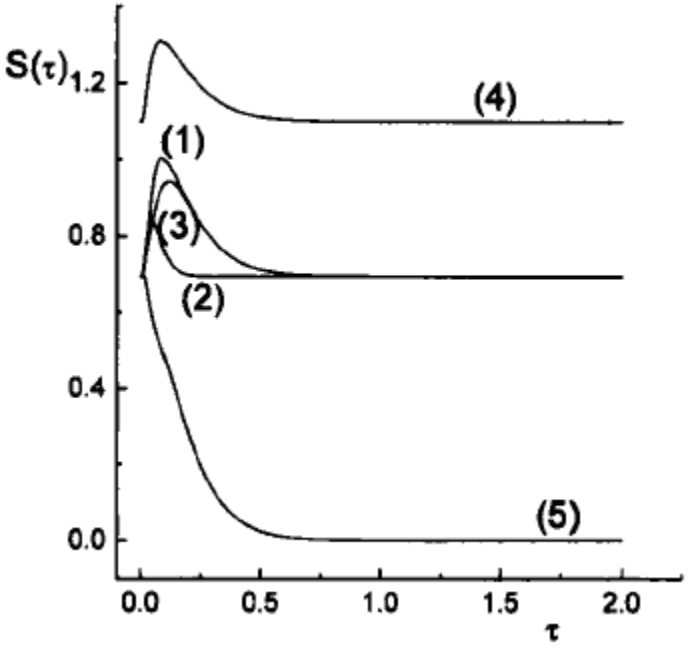

Fig. 4.6. Quantum entropy dynamics at $\varepsilon/k_3 = 20$ and $k_1 = 0, k_2 = 0$ and for the following initial states: (1) $\rho(0) = (|0\rangle\langle 0| + |1\rangle\langle 1|)/2$, (2) $\rho(0) = (|1\rangle\langle 1| + |2\rangle\langle 2|)/2$, (3) $\rho(0) = (|0\rangle\langle 0| + |2\rangle\langle 2|)/2$, (4) $\rho(0) = (|0\rangle\langle 0| + |1\rangle\langle 1| + |2\rangle\langle 2|)/3$, and (5) $\rho(0) = (|0\rangle\langle 0| + |3\rangle\langle 3|)/2$.

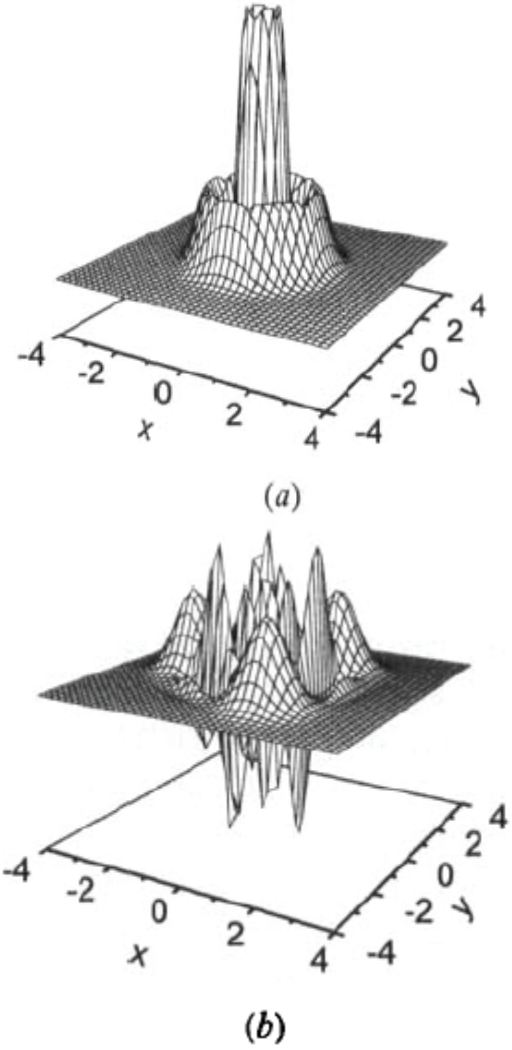

Fig. 4.7. Wigner functions of (a) the initial state $\rho(0) = (|0\rangle\langle 0| + |3\rangle\langle 3|)/2$ and (b) the steady state when there are no one- and two-photon losses and at $\varepsilon/k_3 = 20$.

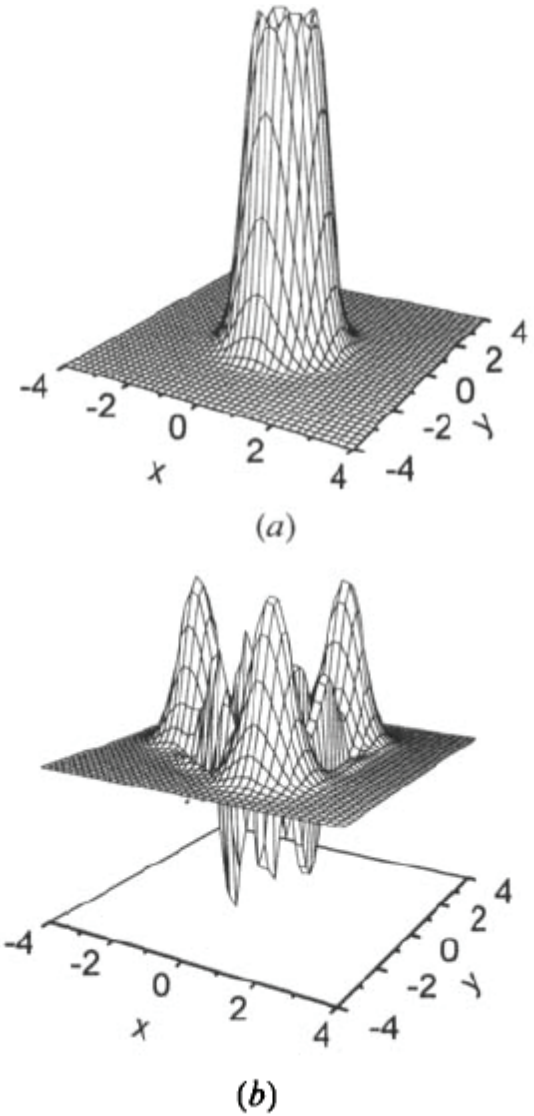

Fig. 4.8. Wigner functions of (a) the initial state ($\rho(0) = (|0\rangle\langle 0| + |1\rangle\langle 1|)/2$) and (b) the steady state at $\varepsilon/k_3 = 20$ and $k_1 = 0, k_2 = 0$.

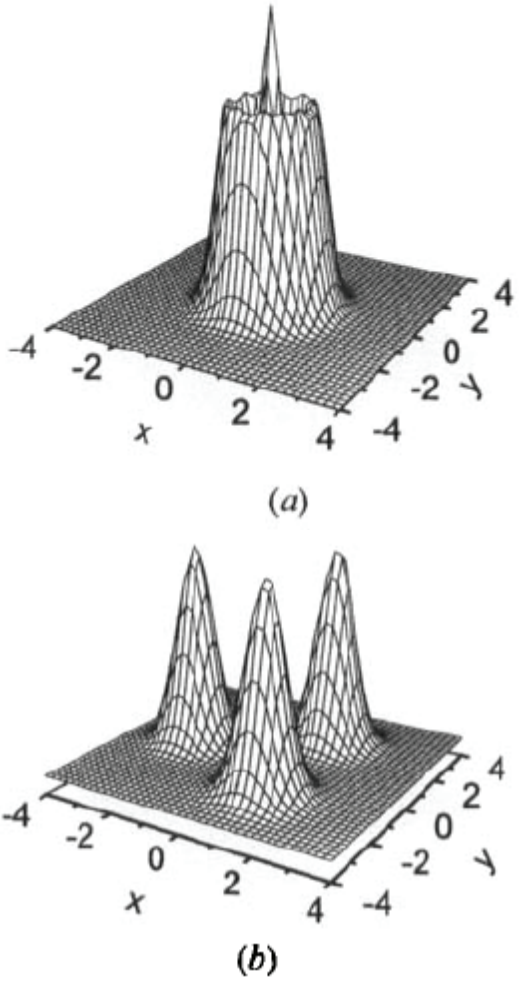

Fig. 4.9. Wigner functions of (a) the initial state ($\rho(0) = (|0\rangle\langle 0| + |1\rangle\langle 1| + |2\rangle\langle 2|)/3$) and (b) the steady state at $\varepsilon/k_3 = 20$, $k_1 = 0, k_2 = 0$, and $k_1 = 0, k_2 = 0$.

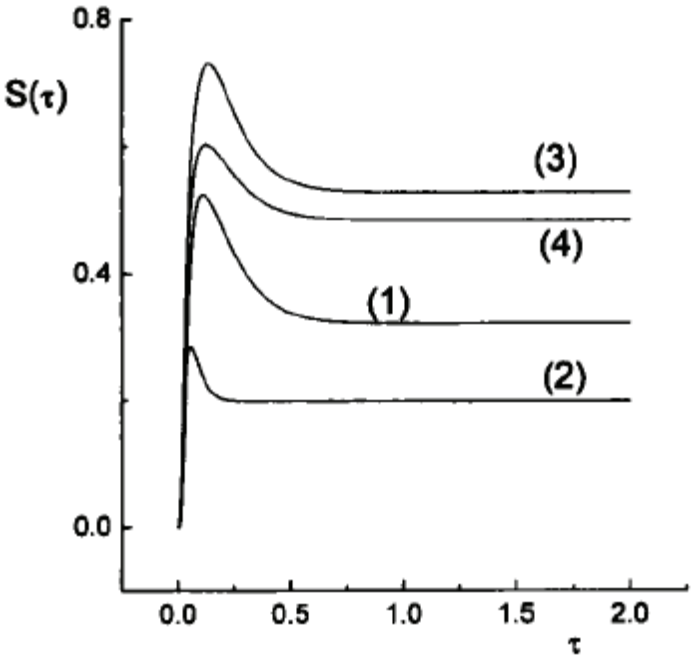

Fig. 4.10. Quantum entropy dynamics of the field for the perturbation value $\varepsilon/k_3 = 20$ in the absence of single- and two-photon absorption ($k_1 = 0, k_2 = 0$) and in the case of evolution of the system from the following initial pure states of the field ($\rho(0) = (|\psi(0)\rangle\langle\psi(0)|)$:$|\psi(0)\rangle = (|0\rangle + |1\rangle)/2^{1/2}$ (curve 1), $|\psi(0)\rangle = (|1\rangle + |2\rangle)/2^{1/2}$ (curve 2), $|\psi(0)\rangle = (|0\rangle + |2\rangle)/2^{1/2}$ (curve 3); and $|\psi(0)\rangle = (|0\rangle + |1\rangle + |2\rangle)/3^{1/2}$ (curve 4).

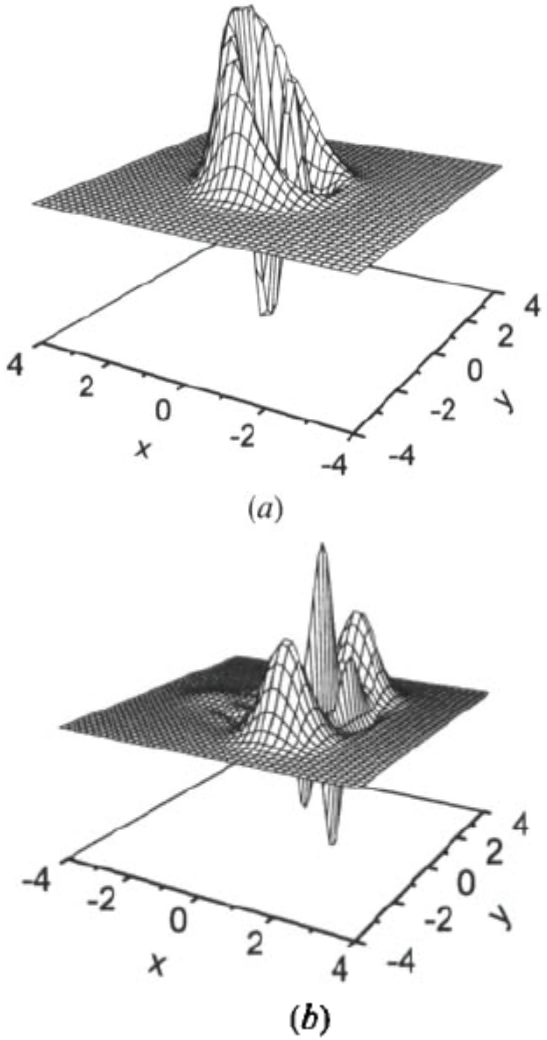

Fig. 4.11. Wigner function of the stationary state of the field (b) for the perturbation value $\varepsilon/k_3 = 20$ in the absence of single- and two-photon absorption ($k_1 = 0, k_2 = 0$) and in the case of evolution of the system from the initial pure state $|\psi(0)\rangle = (|1\rangle + |2\rangle)/2^{1/2}$ ($\rho(0) = (|\psi(0)\rangle\langle\psi(0)|$), the Wigner function of which is presented in (a).

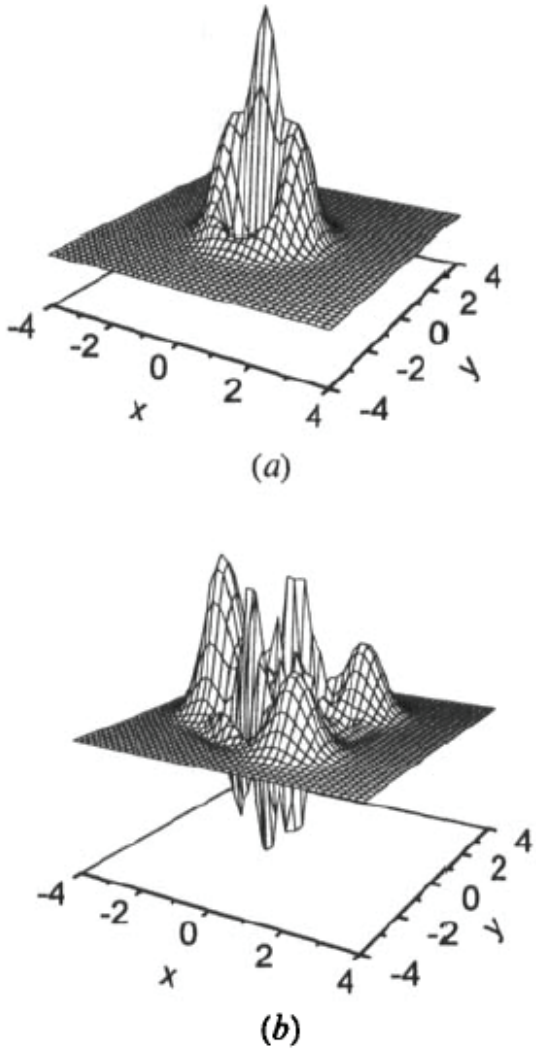

Fig. 4.12. Wigner function of the stationary state of the field (b) for the perturbation value $\varepsilon/k_3 = 20$ in the absence of single- and two-photon absorption ($k_1 = 0, k_2 = 0$) and in the case of evolution of the system from the initial pure state $|\psi(0)\rangle = (|0\rangle + |2\rangle)/2^{1/2}$ ($\rho(0) = (|\psi(0)\rangle\langle\psi(0)|$), the Wigner function of which is presented in (a).

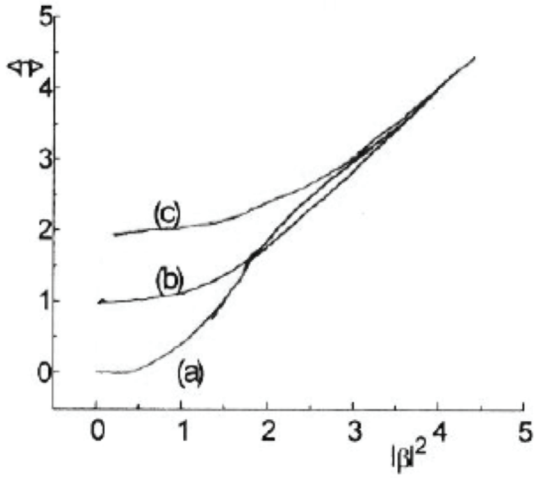

Fig. 4.13. Dependence of the mean value of the number of photons of quantum three-component superposition states $|\beta\rangle_m$ $(m = 0,1,2)$ on the square of the absolute value of the state amplitude $|\beta|^2$. In curve a, $m = 0$ curve; in curve b, $m = 1$; and in curve c, $m = 2$.

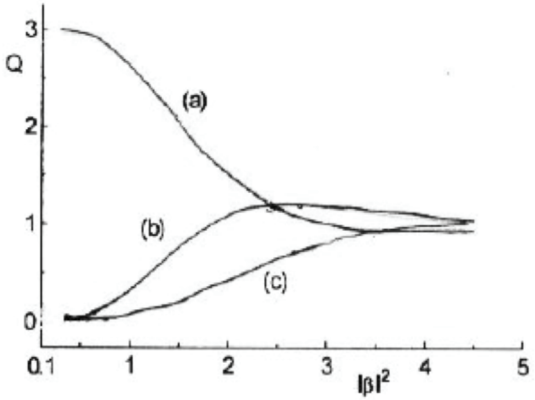

Fig. 4.14. Dependence of the normalized value of the photon number dispersion of quantum three-component superposition states $|\beta\rangle_m$ $(m = 0,1,2)$ on the square of the absolute value of the state amplitude $|\beta|^2$. In curve a, $m = 0$; in curve b, $m = 1$; and in curve c, $m = 2$.

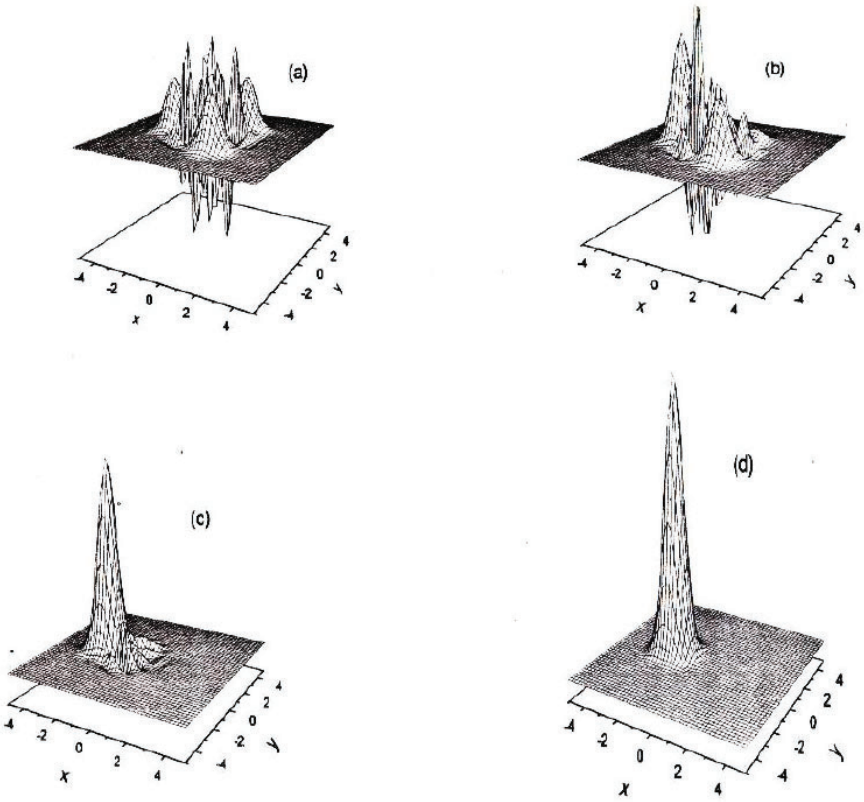

Fig. 4.15. Wigner functions of the field state of one "Quantum state diffusion" trajectory of the initial quantum three-component superposition state$|\beta\rangle_0$: (a) –(d) represent the Wigner functions of the state of the field at the times $\gamma t = 0$, $\gamma t = 0.005$, $\gamma t = 0.1$, and $\gamma t = 0.5$, respectively.

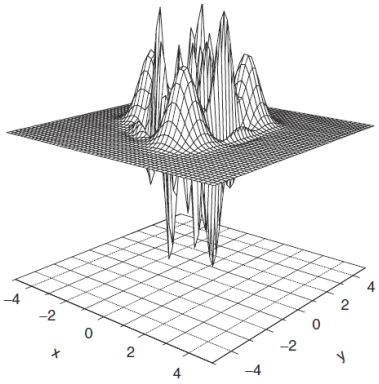

Fig. 4.16. Field state Wigner function of a single quantum trajectory of the system with field evolving from an initial vacuum state and at the time $\gamma_3 t = 10$. The parameters are $\varepsilon/\gamma_3 = 10$ and $\gamma_1 = 0$.

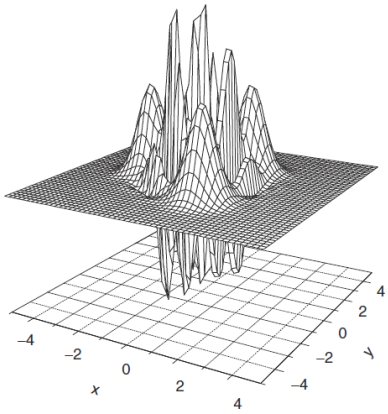

Fig. 4.17. Field state Wigner function of a single quantum trajectory of the system with the field evolving from an initial one-photon Fock state and at the time $\gamma_3 t = 10$. The parameters are $\varepsilon/\gamma_3 = 10$ and $\gamma_1 = 0$.

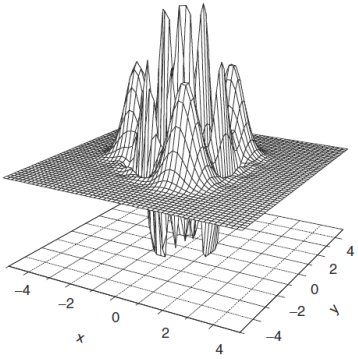

Fig. 4.18. Field state Wigner function of a single quantum trajectory of the system with the field evolving from an initial two-photon Fock state and at the time $\gamma_3 t = 10$. The parameters are $\varepsilon/\gamma_3 = 10$ and $\gamma_1 = 0$.

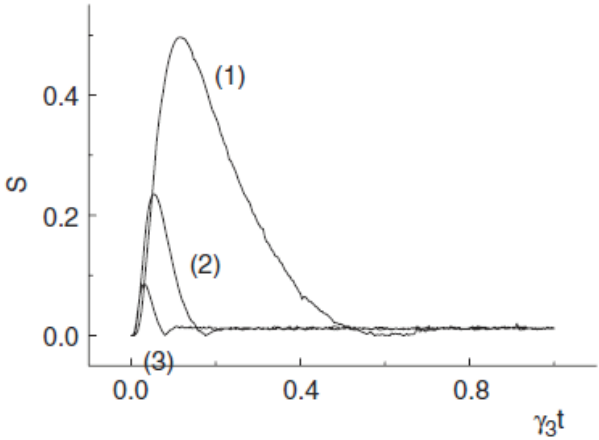

Fig. 4.19. Dynamics of the quantum entropy of the field for field evolution from (curve 1) initial vacuum state, (curve 2) one-photon Fock state, and (curve 3) two-photon Fock state. Each curve is calculated, using 5000 independent quantum trajectories of the system at $\varepsilon/\gamma_3 = 10$ and$\gamma_1 = 0$.

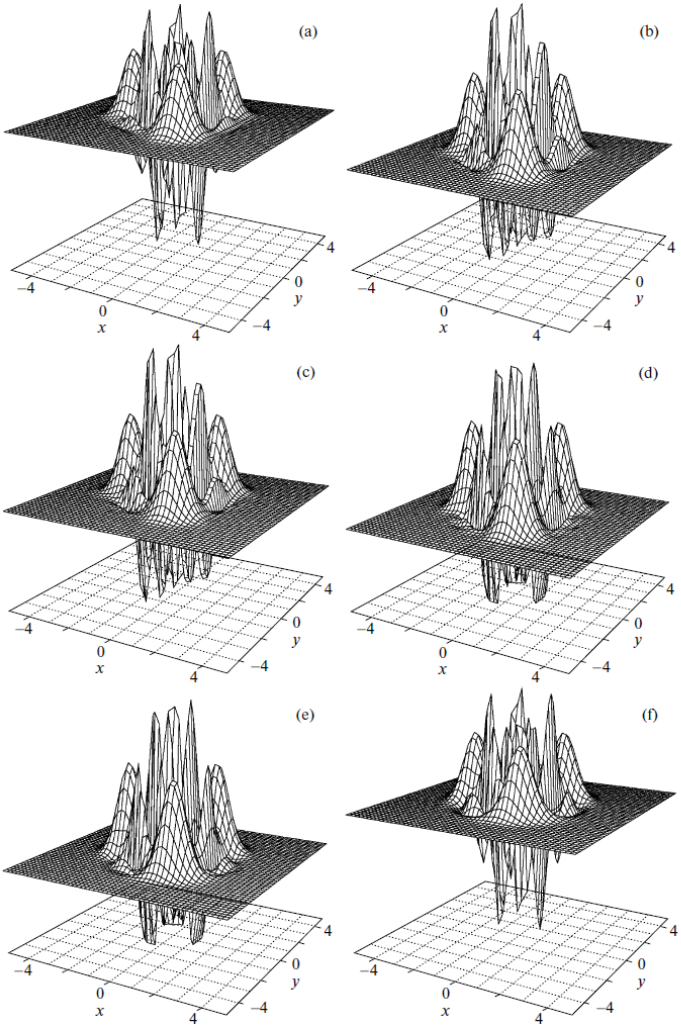

Fig. 4.20. Field state Wigner function of a single quantum trajectory of the system with the field evolving from an initial vacuum state in the presence of weak one-photon absorption ($\gamma_1/\gamma_3 = 0.01$). Panels (a) and (b), (c) and (d), and (e) and (f) show the Wigner functions before and after the first (at $\gamma_3 t \approx 1.64$), before and after the second (at $\gamma_3 t \approx 2.18$), and before and after the third (at $\gamma_3 t \approx 2.33$) single-photon quantum jumps of the field state. $\varepsilon/\gamma_3 = 10$.

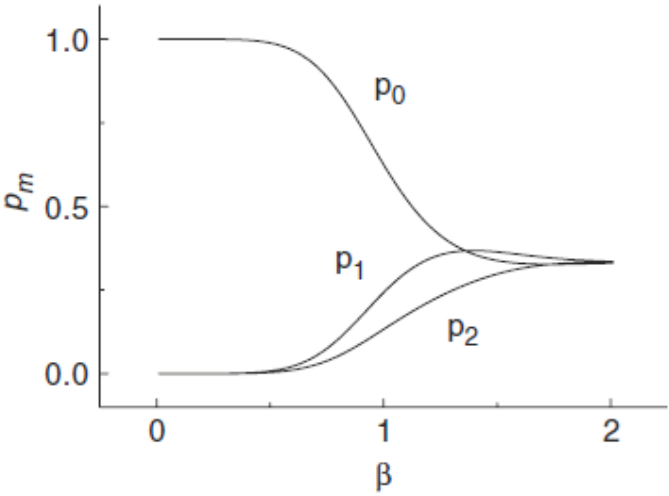

Fig. 4.21. Plot of the p_m probabilities to find the field in the superposition states $|\alpha\rangle_m$ $(m = 0,1,2)$ at long evolution times $\gamma_1 t >> 1$ in the presence of weak one-photon absorption $(\gamma_1/\gamma_3 << 1)$ versus the absolute value of the state amplitude $\beta = |\alpha|$.

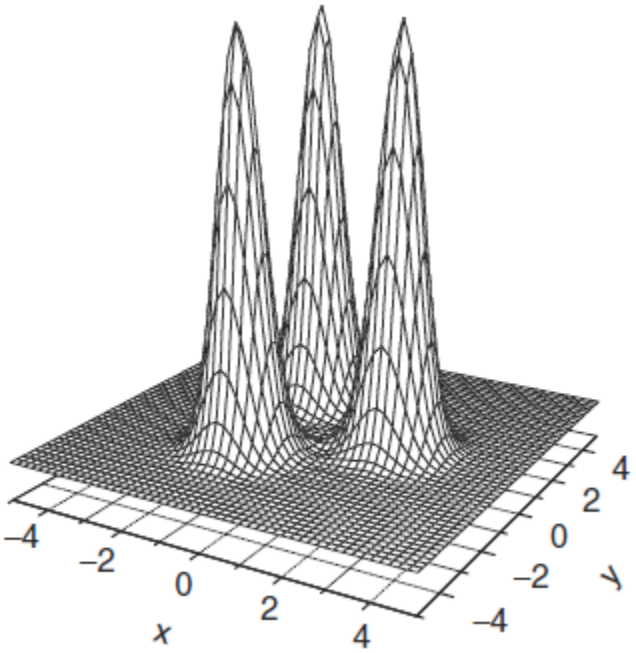

Fig. 4.22. Wigner function of the stationary state of the field in the presence of weak one-photon absorption $\gamma_1/\gamma_3 << 1$ and for a large value of the state amplitude ($\alpha = 2$).

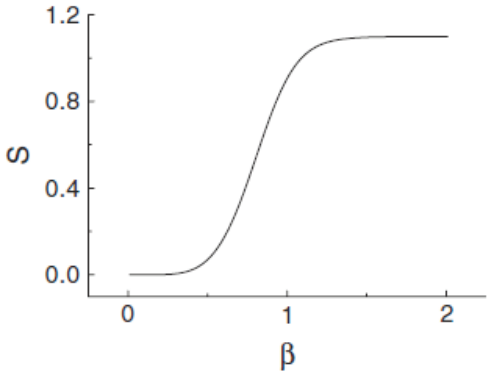

Fig. 4.23. Plot of the quantum entropy of the stationary state of the field in the presence of weak one-photon absorption $\gamma_1/\gamma_3 << 1$ versus the absolute value of the state amplitude $\beta = |\alpha|$.

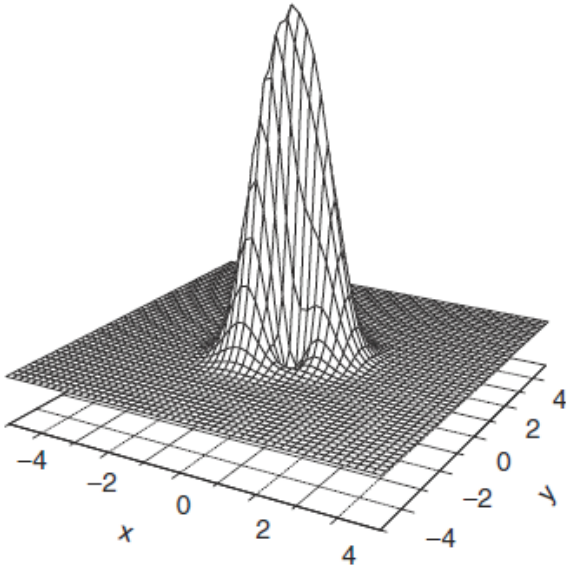

Fig. 4.24. Wigner function of the stationary state of the field in the presence of weak one-photon absorption ($\gamma_1/\gamma_3 << 1$) for a small value of the state amplitude ($\alpha = 0.9$) .

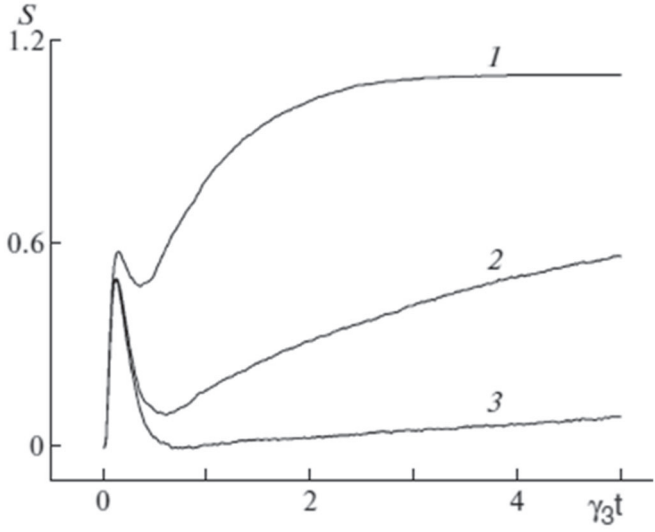

Fig. 4.25. Dynamics of the quantum entropy of the field (curve 1) for field evolution from an initial vacuum state and for $\gamma_1/\gamma_3 = 0.1$; (curve 2) for $\gamma_1/\gamma_3 = 0.01$; and (curve 3) for $\gamma_1/\gamma_3 = 0.001$, respectively ($\varepsilon/\gamma_3 = 10$). Each curve is calculated, using 5000 quantum trajectories of the system.

CHAPTER 5

QUANTUM DYNAMICS OF INTRACAVITY SECOND SUBHARMONIC GENERATION

Introduction

The materials in this chapter have been taken from work [1].

The correlation dynamics of fluctuations in the number of photons of the interacting modes is investigated for the process of intracavity subharmonic generation. It is demonstrated that this correlation depends strongly on the nonlinear mode coupling coefficient. For small values of the coupling coefficient, the correlation between fluctuations in the number of photons is small. With an increase in the coupling coefficient, the correlation increases (the states of the subsystem become entangled) and, starting from a particular value of the coupling coefficient, starts to decrease with a further increase in the coupling coefficient and gradually approaches zero (the entanglement of the subsystem states decreases). The quantum dynamics of the number of photons, quantum entropy, and the Wigner function of the stationary state of the fundamental and subharmonic modes is investigated. It is demonstrated that the dynamics of these quantities also depends strongly on the coupling coefficient of the interacting modes. We show that, for very large values of the mode coupling coefficients and in the region of long interaction times, the subharmonic mode localizes in a two-component state with equal probabilities of finding the state in each component. The quantum entropy

of this state is smaller than the maximum entropy of a two-component state, which is equal to ln2. The latter shows that a quantum-mechanical interference takes place between components of the subharmonic mode. It is also shown that, in the region of small values of the mode coupling coefficient, the subharmonic mode localizes in a squeezed vacuum state, which has a nonzero quantum entropy.

5.1. Nonlinear System, Main Equations, and Calculation Algorithms

We consider a model of intracavity second subharmonic generation in a two-mode cavity. A nonlinear medium is placed in a cavity that is tuned to the frequency ω_1 of the fundamental mode and the frequency ω_2 of the subharmonic mode, where $\omega_1 = 2\omega_2$. The fundamental mode is resonantly perturbed by a classical external field. The density matrix equation describing this optical system can be presented in the form

$$\frac{\partial \rho}{\partial t} = (i\hbar)^{-1}\left[H_{sys}, \rho\right] + L(\rho), \tag{5.1.1}$$

where

$$H_{sys} = \frac{i\hbar\chi}{2}(a_1 a_2^{+2} - a_1^{+} a_2^{2}) + i\hbar E(a_1^{+} - a_1), \tag{5.1.2}$$

$$L(\rho) = \frac{\gamma_1}{2}(2a_1\rho a_1^{+} - \rho a_1^{+} a_1 - a_1^{+} a_1 \rho) + \frac{\gamma_2}{2}(2a_2\rho a_2^{+} - \rho a_2^{+} a_2 - a_2^{+} a_2 \rho). \tag{5.1.3}$$

Here, a_i and a_i^{+} $(i = 1,2)$ are the photon creation and annihilation operators of the fundamental and subharmonic modes, respectively; χ is the mode coupling coefficient proportional to the nonlinear susceptibility$\chi^{(2)}$ of the medium; E is the classical amplitude of the

perturbing field at the frequency ω_1; and $\gamma_i (i = 1,2)$ represents the coefficients of the interacting modes, damping through the resonator mirrors. For simplicity, we omitted the phase of the perturbing field in (5.1.2).

Let us investigate the dynamics of the normalized correlation function of fluctuations in the number of photons in the fundamental and subharmonic modes:

$$g(t) = \frac{\langle((n_1(t)-\langle n_1(t)\rangle)+(n_2(t)-\langle n_2(t)\rangle))^2\rangle}{(\langle n_1^2(t)\rangle-\langle n_1(t)\rangle^2)+(\langle n_2^2(t)\rangle-\langle n_2(t)\rangle^2)}. \quad (5.1.4)$$

Here, $n_i = a_i^+ a_i \ (i = 1,2)$ represents the operators of the number of photons in the fundamental and subharmonic modes, respectively. Formula (5.1.4) can be recast in the form

$$g(t) = 1 + \frac{2(\langle n_1(t) n_2(t)\rangle-\langle n_1(t)\rangle\langle n_2(t)\rangle)}{\langle n_1^2(t)\rangle-\langle n_1(t)\rangle^2+\langle n_2^2(t)\rangle-\langle n_2(t)\rangle^2}. \quad (5.1.5)$$

In the absence of correlation between fluctuations in the number of photons in the interacting modes, correlation function (5.1.5) tends to unity.

To study the quantum properties of the optical system, let us also calculate the Wigner functions of the state of field modes [2] (see also Eqs. (1.9.1) and (1.9.2)).

Let us also study the dynamics of quantum entropy

$$S_i(t) = -Tr(\rho_i(t)\, ln\, \rho_i\,(t)) \ (i = 1,2)$$

of the fundamental and subharmonic modes.

Equation (5.1.1), governing the density matrix of the optical system, is solved by the numerical Monte Carlo wave-function method [3,4].

We investigated the system dynamics in terms of dimensionless time ($\tau = \gamma t$) and dimensionless parameters of the system ($\varepsilon = E/\gamma$ and $k = \chi/\gamma$) for the case of equal mode-damping coefficients in the cavity ($\gamma_1 = \gamma_2 = \gamma$). All calculations were made in the case of system evolution from an initial vacuum state of the fundamental and subharmonic modes. To find the dynamics of each correlation function of fluctuations in the number of photons, of quantum entropy of the modes, and of the Wigner function, we used 1000 independent quantum trajectories of the optical system. We studied the dynamics of the system for the value of the perturbation amplitude of the fundamental mode $\varepsilon = 1.5$.

5.2. System Dynamics in the Case of Weak Coupling of the Modes: Squeezed Vacuum State

In this section, we will investigate the quantum dynamics of the system in the case of a small mode coupling coefficient ($k = 0.1$).

The dynamics of the number of photons in the fundamental (curve a) and subharmonic (curve b) modes for this case is illustrated in Fig. 5.1. The photon number of the fundamental mode increases rapidly and becomes much larger than unity at long interaction times, whereas the photon number of the subharmonic-mode does not change much and remains much smaller than unity at long interaction times. This suggests that the system is in a below-threshold state with respect to the subharmonic generation and the subharmonic mode is close to a vacuum state.

Wigner functions of the stationary state of the fundamental and subharmonic modes are depicted in Fig. 5.2. The Wigner functions are shown at the interaction time $\tau = 20$. At long interaction times, the fundamental mode occupies a one-component state, the Wigner function of which is similar to that of a coherent state, except that it has a nonzero quantum entropy (see below). The Wigner function of the subharmonic mode shows that this mode is close to a squeezed vacuum state at long interaction times (Fig. 5.2b).

The dynamics of the quantum entropy of the fundamental and subharmonic modes is shown in Figs. 5.3 and 5.4, respectively. Both curves show rapid growth at short interaction times and reach a stationary state at long interaction times ($\tau >> 1$). At long interaction times, the quantum entropy of the fundamental mode is quite different from that of the subharmonic mode (the fundamental mode entropy is nearly twice as high as that of the subharmonic mode). The large value of the entropy of the interacting modes shows that neither mode is in a pure state.

A correlation function of photon number fluctuations in the fundamental and subharmonic modes, calculated using formula (5.1.5), is presented in Fig. 5.5. During the entire interaction time, the correlation function of fluctuations of the interacting modes remains close to unity, which indicates the absence of entanglement of the states of the fundamental and subharmonic modes with respect to the photon number variables in the interaction area characterized by a small value of the mode coupling coefficient (k = 0.1).

5.3. System Dynamics in the Case of Strong Coupling of the Modes: Two-Component and Entangled States

In this section, we will analyze the system dynamics in the case of a nonlinear mode coupling coefficient (k = 0.3) somewhat larger than the one we used in the previous chapter (k = 0.1) and the same perturbation amplitude ($\varepsilon = 1.5$). Although the nonlinear mode coupling coefficients do not differ much, the quantum behaviour of the system changes dramatically.

Figure 5.6 illustrates the dynamics of the number of photons of the fundamental (curve a) and subharmonic (curve b) modes. As can be seen from the figure, in contrast to the previous case, the system is in an above-threshold state with respect to subharmonic mode generation. At long interaction times, the photon number of the subharmonic mode exceeds the corresponding photon number of the fundamental mode.

Figure 5.7 illustrates the Wigner functions of the fundamental (Fig. 5.7a) and subharmonic (Fig. 5.7b) modes in a stationary state of the system. The Wigner functions are calculated for the interaction time $\tau = 20$.

Similarly to the case described in the previous section, the Wigner function of the fundamental mode of the stationary state of the system resembles that of a coherent state but with nonzero quantum entropy. In contrast to the fundamental mode, the Wigner function of the subharmonic mode changed drastically. While in the case of k = 0.1 it resembled the Wigner function of a squeezed vacuum state, for k = 0.3, it resembles the Wigner function of a statistical mixture of two states. It has a two-component structure, each of the components of which is similar to the Wigner function of a coherent state. The quantum entropy of this state is

larger than the maximum quantum entropy of a statistical mixture of two coherent states, which is equal to ln2 (Fig. 5.9).

The dynamics of the quantum entropy of the fundamental and subharmonic modes is illustrated in Figs. 5.8 and 5.9, respectively. In this case (k = 0.3), similarly to the previous case (k = 0.1), the stationary values of entropy of the interacting modes are not the same. In contrast to the previous case, in which the stationary value of the quantum entropy of the fundamental mode was larger than that of the subharmonic mode, the stationary value of the quantum entropy of the subharmonic mode is here larger than that of the fundamental mode. Large entropy values of the modes state that the modes are not in pure states.

The dynamics of the correlation function of fluctuations in the number of photons in the fundamental and subharmonic modes for k = 0.3 is depicted in Fig. 5.10. It was calculated using (5.1.5). In contrast to the case of k = 0.1, where there was no correlation between fluctuations in the number of photons in interacting modes, here, at long interaction times, the correlation function is much smaller than unity, which indicates the appearance of a correlation between fluctuations in the number of photons in the fundamental and subharmonic modes, leading to the entanglement of their states.

5.4. System Dynamics in the Case of Very Strong Coupling of the Modes: Two-Component State with Quantum-Mechanical Interference between State Components

In this section, we investigate the system dynamics in the case of relatively large nonlinear coupling coefficients of interacting modes (k = 4).

The dynamics of the number of photons in the fundamental (curve a) and subharmonic modes (curve b) is shown in Fig. 5.11. The number of photons in the stationary states of both modes is less than unity. The number of photons in the stationary state of the fundamental mode is $\langle n_1 \rangle \approx 0.05$, suggesting that the mode is close to a vacuum state. The number of photons in the stationary state of the subharmonic mode is $\langle n_2 \rangle \approx 0.6$.

The Wigner functions of the stationary state of the fundamental and subharmonic modes are shown in Fig. 5.12. The Wigner function of the fundamental mode is similar to that of the vacuum state.

The Wigner function of the subharmonic mode reveals a two-component structure. The mode is in a two-component state with an equal probability of finding it in each component.

The quantum entropy dynamics of the fundamental and subharmonic modes is presented in Figs. 5.13 and 5.14, respectively. The quantum entropy of the fundamental mode is very close to zero, which shows that this mode is in a pure state.

The stationary quantum entropy value of the subharmonic mode is smaller than $ln(2) \approx 0.7$ (the entropy of the stationary state of the mode is approximately equal to 0.6), which suggests the presence of quantum-mechanical interference of state components, the Wigner function of which is presented in Fig. 5.12b.

The dynamics of the correlation function of photon number fluctuations in the fundamental and subharmonic modes is shown in Fig. 5.15. At long interaction times, the correlation function is close to unity, which indicates

a lack of correlation between fluctuations in the number of photons in the interacting modes. In this case, there is no entanglement of the states of the fundamental and subharmonic modes, similarly to the case of the nonlinear coupling coefficient k = 0.1 (Figs. 5.5 and 5.15).

References

1. S. T. Gevorgyan and M. S. Gevorgyan, "Quantum Dynamics of Interacting Modes in the Process of Intracavity Subharmonic Generation," *Optics and Spectroscopy* 116 (2014), no. 4: 619–625 (2014).
2. L. Gilles, B. M. Garraway, and P. L. Knight, “Generation of Nonclassical Light by Dissipative Two-Photon Processes,” *Phys. Rev. A* 49 (1994): 2785–2799.
3. K. Molmer, Y. Castin, and J. Dalibard, “Monte Carlo Wave-Function Method in Quantum Optics,” *JOSA B* 10 (1993): 524–538.
4. J. R. Johansson, P. D. Nation, and F. Nori, "QuTiP 2: A Python Framework for the Dynamics of Open Quantum Systems," *Comp. Phys. Comm.* 184 (2013): 1234.

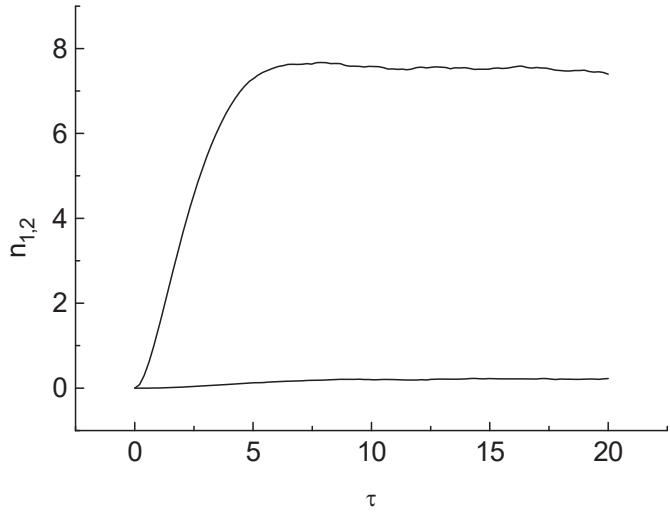

Fig. 5.1. Dynamics of the number of photons in the (a) fundamental and (b) subharmonic modes for the nonlinear mode coupling coefficient k = 0.1.

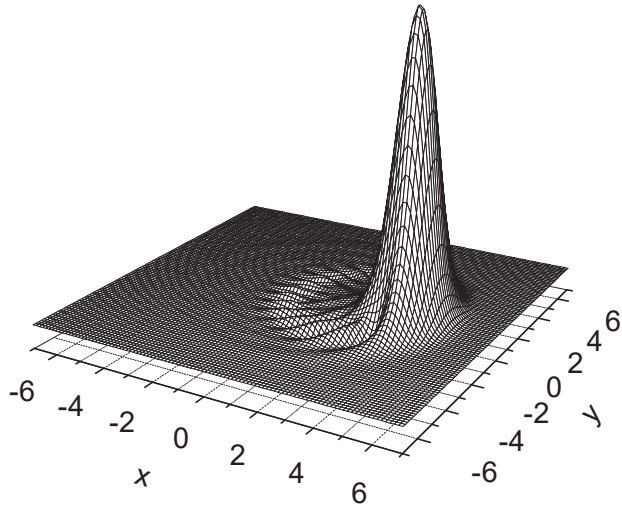

Fig.5.2a

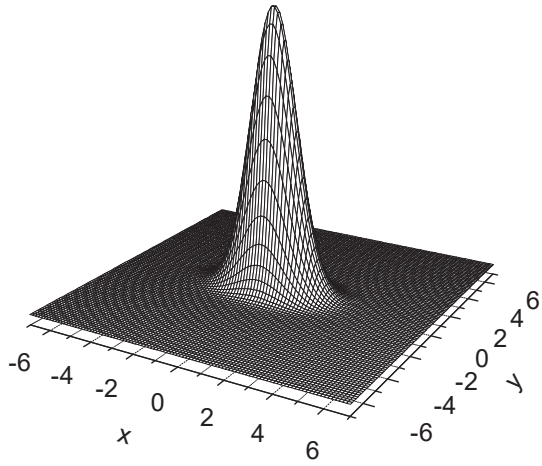

Fig. 5.2b

Fig. 5.2. Wigner function of the stationary state of the (a) fundamental mode and (b) Wigner function of the stationary state of the subharmonic mode for the nonlinear mode coupling coefficient k = 0.1.

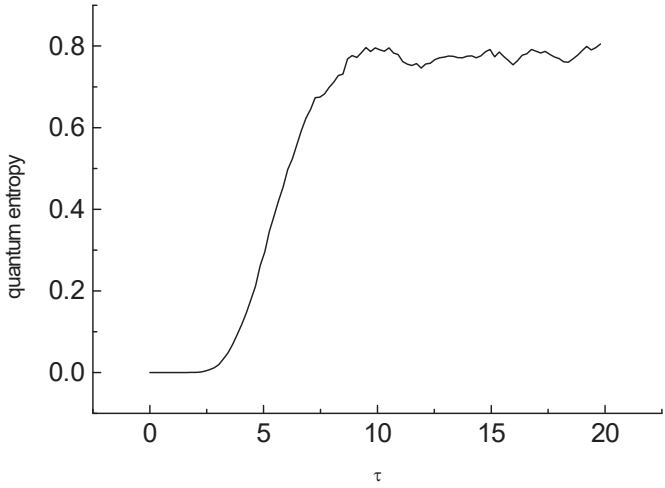

Fig. 5.3. Quantum entropy dynamics of the fundamental mode for the parameter k = 0.1.

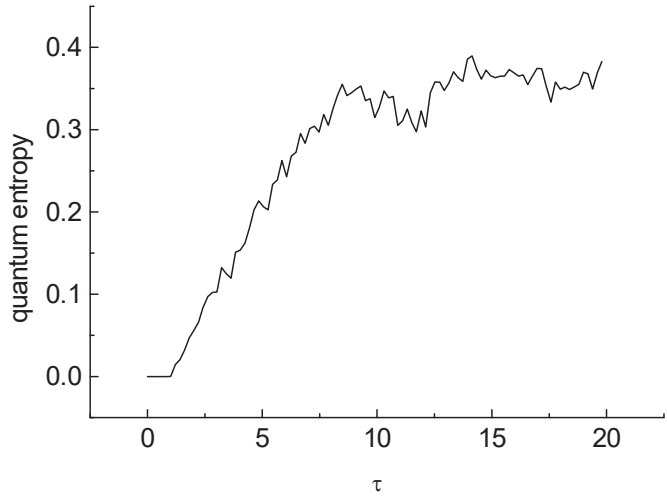

Fig. 5.4. Quantum entropy dynamics of the subharmonic mode for the parameter k = 0.1.

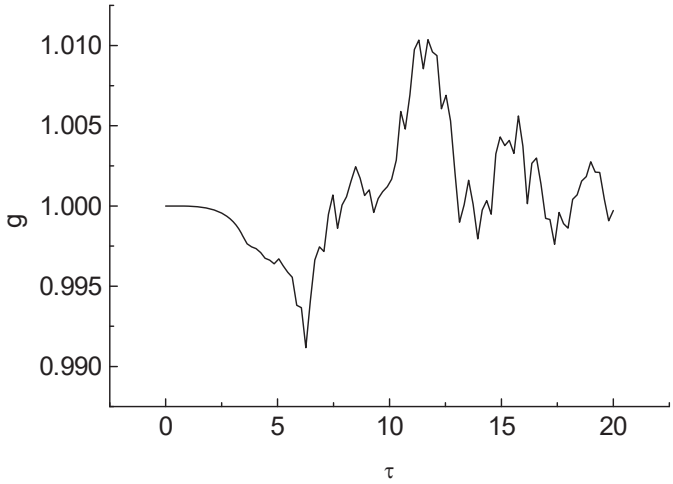

Fig. 5.5. Dynamics of the correlation function of fluctuations in the number of photons in the fundamental and subharmonic modes for the nonlinear mode coupling coefficient k = 0.1.

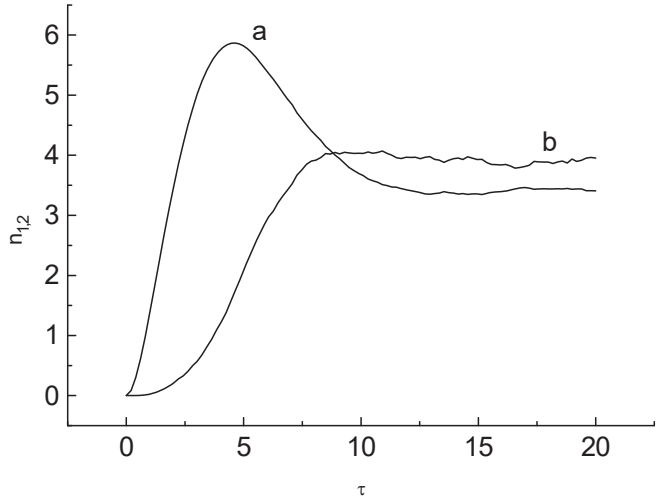

Fig. 5.6. Dynamics of the number of photons in the (a) fundamental and (b) subharmonic modes for the nonlinear mode coupling coefficient k = 0.3.

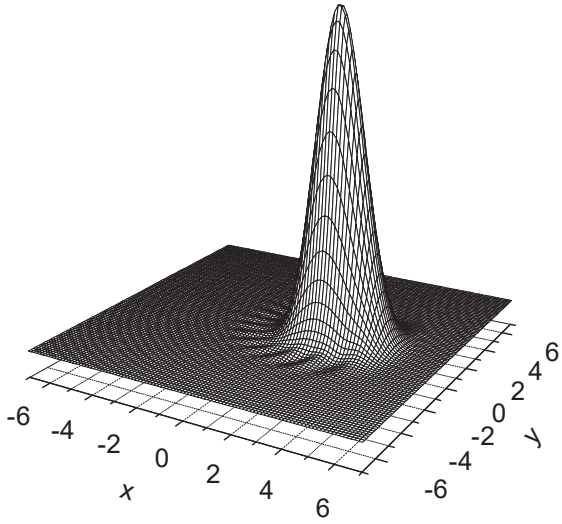

Fig. 5.7a

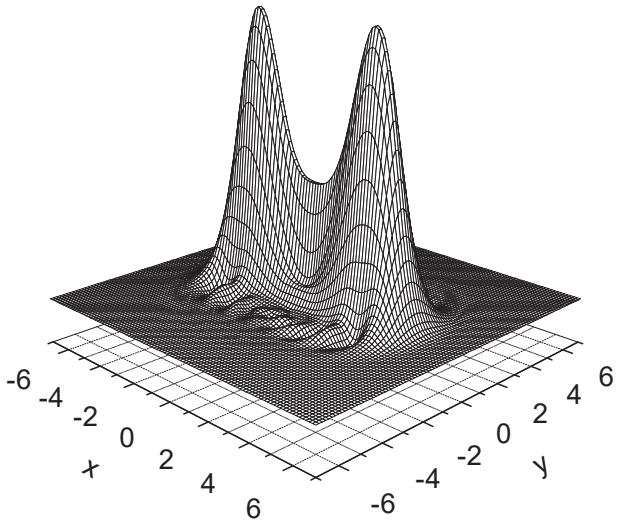

Fig. 5.7b

Fig. 5.7. Wigner function of the stationary state of the (a) fundamental mode and (b) Wigner function of the stationary state of the subharmonic mode for the nonlinear mode coupling coefficient k = 0.3.

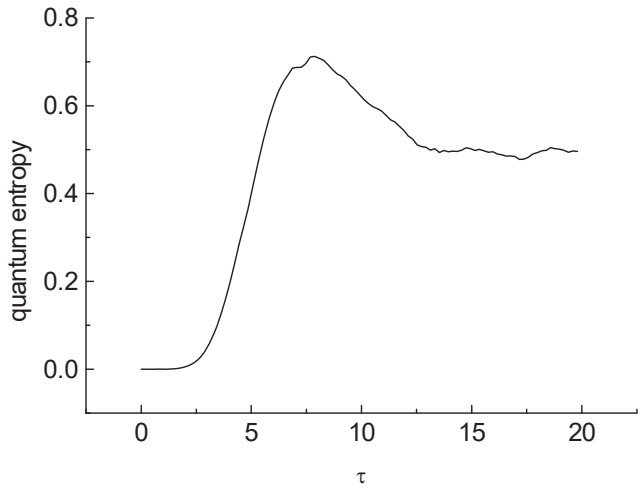

Fig. 5.8. Quantum entropy dynamics of the fundamental mode for the parameter k = 0.3.

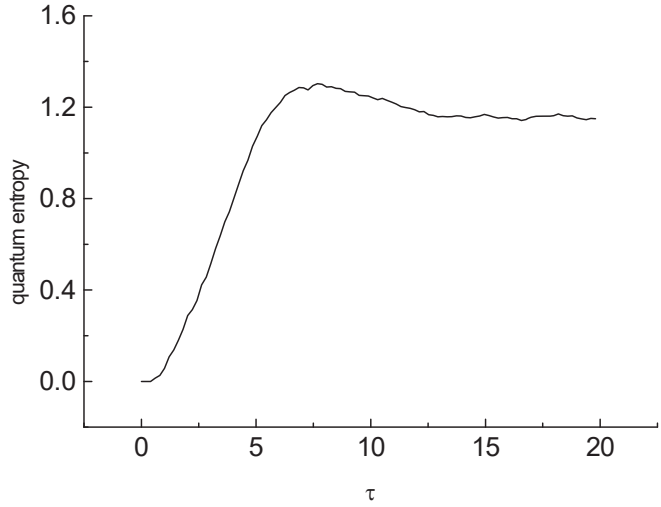

Fig. 5.9. Quantum entropy dynamics of the subharmonic mode for the parameter k = 0.3.

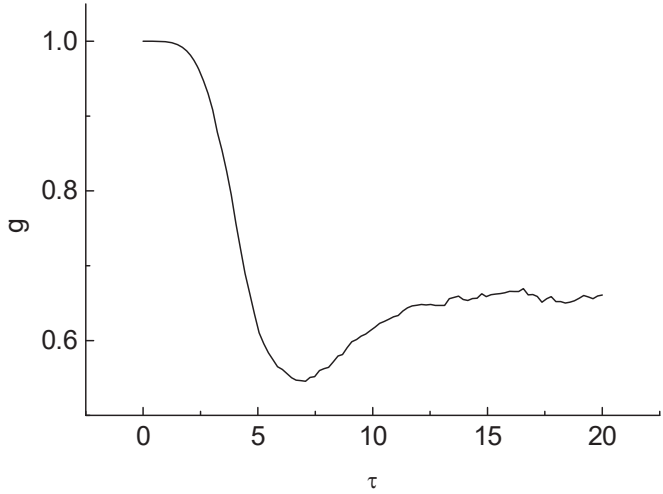

Fig. 5.10. Dynamics of the correlation function of fluctuations in the number of photons in the fundamental and subharmonic modes for the nonlinear mode coupling coefficient k = 0.3.

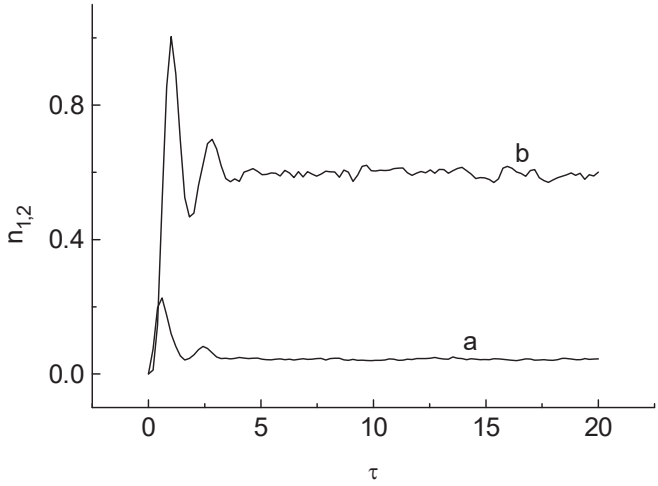

Fig. 5.11. Dynamics of the number of photons in the (a) fundamental and (b) subharmonic modes for the nonlinear mode coupling coefficient k = 4.

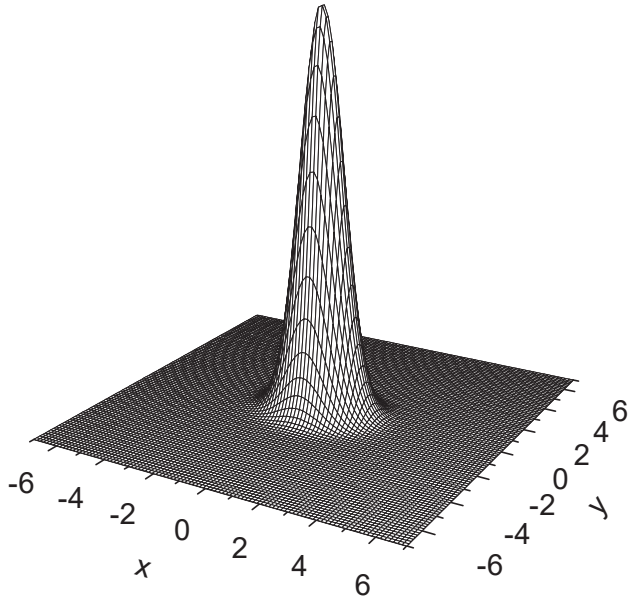

Fig. 5.12a

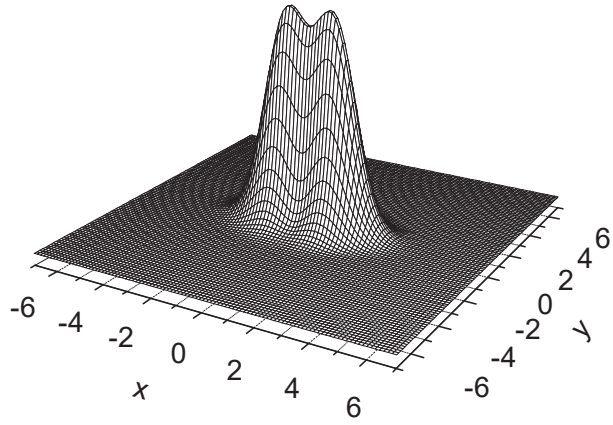

Fig. 5.12b

Fig. 5.12. Wigner function of the stationary state of the (a) fundamental mode and (b) Wigner function of the stationary state of the subharmonic mode for the nonlinear mode coupling coefficient k = 4.

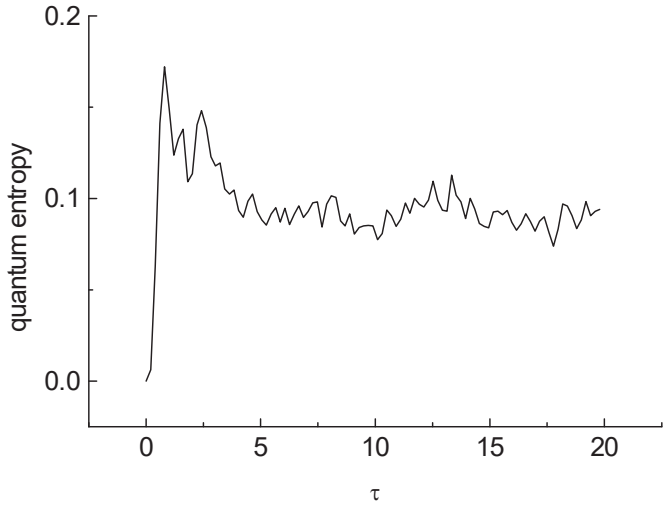

Fig. 5.13. Quantum entropy dynamics of the fundamental mode for the parameter k = 4.

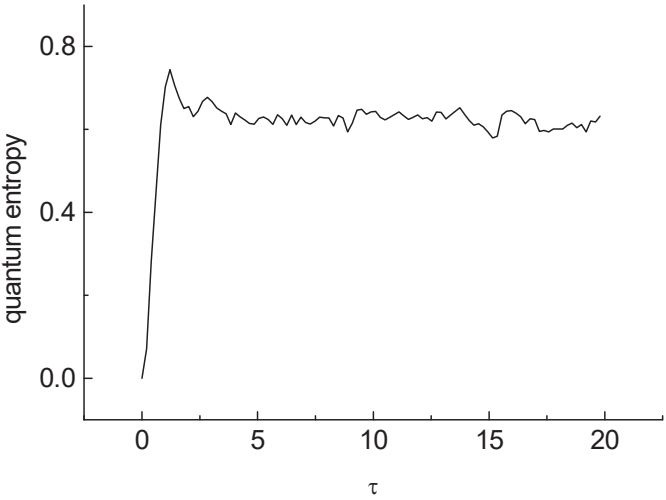

Fig. 5.14. Quantum entropy dynamics of the subharmonic mode for the parameter k = 4.

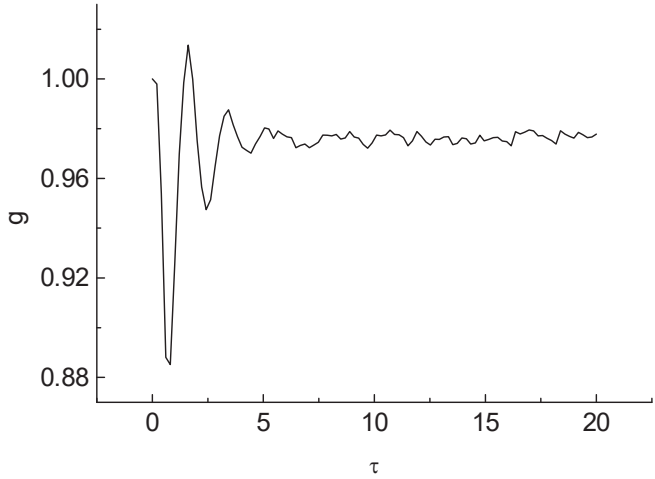

Fig. 5.15. Dynamics of the correlation function of fluctuations in the number of photons in the fundamental and subharmonic modes for the nonlinear mode coupling coefficient k = 4.

CHAPTER 6

QUANTUM DYNAMICS OF INTRACAVITY THIRD SUBHARMONIC GENERATION

Introduction

The materials in this chapter are taken from [1,2].

The quantum dynamics of the mean number of photons and the quantum entropy of interacting modes, as well as the Wigner function of the stationary state of the fundamental and third subharmonic modes, is studied for the intracavity third subharmonic generation. It is shown that the quantum dynamics of the system depends strongly on the nonlinear coupling coefficient between the modes. It is also demonstrated that, in the steady-state limit, depending on the intermodal coupling coefficient, the fundamental mode can be either in a pure coherent, in a squeezed, or in a pure vacuum state. The third subharmonic mode in the subthreshold generation regime of this mode is in a vacuum state. The Wigner function is squeezed over the three sides of an equilateral triangle. The quantum entropy of this state is nonzero. It is also shown that the third subharmonic mode, depending on the nonlinear coupling coefficient in the steady-state limit, can be localized in a three-component state with the same probability of detecting the field in each coherent component of the state and with the presence of quantum-mechanical interference between the state components. The mean number of photons in this state is smaller than unity. Depending on the nonlinear coupling coefficient, the third

subharmonic mode can also be localized in a three-component state, which is a statistical mixture of three squeezed states. The correlation dynamics of photon number fluctuations of the interacting modes is investigated. It is shown that field states, entangled by photon number variables, can be obtained in this system.

6.1. Nonlinear System, Basic Equations, and Calculation Algorithms

We model the generation of the third subharmonic in a two-mode cavity. A nonlinear medium is placed in a cavity, which is tuned to the fundamental mode frequency ω_1 and third subharmonic mode frequency ω_2 ($\omega_1 = 3\omega_2$). The fundamental mode is resonantly perturbed by an external classical field. The equation for the density matrix of this system can be presented in the form

$$\frac{\partial \rho}{\partial t} = (i\hbar)^{-1}\left[H_{sys}, \rho\right] + L(\rho), \tag{6.1.1}$$

where

$$H_{sys} = \frac{i\hbar\chi}{2}(a_1 a_2^{+3} - a_1^{+} a_2^{3}) + i\hbar E(a_1^{+} - a_1), \tag{6.1.2}$$

$$L(\rho) = \frac{\gamma_1}{2}(2a_1\rho a_1^{+} - \rho a_1^{+} a_1 - a_1^{+} a_1 \rho) + \frac{\gamma_2}{2}(2a_2\rho a_2^{+} - \rho a_2^{+} a_2 - a_2^{+} a_2 \rho). \tag{6.1.3}$$

Here, a_i and $a_i^{+} (i = 1,2)$ are the annihilation and creation operators of the fundamental and third subharmonic modes, respectively; χ is the intermodal coupling coefficient, which is proportional to the nonlinear susceptibility $\chi^{(3)}$ of the medium; E is the classical amplitude of the perturbing field at the ω_1 frequency; and $\gamma_i (i = 1,2)$ are the damping

coefficients of interacting modes via cavity mirrors. The perturbing-field phase is omitted for simplicity in Eq. (6.1.2).

The study of the quantum behaviour of this optical system is similar to the study of the quantum behaviour of the intracavity second subharmonic generation process given in Chapter 5. To facilitate the process of reading, we present basic formulas and algorithms necessary for studying the quantum behaviour of the current optical system.

To study the quantum properties of the optical system, we calculate the Wigner functions of the state of the field mode. These functions are calculated in polar coordinates, using the formula [3]

$$W_i(r,\theta) = \sum_{m,n} \rho_{i,mn} w_{mn}(r,\theta)\ (i = 1,2). \qquad (6.1.4)$$

Here, $\rho_{i,mn}$ are the elements of the density matrices of the interacting modes in the Fock basis. The expression for $w_{mn}(r,\theta)$ has the following form:

$$w_{mn}(r,\theta) = \begin{cases} \frac{2}{\pi}(-1)^n \left(\frac{n!}{m!}\right)^{1/2} exp(\, i(m-n)\theta) \times \\ \quad exp(-2r^2)(2r)^{m-n} L_n^{m-n}(4r^2), \quad m \geq n \\ \frac{2}{\pi}(-1)^m \left(\frac{m!}{n!}\right)^{1/2} exp(\, i(m-n)\theta) \times \\ \quad exp(-2r^2)(2r)^{n-m} L_m^{n-m}(4r^2), \quad m \leq n \end{cases}. \qquad (6.1.5)$$

In the last expression, L_p^q are Laguerre polynomials.

We also investigate the quantum dynamics of the mean number of photons of the field modes and the quantum entropy dynamics

$$S_i(t) = -Tr(\rho_i(t)\, ln\, \rho_i\,(t))\ (i = 1,2) \qquad (6.1.6)$$

of the fundamental and subharmonic modes. The quantum entropy of the field can be calculated, using numerical diagonalization of the density matrices of these modes in the Fock basis.

We also investigate the dynamics of the normalized correlation function of fluctuations in the number of photons of the fundamental and the subharmonic modes

$$g(t) = \frac{\langle((n_1(t)-\langle n_1(t)\rangle)+(n_2(t)-\langle n_2(t)\rangle))^2\rangle}{(\langle n_1^2(t)\rangle-\langle n_1(t)\rangle^2)+(\langle n_2^2(t)\rangle-\langle n_2(t)\rangle^2)}. \quad (6.1.7)$$

Here, $n_i = a_i^+ a_i$ $(i = 1,2)$ are the operators of the number of photons in the fundamental and subharmonic modes, respectively. Formula (6.1.7) can be recast in the form

$$g(t) = 1 + \frac{2(\langle n_1(t)n_2(t)\rangle-\langle n_1(t)\rangle\langle n_2(t)\rangle)}{\langle n_1^2(t)\rangle-\langle n_1(t)\rangle^2+\langle n_2^2(t)\rangle-\langle n_2(t)\rangle^2}. \quad (6.1.8)$$

In the absence of correlation between fluctuations in the number of photons in the interacting modes, correlation function (6.1.8) tends to unity.

Equation (6.1.1) for the density matrix of the optical system can be solved by the numerical Monte Carlo method [4]. In this method, the density matrix of the system is presented as the mathematical expectation of the density matrices of quantum trajectories, and each of these matrices characterizes a pure state, which can be found using a certain calculation algorithm:

$$\rho(t) = M\left\{\left|\phi^{(\alpha)}(t)\right\rangle\left\langle\phi^{(\alpha)}(t)\right|\right\} = \lim_{N\to\infty}\frac{1}{N}\sum_{(\alpha)}^{N}\left|\phi^{(\alpha)}(t)\right\rangle\left\langle\phi^{(\alpha)}(t)\right| \quad .(6.1.9)$$

Here, (α) is the trajectory number, and N is the number of independent quantum trajectories.

These calculations can also be done using the python module described in [5].

The dynamics of the system is investigated for identical values of the mode damping coefficients in the cavity ($\gamma_1 = \gamma_2 = \gamma$) in dimensionless time ($\tau = \gamma t$) and with dimensionless parameters of the system ($\varepsilon = E/\gamma$ and $k = \chi/\gamma$). All calculations are performed for system evolution from an initial vacuum state of the fundamental and third subharmonic modes. The dynamics of the mean number of photons, mode quantum entropy, and the Wigner function is obtained using 1000 independent quantum trajectories of the optical system. The dynamics of the system is analyzed for the amplitude of fundamental mode perturbation $\varepsilon = 1.5$.

6.2. System Dynamics in the Case of Weak Coupling of the Modes: Symmetry of Vacuum

In this section, we consider the quantum dynamics of the system for a small intermodal coupling coefficient: $k = 0.03$.

Figure 6.1 shows the dynamics of the numbers of photons of the fundamental (curve a) and third subharmonic (curve b) modes for the above-mentioned case. The number of photons of the fundamental mode increases significantly and exceeds greatly unity for long interaction times (the steady-state value of the number of photons of the fundamental mode, in this case, is approximately 9). At the same time, the number of photons of the third subharmonic barely increases and is much smaller than unity for long interaction times (in this case, the steady-state value of the

number of photons of the third subharmonic mode is approximately 0.06). One can state that the system is in the subthreshold regime of subharmonic generation, and the third subharmonic mode is close to a vacuum state.

The Wigner functions of the stationary state of the fundamental and third subharmonic modes are presented in Figs. 6.2a and 6.2b, respectively, for the interaction time $\tau = 20$. In the region of long interaction times, the fundamental mode is in a one-component state, the Wigner function of which resembles that of a coherent state. The quantum entropy of this state is much lower than unity (approximately 0.0015, see Fig. 6.3). One can state that the fundamental mode is in a pure coherent state.

The Wigner function of the third subharmonic mode resembles the Wigner function of the vacuum state, which is symmetrically squeezed over the three sides of an equilateral triangle. The quantum entropy of this state is approximately 0.1 (Fig. 6.4), indicating that the state is nonpure. Figure 5.2b presents the Wigner function of the stationary state of the second subharmonic mode in the subthreshold generation regime of this mode, which was obtained in [6]. These Wigner functions differ significantly in symmetry, although both describe the vacuum state of the corresponding mode in the subthreshold generation regime of the corresponding subharmonic.

The dynamics of the quantum entropy of the fundamental and subharmonic modes is presented in Figs. 6.3 and 6.4, respectively.

Figure 6.5 represents the correlation function of the photon number fluctuations in the fundamental and third subharmonic modes, which is calculated with the help of Eq. (6.1.7). During the entire interaction time, the value of the correlation function of fluctuations of the interacting

modes is close to unity, which points to the absence of entanglement of the states of the fundamental and subharmonic modes with respect to the number of photons in the interaction region with a small coupling coefficient between the modes (k = 0.03).

6.3. System Dynamics in the Case of Strong Coupling of the Modes: Squeezed State, Statistical Mixture of Three Squeezed States, and Entangled State

In this section, we investigate the quantum dynamics of the system for a nonlinear coupling coefficient exceeding that analyzed in the previous section by a factor of 10 (k = 0.3 and 0.03, respectively). The perturbation amplitude is retained the same ($\varepsilon = 1.5$). In this case, the quantum behaviour of the system differs significantly from the behaviour of the system described in the previous section.

Figure 6.6 shows the dynamics of the number of photons of the fundamental and subharmonic modes (curves a and b, respectively). One can see that in this case (in contrast to that described in the previous section) the system is in the above-threshold regime of subharmonic mode generation. The number of photons of the subharmonic mode for long interaction times is approximately equal to the number of photons of the fundamental mode for the same interaction times.

Figures 6.7a and 6.7b show the Wigner functions of the fundamental and subharmonic modes, respectively, in a stationary state of the system. These functions were calculated for the interaction time $\tau = 20$.

The Wigner function of the fundamental mode in the stationary state of the system differs significantly from the Wigner function of the stationary

state of the same mode in the previous case: at k = 0.03, it is similar to the Wigner function of the coherent state, whereas at k = 0.3 it resembles the Wigner function of the squeezed state. The quantum entropy of this state is approximately 1.2 (Fig. 6.8), being indicative of the nonpurity of this state. The form of the Wigner function of the subharmonic mode also changes sharply: at k = 0.03, it resembles the Wigner function of the vacuum state squeezed over the three sides, whereas, at k = 0.3, it is similar to the Wigner function of the state that is a statistical mixture of three components. Each component resembles the Wigner function of a squeezed state. The field of the third subharmonic mode can be found in each component of the state with equal probability. The quantum entropy of this state exceeds the maximum quantum entropy of a statistical mixture of a three-component state (ln3) (Fig. 6.9). The latter indicates that the field state has a much more complicated structure, which does not follow from the analysis of the Wigner function.

The dynamics of the quantum entropy of the field state for the fundamental and third subharmonic modes is presented in Figs. 6.8 and 6.9, respectively. Both values become steady-state at long interaction times.

Figure 6.10 represents the dynamics of the correlation function of fluctuations in the photon number of the fundamental and third subharmonic modes for the case k = 0.3. It is computed with the use of formula (6.1.8). In contrast to the previous case (k = 0.03), where there was no correlation between fluctuations in the photon numbers of the interacting modes, in this case, the correlation function is less than unity in the region of large interaction times, which points to the origination of correlation between fluctuations in the photon numbers of the fundamental

and third subharmonic modes. This results in the entanglement of the states of these modes.

6.4. System Dynamics in the Case of Very Strong Coupling of the Modes: Three-Component State with Quantum-Mechanical Interference between State Components

In this section, we investigate the dynamics of the system in the case of a large nonlinear coupling coefficient between the interacting modes: $k = 4$.

Figure 6.11 shows the dynamics of the number of photons of the fundamental and subharmonic modes (curves a and b, respectively). The number of photons of the stationary state for both modes is smaller than unity. The number of photons of the stationary state for the fundamental mode is $\langle n_1 \rangle \approx 0.02$, and one can state that this mode is close to a vacuum state. The number of photons of the stationary state for the subharmonic mode is $\langle n_2 \rangle \approx 0.5$.

The Wigner functions of the stationary state of the fundamental and third subharmonic modes are presented in Figs. 6.12a and 6.12b, respectively. The Wigner function of the fundamental mode resembles the Wigner function of a vacuum state. The quantum entropy of this state is also close to zero (Fig. 6.13): it is approximately 0.05. Thus, one can state that, in this case, the fundamental mode is in a pure vacuum state at long interaction times.

In this case, the Wigner function of the stationary state of the third subharmonic mode has a three-component structure. This mode is in a three-component state with the same probability of detecting the field in each component of the state. The quantum entropy of this state is

approximately 0.7 (Fig. 6.14). This value is smaller than the maximum quantum entropy of a three-component state ln3, which indicates the existence of a quantum-mechanical interference between the components of the field state for the third subharmonic mode in this interaction domain. The possibility of creating three-component superposition states of light in optical systems was for the first time indicated in [7]. A mechanism of occurrence of three-component states of light with quantum interference between the field state components in the range of small amplitudes of the state (the mean number of photons is smaller than unity) in a dissipative medium was proposed in [8].

The dynamics of the quantum entropy of the fundamental and third subharmonic modes for k = 4 is presented in Figs. 6.13 and 6.14, respectively. Both entropies become steady-state at long interaction times. The steady-state entropy of the fundamental mode is much smaller than that of the third subharmonic mode.

Figure 6.15 represents the dynamics of the correlation function of photon number fluctuations of the fundamental and third subharmonic modes. In the region of large interaction times, the correlation function is close to unity, which indicates the absence of correlation between fluctuations in the number of photons of the interacting modes. Entanglement of the states of the fundamental and subharmonic modes is absent in this case, as in the case of the k = 0.03 value of the nonlinear coupling coefficient between the modes (see Figs. 6.5 and 6.15).

References

1. S. T. Gevorkyan and M. S. Gevorkyan, “Quantum Dynamics of Intracavity Third Subharmonic Generation,” *Optics and Spectroscopy* 122 (2017), no. 5: 784–790.
2. M. S. Gevorgyan, "Quantum Coherence and Entangled States in Intracavity Third Subharmonic Generation Process," *Journal of Contemporary Physics (Armenian Academy of Sciences)* Vol. 52 (2017), no. 2: 97–104.
3. L. Gilles, B. M. Garraway, and P. L. Knight, “Generation of Nonclassical Light by Dissipative Two-Photon Processes,” *Phys. Rev. A* 49 (1994): 2785–2799.
4. K. Molmer, Y. Castin, and J. Dalibard, “Monte Carlo Wave-Function Method in Quantum Optics,” *JOSA B* 10 (1993): 524–538.
5. J. R. Johansson, P. D. Nation, and F. Nori, "QuTiP 2: A Python Framework for the Dynamics of Open Quantum Systems," *Comp. Phys. Comm.* 184 (2013): 1234.
6. S. T. Gevorgyan and M. S. Gevorgyan, “Quantum Dynamics of Interacting Modes in the Process of Intracavity Subharmonic Generation,” *Optics and Spectroscopy* 116, no. 4 (2014): 619–625.
7. S. T. Gevorgyan and V. O. Chhaltykyan, "Coherent Superposition States of Light and Their Interference in the Three-Photon Absorption Process," *J. of Modern Opt.* 46 (1999): 1447–1463.
8. S. T. Gevorgyan, Min Xiao, and V. O. Chaltykyan, “Superposition States of Light in a Three-Photon Absorbing Dissipative Medium,” *J. Modern Optics* 55, no. 12 (2008): 1923–1935.

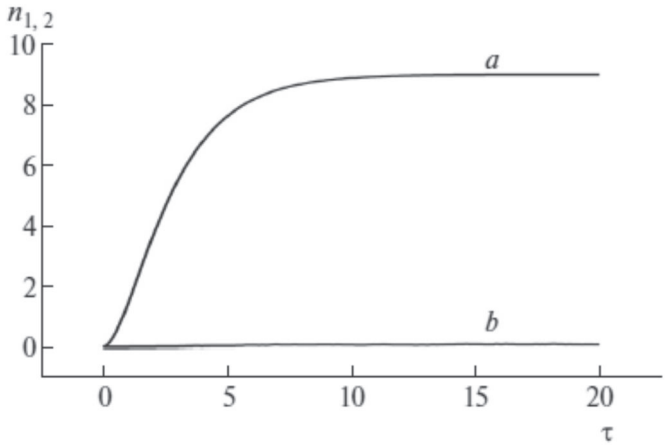

Fig. 6.1. Dynamics of the mean numbers of photons of the (curve a) fundamental mode and (curve b) third subharmonic modes for the coupling coefficient k = 0.03.

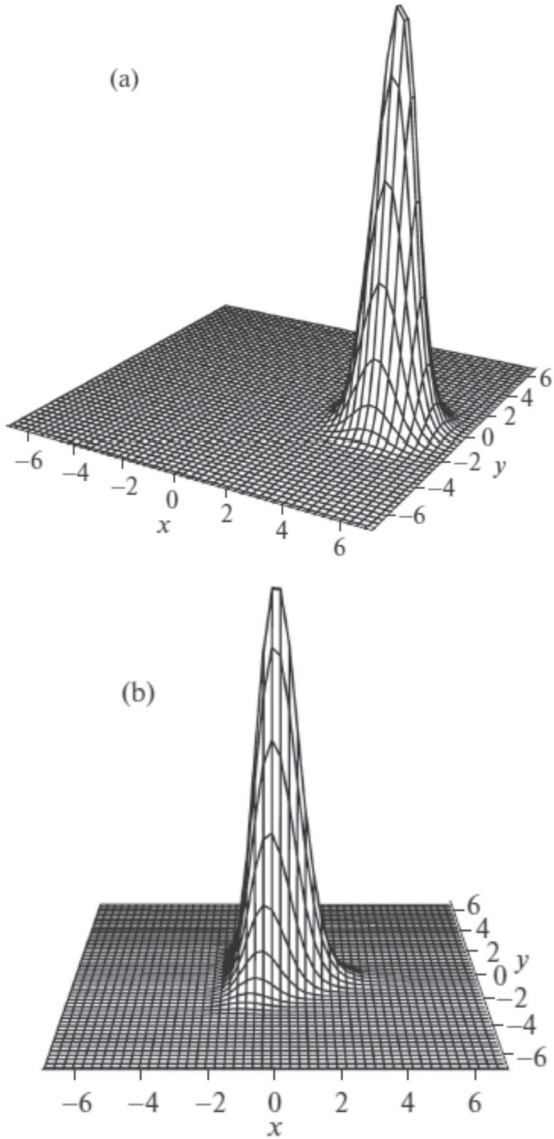

Fig. 6.2. Wigner functions of the stationary states of (a) the fundamental mode and (b) the third subharmonic for the intermodal coupling coefficient k = 0.03.

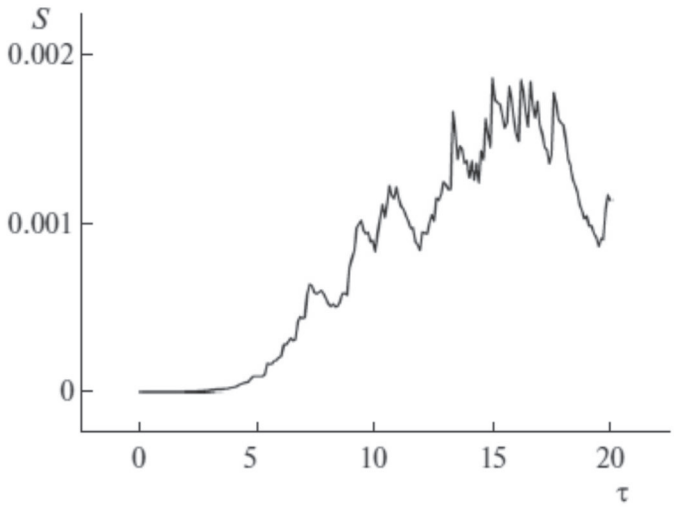

Fig. 6.3. Dynamics of the quantum entropy of the fundamental mode for the intermodal coupling coefficient k = 0.03.

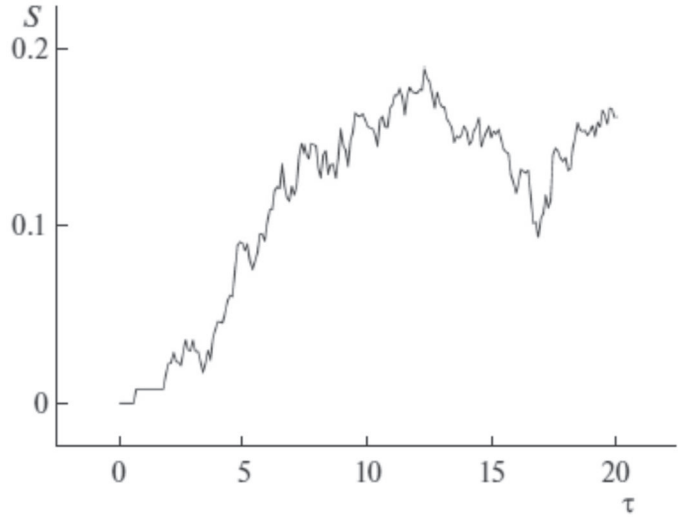

Fig. 6.4. Dynamics of the quantum entropy of the third subharmonic mode for the intermodal coupling coefficient k = 0.03.

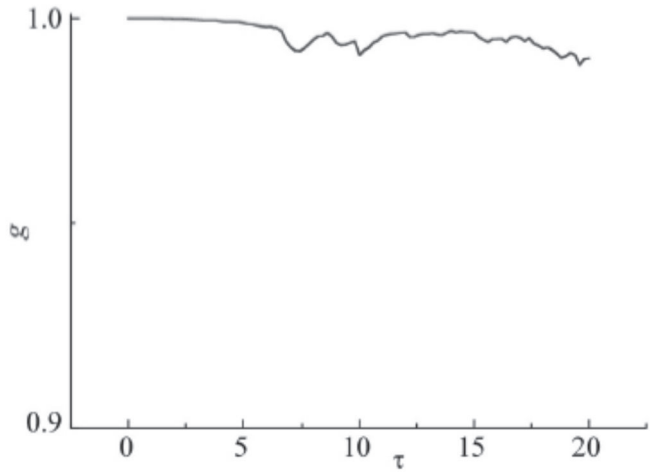

Fig. 6.5. Dynamics of the correlation function of the number of photon fluctuations of the fundamental and the third subharmonic modes for the following coefficient of nonlinear coupling between the modes: k = 0.03.

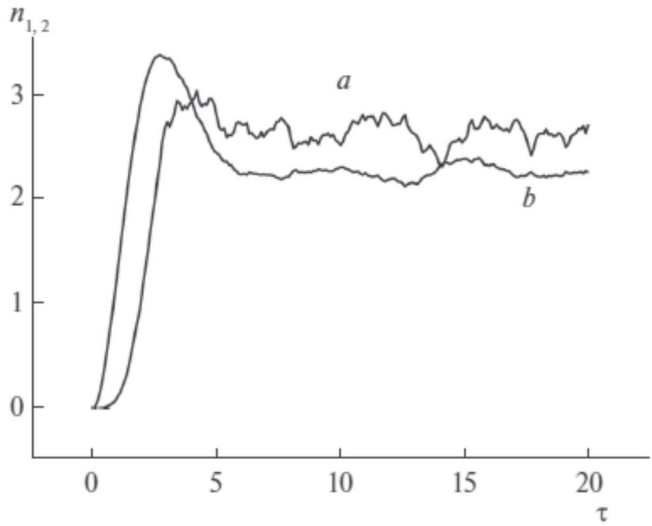

Fig. 6.6. Dynamics of the mean numbers of photons of the (curve a) fundamental and (curve b) third subharmonic modes for the coupling coefficient k = 0.3.

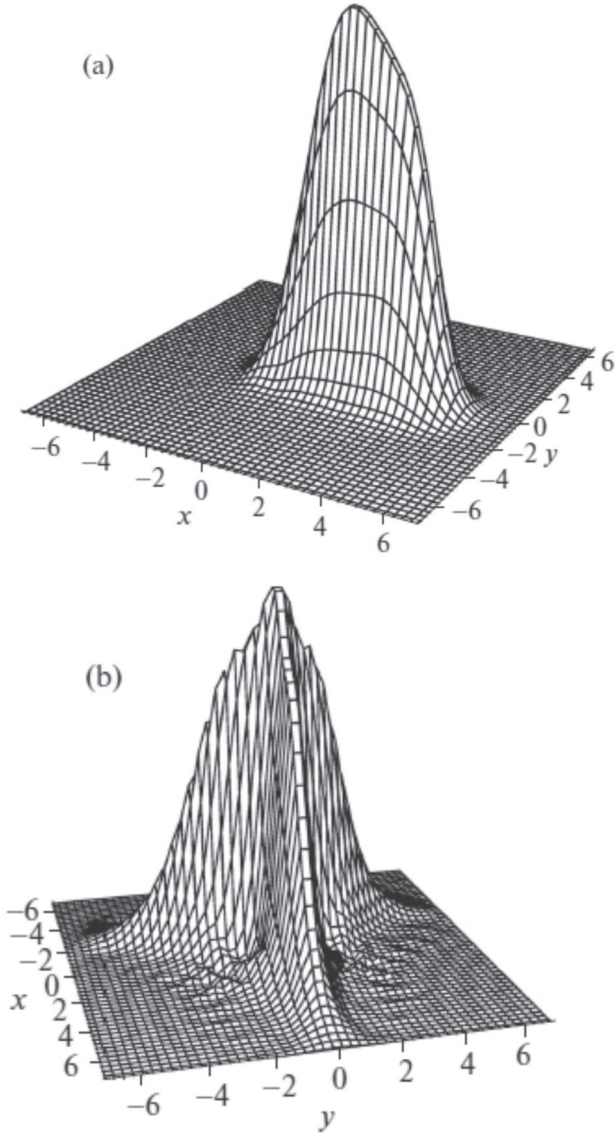

Fig. 6.7. Wigner functions of the stationary states of (a) the fundamental mode and (b) the third subharmonic for the intermodal coupling coefficient k = 0.3.

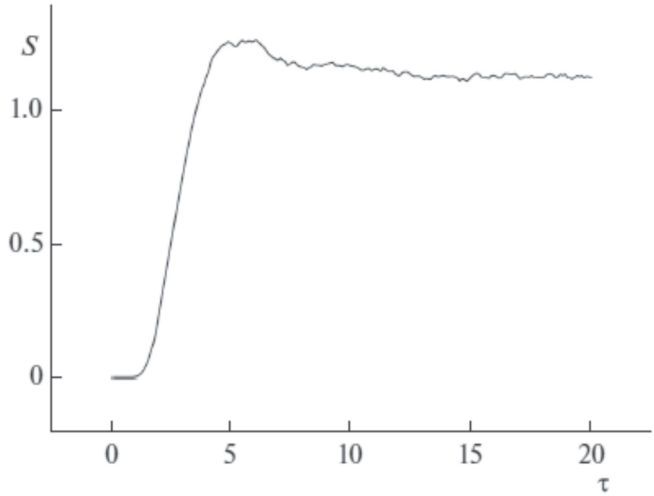

Fig. 6.8. Quantum entropy dynamics of the fundamental mode for the intermodal coupling coefficient k = 0.3.

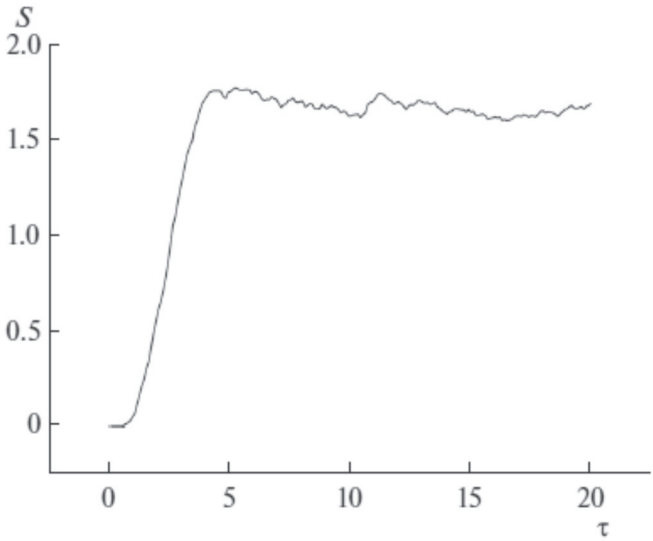

Fig. 6.9. Quantum entropy dynamics of the third subharmonic mode for the intermodal coupling coefficient k = 0.3.

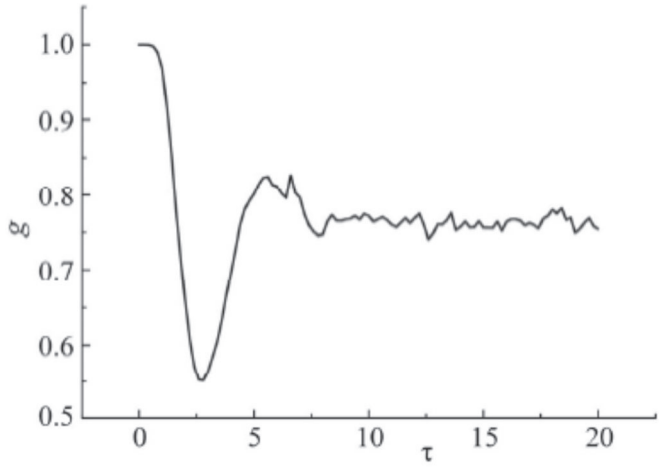

Fig. 6.10. Dynamics of the correlation function of fluctuations in the number of photons of the fundamental and third subharmonic modes for the following value of the coefficient of nonlinear coupling between the modes: k = 0.3.

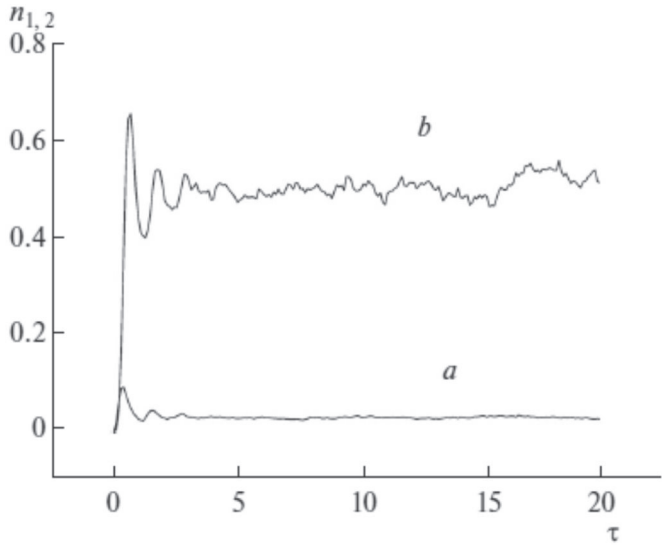

Fig. 6.11. Dynamics of the mean numbers of photons of the (curve a) fundamental and (curve b) third subharmonic modes for the coupling coefficient k = 4.

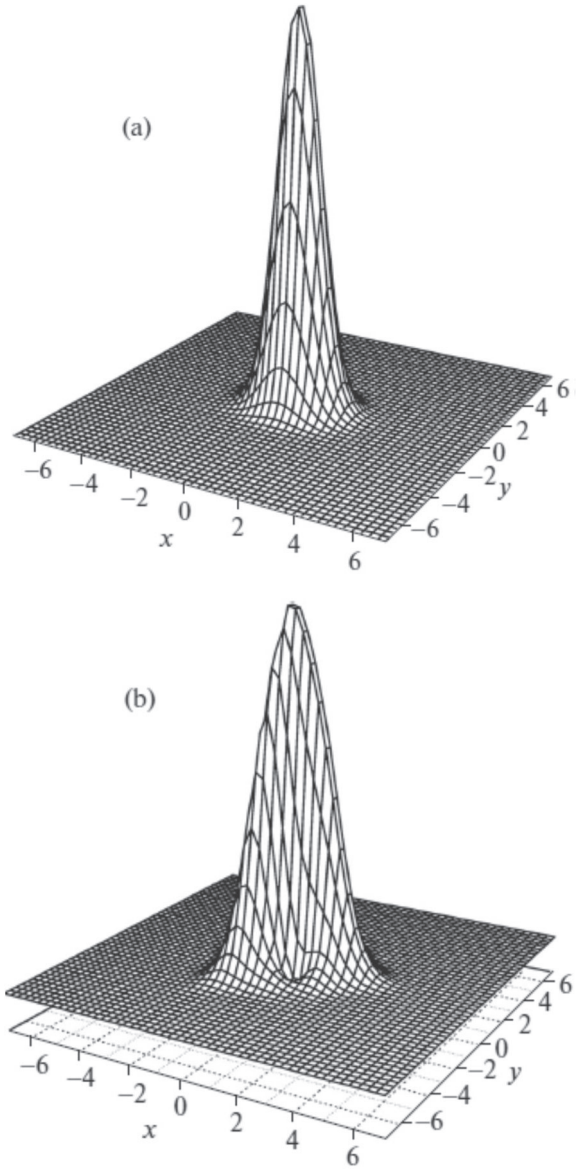

Fig. 6.12. Wigner functions of the stationary states of (a) the fundamental mode and (b) the third subharmonic for the intermodal coupling coefficient k = 4.

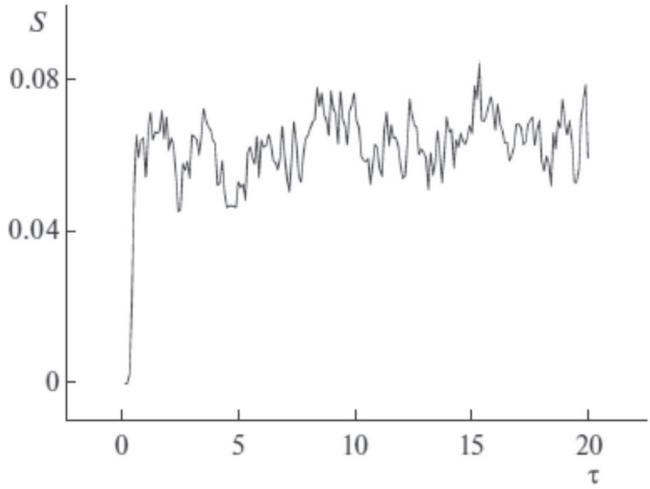

Fig. 13. Quantum entropy dynamics of the fundamental mode for the intermodal coupling coefficient k = 4.

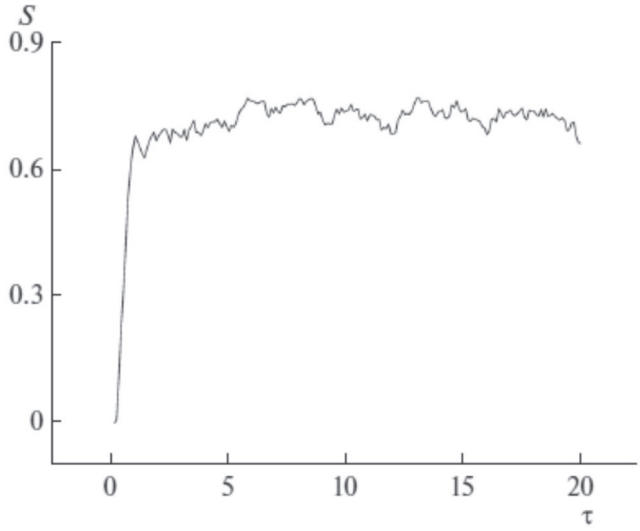

Fig. 6.14. Quantum entropy dynamics of the third subharmonic mode for the intermodal coupling coefficient k = 4.

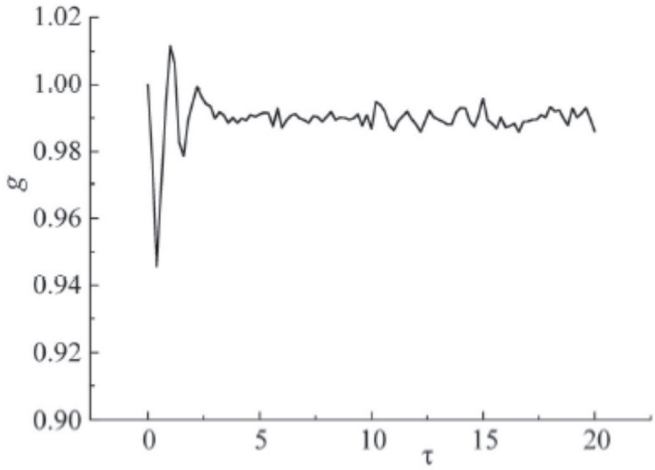

Fig. 6.15. Dynamics of the correlation function of fluctuations in the number of photons of the fundamental and third subharmonic modes for the following value of the coefficient of nonlinear coupling between the modes: k = 4.